Actuation and Control of Lower Limb Prostheses

Yu, Tian

Award date:
2017

Awarding institution:
University of Bath

Actuation and Control of Lower Limb Prostheses

Tian Yu

A thesis submitted for the degree of Doctor of Philosophy

University of Bath
Department of Mechanical Engineering

July 2017

Abstract

Millions of people are suffering from lower limb loss all around the world. Passive ankle prostheses in the market cannot fully restore ankle function and will cause asymmetrical walking gaits. Several powered ankle prostheses, which provide net power in the stance phase to assist walking, have been developed by the researchers, but their walking range is significantly limited by the power requirement.

In this thesis, an electrohydrostatic actuator (EHA) powered ankle prosthesis is proposed. This is intended to actively assist walking at certain points in the gait cycle, namely the plantarflexion (PF) before toe-off and dorsiflexion (DF) in the early swing phase for toe-lifting. In the rest of the gait, the ankle prosthesis actuation system can operate passively with controllable damping. This approach can increase the working time range compared to a continually powered ankle and ensure safe passive prosthetic function after the battery discharged.

A prototype of the EHA powered ankle prosthesis has been developed. A 100 W brushless DC motor is used driving a 0.45 cc/rev bi-directional gear pump. The damping ratios of the ankle PF and DF are controlled by bypass restriction valves. The EHA system and the foot springs at the ankle joint weigh 2.2 kg. The controller and a 2 Ah battery are held in a backpack.

Walking characteristics with a passive ankle were studied in an amputee trial to gather ankle sensor signals for the controller design. A timing control method is proposed which uses the foot spring strain gauge signals to detect heel strike. A middle stance time delay is added between the end of the heel strike and the start of the powered PF phase. This delay time length can be adjusted to fit different walking speeds. Heel strike detection using hydraulic pressure signals is also studied.

The EHA powered ankle prosthesis and its controller has been tested by a 70 kg transtibial amputee. According to the amputee trial results, the EHA can provide

sufficient power to assist walking in the terminal stance and the energy consumption in the passive phases are proximately zero. The on-board battery is able to power over 5500 level walking steps. In the amputee trial, the ankle prosthesis controller correctly recognises the heel strike and triggers the powered PF phase. According to feedback from the amputee, the EHA powered ankle prosthesis provided beneficial level walking assistance and a very natural walking gait. The characteristics of the powered ankle prosthesis are analysed by comparing with the healthy ankle and by testing at different walking speeds.

A simulation model was developed to help analyse the performance characteristics of the EHA. This includes a brushless DC motor model and a symmetric hydraulic actuation model. The laboratory-based experiment results and amputee trial results are used to analyse and validate the simulation model. The model can be used for future development and refinement of EHA powered ankle prostheses.

Acknowledgement

I would like to express my special thanks of gratitude to my lead supervisor Prof. Andrew Plummer for his guidance, support, kindness, immense knowledge and advanced thinking. It is never too much appreciations comparing to the genius advices he gave me without restraint.

My sincere thanks also goes to my supervisor Dr. Pejman Iravani, who always inspires and directs me with his expertise and innovation ideas.

I am grateful to the Chas. A. Blatchford & Sons Ltd for supporting this project and their excellent contribution to help the amputees. With a special mention to Prof. Saeed Zahedi OBE, Dr. Jawaad Bhatti and Dr. David Moser, their support and trust always push this project forward.

I am also grateful to the staffs in Centre for Power Transmission and Motion Control and student workshop for the assistance this project.

Many many thanks to my family for their endless love and support.

Many many thanks to my friends who always listen to my complaint and feed me up with love and positive energy.

Contents

List of Figures

List of Tables

List of Symbols

SYMBOL	DESCRIPTION
A_a	Annulus area/Cylinder working area
A_{ra}	Ankle rotation range
D	Pump displacement
D_p	Piston diameter
D_r	Rod diameter
F_r	Rod force
g	Acceleration due to gravity
I	Motor current
J_m	Motor inertia
J_p	Pump inertia
K	Proportional gain
K_a	Ankle speed lever ratio
K_b	Motor back-EMF coefficient
K_{bd1}	Active DF Bypass Coefficient 1 (square-root)
K_{bd2}	Active DF Bypass Coefficient 2 (linear)
K_{bp1}	Active PF Bypass Coefficient 1 (square-root)
K_{bp2}	Active PF Bypass Coefficient 2 (linear)
K_B	On/off valve coefficient
K_i	Integral gain
K_{in}	Pump internal leakage coefficient
K_l	Manifold pressure loss coefficient
K_{pf}	Pressure-based friction coefficient
K_r	IxR compensation coefficient
K_t	Motor torque constant
K_{vf}	Viscous friction coefficient

L	Motor inductance
L_a	Arm length
L_l	Lever length
L_s	Piston stroke
M_l	Mass of load weights
P_a	Ankle output power
P_m	Motor input power
P_p	Pump output power
Q	Flow rate in hydraulic circuit
Q_a	Actuator flowrate
Q_{pa}	Actual pump output flowrate
Q_p	Pump flowrate
Q_{pt}	Theoretical pump output flowrate
R	Motor resistance
R_l	Lever ratio
s	Differential operator
T_{aa}	Actual actuator output torque
T_{an}	Ankle torque
T_{at}	Theoretical actuator output torque
T_{cf}	Coulomb friction
T_l	Load torque
T_m	Motor torque
T_{ma}	Effective motor output torque
T_{mt}	Theoretical motor output torque
V_b	Saturation voltage
V_d	Motor drive voltage
ΔP	Pressure difference
ΔP_a	Pressure difference across actuator
ΔP_p	Pressure difference across pump
α	Ankle angular position

$\boldsymbol{\beta}$	Shank angular position
$\boldsymbol{\mu_r}$	Rod extension speed
$\boldsymbol{\omega_{an}}$	Ankle rotation speed
$\boldsymbol{\omega_d}$	Motor demand speed
$\boldsymbol{\omega_l}$	Lever angular speed
$\boldsymbol{\omega_m}$	Motor speed

List of Abbreviations

ATSG	Average Toe Strain Gauge
BSP	British Standard Pipe
COT	Cost of Transport
CRIO	Compact Real-time Input/output (Processor)
DC	Direct Current
DF	Dorsiflexion
EHA	Electrohydrostatic Actuation
EMF	Electromotive Force
EMG	Electromyography
ESR	Energy Storage and Return (foot)
FPGA	Field-programmable Gate Arrays
HSG	Heel Strain Gauge
IMU	Inertial Measurement Unit
PF	Plantarflexion
PI	Proportional-integral (Controller)
P/O	Prostheses and Orthoses
PPAM	Pleated Pneumatic Artificial Muscle
PVC	Polyvinyl Chloride Rigid Polyvinyl chloride
RoM	Range of Motion
RPVC	Rigid Polyvinyl chloride
SACH	Solid Ankle Cushion Heel (Foot)
SEA	Series-elastic Actuator

List of Publications

Conference Papers

1. T. Yu et al., "The design of a powered ankle prosthesis with electrohydrostatic actuation," in *Proc. Of the ASME/BATH 2015 Symposium on Fluid Power*, Chicago, Illinois, USA, 2015.

2. T. Yu et al., "Testing an electrohydrostatic powered ankle prosthesis with transtibial and transfemoral amputees," in *Proc. Of the 7th IFAC Symposium on Mechatronic Systems*, Loughborough, UK, 2016.

3. T. Yu et al., "The design, analysis and testing of a compact electrohydrostatic powered ankle prosthesis," in *Proc. Of the ASME/BATH 2016 Symposium on Fluid Power,* Bath, UK, 2016

Journal Papers

4. T. Yu et al., "The design, control and testing of a compact electrohydrostatic powered ankle prosthesis," to be published.

Chapter 1

Introduction

The importance of the development of a new generation ankle prosthesis is now greater due to the increasing number of lower limb amputees. The development of ankle prostheses has gradually restored some of the ankle functions. Recently several approaches, using different types of actuation, have been attempted to actively assist walking. Electrohydrostatic actuation (EHA) is suitable for a powered ankle prosthesis due to its high power density and ability for quick and smooth switching between active and passive operation modes. Therefore research on an EHA powered ankle prosthesis is proposed.

1.1. Background

Millions of people are suffering from limb loss all around world and thousands of people go through limb amputation operations every year. In the UK, there are over 5000 major limb amputations carried out every year according to the National Health Service, most of which are lower limb amputations [1]. In the US, the estimated number of people suffering from limb loss has increased from 1.2 million in 1996 to 1.6 million in 2005 and will be more than doubled by 2050 to 3.6 million [2]. Beside the limb loss due to trauma, amputation operations are also caused by cancer , malignancy or the complications of circulatory, vascular and diabetes disease [3][4]. The vascular disease and diabetes are considered to cause over 80 % of all amputations in the UK [3].

Among all the physiological and psychological approaches to help amputees rehabilitate, limb prostheses are essential to enable the amputees' daily activities [5]. Especially well-functioning lower limb prostheses can restore the missing mobility functions of the lower limb amputees from standing to outdoor walking and even running or stair ascent. The development of a new generation lower limb prosthesis with improved performance is not only highly desired by the amputees, but also a promising product with huge market demand.

According to the amputation level, lower limb amputation can be classified into toe, ray, transmetatarsal, mid-foot, below-knee (transtibial) and above knee (transfemoral) amputations [6]. At different amputation levels, the required prostheses greatly vary in size, weight and function. This research is focusing on the development of a powered transtibial prosthesis to replace the ankle joint functions.

The research has been undertaken in collaboration with Chas A Blatchford & sons Ltd. Chas A Blatchford & sons Ltd, founded in 1890, is a world famous developer and provider of prosthetic and orthotic products and services [7]. The Blatchford Modular Assembly Prosthesis is winner of The Queen's Award and Design Council Award and the Endolite Carbon Fibre System have set industry standards [7]. Their ankle

prosthetic products, e.g. Elan [8] and Echelon [9], significantly enhance the quality of life for lower limb amputees.

1.2. Ankle Motion Introduction

The rotation of the ankle is commonly called dorsiflexion (DF) and plantarflexion (PF) in the sagittal plane. The direction is defined as shown in Figure 1-1. Considering level ground walking (Figure 1-2), the ankle motion in a gait cycle is divided in to early stance phase (or heel strike), middle stance phase, terminal stance phase (or powered PF/ heel rise phase) and swing phase. Usually the early and middle stance phase is divided by the foot becoming horizontal; the middle and terminal stance phase is divided by the maximum DF of the ankle; the stance and swing phase is divided by toe-off. The ankle motion will be further analysed in the following chapters.

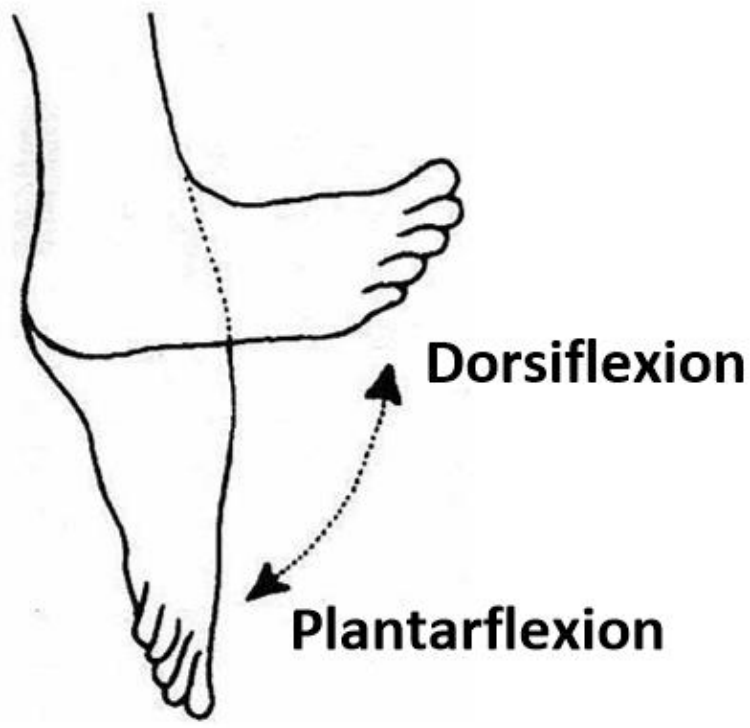

Figure 1-1: Definition of DF and PF of ankle joint [10].

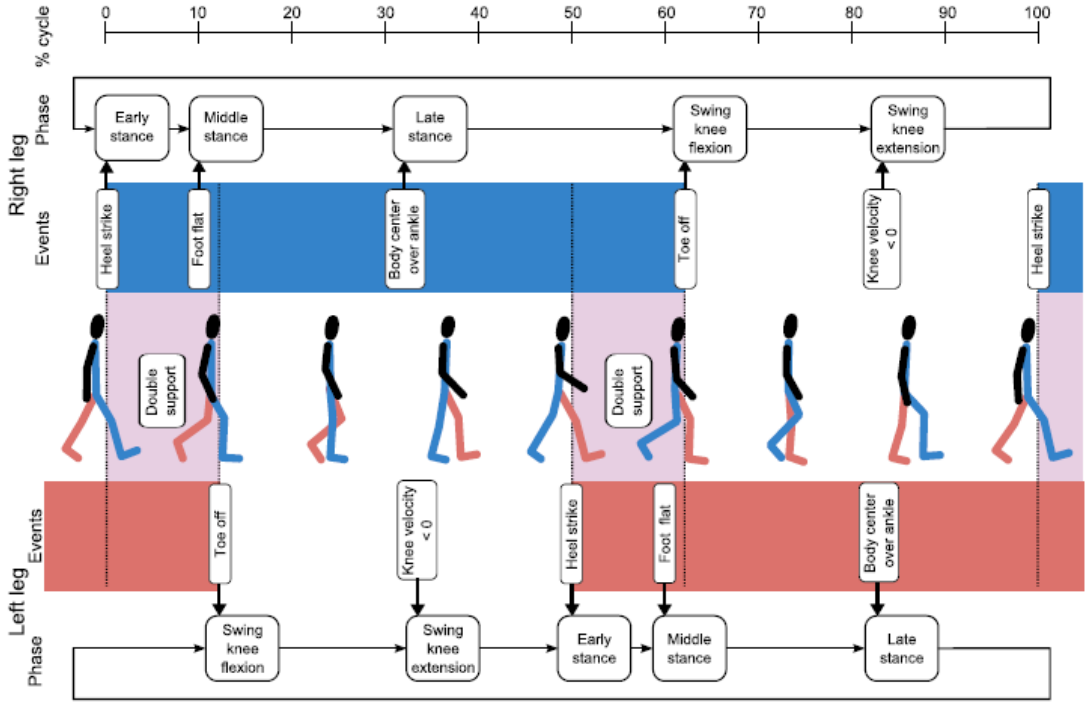

Figure 1-2: Human gait decomposition, reprinted from [11].

1.3. Development History of Ankle Prostheses

The earliest mention of an artificial leg may be traced back to India about 1500 to 800 B.C. [12]. The large number of amputees returning from World War Ⅰ and World War Ⅱ provided impetus for limb prosthesis research [13]. The development of ankle prostheses mirrors the increasing level of human ankle function realization, from body weight support to shock absorption, energy conservation and walking propulsion [5, 14]. Most prosthetic feet before the 1980s were designed to restore basic walking and simple occupational tasks. The SACH (solid ankle cushion heel) foot is the simplest type of non-articulated foot, which supports the body weight during stance and absorbs shock during the heel strike of a walking gait. The ESR (energy storage and return) type uses an elastic structure to absorb and store the energy during weight acceptance and return the energy during push off to assist walking. The energy storage structure

can be carbon composite leaf springs in the artificial feet (Figure 1-3), a shank-ankle-foot structure made of a specially developed carbon composite (Figure 1-4), an elastic bumper spring (Figure 1-5) or other types [5].

Figure 1-3: ESR feet with separated heel and forefoot carbon composite leaf springs, Esprit [15].

Figure 1-4: ESR feet with a shank-ankle-foot carbon composite, Blade XT [16].

Figure 1-5: ESR feet with elastic bumper spring, EliteVT [17].

The rotation of the ankle joint has then been enabled by the single-axis ankle prosthesis with sagittal joint [14]. The practicability of the ankle prosthesis has been further extended to stair ascent and descent, up slope and down slope walking by controlling the damping of the ankle joint using on board microprocessors [5]. Several example products of ESR and single-axis ankle prosthesis will be presented in the next chapter.

Healthy subjects require high net ankle power in the stance phase during walking, which the conventional passive ankle prosthesis cannot achieve [18, 19]. The lack of the push-off function at the ankle results in shorter stance phase on the amputated side (early toe-off), longer double stance phase, asymmetry between sides and higher energy consumption of the amputee [20-22].

To further restore the human ankle function, several powered ankle prostheses with different kinds of actuation have been developed by researchers, including DC (direct current) motors with mechanical transmissions, pneumatic actuation and pneumatic artificial muscles [5]. BiOM is the first commercially available powered ankle prosthesis [23]. These devices will be further reviewed in the next chapter.

For the development of a new generation of ankle prosthesis, the fundamental goal is to provide performance close to that of human locomotion. This requires well controlled ankle impedance and correctly delivered active power during different activities. The main challenge for the ankle joint actuation is to reach the high torque and power requirement within the weight and volume limitation. The power source, user interaction, robustness and safety also need to be considered. For a commercially available ankle prosthesis, even more requirements should be taken into account including cost, market coverage, accessories, operation life, waterproofing, noise, visibility and user satisfaction.

The incorporation of robotic technology provides the opportunity for prosthetic devices with much greater functionality. Especially there is significantly improved capability for embedded control. The development of battery technology with high energy density also gives the possibility for the powered prosthetic devices with longer working range.

1.4. Electrohydrostatic Actuators (EHAs)

An EHA, an actuator combining electric servo-motor and hydraulic transmission circuit, is widely used in the aerospace industry and increasingly used in other industrial hydraulics. It is developed for the power-by-wire systems for aerospace, which distributes power to the actuation modules using electrical power networks only [24, 25]. An example EHA used in an aerospace application is shown in Figure 1-6.

A sample EHA circuit diagram is shown in Figure 1-7. An EHA system normally consists of the following elements:

- An electric motor
- A bi-directional hydraulic pump
- An accumulator or other make-up fluid system

- Bypass relief valves or restriction valves
- A symmetrical linear actuator or rotary hydraulic motor

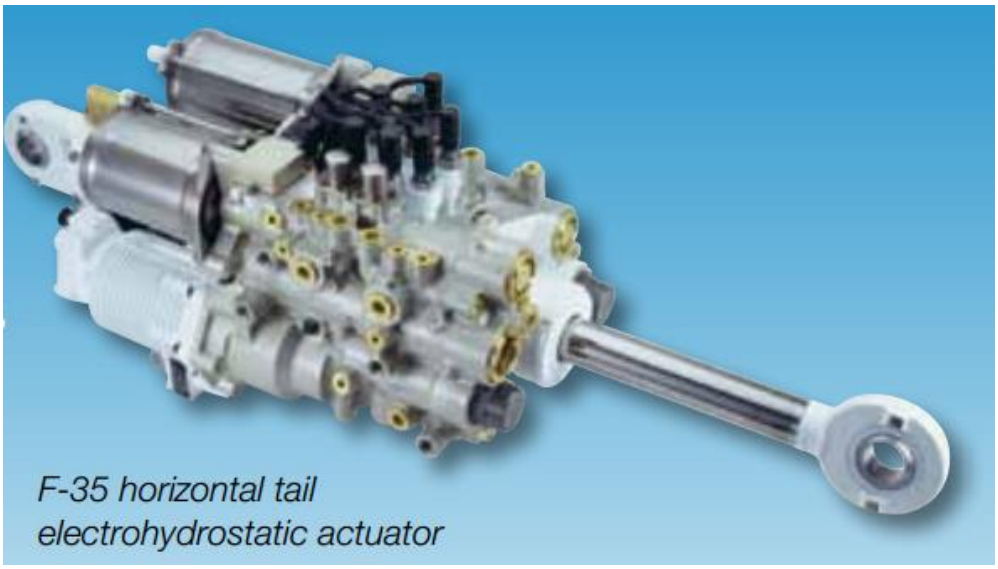

Figure 1-6: F-35 horizontal tail EHA [26].

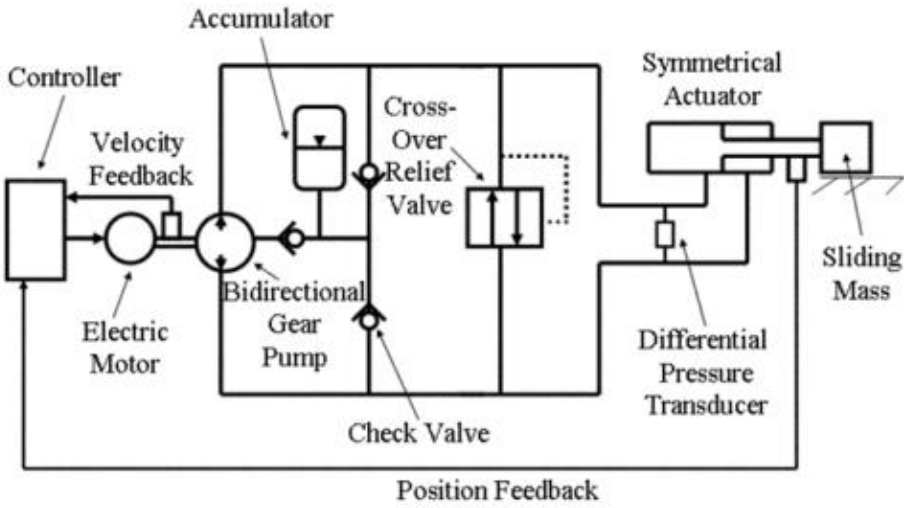

Figure 1-7: Circuit diagram of an EHA system with position feedback control, reprinted from [27].

The advantages of an EHA includes high power to weight/volume ratio, high torque to weight/volume ratio, good controllability and robustness, which give its great potential to be used in lower limb prosthesis applications [28]. By controlling the speed of the servomotor, the EHA can deliver power on demand and use energy efficiently. A passive operation mode with controllable damping is easily achieved by incorporating bypass restrictors. The switch between active and passive operation mode can be quickly and smoothly completed by controlling the motor-pump and bypass valve in an EHA.

1.5. Aims and Objectives

The aim of this research is to develop a powered ankle prosthesis and its controller to assist walking and other daily activities of lower limb amputees. By using an EHA, which gives the ability to switch quickly and smoothly between passive and active modes, the new ankle prosthesis is intended to assist walking with an improved walking experience and extended range compared to traditional passive devices and continually powered devices.

The objectives of this research are summarized below:

- Based on analysis of the ankle locomotion of healthy subjects, an EHA system should be designed which can quickly and smoothly switch between a passive mode with controllable damping and an active mode to assist walking.
- An experimental powered ankle prosthesis prototype should be developed. This prototype should satisfy the weight limitation and provide sufficient output power. The performance capability of this prototype should be validated in the laboratory.
- An amputee trial with the ankle prosthesis functioning passively should be undertaken to gather the signal characteristics of the sensors on the prototype in different walking conditions which will help the controller design.
- A controller for the EHA powered ankle prosthesis should be developed which can correctly control the output power of the ankle prosthesis in the active

mode, the ankle joint damping ratio in the passive mode and the timing of switching modes.

- The performance of the EHA powered ankle prosthesis prototype and its controller should be evaluated in an amputee trial.
- A simulation model should be developed to analyse the performance of the EHA and be used for the future controller improvement.

Since this research project is in collaboration with Chas A Blatchford & sons Ltd, higher priority has been given to the development and testing of the EHA powered ankle prosthesis prototype and its controller. Some simulation and modelling works have been carried out during the research progress, e.g. the simulation model and analysis in appendix 1, but these do not provide useful inputs for the system design and development. The simulation model involved in this thesis is developed for the analysis of the performance of the prototype presented in the thesis and is intended to be used for the future controller improvement.

1.6. Original Research Contribution

The EHA powered ankle prosthesis proposed in this research is a novel approach which can increase the working time range compared to a continually powered ankle and ensure safe passive prosthetic function after the battery is discharged.

A timing control method for this approach is proposed, which can achieve the mode switching at the certain time points in the gait cycle based on the heel strike detection and middle stance time delay. The effectiveness of the approach is evaluated.

The proof of principle prototype and its controller developed in this research can provide beneficial level walking assistance and a very natural walking gait which has been validated in an amputee trial. The characteristics of the powered ankle prosthesis at different walking speeds, obtained in the amputee trial, are analysed in this thesis which can be used for future device improvement and controller design.

1.7. Thesis Structure

Chapter 1 introduces the research background and development history of ankle prostheses. An EHA is proposed to be used in the powered ankle prosthesis application.

Chapter 2 reviews the published studies of lower limb locomotion, developments of ankle prostheses and control algorithms. Several examples of commercially available passive and semi-active ankle-foot prostheses are presented. The active ankle prostheses with different types of actuation are summarized and discussed.

Chapter 3 specifies the EHA powered ankle design requirements by analysing the ankle motion and moment characteristics of a healthy subject during level walking.

Chapter 4 presents the design of the compact powered ankle prosthesis prototype and its bench test results.

Chapter 5 analyses the ankle sensor signal features during an amputee trial with the ankle prosthesis functioning passively. This information is used to help develop the controller for the active ankle prosthesis.

Chapter 6 explains the timing control method based on heel strike recognition and middle stance time delay.

Chapter 7 shows and discusses the results of the amputee trial with the powered ankle prosthesis. The EHA performance and its timing control method are validated in the amputee trial.

Chapter 8 describes the simulation model developed to help analyse the performance of the EHA. The comparison of the simulated results and experiment results are discussed.

Chapter 9 concludes the development of the EHA powered ankle prosthesis and the main findings of this research.

Chapter 2

Literature Review

This chapter reviews the literature related to the development of a powered ankle prosthesis. The studies on lower limb locomotion during level ground walking, stair ascent and descent are reviewed first. Examples of commercially available ankle-foot prostheses are given including energy storage and return feet, microprocessor controlled semi-active ankles and an active ankle prosthesis. Several studies on electric motor based powered lower limb prostheses are presented. The actuation design, on board sensors, control strategy and published amputee trial results of each research group are summarized and discussed. Pneumatic actuation is another popular approach, although all the proposed prototypes reviewed in this chapter are tethered. Control strategies for powered ankle prostheses are discussed at the end based on a hierarchical controller structure.

2.1. Lower Limb Locomotion

The clinical tests in [18] investigate the gait cycle characteristics, ground reaction force, kinematic, joint moment and joint power of hip, knee and ankle joints of healthy subjects during level ground walking, stair ascent and descent. The stair case used in this study, as shown in Figure 2-1, is composed of four steps and a platform at the top. Six strain gauge based force transducers have been mounted on each of the lower three steps. The three components of the ground reaction force (vertical, anterior/posterior and medial/lateral) and the location of the centre of pressure on the step surface can hence be computed. A movement analyser based on 4 cameras has been used to measure the kinematics of the three lower limb joints. Ten healthy subjects have been asked to ascend and descend the stairs of 24°, 30° and 42° inclinations. The results are compared with level ground walking data from Centro di Bioingegneria gait laborator [18].

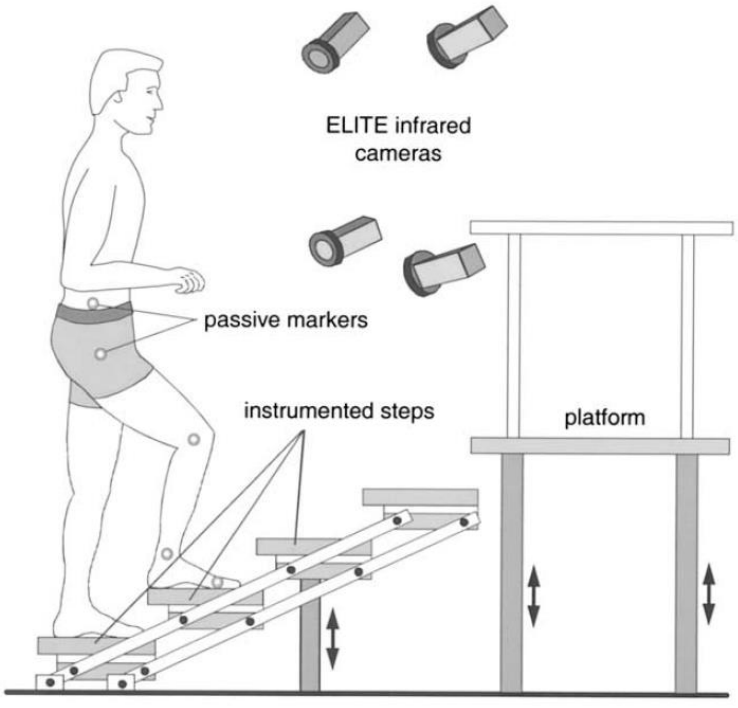

Figure 2-1: Clinical test rigs with instrumented steps and a movement analyser. Reprinted from [18].

According to the results presented in [18], the cycle duration during stair ascent (1.40~1.47 s) is significantly longer than during descent (1.19~1.22 s) and level ground walking (1.11 s). The stance phase percentages are 61.1±1.7% when level ground walking; 61.1±1.7% when 30° stair descent and 63.6±1.9% when 30° ascent, which indicate the swing phase duration (single stance duration) during stair ascent (515 ms) is distinctly longer than during level ground walking (435 ms).

The ankle kinematic and kinetic data is shown in Figure 2-2, Figure 2-3 and Figure 2-4 [18]. The gaits shown in these three figures start with foot contact. The vertical grey bars in the figures (at approximately 60% of the gait cycle) indicate toe-off, which separates the gait into stance phase and swing phase. The vertical thin yellow bars at approximately 9% of the gait cycle indicate the foot becoming horizontal when level walking and the vertical thin yellow bars at approximately 47% of the gait cycle indicate the maximum DF of the ankle when level walking. The stance phase of the gait cycle is divided into initial (or early), middle and terminal stance phases by these vertical bars.

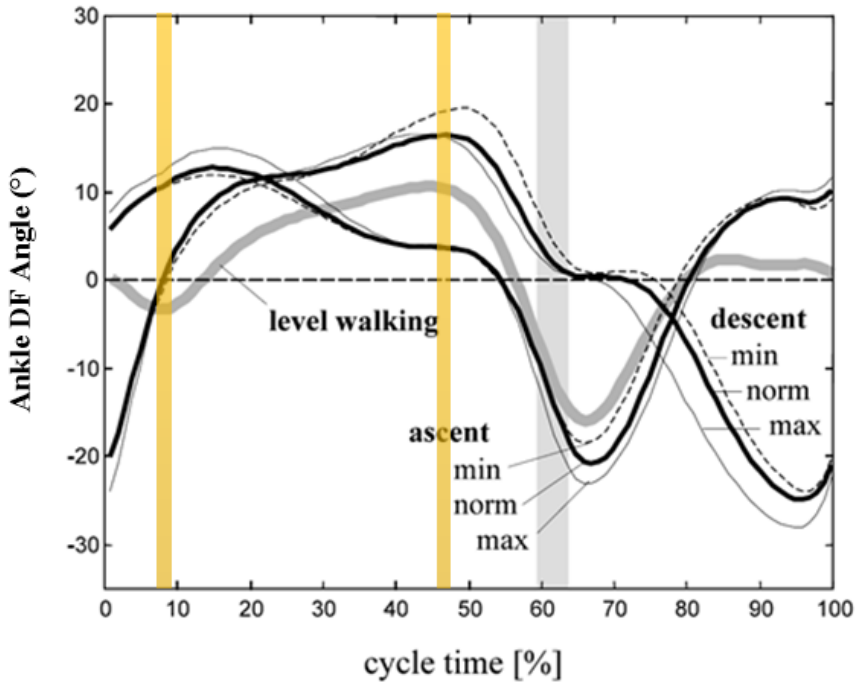

Figure 2-2: Ankle DF angle during level ground walking, stair ascent and descent. Reprinted from [18].

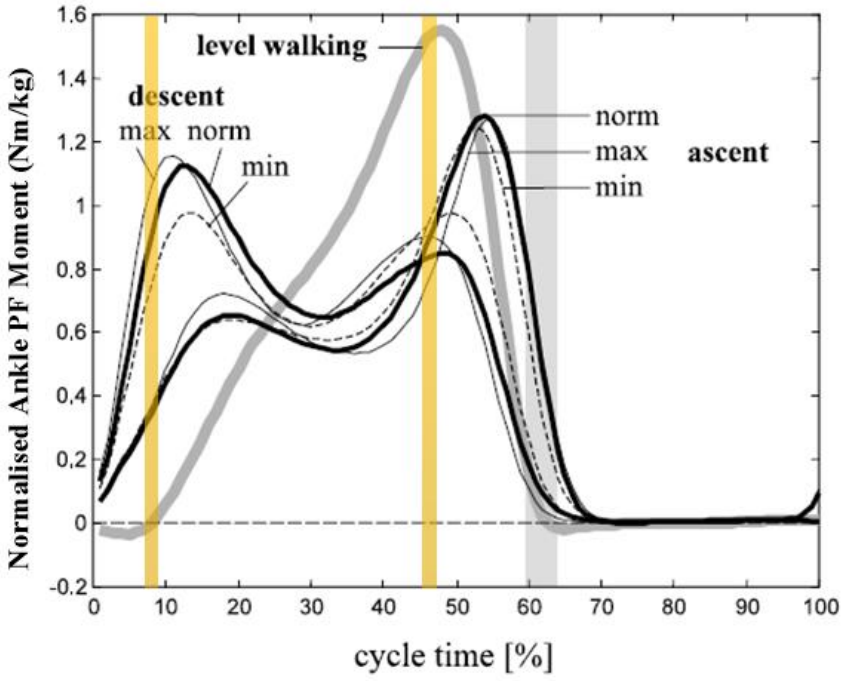

Figure 2-3: Ankle PF moment (normalised for subject mass) during level ground walking, stair ascent and descent. Reprinted from [18].

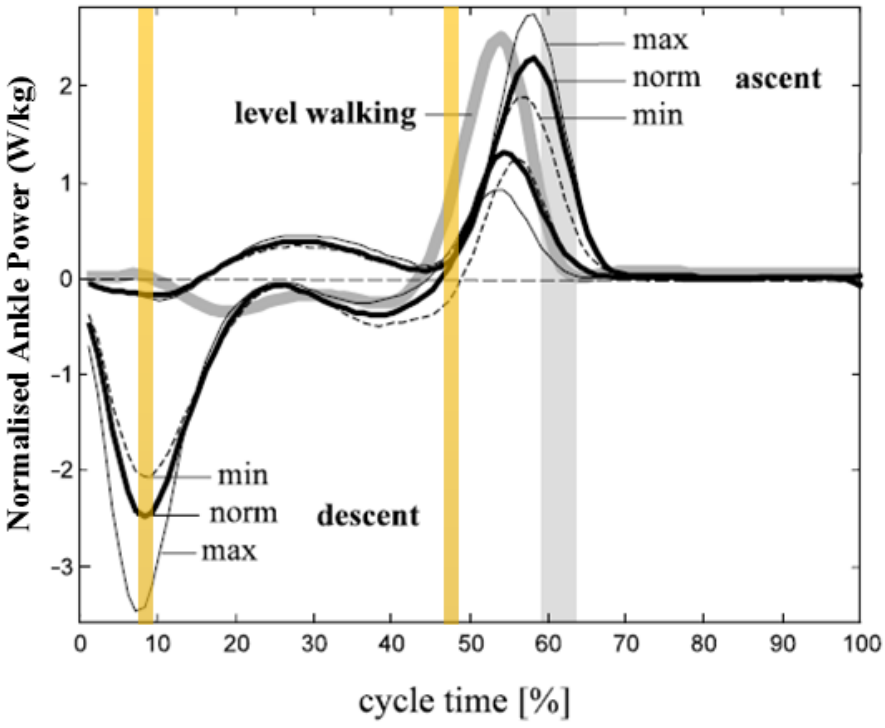

Figure 2-4: Normalised ankle power during level ground walking, stair ascent and descent. Reprinted from [18].

As shown in Figure 2-2, the RoM (range of motion) during stair climbing (34° for ascent and 50° for descent) is larger than during level ground walking (23°). Different from the gaits start from the heel strike during level ground walking, all the gaits start from the forefoot contacting steps during stair walking in both the directions, which results in the high PF moment during the initial stance phase to keep the heel lifted (Figure 2-3). An assumption can be made that there is a certain inclination angle or angular range (below 24°) where the initial foot placement switches from heel contact to forefoot contact, which will lead to different control strategies of the lower limb prostheses.

This peak moment at 15% of the gait cycle is higher during stair descent. In the terminal stance phase (47~60% of the gait cycle), the ankle joint performs a PF movement and a peak moment in all inclinations (including level ground walking). Different from the DF for ground clearance in the swing phase during stair ascent and level ground walking, the ankle mainly plantarflexes for the forefoot contacting of the next step during stair descent. The ankle joint absorbs power at 8~10% of the gait cycle during stair descent as shown in Figure 2-4. In all the inclinations, the ankle joint exhibits maximum power production at the end of the stance phase (53~59% of the gait cycle). The ankle kinematics, moments and power during level walking are used as design references which will be further discussed in Chapter 3.

Several conclusions could be derived according to [18]. Compared to a single power peak at the ankle joint in the terminal stance phase during level ground walking and stair ascent, a single power peak at the knee joint in the initial stance phase during stair ascent is observed, which indicates the un-simultaneous power requirements between the two joints. For a powered lower limb prosthesis, this shows the potential for the ankle and knee actuators sharing one power source [29]. The influence of the inclination angle on joint angle patterns, gait phase parameters and joint moment patterns are small. The largest difference resulting from the inclination angle is the joint power during stair ascent (Figure 2-4).

The lower limb kinematic and kinetic patterns in healthy human gait have also been studied in [19, 30]. In [19], the ankle function is described as controlling the forward

moving leg during weight acceptance phase (heel strike) and middle stance phase and providing active PF and generating the major positive energy burst during push-off. Walking without the active ankle joint power, e.g. below knee amputees with passive ankle prostheses, will cause modified motor patterns from the residual lower limb muscles [21]. The comparison of the normalised ankle moments for fast, natural and slow cadence groups are shown in Figure 2-5 [30]. The ankle moments are totally dominated by the requirements of stance with the foot flat on the ground during most of the stride period. The moment patterns of the ankle for slow to fast cadences are basically in the same shape and increased in magnitude as cadence increases, except the ankle moment during 20~40% of the gait cycle is smaller in the fast cadence group.

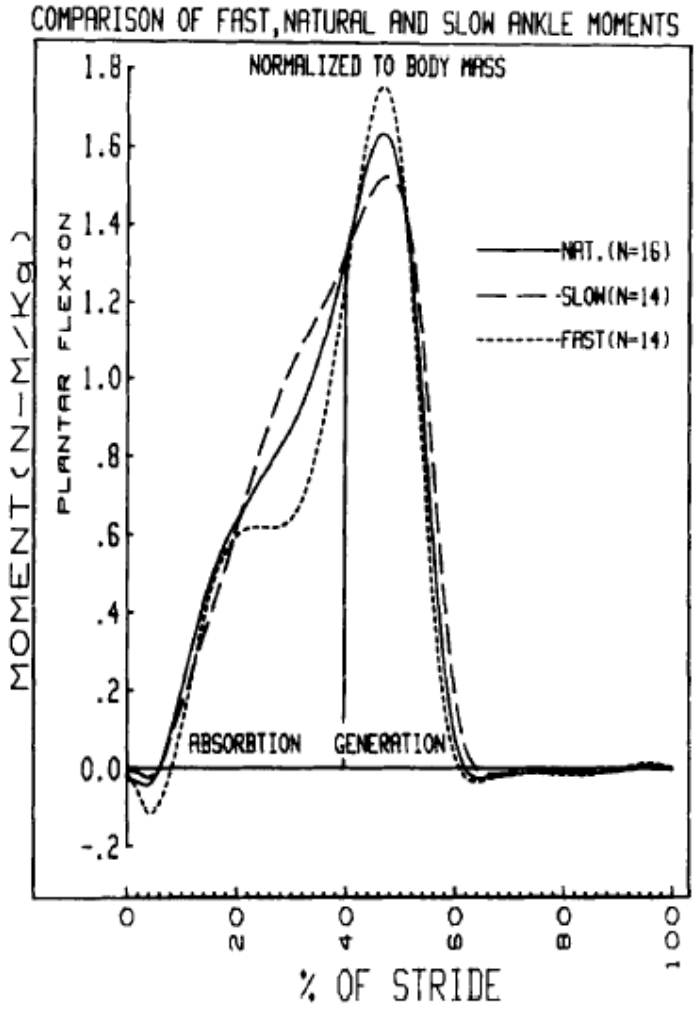

Figure 2-5: The comparison of the normalised ankle moments for fast, natural and slow cadence groups. Reprinted from [30].

The intra and inter-subject variability of the joint angles and moment patterns have also been studied in [30]. The intra-subject variability of joint angles are low, i.e. the kinematic pattern for the same subject is highly repeatable. The intra and inter-subject variability of joint moments are high at the hip and knee, relatively low at the ankle, but the support moment (defined as the combination of the three individual joint moments in [30]) is relatively constant.

The study in [4] gathers and analyses the lower limb kinematic and kinetic data during level ground walking and stair ascent/descent from three different references [18, 31, 32], which provides guidelines to estimate the lower limb prosthesis actuation system requirements during daily living activities. The main criteria for the selection of the actuator and actuation mechanism, including the joint RoM, torque-angle profile, maximum angular velocity, peak braking torque, peak driving torque, rated continuous torque, energy absorption and generation of each joints, are summarized and analysed in the study. The parameters for ankle joints during level ground walking are very helpful to identify the actuation system requirements. For examples: the total average RoM of ankle is 29.5°±2.9°; the maximum PF torque (1.5±0.157 Nm/kg) during stance phase happens at the starting of the terminal stance phase at the ankle angular position of 10.98°±3.02°; the maximum PF ankle angular velocity (39.97±7.5 rpm) happens during terminal stance phase at approximately 0.4 Nm/kg ankle torque; the required positive energy for body propulsion is much higher than the absorbed negative energy during the whole gait. Comparing to level ground walking, the RoM of the ankle joint during stair ascent and descent are higher since the ankle joint is required to further dorsiflex to comply with the step height and inclination [4].

2.2. Ankle Prostheses Development

2.2.1. Energy Storage and Return Feet

The most common type of ankle prosthesis in the market is ESR type, which has a fixed ankle joint and foot springs. The foot springs are made from carbon fibre

materials, which could be a single spring shown in Figure 1-4 or separated heel and forefoot springs shown in Figure 1-3 [15, 16]. Some energy is stored in the foot springs during the heel strike and the DF stance phase. The energy is returned to the subject with the release of the springs. These passive prostheses can provide sufficient and safe support of the amputee with minimized size and weight. They also exhibit low price, wide market coverage and long operation life. The two examples shown in section 1.3 also have split toe springs which provide more comfortable ground adaptation. Normally ESR ankle-foot prostheses are available in different stiffnesses, which could be chosen according to the user weight and activity level from indoor walking to jogging and even running. The limitations are the fixed ankle angle and the lack of the active power assist during walking. The study in [33] shows the reduction of the COT (cost of transport) with ESR feet is only 2.7% smaller than the cost with SACH (solid ankle cushion heel) feet.

2.2.2. Microprocessor Controlled Semi-active Ankle prostheses

Several microprocessor controlled semi-active ankle prostheses are commercially available nowadays to expand the daily activities for lower limb amputees. Three example products have been chosen by the author to demonstrate the function and activity level of this type of ankle prosthesis. Several shared features are similar device weight (1.2~1.4 kg), composed of a rotatable ankle joint and carbon-fibre foot springs, embedded sensors and microprocessor, awareness of the environment and user intent to some extent and rechargeable battery for at least 24 hours of operation.

The Elan ankle shown in Figure 2-6 is developed by Chas. A. Blatchford & Sons Ltd [8]. The ankle joint is composed of a hydraulic cylinder and two bypass restriction valves controlled by two micro motors respectively. The damping ratio in DF and PF directions can be actively controlled according to the subjects' preference and ground conditions. Without an actuator at the ankle joint, the Elan foot cannot actively adjust

the ankle angle, but this microprocessor controlled hydraulic prosthesis can provide a fairly smooth and natural walking gait [34].

The Triton Smart Foot shown in Figure 2-7 was developed by Ottobock [35]. The hydraulic valves at the ankle joint can be used to lock or release the rotation of the ankle, which gives this prosthesis the ability to adjust the ankle angle incrementally during the rollover of the foot recording to the walking speed and ground slope. This function also allows the user to adjust the heel height and free the ankle rotation when sitting or in other un-load situations [37]. The built-in relief function is controlled by the embedded microprocessor and the ankle can communicate with the user wirelessly.

Figure 2-6: Elan ankle [8].

Figure 2-7: Triton Smart Foot [35].

Figure 2-8: Proprio Foot [36].

The Proprio Foot developed by Össur [36], shown in Figure 2-8, is a commercially available ankle prosthesis integrated ankle joint actuator. The ankle angle can be actively adjusted by the actuator driven by a DC motor, which is controlled by an embedded microprocessor. The actuator is not capable of providing high net power in the stance phase to propel the amputee forwards.

Instead, this semi-active ankle is designed to dorsiflex the foot springs in the early swing phase to improve ground clearance which significantly improves the safety [38]. Other functions will enhance the user's ability and provide a more natural appearance , including plantarflexing the ankle to a certain angle when the amputee is lying down, kneeling or sitting, adjusting heel height and adapting the ankle position when stair ascending/descending [38].

2.2.3. Active Ankle Prosthesis with Series-elastic Actuator

The first commercially available powered ankle prosthesis which can inject net power in stance phase is the BiOM Ankle (Figure 2-9) [23]. This powered ankle is developed by the Biomechatronics Group within MIT Media Lab directed by Professor Hugh Herr.

The series-elastic actuator (SEA) in the prototype described in [39] comprises a 200W DC brushless motor, ball-screw transmission and a carbon-composite leaf spring in series with the transmission as shown in Figure 2-10 and 2-11. There is another unidirectional leaf spring in parallel with the SEA. The prototype shown in Figure 2-11 weights 2 kg, including a 0.22 kg Lithium-polymer battery and two pieces of foot leaf springs. The importance of the series spring and the parallel spring have been explained in [22]. The series motor elasticity is necessary to protect the motor and ball-screw transmission from the excessive shock loads in the heel strike phase. The unidirectional parallel motor elasticity effectively lowers the forces borne by the

actuator [40] and is necessary to increase the force bandwidth to achieve the required biomimetic ankle-foot behaviour [22].

Figure 2-9: BiOM ankle [23].

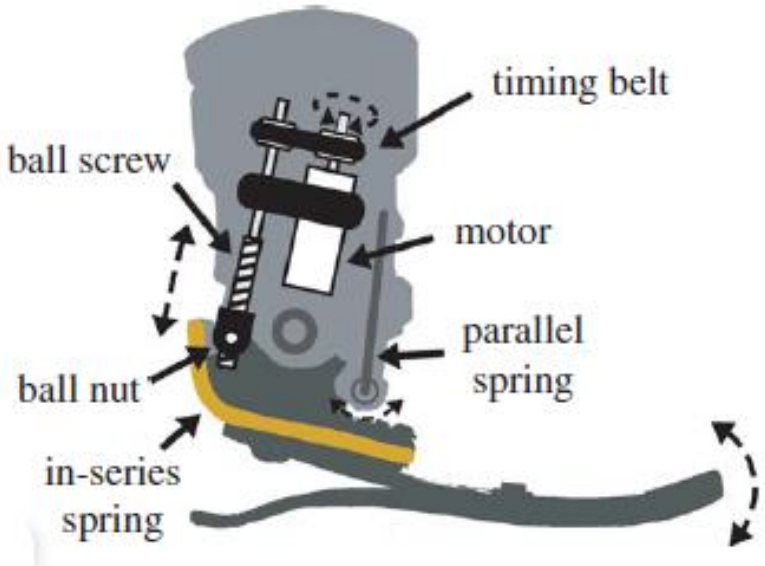

Figure 2-10: Inner structure of BiOM prototype. Reprinted from [39].

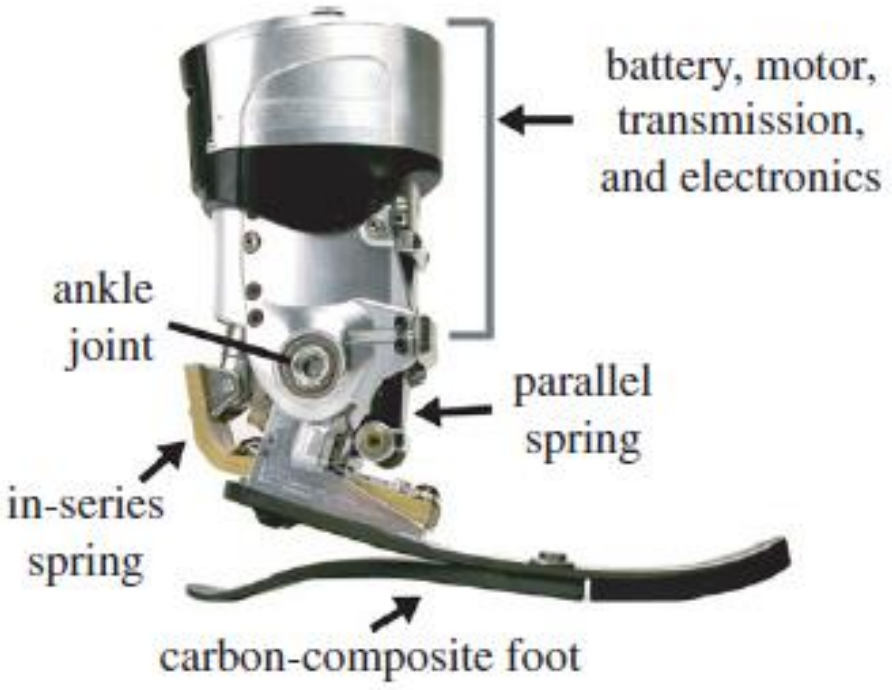

Figure 2-11: Components of BiOM prototype. Reprinted from [39].

The operation of this ankle prosthesis can be divided into six states: controlled PF (heel strike phase); controlled DF (middle stance phase); powered PF (terminal stance phase) and three sub states in the swing phase [40]. The states are recognised using four sensor signals: the heel contact signal measured by two force transducers beneath the heel; the toe contact signal measured by four force transducers beneath the toe; the ankle rotation angle measured by an encoder at the ankle joint and the ankle joint torque calculated from the series spring displacement obtained by a linear spring potentiometer and the spring stiffness. For example, the powered PF state is triggered when the ankle torque exceeds a threshold. Three low-level servo controllers are used to control the SEA: a torque controller to provide positive output torque in the powered PF phase; an impedance controller to modulate joint stiffness in the stance phase and a position controller to adjust ankle angle in the swing phase [40].

The prototype described in [40] outputs about 120 Nm peak ankle torque at 47% of a gait cycle in their amputee trial. Each step consumes approximately 20 J during the

tests. COT of the amputee with the BiOM prototype has also been studied in [22]. The results show that the COT of an amputee walking with the BiOM prototype is about the same as a healthy subject and is much better than the amputee wearing a passive ankle prosthesis. A charged battery in the BiOM prototype can support 4-5 km walking [22].

An evaluation on the BiOM prosthesis is given in [41]. The BiOM is compared with a passive ankle prosthesis, the contralateral intact limb and non-amputee control limbs. According to the patient trial results, the BiOM demonstrates much greater ankle RoM than the selected passive ankle prostheses in the study, but still less than that of the healthy subject. The peak ankle PF power in the terminal stance phase generated by the BiOM ankle is even higher than that of a healthy ankle. The stance and swing phase duration asymmetries, which is common with the passive devices, is reduced with the BiOM ankle. The step length of the amputee with BiOM is significantly longer than the amputee with a passive device. Another interesting finding is that the preferred walking speed of the amputee with BiOM is faster than other participants.

The study in [42], beyond the traditional prosthetic leg research focused on improving mobility of the amputees' daily activities, pursues a control system for a bionic ankle prosthesis to be used when dancing. The BiOM ankle has been modified to enable easy adjustment of the prosthesis alignment and avoid leg-to-leg interference. The ankle torque-angle relationship when the participant wearing the BiOM ankle with new control system and the traditional passive ankle prosthesis ([43]) were recorded and compared with non-amputee data. Though no net-positive power is added by the bionic prosthesis during the dance steps, this study still shows the bionic dance prosthesis outperforms the passive prosthesis in this particular dancing condition. This study also points out the challenges for a dance prosthesis including: larger RoM, more impact device, specialized control systems provide time-varying behaviour and dance step recognition.

2.2.4. Self-contained Knee-Ankle Prosthesis with Electric Actuators

The transfemoral prosthesis prototype shown in Figure 2-12 has been developed by Frank Sup et al [44]. This self-contained powered bi-articular lower limb prosthesis uses two 200W motor and ball screw assemblies for the ankle and knee joints. The prosthesis is capable of a RoM of 120° for the knee joint and 45° for the ankle joint. In additional to the ankle joint actuator, a spring in parallel with the ball screw is applied to bias the motor's axial force output toward ankle PF and to supplement power output during the powered PF phase. This prototype uses a sensorized prosthetic foot with solid heel and toe segments, which has similar weight and size to a commercially available foot prosthesis. This sensorized foot trades off the ESR function of the foot springs for the strain gauge installation space. As an advantage of the integrated bi-articular prosthesis, the space at the shank is used for an embedded system including controller, servo amplifier and a 0.62 kg battery. The whole prototype weights 4.2 kg, which is similar to the normal lower limb of a healthy subject [44].

The sensor signals for the prototype controller include the moment signal from a strain gauge moment sensor mounted in the adapter dome between the prosthesis and the residual limb; ankle and knee angular position signals from potentiometers; force signals from two uniaxial load cells in series with the actuator in each joint and ground reaction force signals from the heel and toe strain gauges. A three level control architecture is applied in the prototype. The high level activity intent recognition controller is implemented off board and the middle level impedance controller and the low level actuator force controller are self-contained in the prototype. In the control system of this prototype, the terminal stance phase is triggered when the ankle angle crosses a threshold [44].

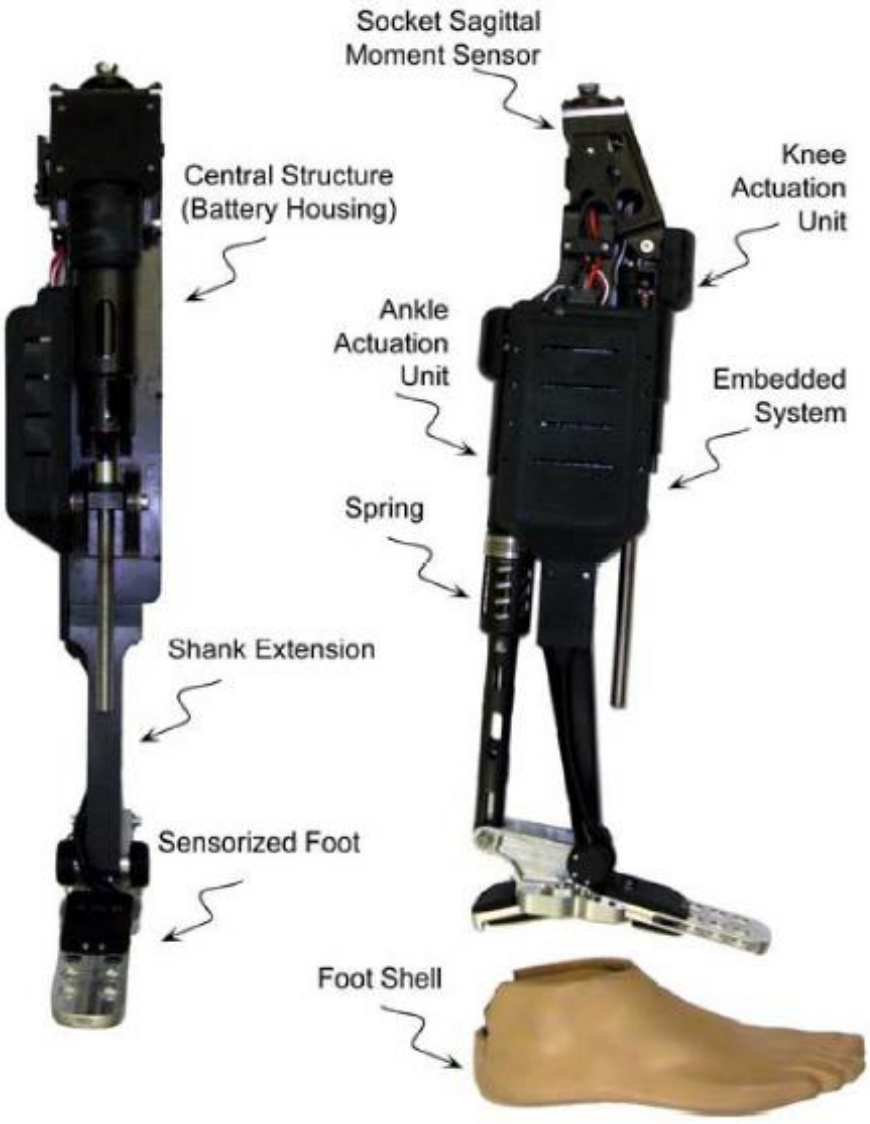

Figure 2-12: Self-contained transfemoral prostheses with electric actuators. Reprinted from [44].

According to the amputee test results shown in [44], the ankle joint actuator outputs approximately 120 Nm at 40% of the gait cycle. The average power consumptions of the prosthesis ankle and knee are 45 W and 19 W respectively at a walking speed of 5.1 km/h. A charged battery in the prototype can support 9 km of level walking. This prototype has also been tested for upslope walking with an upgraded control system [45]. An accelerometer is attached to the ankle for ground slope estimation by using

the magnitude of acceleration measured orthogonal to the long axis of the foot. The tests results in [45] show this powered transfemoral prototype provides increased knee flexion with increased slope after heel strike, a net knee extension during stance phase and an increasing bias towards ankle DF with increasing slope. [45] also points out the requirement for the optimization of the control system to accommodate the changes on the self-selected cadence.

2.2.5. Active Ankle Prosthesis with Robotic Tendon Actuator

An active foot-ankle prosthesis using a robotic tendon actuator [46] is developed by Thomas Sugar et al. The robotic tendon actuator, including a 150W DC motor, gear box and lead screw transmission and series helical 'tendon' springs (Figure 2-13), is used in this prototype to minimize the peak motor power requirement by storing and releasing the energy in the tendon springs. An efficiency model is established and discussed in the work [46], which pursues the lowest power requirements and is used to optimize the prototype design. A switch embedded in the heel is used to detect heel strike. A closed-loop position controller is used to control the motor under a predetermined reference ankle angular position pattern in a gait cycle [46, 47]. The ankle angular position is recorded by an encoder at the ankle joint. Amputee test results shown in [46] indicate the prototype provided 90 Nm peak torque at about 48% of a gait cycle during level ground walking at a speed of 1 m/s. An active robotic ankle with two actuated degrees of freedom has been described in [48], which consists of a coronal ankle axis and a pair of robotic tendon actuators (Figure 2-14). The motor in this design is rated to 200 W.

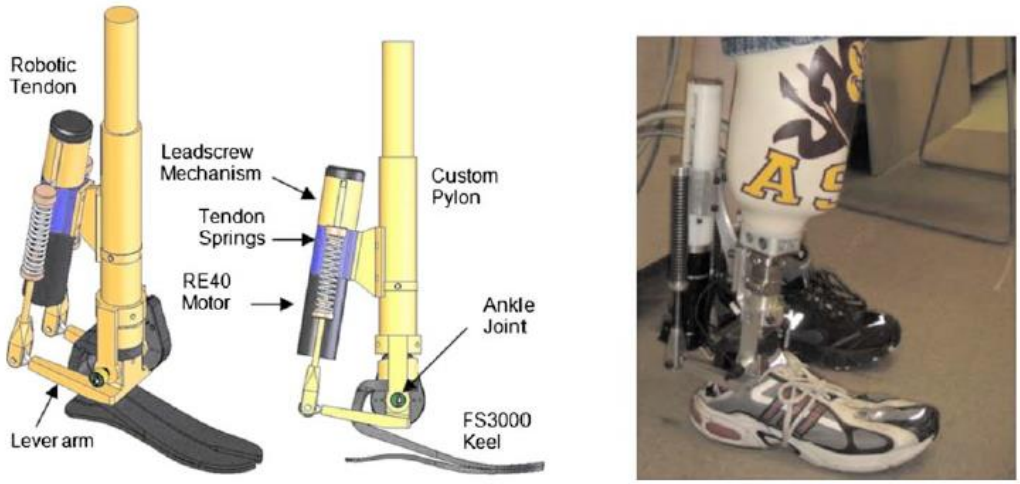

Figure 2-13: Active ankle prosthesis with robotic tendon actuator. Reprinted from [46]. (a) The isometric view of the ankle design. (b) The side view of the ankle design. (c) A photo of the ankle on a transtibial amputee.

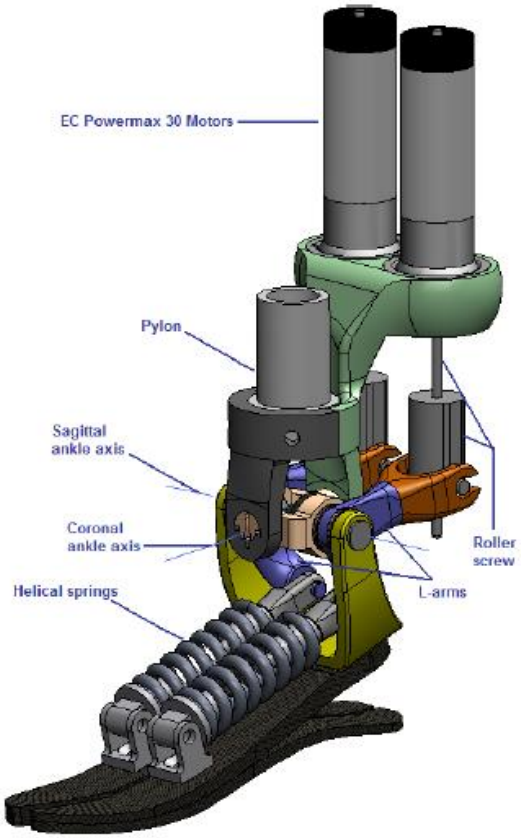

Figure 2-14: Active robotic ankle with two actuated degrees. Reprinted from [48].

2.2.6. Semi-active Transfemoral Prosthesis with EHA

[29] proposes a design of an integrated semi-active transfemoral prosthesis. A hydraulic pump driven by electric motor is used to power both the knee and the ankle joint which allows the size and weight of the prosthesis to be minimized. As shown in Figure 2-15, the prosthesis structure includes a hydraulic transmission unit, an ankle actuator, a knee actuator, a carbon-fibre foot and a stance controlled joint. The stance controlled joint is applied to lock the ankle joint when it is loaded (in stance phase) and allows the ankle actuator to lift the foot up freely during swing phase. Via a wire rope, the ankle actuator will charge the foot spring in the middle stance phase. The additional energy stored in the spring will be released at the end of terminal stance phase to propel the amputee forwards. In the early swing phase, the ankle actuator dorsiflexes the foot for ground clearance. The design concept of the transfemoral prosthesis is based on the un-simultaneous large positive power requirements for knee and ankle during walking and stair ascending. The four-way valve, shown in the hydraulic circuit in Figure 2-16, is driven by a micro motor which enables 4 primary states: passively damping the knee actuator while powering the ankle actuator (middle-stance phase); powering the ankle and knee actuator simultaneously (early swing phase); passively damping the knee actuator while locking the ankle actuator (heel strike phase) and powering knee actuator while locking the ankle actuator (early stance phase when stair ascent). No evidence that a prototype has been built and tested has been found.

This semi-active integrated transfemoral prosthesis is developed from the concept of the semi-active knee prosthesis described in [49]. The EHA in this study, shown in Figure 2-17, is proposed to achieve a switch between active powered swing mode and passive mode with controlled damping. During toe off, the knee actuator is actively flexed to rise the heel by controlling the 3 port variable position valve (rotary valve driven by a motor shown as ‘control valve’ in Figure 2-17) and activating the motor-pump. The motor-pump can then reverse the direction for knee extension while the control valve is moved to open the parallel free extension path (middle position). In

the stance phase, the pump-motor is disabled and the required impedance is provided by the partially opened control valve. In other words, the impedance to flow is adjusted by varying the valve angle between the primary positions.

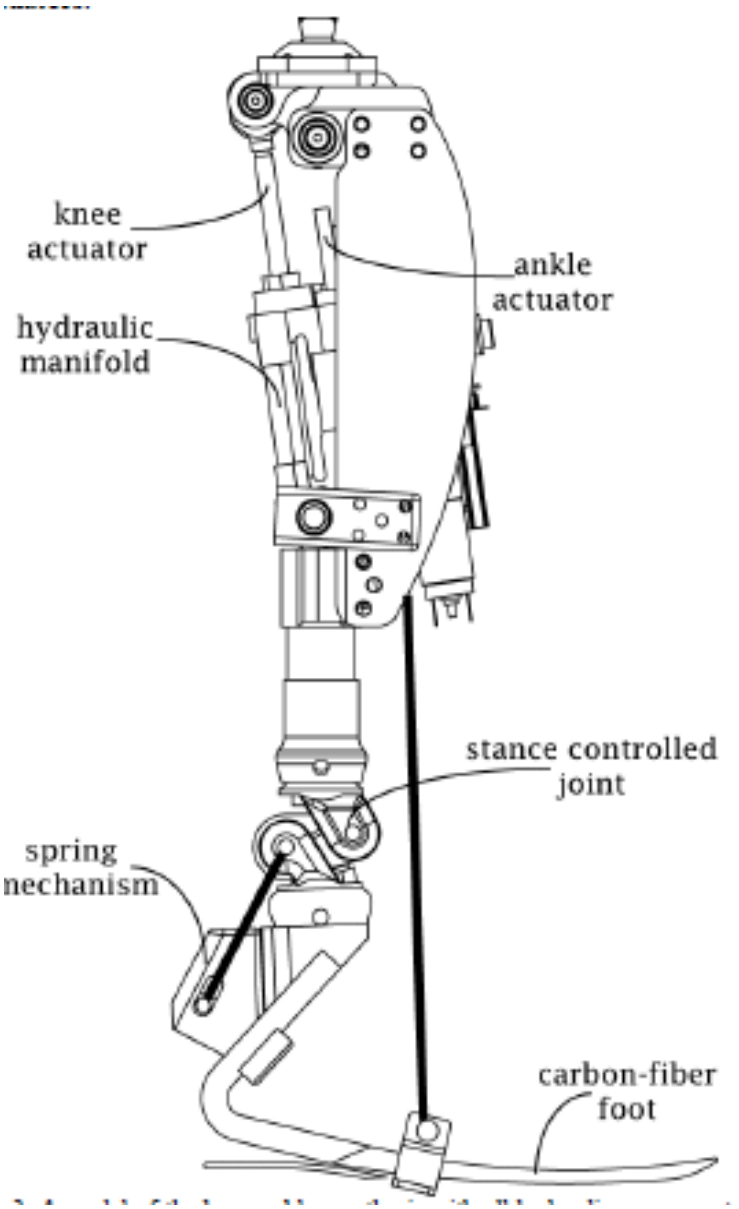

Figure 2-15: Semi-active transfemoral prosthesis with EHA. Reprinted from [29].

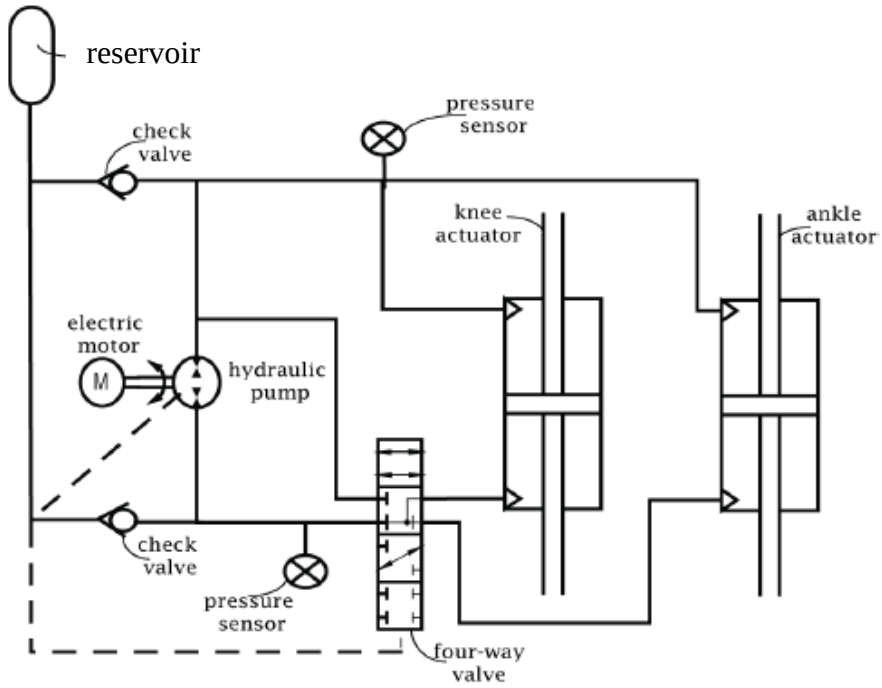

Figure 2-16: Hydraulic circuit of the EHA powered transfemoral prosthesis. Reprinted from [29].

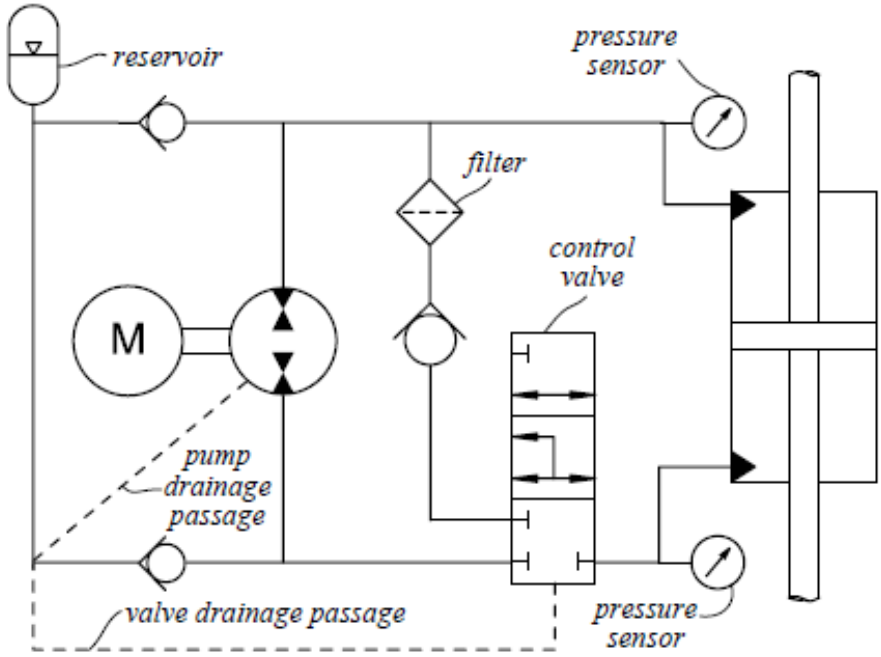

Figure 2-17: Hydraulic circuit of Berkeley's semi active knee [49]

This hydraulic circuit can also enable the free extension of the knee when the battery power is lost, so that the leg can return to a fully straight position to prevent the lock of the knee. This concept takes the advantages of both the fully powered and passive damping types of knee prostheses by using an EHA, which achieves a compact (28cm in length) and low weight (4 kg) prototype that provides sufficient heel rise to reduce hip hike and reduced hip torque [49]. Similar to the operation of this semi-active knee prosthesis, an EHA is also suitable for an ankle prosthesis by switching between the active mode (powered PF in the terminal stance phase and DF in the early swing phase) and passive mode with controlled damping (in the heel strike and middle stance phase).

2.2.7. Pneumatically Actuated Lower Limb Prostheses

Pneumatically actuated lower limb prostheses are also popular for research since the pneumatic actuators, either a pneumatic muscle or a cylinder-type pneumatic actuator, are able to generate large forces and power output with a light weight and compact structure. The portable pneumatic power source, e.g. compressed carbon dioxide bottle, might be the only alternative to a battery for a self-contained powered lower limb prosthesis. The active ankle joint described in [50] by Klute, G.K. et al., which is considered as the first powered ankle prosthesis performing net power during stance phase [39], uses a pneumatic actuator with off-board power.

A powered transfemoral prosthesis which includes two double-acting pneumatic actuators at knee and ankle joints respectively [51] is shown in Figure 2-18. The tethered prototype weights 2.65 kg and provides 70 Nm peak ankle in the indoor walking experiment where the prototype is tested on a healthy subject with an able-bodied testing adaptor [51, 52].

Figure 2-18: Pneumatic cylinder actuated transfemoral prosthesis. Reprinted from [51].

The pneumatically powered ankle prosthesis shown in Figure 2-19, developed by Rino Versluys et al. uses three Pleated Pneumatic Artificial Muscles (PPAMs) to move the ankle joint: one at the forefoot for DF movement and the other two PPAMs at the heel for PF movement [53]. According to the treadmill walking experiment results with a transtibial amputee presented in [53], this ankle prosthesis prototype provides 100 Nm peak torque at the toe off. The limitation of the pneumatic muscle actuator for lower limb prosthesis application is that the radial expansion during operation requires additional space at the lower limb joints [54].

The ankle prosthesis prototype shown in Figure 2-20, developed by Xiangrong Shen et al., is powered by a pneumatic cylinder placed horizontally on the foot plate [54]. This design makes the most use of the foot space and reduces the height of the device. The tethered prototype has been tested with a transtibial amputee and the results indicate that the pneumatic actuator can provide 90 Nm peak torque in the terminal stance phase [54].

The main challenges for the pneumatic actuation approach, comparing with the electric motor and battery based lower limb prostheses, include the need for a pneumatic power source, high noise level and nonlinear system dynamics [54]. The pneumatically actuated ankle prostheses included in this section have only been tested on treadmills with off board power. No published experiment results with a portable pneumatic power source has been found by the author.

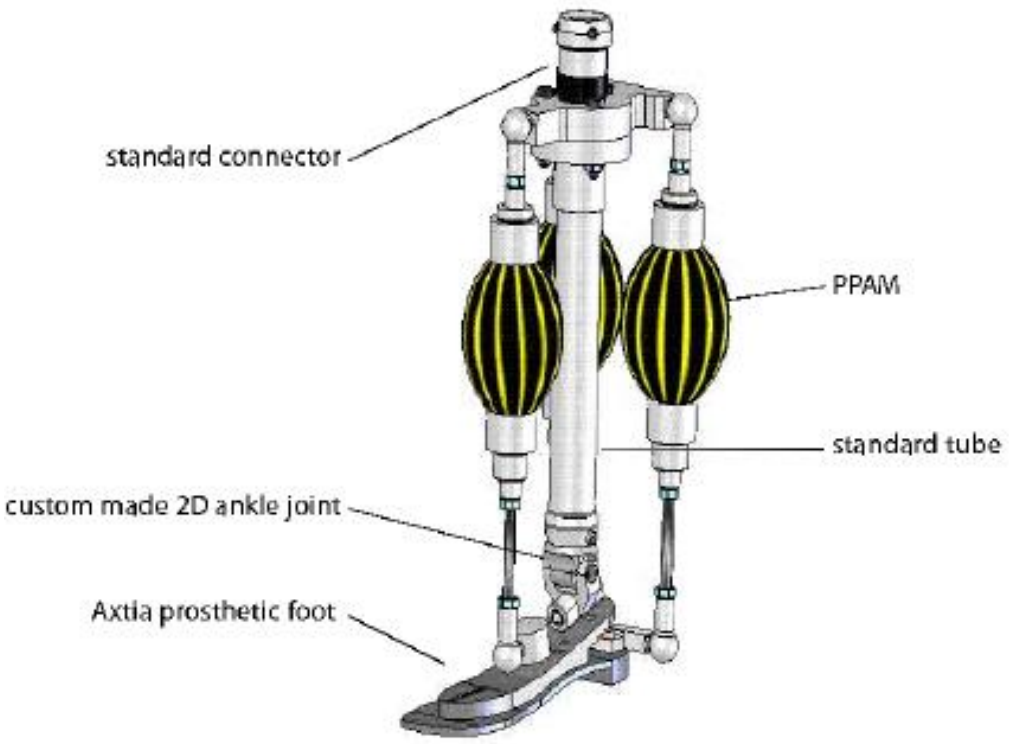

Figure 2-19: Powered ankle prosthesis with PPAMs. Reprinted from [53].

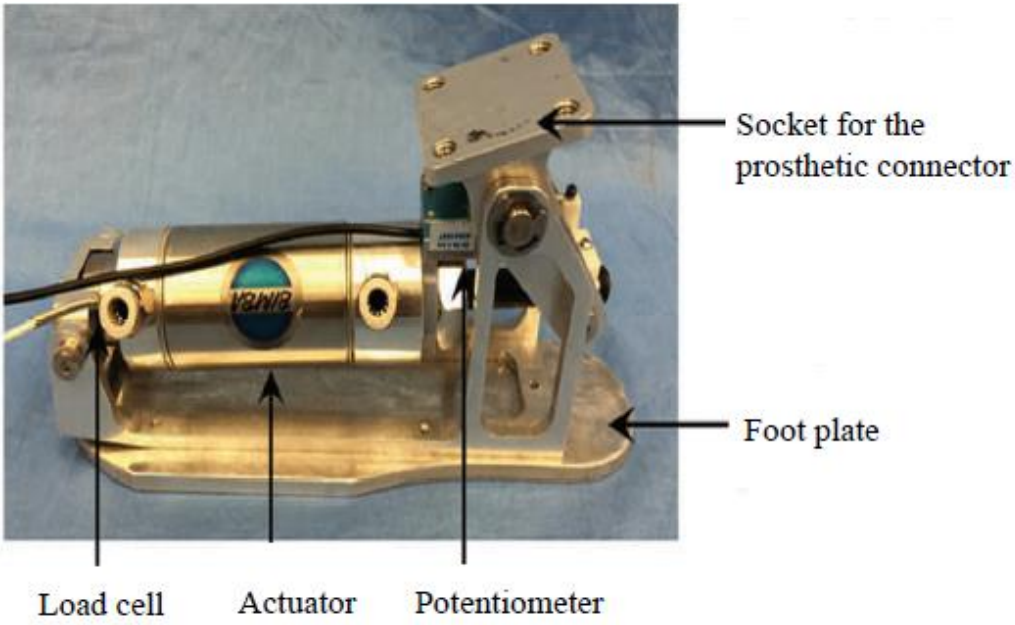

Figure 2-20: Compact design of the powered ankle prosthesis with pneumatic cylinder actuator. Reprinted from [54].

2.3. Ankle Prosthesis Control

The control algorithms for active and semi-active ankle systems in lower limb prostheses, orthoses, and exoskeletons have been summarized and analysed in [55]. [11] extends the previous review by including controllers for the hip, knee and ankle joints (exoskeleton devices not included).

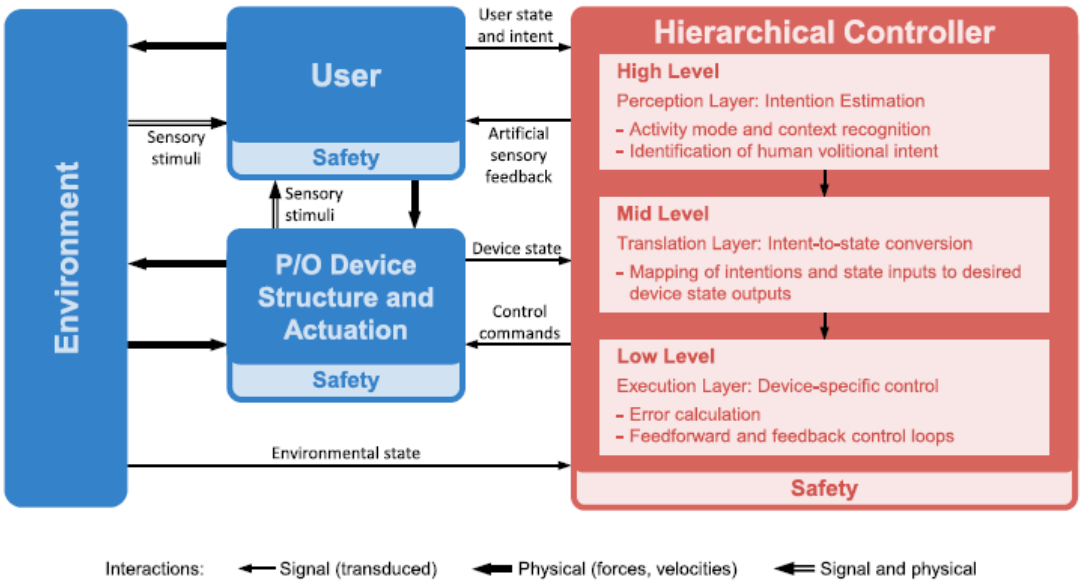

Figure 2-21: Control framework for active lower limb prostheses and orthoses (P/O). Reprinted from [11].

A framework given in [11] illustrates a general hierarchical controller structure for lower limb prostheses and orthoses (Figure 2-21). The interactions between the power lower limb devices, the user and environment are identified by the arrows in the Figure. As shown in Figure 2-21, the lower limb controller could acquire the environment information via the sensors in the actuation system (biomechanical signals) or via the user (electromyography signals, peripheral nervous system signals or central nervous system signals) [56]. At the high level of the controller structure, the user's intent of different activities (sitting, standing, level walking or stair ascent etc.) is recognised. The middle level controller then translates the user's intent to the required movement of the actuators, i.e. a demand signal for the low level controller is generated. The low level controller directly controls the output of the actuators. The development of robust and efficient algorithms to correctly recognise the user's intention and to generate suitable trajectories for the lower level controller is the main challenge for controlling the powered lower limb devices, considering the electronics miniaturization (hardware level) and actuation control (low level) are more mature [55].

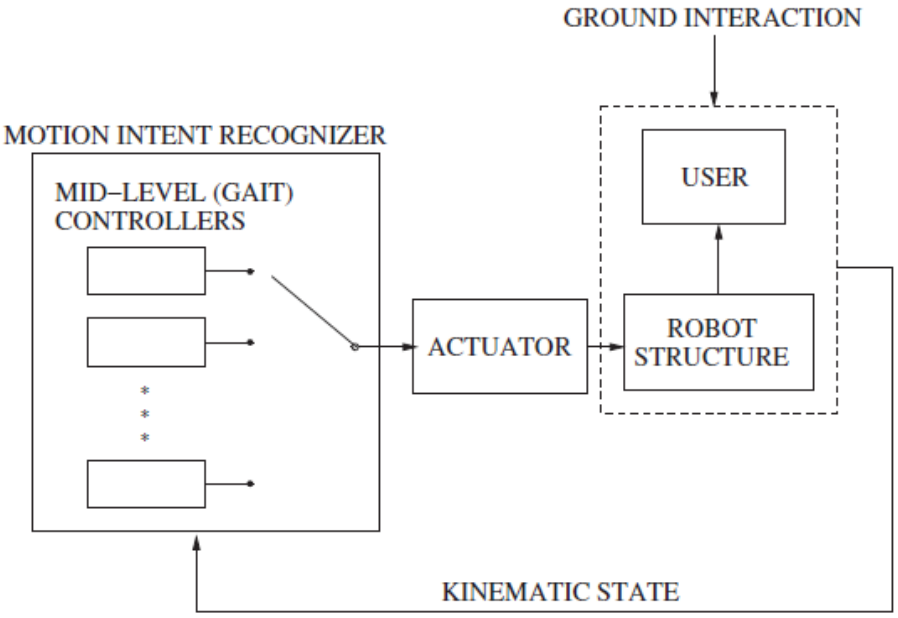

Figure 2-22: Control architecture with motion intent recognizer for the knee–ankle prosthesis. Reprinted from [55].

Some examples are included to demonstrate the development of a high level controller for lower limb prosthesis. Based on the measurement of the interaction force and moment between the user and the prosthesis, a *k*-nearest-neighbor algorithm is used to classify the user's intention into standing or three different speeds walking in [55, 57]. A motion intent recognizer in [57, 58] is used to switch between different middle level controllers (walking, standing, sitting and stair ascent/descent) as shown in Figure 2-22. The decision is made by comparing the sensor signals with a walking pattern database [58].

Comparing to the mechanical signal based high level controllers, the EMG (Electromyography) control allows the user to regulate the assistance devices more naturally using their own muscles. [59] proposes to use EMG signals from the gastrocnemius and tibialis anterior muscles to switch between level ground walking and stair descent modes. The raw EMG signals need to be filtered, amplified and digitized before using. The processed EMG signals can also be used to control the ankle joint angle [60]. The development of an active ankle orthosis in [61] uses the

EMG signals from the soleus and/or tibialis anterior muscles to control the pressure in artificial muscles. The EMG signals are processed in real time and converted to an analogue signal. The main challenge for the EMG signal controlled lower limb prostheses is to correctly correlating the EMG signals with the actuator outputs. Also, the availability and quality of the EMG signals are highly dependent on the user, e.g. inter-patient variability on available residual muscles. The fragility and installation requirements of electrodes increases the difficulty for use in outdoor environments [55].

The majority of the active and semi-active ankle P/O (prostheses and orthoses) adopt a phase based (or finite-state based) control strategy for the middle level controller [40, 44, 62-66]. This results from the fact that the ankle kinematic and kinetic characteristics are quasi-periodic and can be simplified into several phases. As shown in Figure 1-2 (section 1.2), the ankle motion in a gait cycle when level walking is divided into early stance phase (or controlled PF phase), middle stance phase (or controlled DF phase), terminal stance phase (or powered PF phase) and swing phase (or powered DF phase and initial heel strike phase). In each phase, the ankle can be considered as a passive element with fixed stiffness and damping or a power source. In other words, the demand signal in each phase for the low level controller is simplified as a static demand impedance or a demand output torque. This strategy is also expanded for the control of knee joint actuation [63, 66, 67] or other activities [57, 58].

The main problem is then focused on the real time detection of the gait phase or the correct identification of the transitions between phases [55]. In [61], this transition is determined using thresholds for the ankle angle, the ankle torque, the knee velocity and the axial load respectively. [67] includes strain gauges to measure the ground reaction force for the transition from a pre-swing to swing flexion phase [55]. In [40], the states are detected using the ground reaction force measured by force transducers, the ankle angle measured by joint encoder and the ankle torque calculated by the displacement of the spring.

Beside the most popular foot switches and angle sensors, acceleration-based schemes can also be used for state detection [55, 68, 69]. [70] proposes to use a single shank mounted inertial measurement unit (IMU) to achieve real-time gait event detection. Instead of the signal based switch between phases with different impedance, this is achieved 'hydraulically' by two bypass lines with restriction valves and check valves in [8], which will be further discussed in the following chapters.

The weakness of the phase based middle control strategy is that the gait pattern changes of the user may cause the unreliability of the controller, especially in an outdoor walking environment or switching between activities [11, 71]. [47] proposes using a preprogramed ankle motion pattern, expressed as a time-based function, as the actuator position reference to mimic the ankle behaviour. The gait is initiated by the detection of the heel strike and the controller can adapt to the changing pace of gait by monitoring the duration of the previous gait cycle.

2.4. Conclusions

The ankle kinematics, moments and power during level walking and stair climbing are reviewed and analysed, which can be used for the design of the EHA system in the powered ankle prosthesis.

Several ESR prosthetic feet and microprocessor controlled semi-active prostheses presented in this chapter improve the walking experience without providing active walking assistance in the stance phase. The performance of these devices is limited by the lack of net power injection in the stance phase, which results in asymmetric gaits between the healthy leg and the leg with amputation.

The development of powered ankle prostheses with different actuation methods are reviewed, including their power source, sensors, output power level and control method. These powered ankle prostheses provide continuous active power in the stance phase to assist walking and are capable of exerting output over 70 Nm peak torque. The main features of these powered ankle prostheses are summarized in Table

2-1 (according to the materials referenced in this chapter). The powered ankle prostheses, actuated by a DC motor with mechanical transmission, require continuous electrical power for all ankle movements. Their power requirement significantly limits walking range and will disable the ankle movement after the battery discharges. The pneumatically actuated ankle prostheses are also limited by their power density and controllability. The main challenges of the development of a powered ankle prosthesis are: 1. to reach the kinematic and kinetic characteristics of a human's ankle-foot within the weight and volume limitation; 2. to assist walking of lower limb amputees with natural gait; 3. to extend walking range and ensure safety passive operation.

This research project is to develop a light and compact powered ankle prosthesis with improved walking experience, reduced average power draw and to allow safe passive prosthetic function after the battery discharged. This can be achieved by using an EHA system to assist walking within certain time windows within a gait cycle, specifically the PF before toe-off, and DF in the early swing phase for toe-lifting. In the rest of the gait, the EHA system can operate passively with controllable damping which cannot be achieved by most of the other actuation solutions. Its high torque to weight/volume ratio, good controllability and robustness, compared to pneumatic actuation solution, also make it highly suitable for use in lower limb prosthesis applications. The semi-active transfemoral prostheses proposed in [29, 49] are intended to achieve a switch between active mode and passive mode using the proposed EHA system, but a prototype has not been built.

The control framework and methods of the lower limb prostheses are discussed. A hierarchical controller structure with three levels is provided in [11]. The user’s intent can be recognised by interacting with the environment using mechanical signals or the user using EMG signals (high level controller). The phase based middle level control strategy monitors the phase changes in a gait cycle and generates demand signals for the low level controller (controlling the output of the actuators) in each phase.

Table 2-1: Summary of the developments of the powered ankle prostheses.

	Principle	Actuation Method	Power Source	Foot Type	Development Status
BiOM (MIT Media Lab) [39]	Active Ankle Prosthesis with Series-elastic Actuator	DC motor with ball-screw transmission, series spring and parallel spring	On board battery	ESR	Commercially available
Self-contained Knee-ankle Prosthesis (Vanderbilt University) [44]	Self-contained Knee-ankle Prosthesis with Electric Actuators	DC motor with ball-screw transmission and parallel spring	On board battery	Solid	Research prototype
SPARKy (Arizona State University) [46]	Active Ankle Prosthesis with Robotic Tendon Actuator	DC motor with gear box, lead screw transmission and series 'tendon' springs	Off board power	ESR	Research prototype
Semi-Active Knee-Ankle Prosthesis (University of California) [29]	Semi-active Transfemoral Prosthesis with EHA	EHA with wire rope	-	ESR	Proposed concept
Pneumatically Actuated Transfemoral Prosthesis (Vanderbilt University) [51]	Pneumatic Cylinder Actuated Transfemoral Prosthesis	Pneumatic cylinder actuator	Off board power	Solid	Research prototype
Pneumatically Powered Below-Knee Prosthesis (Vrije Universiteit Brussel) [53]	Artificial Muscles Actuated Ankle prosthesis	Pneumatic artificial muscles	Off board power	Solid	Research prototype

Pneumatically Actuated Transtibial Prosthesis (Jilin University) [54]	Pneumatic Cylinder Actuated ankle Prosthesis	Pneumatic cylinder actuator	Off board power	Solid	Research prototype

Chapter 3

Powered Ankle Design Requirements and Concept

This chapter describes the powered ankle design requirements. By analysing the ankle motion and moment characteristics of a healthy subject while level walking, requirements for a new powered ankle prosthesis have been specified. A design concept using an electrohydrostatic actuator (EHA) is then proposed. The output requirement of the EHA has been derived from the ankle rotation speed and peak moment in the PF phase before toe-off of a healthy subject. The flow rate and pressure difference requirements for the EHA pump were then calculated based on the dimension of an existing hydraulic cylinder. The output requirement of the electric motor was derived at the end of this chapter depending on different pump displacements.

3.1. Design Concept

3.1.1. Performance Requirements

Figure 3-1 shows the ankle dorsiflexion angle, moment and power of a healthy subject (70 kg) in a whole gait cycle. The gait cycle in Figure 3-1 starts from the heel strike (Phase <1>). The thick grey bar between phases <3> and <4> indicates the toe leaving the ground. Several main features of the ankle of a healthy subject are summarized in Table 3-1.

In the heel strike (Phase <1>), the ankle plantarflexes a small angle when the heel contacts the ground. The strike on the heel is absorbed by the cushion effect of the heel. The foot then fully contacts the ground and supports the body weight. At the beginning of the middle stance phase (Phase <2>), the ankle reverses the rotation direction. Along with the human body moving forward, the centre of gravity of the human body is transferred from the heel to the toe and from the other leg to the leg being observed. The ankle moment increases until the foot of the other leg contacts the ground. Within the middle stance phase (Phase <2>), the ankle power is negative. In the terminal stance phase (Phase <3>), the ankle moment will peak at 110 Nm, which is because the ankle is actively plantarflexing the foot against the majority of the body weight acting on the toe. Maximum net power is used in this period to push the human body forward. The ankle moment will be released when the toe left the ground (toe-off). The toe is immediately lifted in the beginning of the swing phase (Phase<4>) to clear the ground. This DF movement requires active but limited power. The ankle will then keep at a relatively constant angle until the start of the next gait cycle.

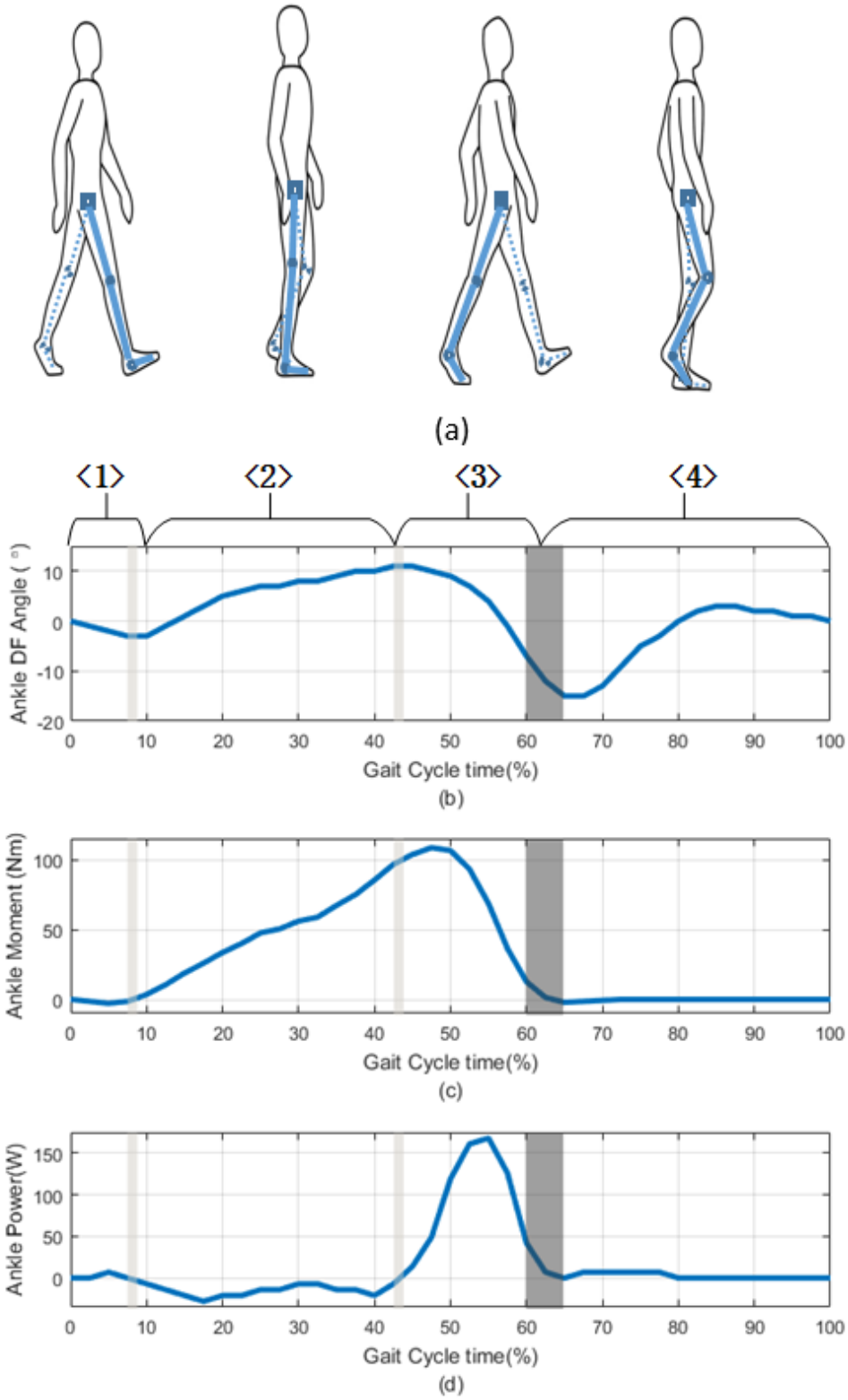

Figure 3-1: Ankle motion of a 70kg healthy subject in a gait cycle [18]. (a) Human postures in a gait cycle. (b) Ankle DF angle in a gait cycle. (c) Ankle moment in a gait cycle. (d) Ankle power in a gait cycle.

Table 3-1: Summary of ankle motion features for a 70kg healthy subject [18].

Phase Number	<1>	<2>	<3>	<4>	
Gait Phase	Heel strike	Middle stance	Terminal stance	Swing	
Phase Period	7.50%	37.50%	20%	15%	20%
Ankle Rotation Direction	PF	DF	PF	DF	-
Ankle Rotation Range (°)	0 ~ -3	-3 ~ 11	11 ~ -15	-15 ~ 0	
Average Rotation Speed (°/s)	30	27	104	75	
Ankle Torque	0	Increase	110 Nm (Peak)	0	
Peak Ankle Power (W)	0	-28	168	7	

As can be seen from Figure 3-1 and Table 3-1, the ankle power consumption is very low, even negative, in the majority of the gait cycle (about 80%). Significant power input is only required in the terminal stance phase, about 20% of a gait cycle. The PF movement in the terminal stance phase needs about 168 W peak from a 70 kg subject for level walking. The ankle is rotating at a speed of about 104 °/s against a peak load torque of 110 Nm. In the other period of the stance phase, the ankle-foot is supporting the whole or part of the body weight and absorbs the shock of the heel strike. In the early swing phase, it is necessary to dorsiflex the ankle to prevent the toe hitting the ground and to avoid the usage of power from the upper limb to lift the ankle-foot. This dorsiflexion movement requires high rotation speed but is against a small load torque. Since the ankle motion in a gait cycle shows a clear split between active power delivery phases (terminal stance and early swing) and power absorption phases, a new powered ankle prosthesis is proposed to achieve a quick switch between passive and active modes to assist walking. The major power should be input into the ankle joint actuator to assist push-off at the end of stance phase and lift up the toe in the early swing phase. In the other period of a gait cycle, the ankle prosthesis should be operated passively with controllable damping. In this way, the new powered ankle prosthesis can expand the function of a passive ankle prosthesis and extend the operation life compared to a fully powered ankle prosthesis.

3.1.2. EHA Powered Ankle Prosthesis Concept

To achieve a quick and smooth switch between active and passive modes, an EHA can be used for this powered ankle prosthesis. The hydraulic circuit of the EHA is shown in Figure 3-2.

A servo motor is coupled to a bi-directional pump. When the actuation is operated actively, the motor-pump is running, and hydraulic oil is pumped into either side of the hydraulic cylinder. The leakage in the pump is gathered in an accumulator via the case drain of the pump. The hydraulic oil in the accumulator can be re-fed into the closed circuit via a pair of check valves. The accumulator is pre-pressured and is used to maintain a minimum pressure in the hydraulic circuit.

When the ankle is operated passively, the motor-pump is stationary, only the hydraulic cylinder and the two bypass lines are working. The passive hydraulic circuit is equivalent to Figure 3-3. The hydraulic cylinder and the two bypass restriction valves form a damper. The damping in either direction can be controlled by adjusting the orifice areas of the restrictor valves respectively.

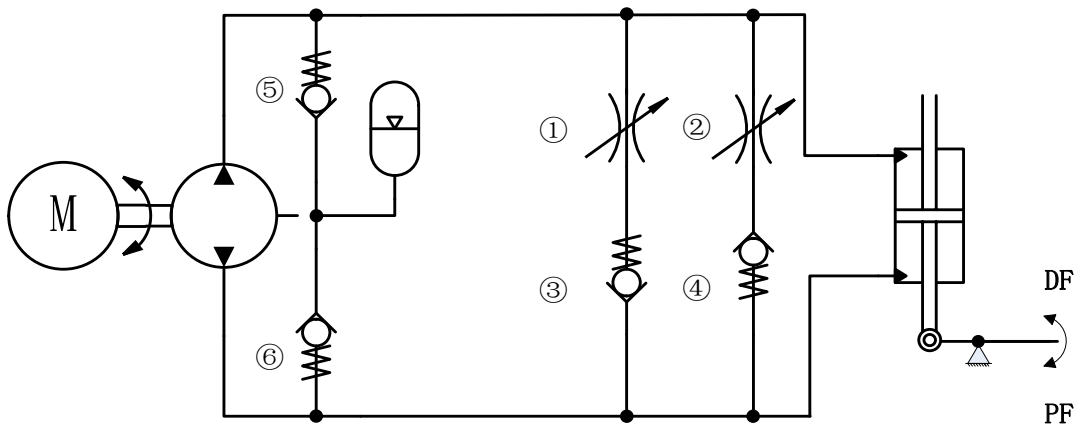

Figure 3-2: Hydraulic circuit of the EHA for the powered ankle prosthesis.

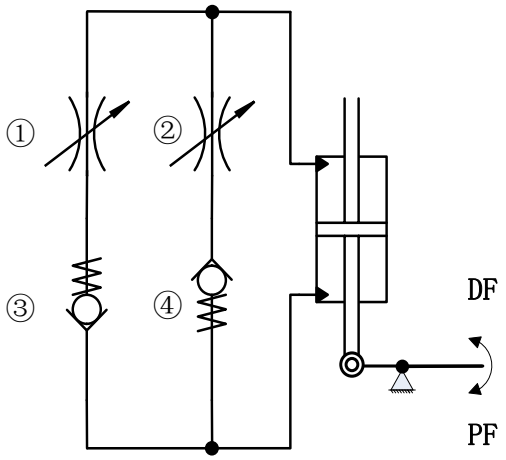

Figure 3-3: Equivalent hydraulic circuit of the EHA in passive mode.

The operation of the EHA in a gait cycle is summarized in Table 3-2. When the heel contacts the ground at the beginning of the heel strike, the PF of the ankle pushes the rod of the hydraulic cylinder upwards. The hydraulic oil in the top chamber of the cylinder is compressed and the pressure increases. When the pressure in the top chamber is higher than the pressure in the bottom chamber, check valve ④ is open and lets the fluid goes through restriction valve ②. The damping provided by restriction valve ② is used to limit the PF speed of the heel strike. The ankle dorsiflexes along with the body weight moving forward in the middle stance phase. In this period, the oil in the bottom chamber of the hydraulic cylinder is compressed, check valve ③ is open and restriction valve ① is activated. In the terminal stance phase, the EHA can be switched into active mode. To actively plantarflex the ankle, the motor-pump is driven to pump the oil into the bottom side of the cylinder. Since the load torque is quite high in this period, the pressure difference is high across the cylinder. Restriction valve ① should be closed to flow bypassing instead of going into the cylinder. At the same time, check valve ⑤ will open and the oil in the accumulator will fed into the low pressure side (top side of the cylinder). The low pressure will be maintained at the pre-set pressure in the accumulator to prevent cavitation. After the toe leaves the ground, the motor-pump will reverse direction. The hydraulic oil will be pumped into the top chamber of the cylinder. The actuator dorsiflexes the ankle

joint to lift the toe. Check valve ④ is open and restriction valve ② is in use. Since there is very small load torque to lift the toe in the swing phase, the pressure difference is low across the cylinder. The bypass flow rate through restriction valve ② is expected to be quite small, so closing the valve is not necessary.

In the active mode, the ankle joint is powered by the motor-pump of the EHA and in the passive mode the ankle joint with two bypass restriction valves works as a damper. In this way, a quick and smooth switch between active and passive modes can be achieved by controlling the motor and restrictor ①.

Table 3-2: The operation of the EHA powered ankle prosthesis in a gait cycle.

Phase Number	<1>	<2>	<3>	<4>	
Gait Phase	Heel strike	Middle stance	Terminal stance	Swing	
Active/Passive Mode	Passive	Passive	Active	Active	Passive
Ankle Rotation Direction	PF	DF	PF	DF	-
Motor-pump Direction	-	-	Positive	Negative	
Cylinder High Pressure Side	Top	Bottom	Bottom	Top	
Activated Restriction Valve	②	①	①	②	
Check Valve ③	Close	Open	Open	Close	
Check Valve ④	Open	Close	Close	Open	
Check Valve ⑤	-	-	Open	Close	
Check Valve ⑥	-	-	Close	Open	

3.2. Component Sizing

3.2.1. Ankle Output Requirement

As shown in Figure 3-1 and Table 3-1, the ankle output requirements of a 70 kg amputee can be used as the design reference. From the study in [18], the ankle output requirement of an 80 kg amputee can also be derived for comparison. Ankle output requirements of a 70 kg amputee and an 80 kg amputee are summarized in Table 3-3.

Table 3-3: Ankle output requirement of a 70kg amputee and an 80kg amputee [18].

Body Weight (kg)	70	80
Rotation Range (°)	26	
Rotation Speed (°/s)	104	
Peak Torque (Nm)	110	126
Peak Power (W)	168	192
Mean Power (W)	112	128

3.2.2. Elan Ankle Cylinder

The Elan foot is a commercially available passive ankle prosthesis with controllable damping, which is manufactured by Chas A Blatchford & Sons Ltd [8]. This passive ankle prosthesis can be used as the passive portion of the new powered ankle prosthesis. The Elan foot is shown in Figure 2-6 and its hydraulic circuit is the same as shown in Figure 3-3. The double acting hydraulic cylinder at the ankle joint rotates the foot carriage via a short arm. The restrictor valves (Valve ① and ② in Figure 3-3) are controlled by two micro motors and a microprocessor. The operation of the Elan foot in a gait cycle is summarized in Table 3-4.

Table 3-4: Elan foot operation in a gait cycle.

Phase Number	<1>	<2>	<3>	<4>
Gait Phase	Heel strike	Middle stance	Terminal stance	Swing
Ankle Rotation Direction	PF	DF	DF	-
Cylinder High Pressure Side	Top	Bottom	Bottom	
Activated Restriction Valve	②	①	①	
Check Valve ③	Close	Open	Open	
Check Valve ④	Open	Close	Close	

This Elan foot has separate elastic carbon forefoot and heel, which can absorb energy in early-middle stance and return energy before toe-off. When the heel contacts the ground at the beginning of the heel strike, the heel spring is deformed, which is working as a cushion, to absorb the impact of the foot. Some energy is stored in the compressed heel spring. In the middle stance phase, both the heel spring and the toe spring are compressed to hold the body weight. In the terminal stance phase, nearly all the body weight is supported by the toe spring and the heel spring is released to feedback the energy to assist walking. When the toe is about to leave the ground, the energy stored in the toe spring is also fed back to assist walking.

As the Elan foot can achieve the passive function very well, provide controllable damping and support body weight, an EHA powered ankle can be developed based on it. The dimensions of the ankle cylinder is shown in Figure 3-4 and Table 3-5.

The cylinder working area in Table 3-5 is the piston annulus area of a double acting cylinder, which is calculated from:

$$A_a = \frac{\pi}{4}\left(D_p^2 - D_r^2\right) \qquad (3-1)$$

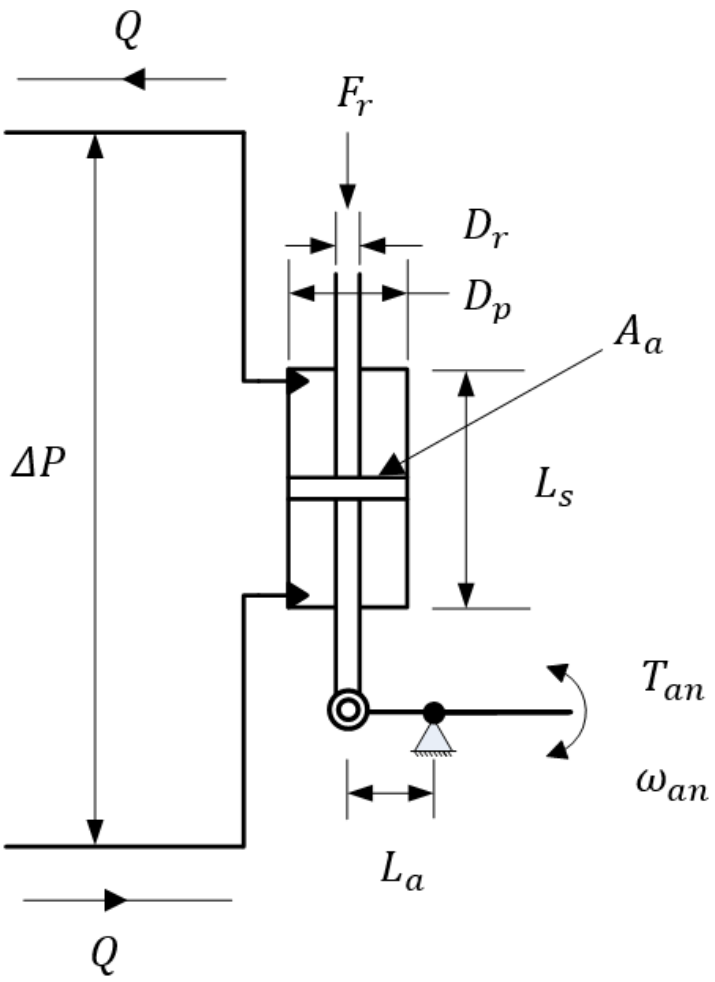

Figure 3-4: Dimensions of the Elan foot hydraulic cylinder.

Table 3-5: Summary of the dimensions of the Elan foot hydraulic cylinder.

Symbol	Specification	Value
D_r	Rod Diameter	1 cm
D_p	Piston Diameter	3 cm
A_a	Cylinder Working Area	6.28 cm²
L_s	Piston Stroke	8.6 mm
L_a	Arm Length	2 cm
A_{ra}	Ankle Rotation Range	21 °

3.2.3. Ankle Cylinder Input Requirements

The force on the cylinder rod F_r can be calculated from the ankle torque T_{an} and the arm length:

$$F_r = \frac{T_{an}}{L_a} \qquad (3-2)$$

The required rod extension speed μ_r can be calculated from the ankle rotation speed ω_{an} and the arm length:

$$\mu_r = \omega_{an} L_a \qquad (3-3)$$

The required pressure difference across the cylinder ΔP can be calculated from the force on the rod and the cylinder working area:

$$\Delta P = \frac{F_r}{A_a} \qquad (3-4)$$

The required flow rate Q into/out the cylinder as shown in Figure 3-4 can be calculated from the required rod extension speed and the cylinder working area:

$$Q = \mu_r A_a \qquad (3-5)$$

Taking the maximum ankle output requirements for a 70 kg amputee from Table 3-3 as the reference, the ankle cylinder input requirements are summarized in Table 3-6.

Table 3-6: Input requirements of the ankle cylinder.

Symbol	Specification	Value	Symbol	Specification	Value
ω_{an}	Peak Ankle PF Speed	104 °/s	T_{an}	Peak Torque	110 Nm
μ_r	Peak Rod Extension Speed	3.63 cm/s	F_r	Peak Rod Force	5500 N
Q	Peak Required Flow Rate	22.8 cc/s	ΔP	Peak Pressure Difference	87 bar

3.2.4. Motor Output Requirements

Assuming the EHA efficiency is 100% and the bypass restriction valve is fully closed in the powered phase, the required motor speed and motor output torque can be derived.

The required motor output torque T_m can be calculated from the required pressure difference across the cylinder and the pump displacement:

$$T_m = \Delta P D \qquad (3-6)$$

where D is the pump displacement. The required motor speed ω_m can be calculated from the required flow rate into/out of the cylinder:

$$\omega_m = \frac{Q}{D} \qquad (3-7)$$

According to the required pressure difference and flow rate from table 3-6, the motor output requirements for different pump displacements are summarized in Table 3-7. The pump displacements in Table 3-7 are referred to the three potential commercially available gear pumps.

Table 3-7: Output requirements of the motor.

Symbol	Specification	Value	Symbol	Specification	Value
Pump Displacement: $D = 0.45$ cc/rev					
Q	Required Flow Rate	22.8 cc/s	ΔP	Required Pressure Difference	87 bar
ω_m	Required Motor Speed	3041 rpm	T_m	Required Motor Torque	0.62 Nm
Pump Displacement: $D = 0.4$ cc/rev					
Q	Required Flow Rate	22.8 cc/s	ΔP	Required Pressure Difference	87 bar
ω_m	Required Motor Speed	3375 rpm	T_m	Required Motor Torque	0.55 Nm
Pump Displacement: $D = 0.33$ cc/rev					
Q	Required Flow Rate	22.8 cc/s	ΔP	Required Pressure Difference	87 bar
ω_m	Required Motor Speed	4090 rpm	T_m	Required Motor Torque	0.46 Nm

3.3. Conclusions

The ankle locomotion of healthy subjects indicates the ankle power consumption is very low in about 80% of the gait cycle. In the other 20% of the gait cycle (terminal stance phase), the ankle performs 104°/s average rotation speed, 110 Nm peak torque (70 kg subject) and 168W peak power (70 kg subject). The design concept using an EHA is proposed to achieve quick and smooth switching between the passive mode and active mode. The output requirements of the hydraulic pump, 22.8 cc/s peak flow rate and 87 bar peak pressure difference, are obtained based on the ankle output requirements in the terminal stance phase and the dimensions of a passive ankle prosthesis product [8]. The motor output requirements are derived according to different pump displacements.

Chapter 4

Prototype Development and Bench Test

This chapter describes the powered ankle prosthesis prototype and explains its development process. The final prototype, called the MK4, achieves a compact design which integrates the whole actuation system at the ankle joint and a weight of 2.2 kg, which is less than half of the previous prototype. The components of MK4 prototype are presented in detail. By comparing the MK4 bench test results with the ankle output requirement of a healthy subject, it is seen that the MK4 powered ankle prosthesis prototype should be able to power the ankle PF movement in the terminal stance phase to assist walking in the real walking load condition.

4.1. Development Process

4.1.1. MK1 Prototype

The MK1 prototype was built by Jawaad Bhatti and Bernard Roe in the University of Bath, which was using a Brushless DC motor and a unidirectional gear pump to deliver power into the ankle cylinder. The hydraulic circuit of MK1 is shown in Figure 4-1 and its motor-pump unit is shown in Figure 4-2.

Since the unidirectional pump applied in this prototype could only pump the hydraulic oil into the bottom side of the cylinder, the EHA could only power the PF movement. A spring has been inserted into the cylinder as shown in Figure 4-1 to help retract the cylinder rod. In this way, the ankle could be dorsiflexed in the swing phase by the energy stored in the spring. But in the powered PF phase, the output torque will be reduced since the actuator is acting against the spring. As a result, the assist received by the amputee is limited.

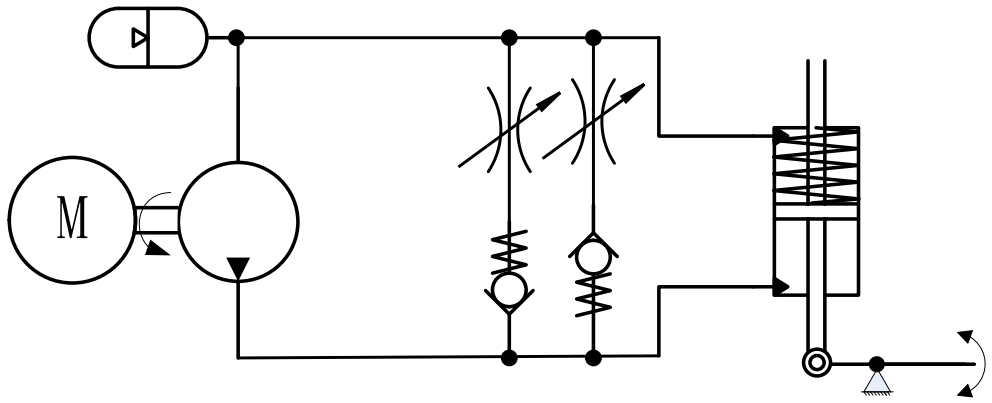

Figure 4-1: Hydraulic circuit of MK1 prototype.

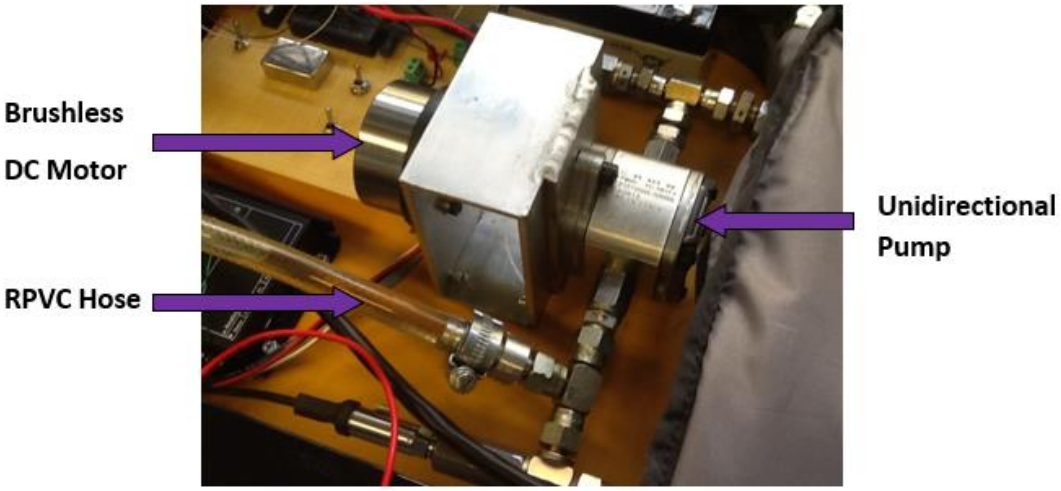

Figure 4-2: Motor-pump unit of MK1 prototype.

The accumulator symbol in Figure 4-1 indicates a piece of RPVC (Rigid Polyvinyl chloride) hose connected to the low pressure side of the pump, which was used as a simplified fluid reservoir. The hydraulic oil contained in the hose was used to compensate the leakage in the hydraulic circuit and to maintain the low pressure in the hydraulic circuit.

The motor-pump unit was kept in a backpack and was connected to the ankle actuator by a pair of hydraulic hoses.

4.1.2. MK2 Prototype

The second prototype was developed by the author to achieve a bi-directional movement of the ankle prosthesis. A bi-directional gear pump was used to replace the previous unidirectional pump. At the same time the spring in the ankle cylinder was removed, which prevented energy being wasted to compress the spring and maximized the power to plantarflex the ankle. The hydraulic circuit of MK2 is shown in Figure 4-3 and its motor-pump unit is shown in Figure 4-4.

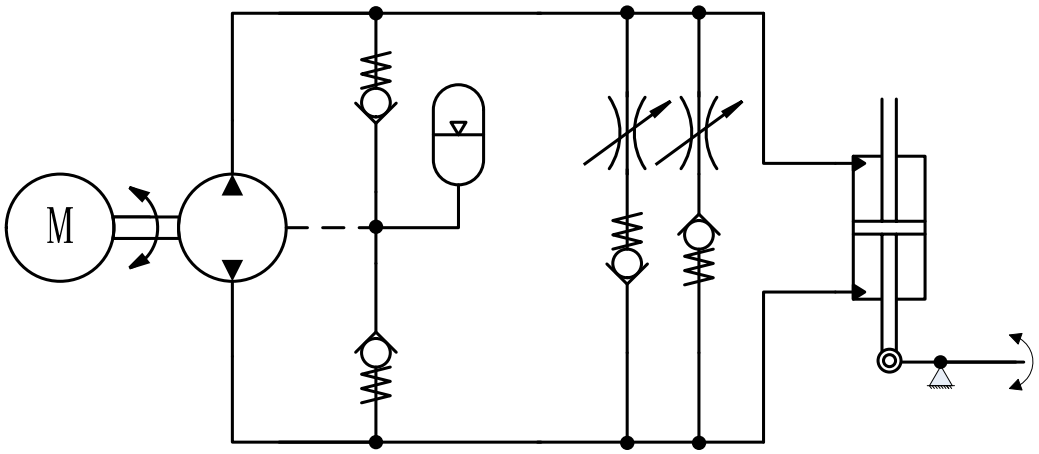

Figure 4-3: Hydraulic circuit of MK2 prototype.

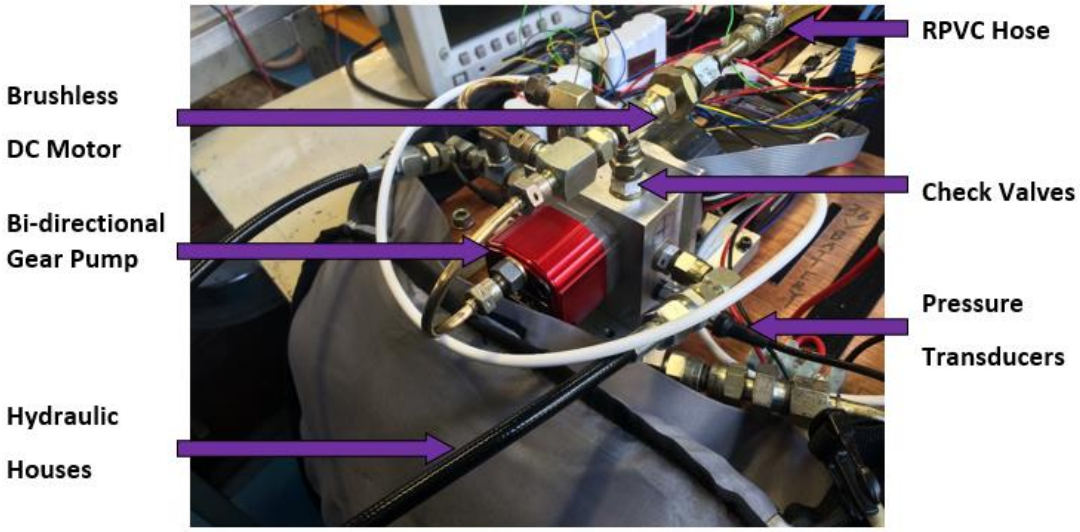

Figure 4-4: Motor-pump unit of MK2 prototype.

The motor, pump, accumulator and check valves are kept in a backpack, as shown in Figure 4-4. The motor is a 24 V brushless DC motor and the pump displacement is 0.45 cc/rev. An accumulator is connected to the case drain of the bi-directional pump to collect the leakage in the pump. The oil in the accumulator can be re-fed to the low pressure side of the closed loop circuit to maintain the low pressure in the circuit at about 5 bar. To reduce the weight of the prototype, a piece of RPVC hose has been used as the accumulator. The hydraulic oil in the accumulator hose is pre-pressured to

5 bar. The two new check valves are from Lee Products Ltd [72], which has been fitted into two 1/8'' BSP (British Standard Pipe) fittings, as shown in Figure 4-5. The motor-pump unit is connected to the other parts with a pair of Micro-bore hydraulic hoses.

The motor is controlled by a Maxon 50-5 ESCON controller [73]. A CRIO (Compact Real-time Input/output Processor) from National Instruments is used to run the control programme and record sensor signals [74]. The controllers and batteries were also kept in the backpack.

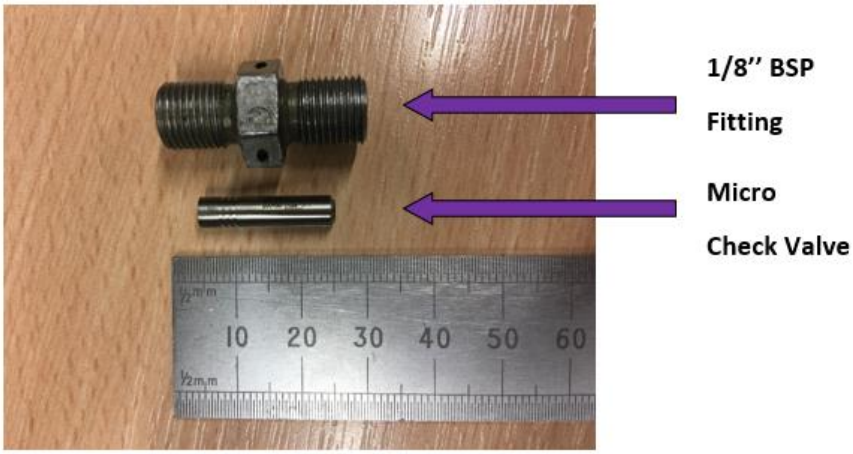

Figure 4-5: Micro check valve used in MK2 prototype [72].

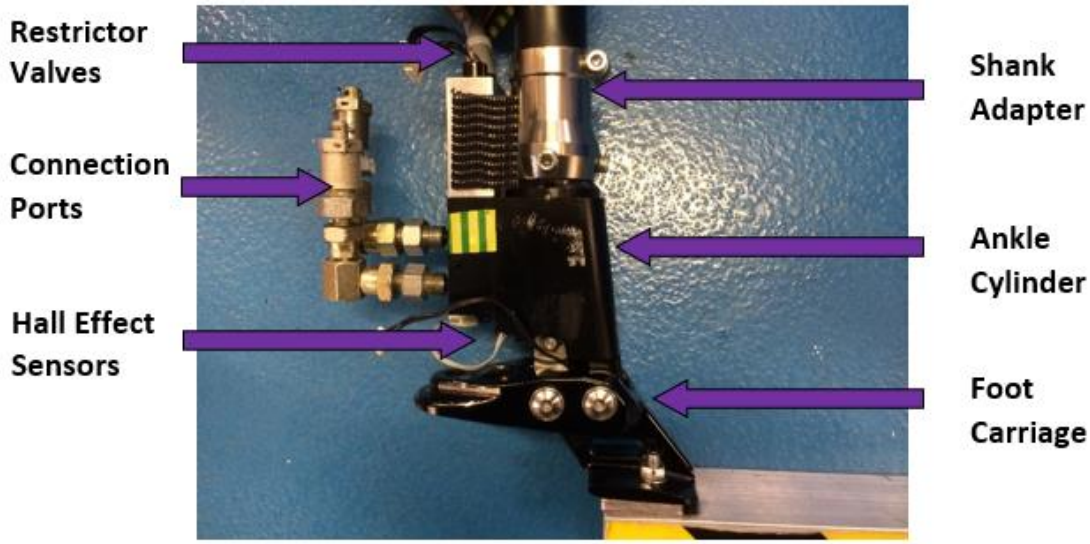

Figure 4-6: Ankle assembly of MK2 prototype.

The ankle assembly of MK2 prototype is shown in Figure 4-6. There are two connection ports in the figure to connect with the Micro-bore hoses. The rotary restrictor valves are driven by two micro motors, as shown in Figure 4-7. The micro motor is controlled by a micro board controller which is developed by Chas A Blatchford.

The ankle cylinder rotates the foot carriage to dorsiflex or plantarflex the foot spring (not shown in Figure 4-6) and connects to the shank or knee prosthesis of the amputee via the shank adapter. The mounting angle of the ankle prosthesis can be adjusted by the shank adapter. A hall effect sensor and a permanent magnet have been mounted on the ankle cylinder and foot carriage respectively, which is used to monitor the ankle rotation angle. The analogue voltage signal from the hall effect sensor is used to detect the state in a gait cycle and used to trigger the powered PF phase. The specifications of some of the components used in the MK2 are summarized in Table 4-1.

Figure 4-7: Restrictor valve with micro motor used in MK2 prototype.

Table 4-1: Specifications of MK2 prototype components.

Components & Sensors	Main Features	
Maxon EC 60 Flat Brushless DC Motor [75]	Nominal Voltage	24 V
	Rated Power	100 W
	Nominal Speed	4250 rpm
	Stall Torque	3.74 Nm
	Weight	470 g
ESCON 50/5 Servo Controller [73]	Nominal Voltage	10-50 V
	Maximum Output Current	15 A
	Weight	204 g
Hydraproducts KV0R04RBZZE Reversible Gear Pump [76]	Displacement	0.45 cc/rev
	Weight	306 g
Axial Flow Screened 187 LEE Chek Check Valve [72]	Valve Diameter	4.75 mm
	Weight	2.3 g
Hydrotechnik DN4 Microbore Hose [77]	Diameter	4 mm
	Maximum Working Pressure	315 bar
Blatchford Elan Ankle Joint Actuator & Foot Springs [8]	Actuator Working Area	6.28 cm^2
	Movement Range	21°
Variohm EPT1200 Pressure Transducer [78]	Rated Pressure	160 bar

The MK2 ankle prosthesis prototype has been tested with a transtibial amputee (70 kg) and a transfemoral amputee (80 kg). In the patient trial, the EHA powered ankle prosthesis could achieve an automatic operation mode switch between passive and active modes and could power both the DF and PF movement. According to the feedback from the amputees, the torque received from the powered ankle prosthesis was not sufficient to assist walking adequately. As suggested by the transfemoral amputee who took part in the trial, the MK2 prototype has also been tested to assist the DF in the middle stance phase. This DF testing result and potential DF assist prosthesis will be discussed in chapter 9.

From bench test results, the efficiency of MK2 was found to be very low which resulted in the low output power which was not enough to assist walking. The efficiency in a high load situation of MK2 is summarised in Table 4-2. Mechanical

efficiency compares the ideal and actual torques and pressures, and volumetric efficiency compares the ideal and actual velocity and flows. For the volumetric efficiency, there is significant wasted bypass flow through the restrictor. In the high load situation, over half of the fluid will be bypassed through the restriction valve even when the smallest orifice of the restriction valve has been applied.

For the mechanical efficiency, both the friction in the motor-pump and the pressure loss in the delivery are significant. Especially the narrow galleries in the manifold, the long Micro-bore hose, and the connectors at ankle ports (Figure 4-8) contribute to the pressure loss.

Table 4-2: Efficiency summary of MK2 prototype.

	Mechanical Efficiency	Volumetric Efficiency	Total Efficiency
Motor ~ Pump	67%	84%	67%
Pump ~ Load	61%	35%	21%
Total	41%	29%	12%

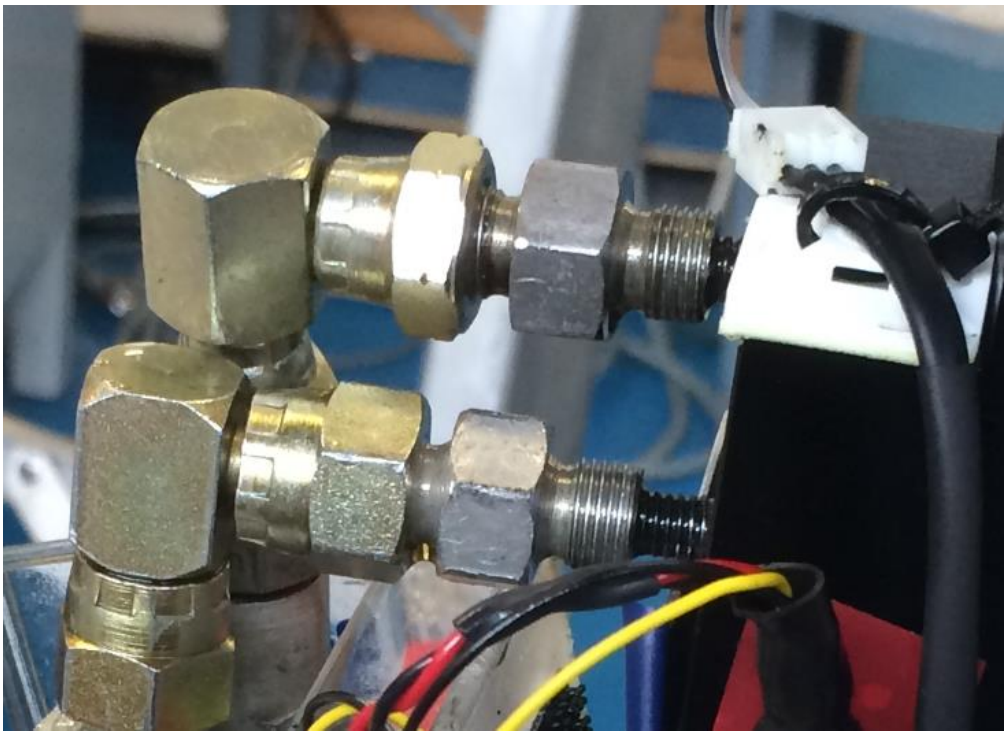

Figure 4-8: Connectors at ankle ports of MK2 prototype.

4.1.3. MK3 Prototype

To improve the efficiency of the MK2 and to maximize the output power to effectively assist walking, the MK3 has been built. The hydraulic circuit of the MK3 is shown in Figure 4-9. The main improvements are:

- A new 48 V motor and 48 V supply voltage from batteries
- Fittings with bigger inner diameter
- Shorter hydraulic hoses with bigger inner diameter
- On/off valve to fully close the bypass line.

The ankle assembly of MK3 is shown in Figure 4-10. The manifold galleries are machined to about 3 mm diameter to minimise the pressure loss within the space constraints of the ankle block. The Micro-bore hydraulic hoses, which were connecting the pump to the ankle, are replaced by a pair of 1 meter length and ¼ inch diameter hydraulic hoses. The on/off valve is a 3 way/2 position normally closed solenoid valve from Lee Products Ltd [79]. When the valve is opened, the fluid could only flow though the valve in one direction, which also included the function of the check valve in the line. The specifications of the new motor and the on/off valve of MK3 are summarized in Table 4-3.

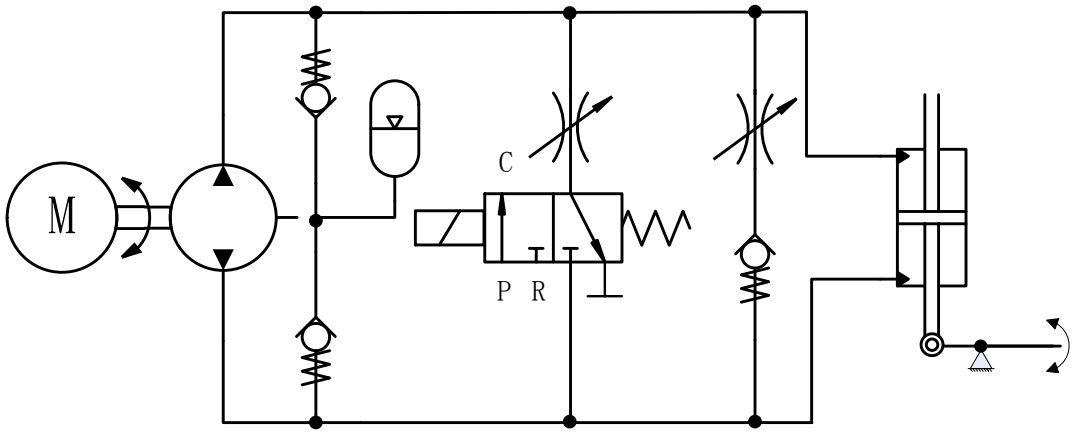

Figure 4-9: Hydraulic circuit of MK3 prototype.

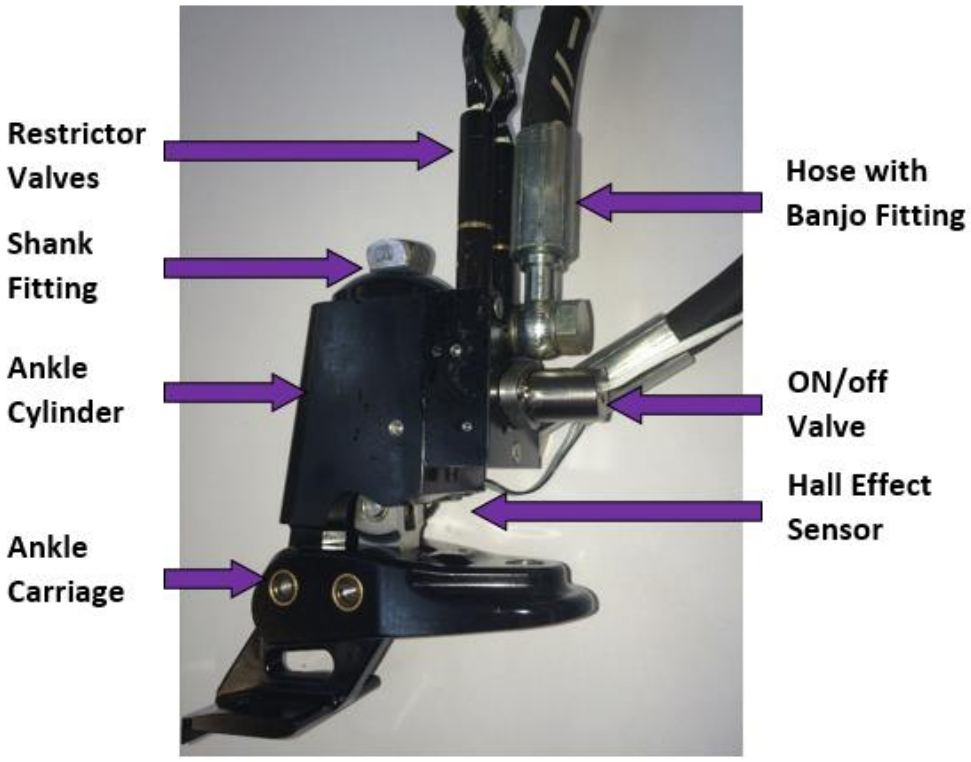

Figure 4-10: Ankle assembly of MK3 prototype.

Table 4-3: Specifications of the motor and on/off valve used in MK3 prototype.

Components	Main Features	
Maxon EC 60 Flat Brushless DC Motor [75]	Nominal Voltage	48 V
	Rated Power	100 W
	Nominal Speed	3970 rpm
	Stall Torque	4.19 Nm
	Weight	470 g
Lee SDBA2531013B 3-way Normally Closed Solenoid Valve [79]	Pull-in Voltage	12 V
	Current Drain	0.4 A
	Weight	40 g

The efficiency comparison between the MK2 and the MK3 is shown in Table 4-4. The MK3 powered ankle prosthesis prototype has been tested with a transtibial amputee (70 kg) and a transfemoral amputee (80 kg) respectively at Chas A Blatchford & Sons Ltd. According to the test results [80] and the feedback of both the amputees involved in the testing, the new powered ankle prosthesis can provide high ankle torque and

high ankle rotation speed in the active phase to effectively assist them walking, and provide damping to absorb impact and support body weight in the passive phase to avoid the consumption of net power.

A problem found in the patient trial is that the hydraulic hoses which link the motor-pump in the backpack to the actuator in the ankle not only limit the motion of the amputee, but also reduce the stiffness of the hydraulic transmission.

Table 4-4: Efficiency comparison between MK2 and MK3.

	Mechanical Efficiency		Volumetric Efficiency		Total Efficiency	
	MK2	MK3	MK2	MK3	MK2	MK3
Motor ~ Pump	67%	79%	84%	84%	56%	66%
Pump ~ Load	61%	80%	35%	100%	21%	80%
Total	41%	63%	29%	84%	12%	53%

4.2. MK4 Prototype Design Overview

Based on the development of the MK3 prototype, the MK4 prototype is designed to be a compact powered ankle prosthesis which integrates the EHA at the ankle joint. This prototype can deliver the same level of assistance power as the MK3 with a 2.2 kg integrated actuation system and a 1 kg battery in the backpack. The hydraulic circuit is shown in Figure 4-11 and the ankle assembly is shown in Figure 4-12.

As can be seen in Figure 4-12, the whole EHA is integrated with the ankle joint. The long hydraulic hoses have been removed. The total weight of the ankle assembly is about 2.2 kg. The weight contribution of the MK4 ankle assembly is shown in Figure 4-13. The motor and pump make up about 1/3 of the total weight of the ankle assembly, the manifold blocks make up another 1/3 and the foot, carriage and other parts make up the other 1/3.

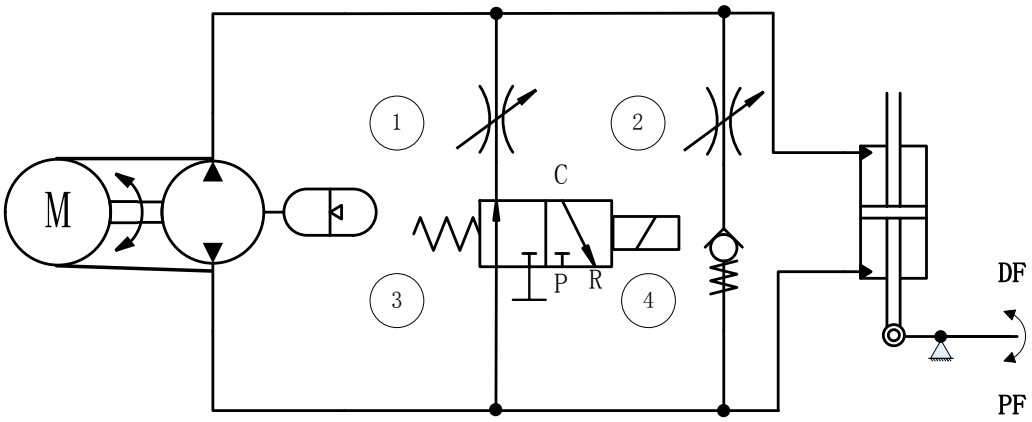

Figure 4-11: Hydraulic circuit diagram of MK4 prototype.

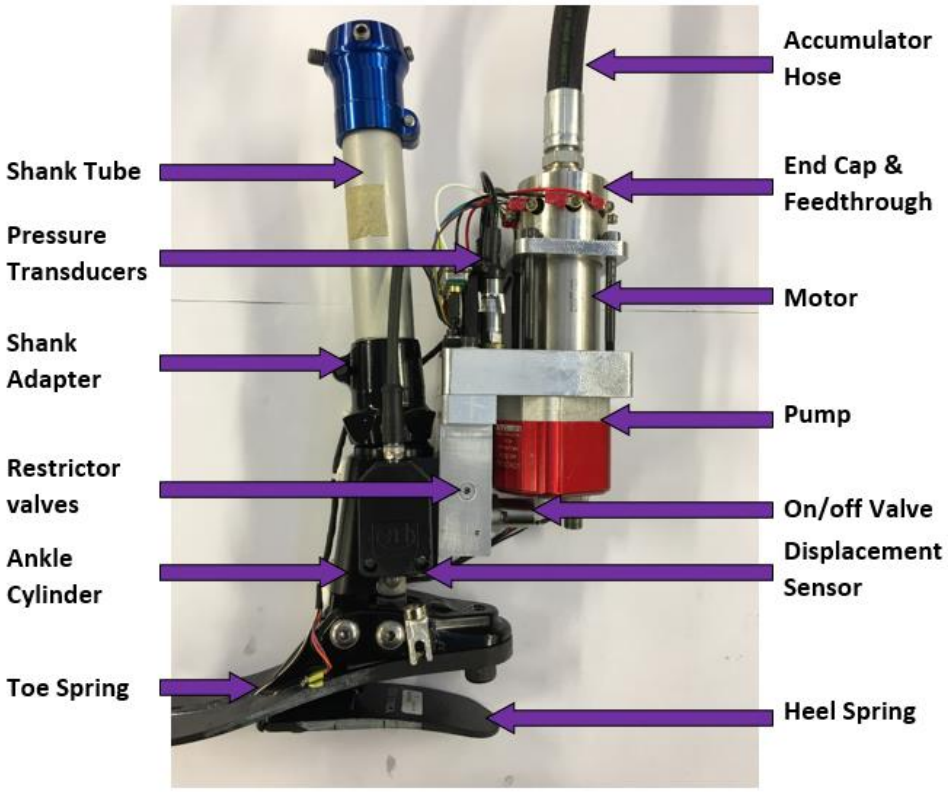

Figure 4-12: Ankle assembly of MK4 prototype.

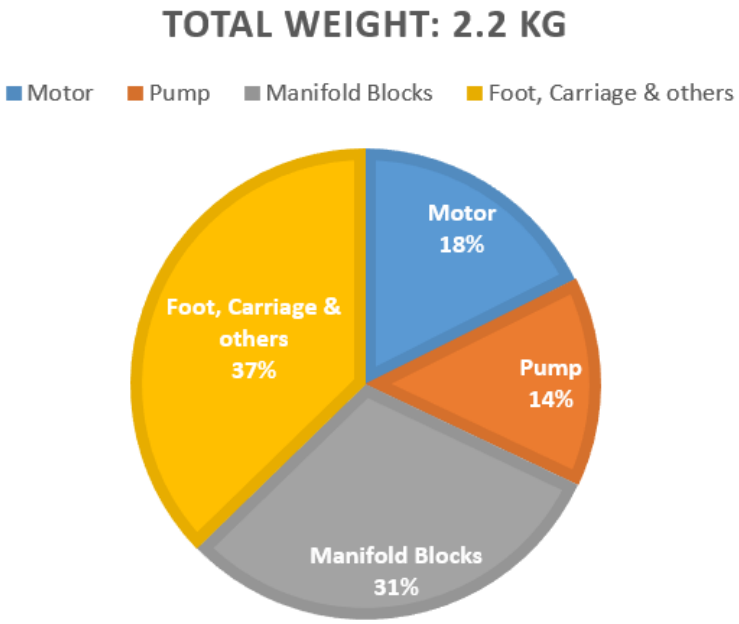

Figure 4-13: Weight contribution of MK4 ankle assembly.

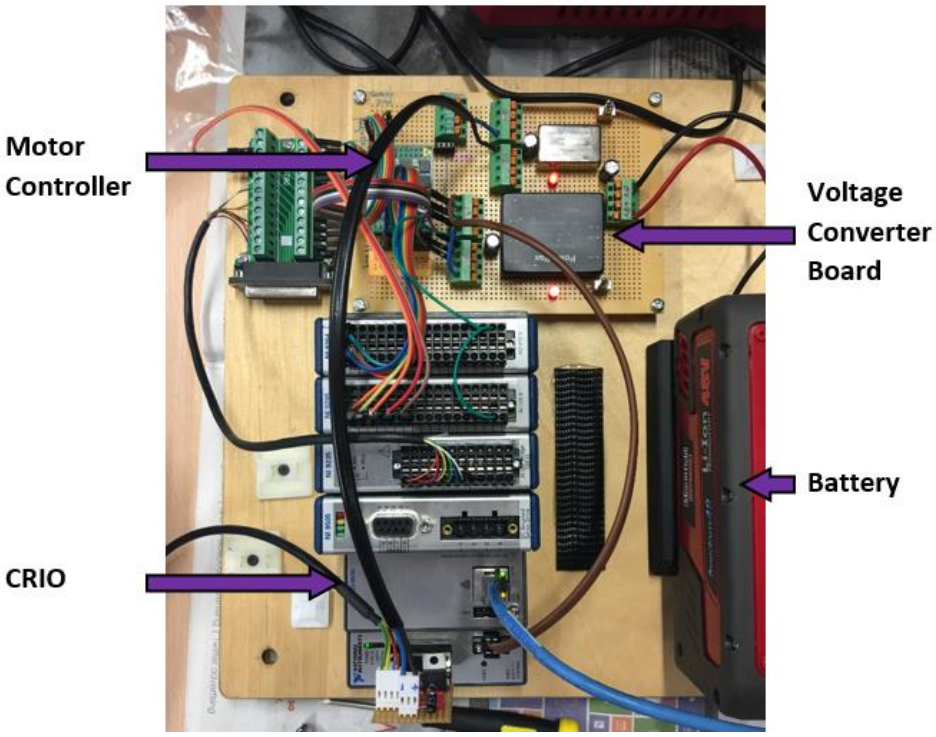

Figure 4-14: Electronics board of MK4 prototype.

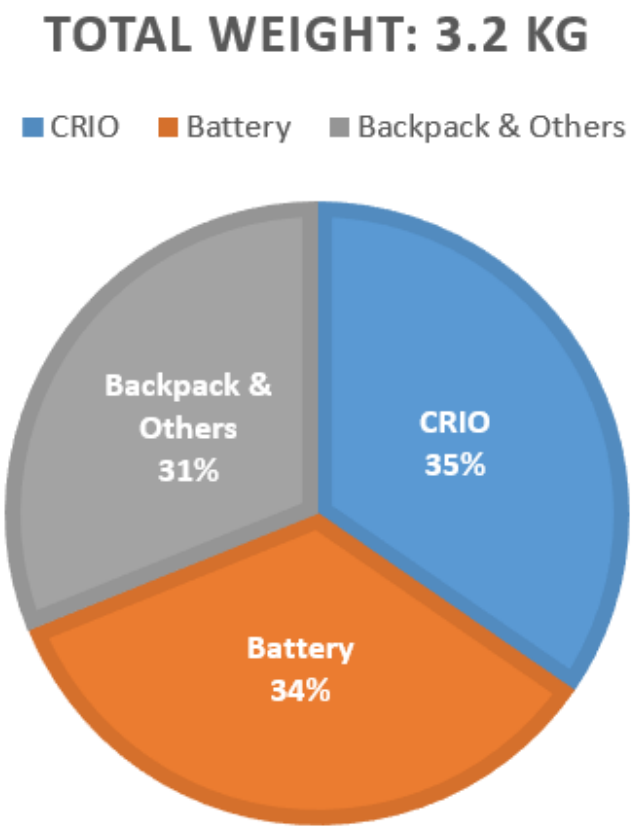

Figure 4-15: Weight contribution of MK4 backpack.

The controller, battery and other electronics are held on a wooden board and kept in a backpack in the MK4, as shown in Figure 4-14. There are two electric cables to communicate with the EHA and sensors at the ankle joint, one of which is the motor power cable and the cable is the signal cable. The weight contribution of the backpack and the included electronics is shown in Figure 4-15. The battery weighs 1.1 kg, which is about 1/3 of the total weight of the backpack. The CRIO controller with 4 interface modulus is 1/3 of the total weight. The backpack itself, wooden board and other parts make up the other 1/3 of the weight.

The total weight of the MK4 prototype is about 5.4 kg, which is about half the weight of the MK3 prototype (11 kg). This compact prototype design gives the ability to undertake long-term testing with amputees in both indoor and outdoor environment.

4.3. Component Specifications

4.3.1. Pump Selection

Three different pump displacements have been compared in Table 3-7, which correspond the optional pumps summarized in Table 4-5. All of the four pumps in the table are commercially available and have been widely used in different applications. The Oildyne Cartridge Piston Pump [81] is the smallest pumps in Table 4-5, but its uni-directional feature is not suitable for this application. The Takako Micro Axial Piston [82] is limited by its maximum speed. The Jung internal gear pump [83] is expected to be a good option due to its low noise characteristic. But the peak pressure may exceed its pressure limit considering mechanical losses and possible extreme load situations.

The Hydraproducts Reversible Gear Pump [76] is selected for this prototype because of its simple structure and wide operation range. It is shown in Figure 4-16.

Table 4-5: Comparison between the optional pumps.

	Displacement (cc/rev)	Maximum Speed (rpm)	Maximum Pressure (bar)	Rotation Direction
Oildyne Cartridge Piston Pump [81]	0.33	5000	276	Uni-directional
Takako TFH-040 Micro Axial Piston Pump [82]	0.4	2000	140	Bi-directional
Jung IPZ 1-HRL-7 Reversible Internal Gear Pump [83]	0.45	5000	110	Bi-directional
Hydraproducts KV0R04RBZZE Reversible Gear Pump [76]	0.45	9000	280	Bi-directional

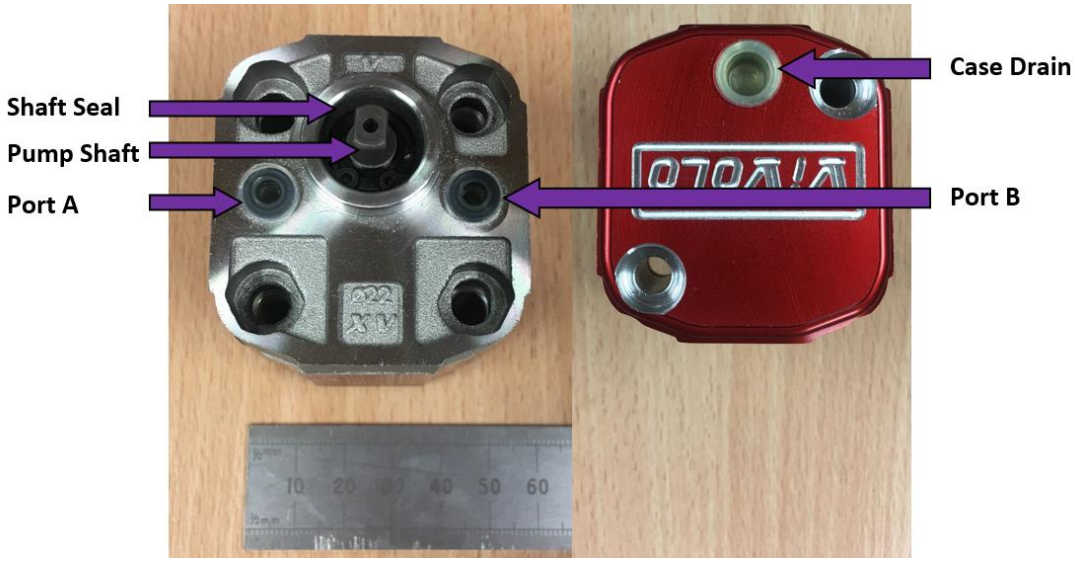

(a) **(b)**

Figure 4-16: Reversible gear pump used in MK4 prototype [76]. (a) Front view. (b) Back view.

4.3.2. Brushless DC Motor

In this compact motor-pump unit, the motor runs in hydraulic fluid of about 60 bar nominal pressure. The pump shaft seal shown in Figure 4-16 is removed to let the pressurised fluid in the motor cavity be refed into the closed circuit via the leakage path of the pump to compensate for oil volume variation in the closed circuit. The motor is required to withstand an internal pressure. The Maxon EC 60 Flat Motor [75] used in the MK3 has its rotor outside and windings in the centre, which is not suitable for this new prototype because of the difficulty of sealing. A new motor of similar characteristics has been chosen, which is Maxon EC-I 40 High Torque Brushless DC Motor [84]. This motor has the rotor in the centre and windings at outside. Its welded steel casing gives its ability to withstand high internal pressure. The motor is shown in Figure 4-17 and its specifications are summarized in Table 4-6.

(a) **(b)**

Figure 4-17: Brushless DC motor used in MK4 prototype [84]. (a) Front view. (b) Side view.

Table 4-6: Specification of the brushless DC motor of MK4 prototype [84].

Maxon EC-i 40 High Torque Brushless DC Motor [84] P/N 488607	
Rated Power	100 W
Nominal Voltage	48 V
Nominal Speed	4390 rpm
Stall Torque	4.33 Nm
Rotor Inertia	44 gcm²
Length	56 mm
Diameter	40 mm
Weight	326 g

4.3.3. End Cap Assembly

An end cap with O-ring has been designed to seal onto the end of the motor, which is shown in Figure 4-18. This end cap is made by aluminium alloy 6082-T6 and weighs

100g. Since commercially available electrical multi-wire high pressure feedthroughs are too large for this application, a special feedthrough structure has been designed for the end cap, as shown in Figure 4-19, which uses a ring piece of PVC (Polyvinyl Chloride) material as an insulator and 8 metal screws (3 for motor power wires and 5 for motor hall effect sensors) as conductors. Instead of an accumulator, a piece of compliant power steering hose is attached on the top of the end cap to supplement the volume in the motor cavity, which is shown as an accumulator symbol in Figure 4-11. This accumulator hose is 15 cm long and is shown in Figure 4-20. The compliance this accumulator hose provides helps to maintain pressurisation at a constant value despite small change in volume (e.g. due to temperature changes).

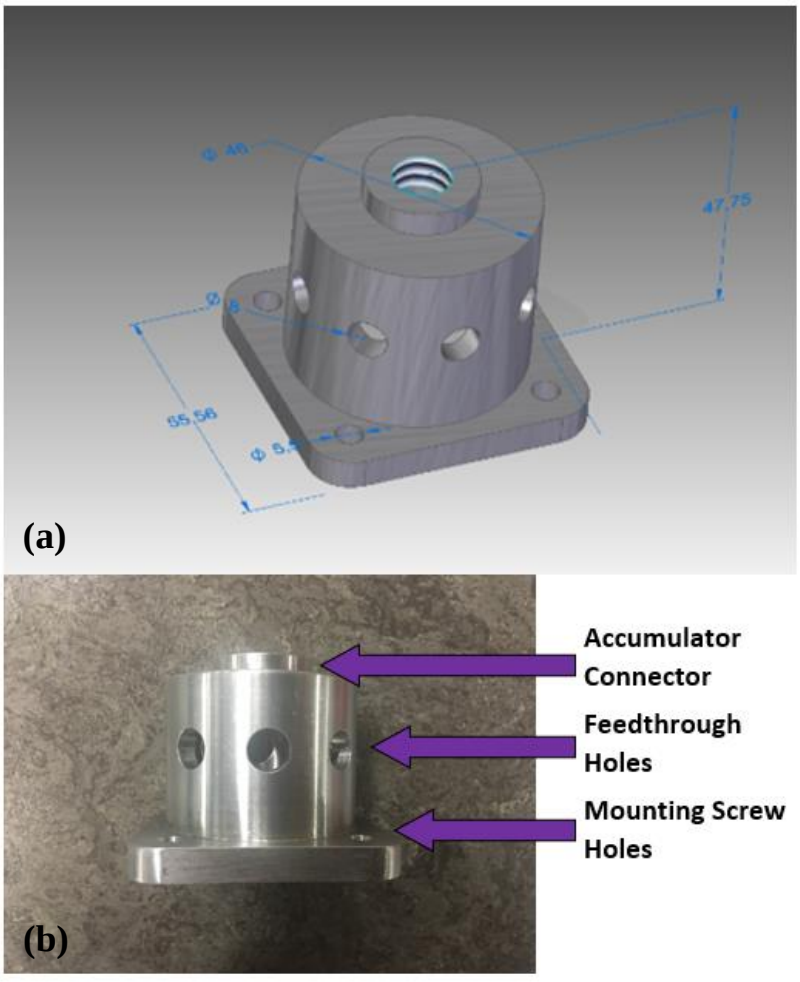

Figure 4-18: End cap for motor end seal. (a) End cap model and dimensions. (b) Side view of the End cap

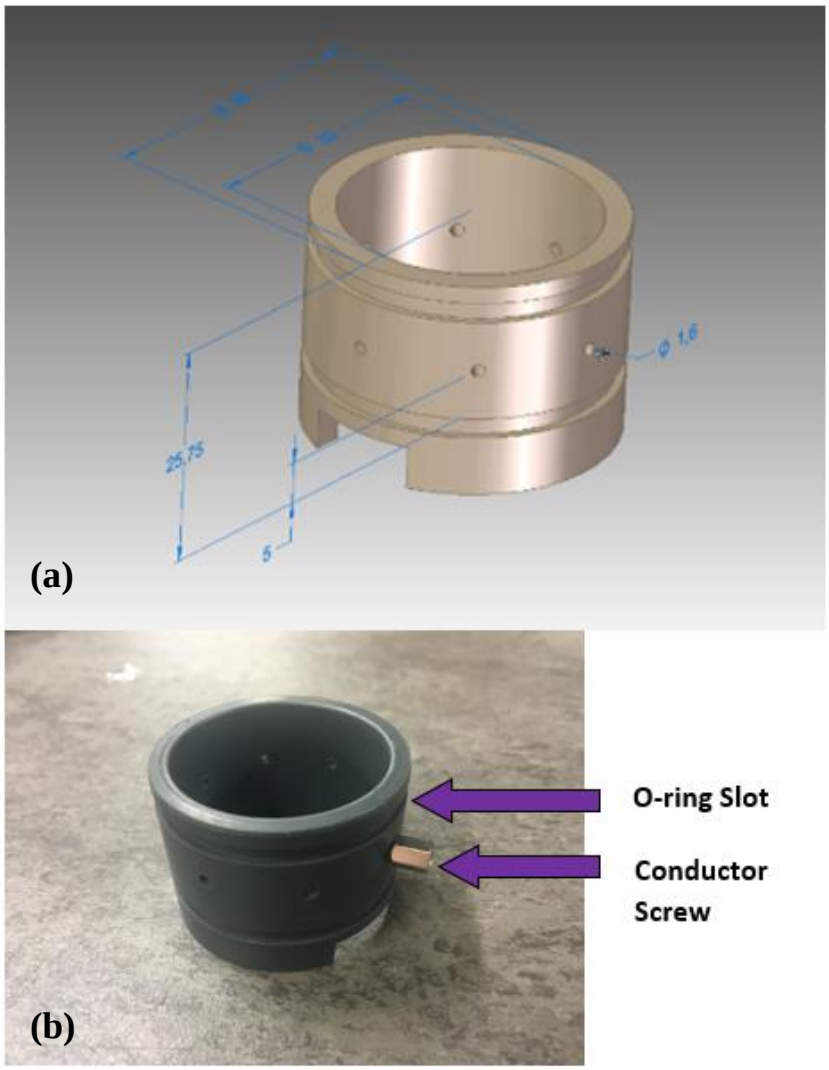

Figure 4-19: PVC ring for feedthrough. (a) PVC ring model and dimensions. (b) Side view of the PVC ring with conductor screw.

Figure 4-20: Accumulator hose (with fitting and cap).

4.3.4. Valves

The bypass restriction valves (valve ① and valve ② in Figure 4-11) used in the MK4 prototype are Echelon valves provided by Chas A Blatchford & Sons Ltd [9]. These manually controlled restrictor valves are used to replace the micro motor controlled restrictor valves in the MK3 prototype. According to the MK2 and the MK3 patient trial experience, the setting of the restrictor valves could be pre-tuned for different amputees before testing and kept the same through the test, unless the walking speed or slope are significantly changed. A drawing of the Echelon valve is shown in Figure 4-21.

The 3 way/2 position solenoid valve shown in Figure 4-11 (valve ③) is working as an on/off valve with its R port blocked. In the passive phase, the valve is normally open without consuming energy. The fluid can only flow in the direction which is from port P to port C, and then goes through the restriction valve (valve ①) in that bypass line. In the active PF phase, this on/off valve will be closed, port P and R blocked, to avoid flow loss through the bypass restriction valve (valve ①). This small 3 way valve is provided by Lee Products Ltd. and is shown in Figure 4-22 [79]. Its specification is summarized in Table 4-7.

Without the on/off valve above, the other bypass restriction valve ② is activated or closed by a micro check valve (valve ④). This check valve is provided by Chas A Blatchford & Sons Ltd. and is shown in Figure 4-23.

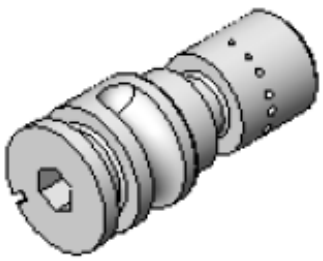

Figure 4-21: Echelon bypass restriction valve [9].

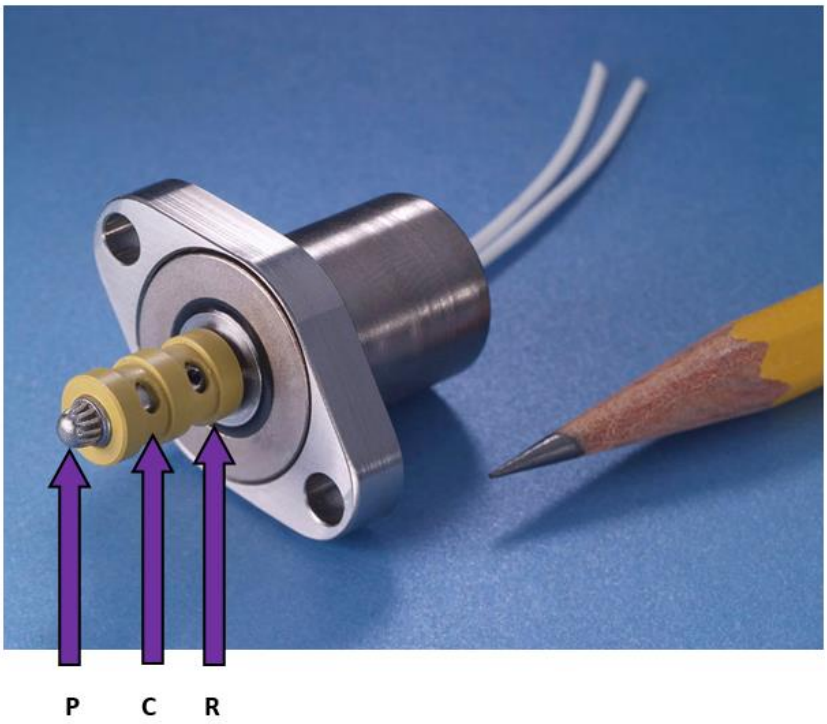

Figure 4-22: LEE 250 Series Solenoid Valve [79].

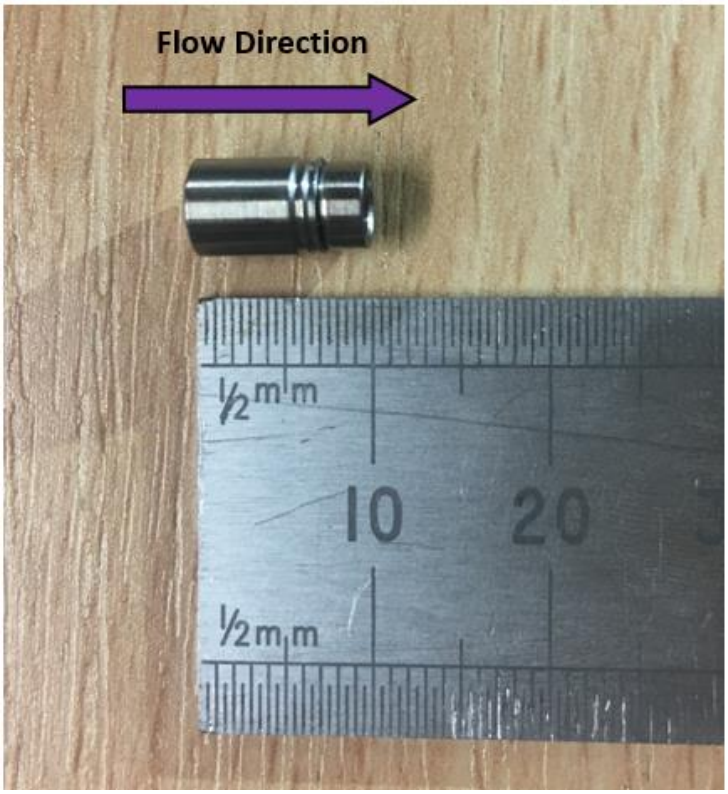

Figure 4-23: Micro check valve used in MK4 prototype.

Table 4-7: Specification of the LEE 250 Series Solenoid Valve [79].

LEE valve 250 Series Solenoid Valve [79] SDBA2531012B	
Nominal System Pressure	207 bar
Configuration	3- Way N.O.
Weight	45 g
Current Drain	0.4 A
Max Operating Voltage	15 V
Pull-In Voltage	12 V
Response Time: Pull-in	0.040 s max
Response Time: Drop-out	0.015 s max

4.3.5. Manifold Blocks

A motor-pump mounting plate is designed by the author, which is shown in Figure 4-24. This piece is made from aluminium alloy 6082-T6 and weights 330g.

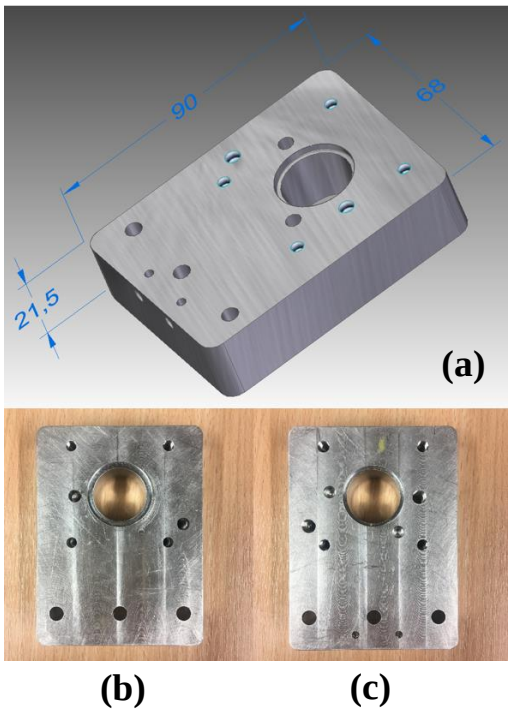

Figure 4-24: Motor-pump mounting plate. (a) Motor-pump mounting plate model and dimensions. (b) Motor side. (c) Pump side.

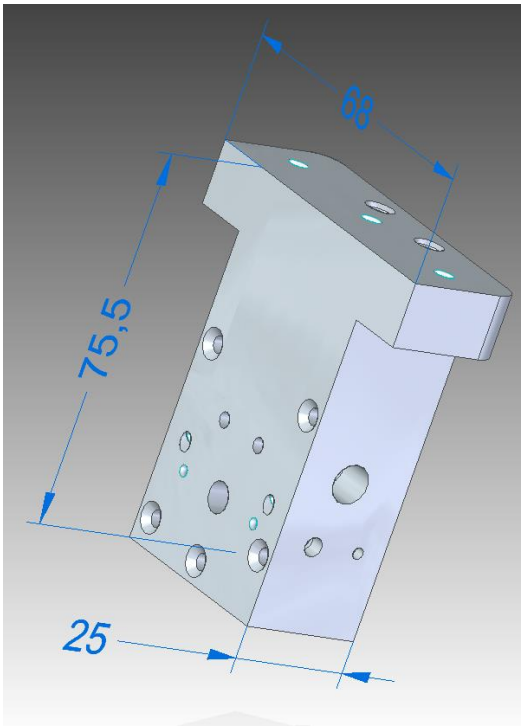

Figure 4-25: T shape manifold block.

Another T shape manifold block has been designed by the author, which is shown in Figure 4-25. This piece is made from aluminium alloy 6082-T6 and weighs 278g. All the valves are assembled in this manifold block. This T block is designed to be the minimum size.

4.3.6. Coupling

In this compact motor-pump unit, the accumulator hose is placed at the top of the motor end cap and is interconnected with the pump case drain via the motor internal chamber and the shaft chamber between motor and pump. All these internal spaces are closed and pressurised, which means once the motor-pump unit has been assembled on the mounting plate in Figure 4-24, the access to the coupling will be lost. A special coupling has been machined which has a compliant core and a reinforce ring on the outside as shown in Figure 4-26. The compliant core to couple the motor and pump is made from Nylon and the reinforce ring is made from steel.

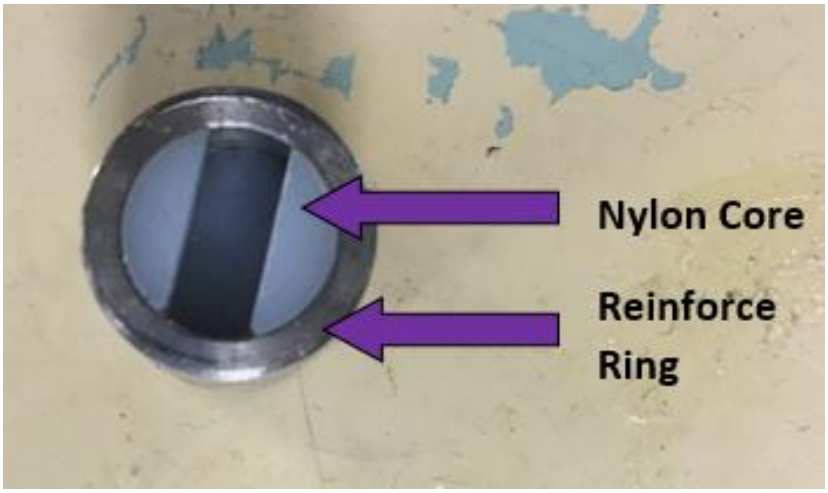

Figure 4-26: Coupling with Nylon core and reinforce ring.

4.4. Sensors and Electronics

4.4.1. Pressure Transducers

Two pressure transducers are used to monitor the pressure difference across the pump. Their locations are shown in Figure 4-12 and Figure 4-27. The pressure transducers are shown in Figure 4-28 and their specification are summarized in Table 4-8.

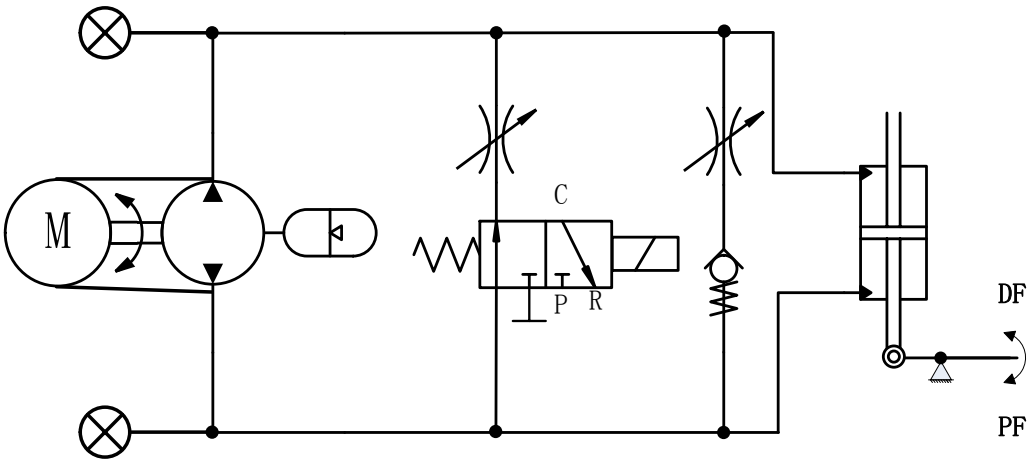

Figure 4-27: Circuit diagram with pressure transducers of MK4 prototype.

Figure 4-28: Variohm EPT1200 Pressure Sensor [78].

Table 4-8: Specification of Variohm EPT1200 Pressure Sensor [78].

Variohm Pressure Sensor [78] EPT1200-K-1600-B-4-A	
Pressure Range	0 ~ 160 bar
Accuracy	< +/- 0.8%
Supply Voltage	10 ~ 32VDC
Current Drain	< 10 mA
Weight	25 g

4.4.2. Displacement Sensor

The ankle rotation is another important measurement for both the EHA testing and prosthesis control. Instead of the hall effect sensor used in the previous prototype, a magneto-inductive displacement sensor with better linearity has been used. The displacement sensor and its magnet target are shown in Figure 4-29 and its specification is summarized in Table 4-9.

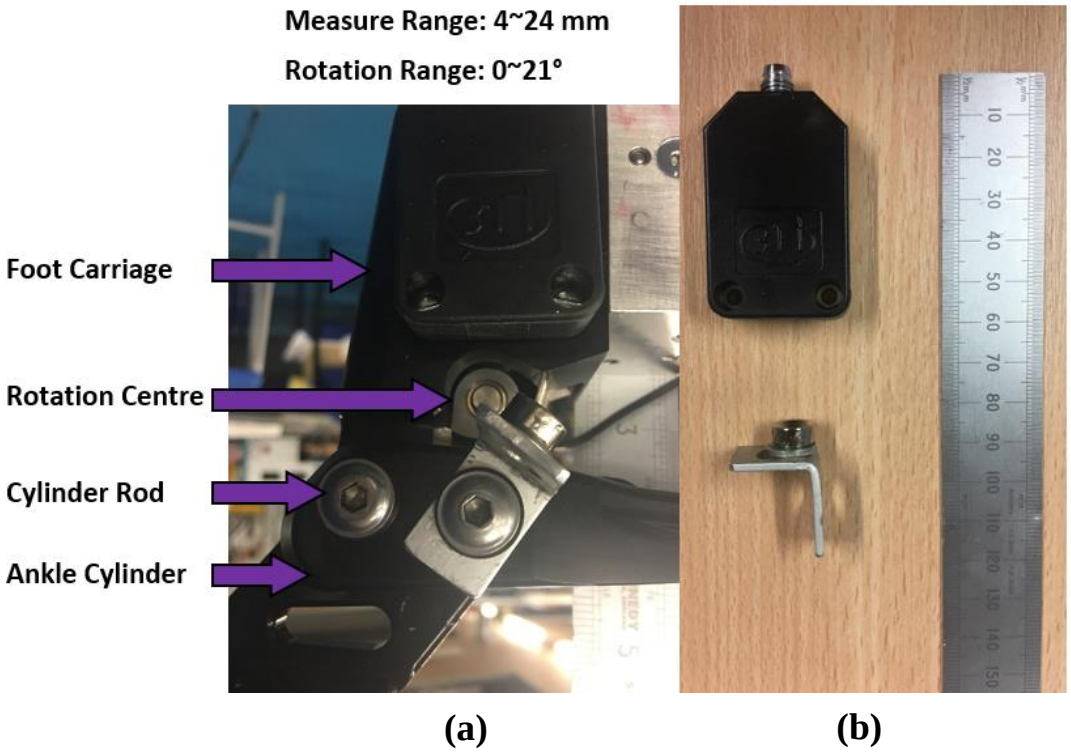

Figure 4-29: Displacement sensor used in MK4 Prototype. (a) Displacement sensor and its magnet target on MK4 Prototype. (b) Maximum measurement distance.

Table 4-9: Micro-Epsilon MDS-45-K-SA displacement sensor specification [85].

Micro- Epsilon Magneto-inductive Displacement Sensor [85] MDS-45-K-SA	
Magnet Target Diameter	10 mm
Mearing Range (Selected Target)	4 ~ 24 mm
Linearity	< +/- 3%
Supply Voltage	12 ~ 30 VDC
Current Drain	< 20 mA
Weight	25 g

The position where the displacement sensor and its magnet target is mounted on the MK4 prototype is shown in Figure 4-29. The distance between the displacement sensor and its magnet target shown in Figure 4-29 is approximately the maximum measuring distance and the ankle is at the maximum DF angle (reference 0°). The

relationship between the displacement sensor output voltage and the ankle rotation angle is calculated from a straight line approximation fitting the recorded data shown in Figure 4-30.

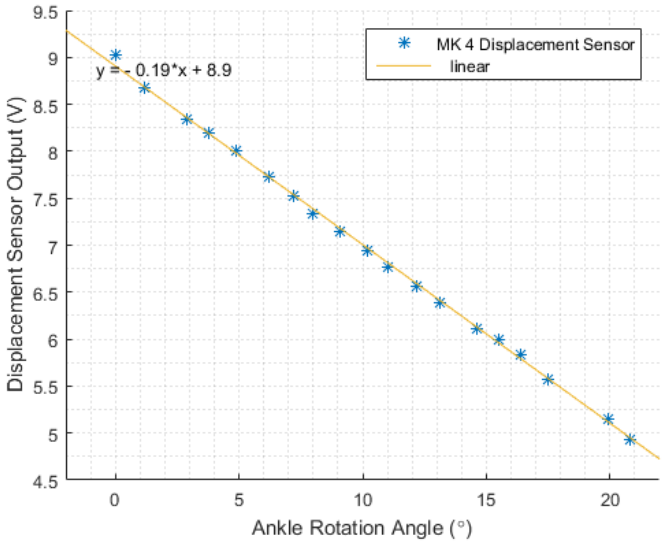

Figure 4-30: Displacement sensor output and ankle rotation angle relation.

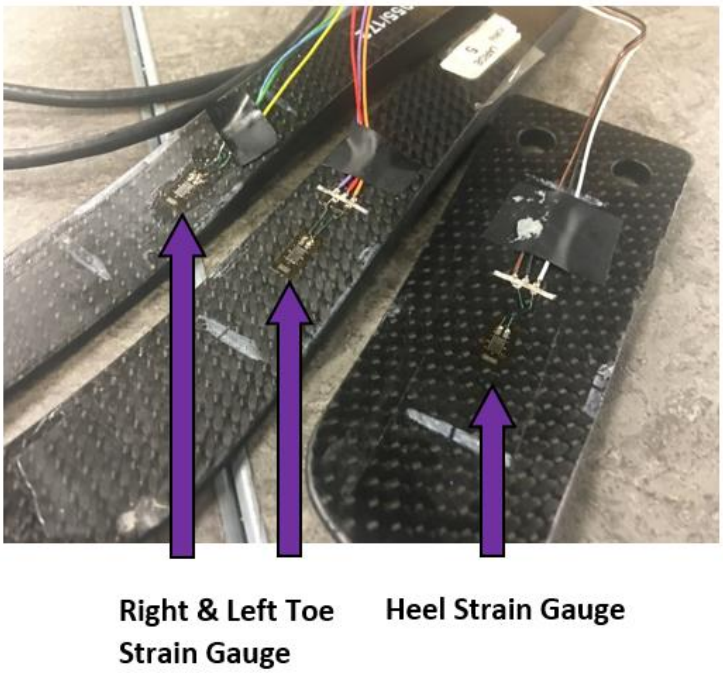

Figure 4-31: Foot spring with strain gauges.

4.4.3. Foot Spring Strain Gauges

Three strain gauges have been attached on the foot spring as shown in Figure 4-31. The strain change between the foot springs (heel spring and toe springs) indicates the movement of the body weight location, which will be used as one of the trigger signals for powered PF and helps to detect the intent of the amputee.

4.4.4. Shank IMU

An IMU provided by Chas A Blatchford & Sons Ltd. has been attached to the MK4 prototype as shown in Figure 4-32. This IMU is glued on the ankle cylinder, which will record the shank rotation and acceleration in the three axes of its own coordinate system. By processing the IMU output signal, the shank orientation and the position in the global coordinate system can be obtained.

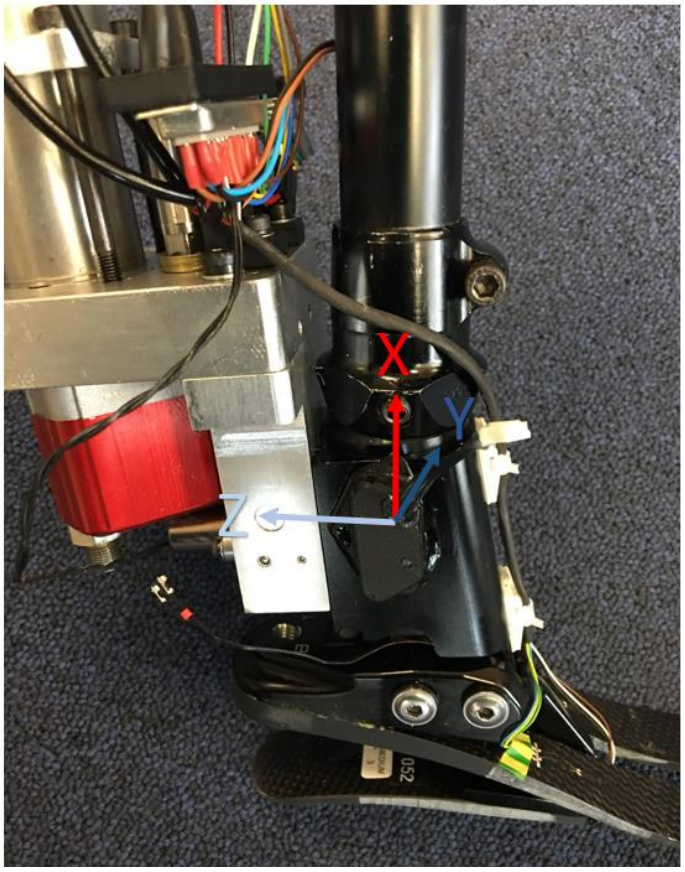

Figure 4-32: IMU on MK4 prototype and its coordinate.

4.4.5. CRIO Controller

A CRIO from National Instruments is used to run the control program and record data. The CRIO and the modules used in the MK4 prototype are shown in Figure 4-33 and their specifications are summarized in Table 4-10.

Table 4-10: The CRIO and the modulus used in MK4 Prototype [74, 86-89].

National Instruments CRIO [74]	
cRIO-9076	
Run control program and Record data	
Communicate with computer via RJ-45 Ethernet Port	
Receive data from IMU via RS0232 Serial Port	
Supply Voltage	9 ~ 30 VDC
Weight	643 g
Current Drain	< 1 A
SLOT 1: NI 9505 DC Brushed Servo Drive [86]	
Drive the solenoid on/off valve	
Record the solenoid /on/off valve current drain	
Drive Voltage	12 V
Weight	155 g
Continuous Current	5 A
SLOT 2: NI 9235 120Ω Quarter Bridge Completion [87]	
Measure strain gauges on the foot spring	
Weight	153 g
Excitation Voltage	2 V
SLOT 3: NI 9205 Analog Input Module [88]	
Receive signals from: motor controller, pressure transducers and displacement sensor	
Weight	158 g
Input Range	+/- 10 VDC
SLOT 4: NI 9264 Analog Voltage Output Module [89]	
Send motor enable and demand speed signals to motor controller	
Weight	156 g
Output Range	+/- 10 VDC
Current Drive	+/- 16 mA all channels max

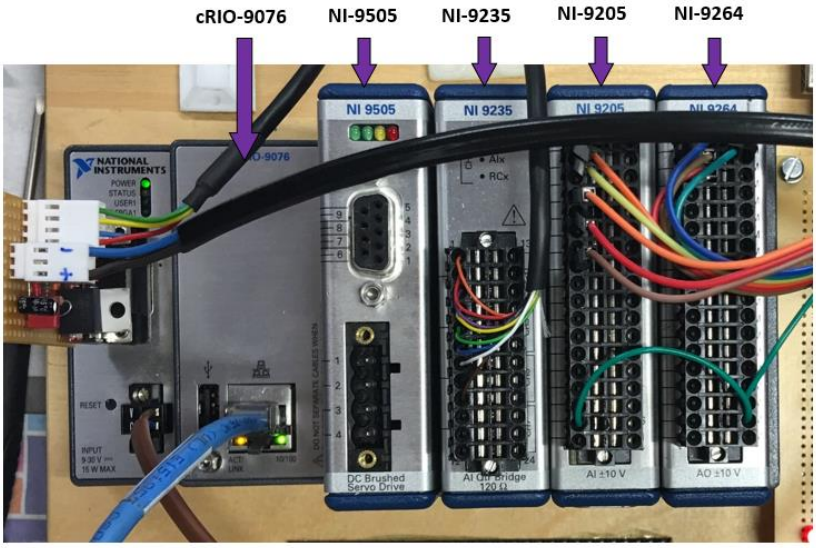

Figure 4-33: CRIO and the modules used in the MK4 prototype [74, 86-89].

4.4.6. Motor Controller

The Maxon EC-i 40 Brushless DC Motor used in MK4 is controlled by an ESCON servo controller from Maxon [90]. This motor controller is shown in Figure 4-34 and its specification is summarized in Table 4-11. The motor control mode (closed loop or open loop speed control, or current control) can be chosen using the ESCON studio software [91], which can also be used to tune the controller parameters, customize the input/output signals and monitor the motor performance.

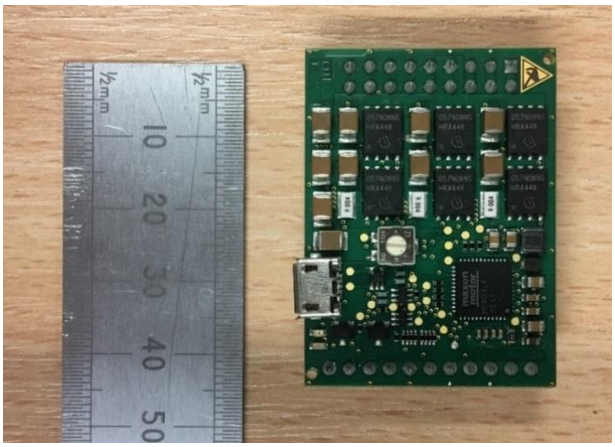

Figure 4-34: ESCON Module 50/5 Servo Controller [90].

Table 4-11: Specification of the ESCON Module 50/5 Servo Controller [90].

ESCON Module 50/5 Servo Controller [90] P/N 438725	
Specification	
Nominal Operating Voltage	10 ~ 50 VDC
Output Current (continuous)	5 A
Output Current (peak)	15 A
Maximum Voltage Drop	1 V @ 5A
Weight	12 g
Voltage Output	
Hall Effect Sensor Supply Voltage	+5 VDC
Brushless DC Motor Connections	Motor winding W1, W2, W3
Signal Input	
Digital Input 1	Motor enable
Analog Input 1	Demand speed
Hall Effect Sensor Signals	Motor hall effect sensor H1, H2, H3
Signal Output	
Analog Output 1	Actual motor current
Analog Output 2	Actual motor speed

4.4.7. Battery & Voltage Converters

A 48V / 2Ah battery [92] is used to power the motor and all the electronics. The battery is shown in Figure 4-35 and its specification is summarized in Table 4-12. The supply voltage from the battery is converted to different voltages by a voltage converter board which is shown in Figure 4-36. The 12 V supply is for the IMU (via its own voltage converter) and the on/off valve (via NI 9505 Servo Drive module [86]). The 15 V supply is for the CRIO, displacement sensor and pressure transducers.

Table 4-12: Specification of Mountfield 48V/2Ah Lithium-Ion battery [92].

Mountfield Lithium-Ion Battery [92] MBT4820Li	
Battery Type	Lithium-Ion
Output Voltage	48 VDC
Capacity	2 Ah
Weight	1.1 kg

Figure 4-35: Mountfield 48V/2Ah Lithium-Ion battery [92].

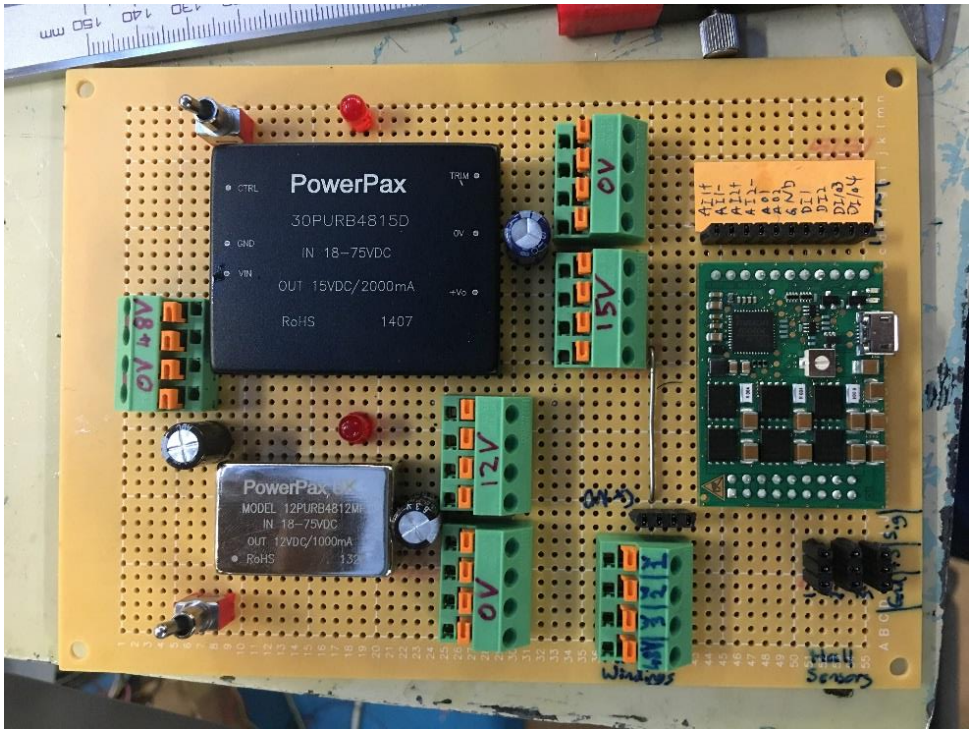

Figure 4-36: Voltage converter board used in MK4 prototype.

4.4.8. Accessories

An emergency stop button has been inserted between the battery and the motor controller, which is used to disable the motor.

A wireless router is connected on the RJ-45 Ethernet Port of the CRIO controller, which allows the operator to control and monitor the system remotely.

4.5. Bench Test and Results Analysis

4.5.1. Bench Test Introduction and Setup

In order to examine the performance of the ankle prosthesis EHA in different load conditions, a series of bench tests have taken place. To fulfil the power level of human ankle when level walking, the EHA powered ankle prosthesis is required to output a peak PF torque of 110 Nm (Table3-6) and rotate the ankle to the maximum 23° within 300ms in the active PF phase (Figure 3-1). Since the real load on human ankle when level walking is difficult to imitate, the EHA was demanded to move the ankle against a constant load. By analysing the bench tests results and comparing with the motion requirements of healthy subject ankle, whether this EHA powered ankle prosthesis can provide sufficient powered PF assist in patient trial can be estimated.

The bench test rig is shown in Figure 4-37. The ankle prosthesis EHA is mounted upside down to lift a lever. Weights could be hung at the end of the lever to provide a certain load. The PF of the prosthesis will lift up the weights. The horizontal distance between the hanging weights and the pivot is $L_l = 27$ cm and horizontal distance between the actuator rod and the pivot is $L_a = 2$ cm, which gives the lever ratio $R_l = L_l/L_a = 13.5$.

Figure 4-37: Bench test rig.

A list of test settings are shown in Table 4-13. Since only the PF direction is loaded in the test, only the bypass restriction valve ① in Figure 4-11 is in use. The heaviest weights used in the bench tests (16kg) is equivalent to 43 Nm of ankle load torque. This load torque is lower than the peak ankle PF moment when level walking, but it is considered to be enough for analysing the EHA performance since it is a constant high load. Another three load levels (0, 5 and 10kg weights) are chosen to examine the performance of the ankle prosthesis EHA in different load conditions.

Table 4-13: MK4 bench test settings.

No	Weights (kg)	Equivalent Load Torque (Nm)	Demand Speed (rpm)	Demand Time Length	On/off Valve	Bypass Restriction Valve
1	0	0	1000 2000 3000 4000 5000 6000	1000 ms for Each Demand Speed	Close	Fully close
2	5	13				
3	10	27				
4	16	43				

4.5.2. MK4 Bench Test Results Analysis

The test results with highest demand motor speed (6000rpm) at different load levels are shown in Figure 4-38, 4-39, 4-40 and 4-41 respectively. The high motor demand speed (6000rpm) is intended to maximize the motor output power, which will maximize the EHA output power in different load conditions to help estimate the ankle prosthesis performance in level walking condition. As shown in these four figures, the maximum recorded motor speed is 4300rpm in Figure 4-38 (0kg of weights) which is limited by the battery output voltage (48V) and the voltage limitation of the motor controller [90]. The time gap between the start of the demand signal at 0.1s and the start of the motor rotation is resulted from the time delay for the motor controller switching from disabled mode to enabled mode. This will not affect the performance of the EHA powered ankle prosthesis in the amputee trial when the motor controller is set at enabled mode at all time.

The pressure difference shown in the bench test results was measured across the pump. In each of these four load conditions, there is a pressure difference peak to accelerate the motor-pump and the load. After the acceleration period, the EHA lifts the load at a constant speed and pressure difference. The pressure difference and motor current increase with the increment of the load. The increments of the load reduce the maximum motor speed from 4300rpm at 0kg of weights to 3000rpm at 16kg of weights. As a result, it takes longer for the EHA to plantarflex the ankle to the maximum PF angle in high load conditions, which is 300ms at highest load condition. When the actuator piston reaches the end, the high pressure was observed to shoot up to the highest value, double the nominal pressure, and the low pressure drops to 0 bar, which is shown as the peak pressure difference at 0.43s in Figure 4-41(b). The efficiency analysis of the MK4 prototype at highest load (43Nm) is summarized in Table 4-14.

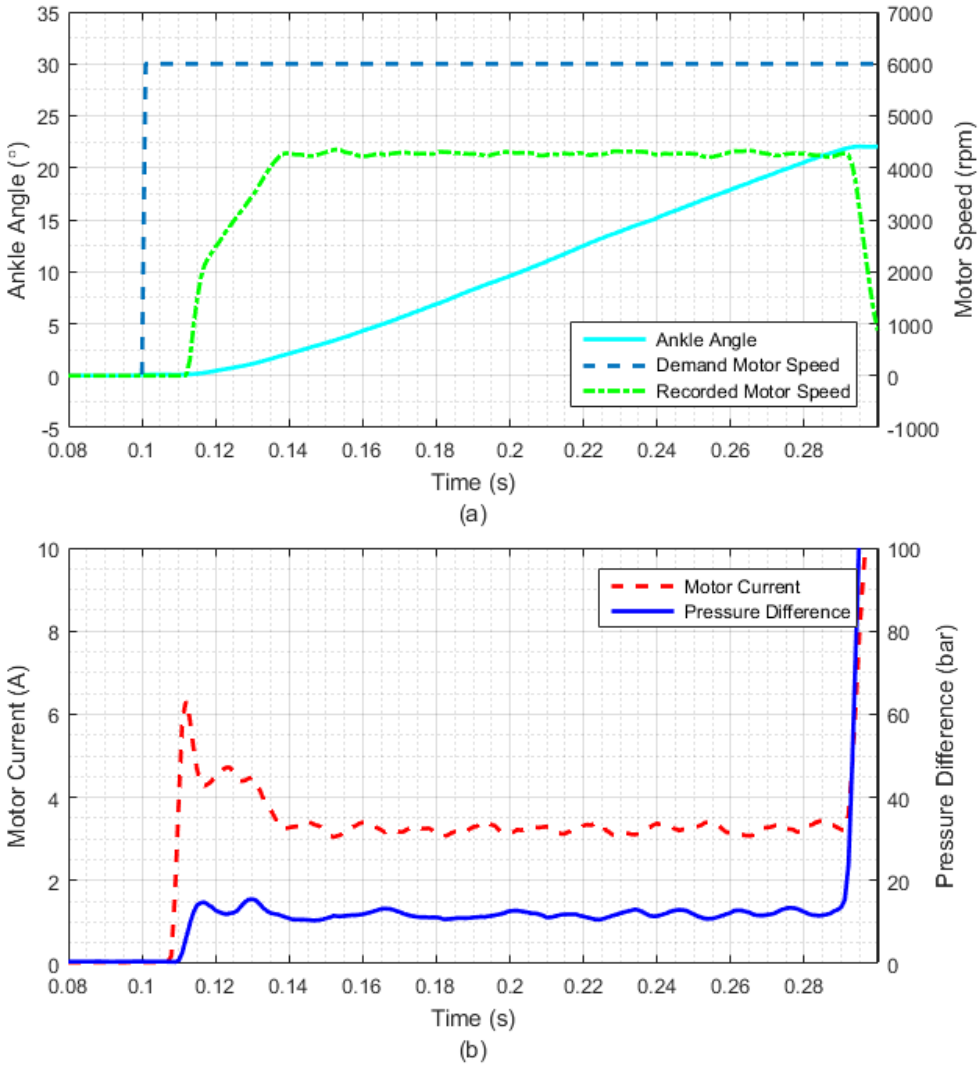

Figure 4-38: Bench test with 0kg load. (a) Ankle PF angle and motor speed. (b) Motor current and pressure difference across pump.

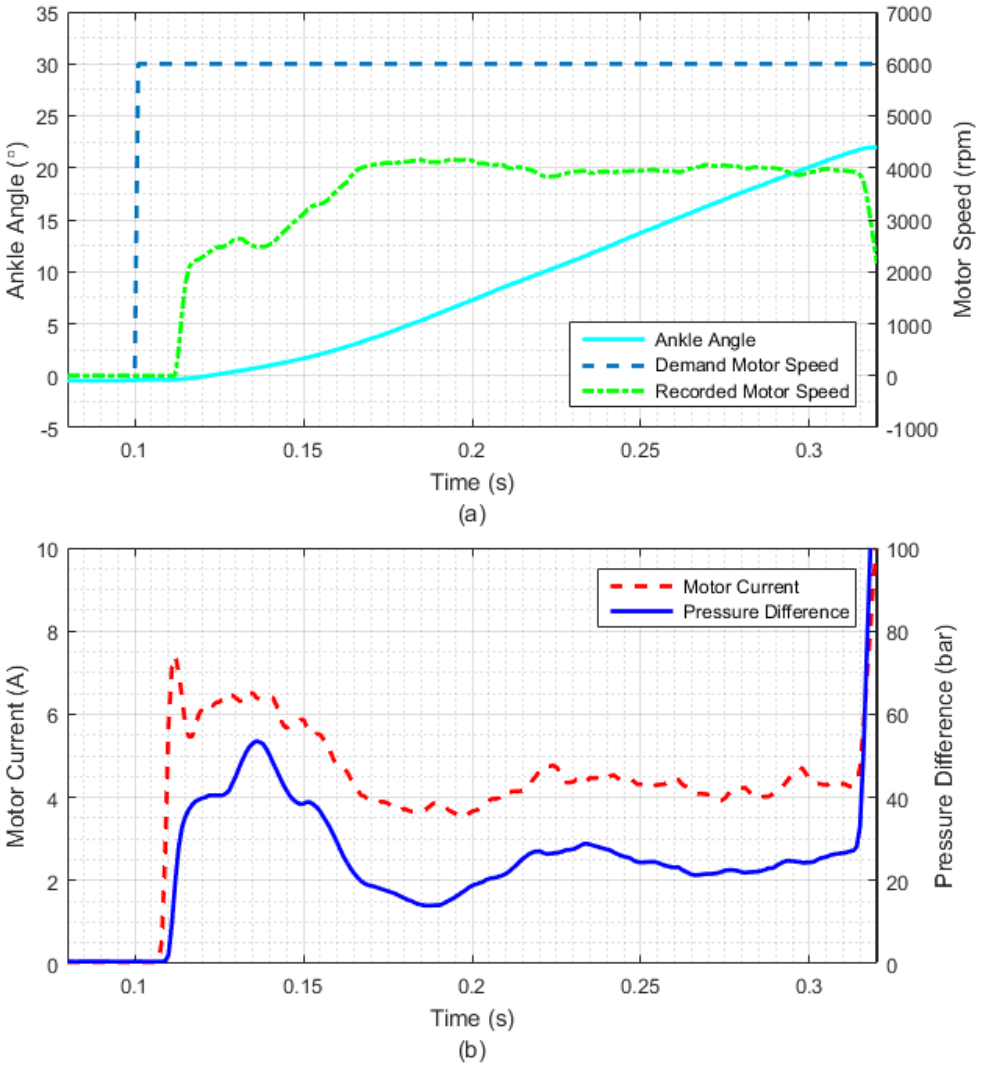

Figure 4-39: Bench test with 5kg load. (a) Ankle PF angle and motor speed. (b) Motor current and pressure difference across pump.

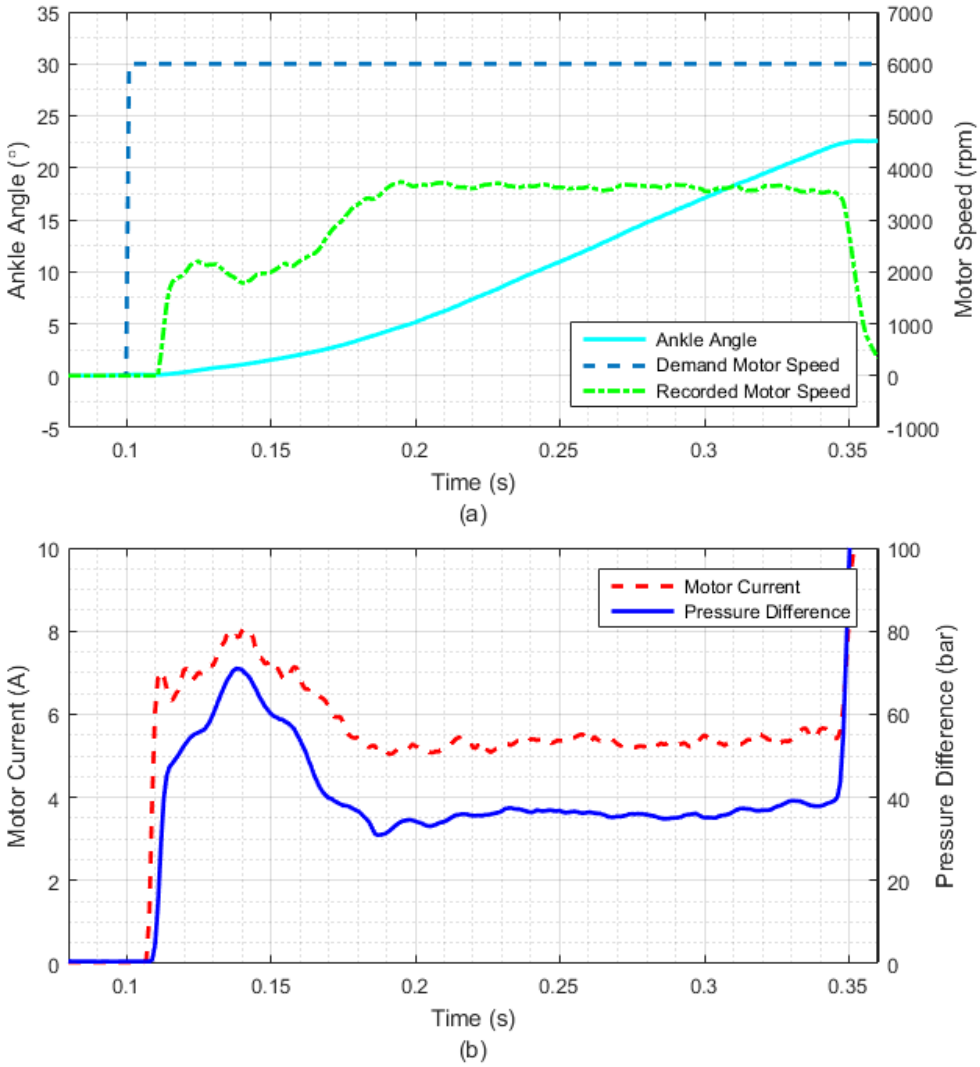

Figure 4-40: Bench test with 10kg load. (a) Ankle PF angle and motor speed. (b) Motor current and pressure difference across pump.

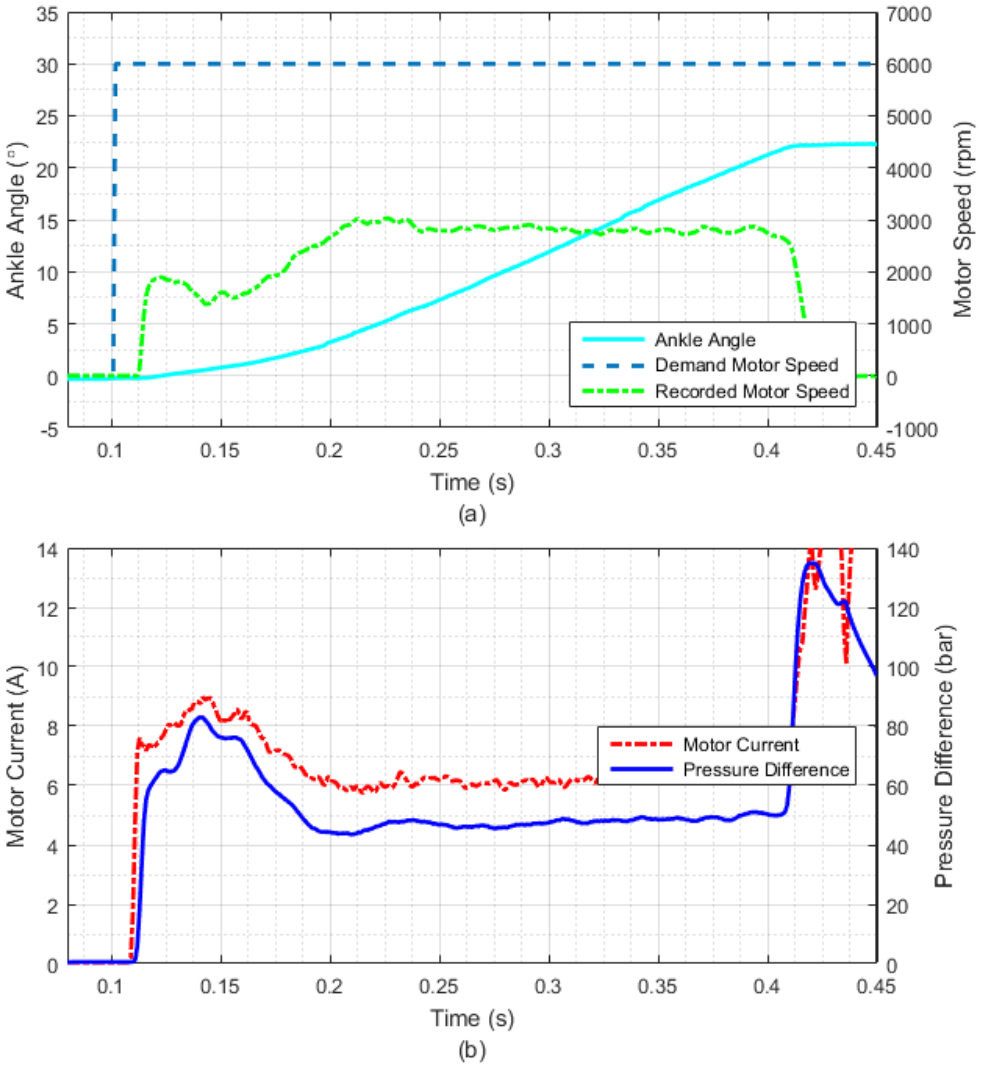

Figure 4-41: Bench test with 16kg load. (a) Ankle PF angle and motor speed. (b) Motor current and pressure difference across pump.

Table 4-14: The efficiency analysis of the MK4 prototype.

Motor Input	Motor Output		Pump Output		Actuator Output		Load
Recorded	Theoretical	Actual	Recorded		Theoretical	Actual	Recorded
Current	Torque	Torque	Pressure		Torque	Torque	Weight
6 A	0.558 Nm	0.329 Nm	46 bar		58 Nm	43 Nm	16kg
59%							
			74%				
Mechanical Efficiency: 44%							
	Recorded		Theoretical	Actual	Recorded		
	Average Speed		Flow Rate	Flow Rate	Average Speed		
	2600 rpm		19.2 cc/s	16.88 cc/s	77 °/s		
	Volumetric Efficiency: 86%						
Overall Efficiency: 38%							

The theoretical motor output torque T_{mt} in Table 4-14 is calculated by:

$$T_{mt} = IK_t \qquad (4-1)$$

where I is the recorded motor current and K_t is the motor torque constant (91mNm/A). The actual motor torque T_{ma} is calculated by:

$$T_{ma} = \Delta PD \qquad (4-2)$$

where ΔP is the recorded pressure difference across the pump and D is the pump displacement. As shown in the table, the friction loss in the motor-pump unit in this continuous high load situation is significant, which is about 0.23 Nm.

The theoretical actuator output torque T_{at} is calculated by:

$$T_{at} = \Delta PA_aL_a \qquad (4-3)$$

where A_a is the annulus area. The actual actuator output torque T_{aa} is calculated by:

$$T_{aa} = M_lgL_l \qquad (4-4)$$

where M_l is the mass of the load weights and g is the acceleration due to gravity.

The theoretical pump output flowrate is calculated by:

$$Q_{pt} = \omega_m D \qquad (4-5)$$

where ω_m is the recorded average pump speed. The actual pump output flow rate Q_{pa} is calculated by:

$$Q_{pa} = \omega_l L_a A_a \qquad (4-6)$$

where ω_l is the recorded angular speed of the lever. Since the on/off valve is closed in this test, the bypass flow rate loss is assumed to be 0. The majority of the flowrate loss is assumed to be from the pump leakage.

4.5.3. Comparison with Healthy Subject Ankle Motion

According to Figure 3-1 and Table 3-1, the ankle joint moment of a healthy subject shows a peak at the beginning of the powered PF phase (terminal stance phase). This peak moment will quickly be released before the toe leaves the ground. According to Table 3-6, the peak moment is about 110Nm, which requires 87bar pressure difference across the actuator cylinder. In the bench test results (16kg) shown in Figure 4-41, the motor-pump generates about 80bar to accelerate the load weights. After the actuator reaches the end stroke, the motor-pump unit keeps pushing the piston and holds a pressure difference of about 100bar for 700ms. From the torque aspect, the MK4 prototype is able to meet the ankle peak moment requirement.

As shown in Table 4-14, the average output ankle rotation speed is 77°/s, which is smaller than the ankle PF speed requirement for level walking of a healthy subject (104°/s as shown in Table 3-6). But the bench test described in this chapter is under a constant high load situation, and the EHA is expected to re-accelerate the ankle along with the release of the ankle joint moment before the toe-off.

By comparing the MK4 bench test result with the ankle output requirement of a healthy subject, the MK4 powered ankle prosthesis prototype is expected to be able to power the ankle PF movement in the terminal stance phase to assist level walking.

4.6. Conclusions

The development of the EHA powered ankle prosthesis prototype is presented in this chapter. The actuation system at the ankle joint weights 2.2 kg, including a 100 W brushless DC motor, a 0.45 cc/rev bi-directional gear pump, control valves, a specially designed end cap assembly, manifold blocks, etc. The sensors applied on the prototype include two pressure transducers, a displacement sensor, foot spring strain gauges and a shank IMU. A 2 Ah, 1.1 kg Lithium-Ion battery, a CRIO controller and other electronics are held in a backpack.

According to the bench test results on the MK4 prototype, the EHA can rotate the ankle at 77 °/s average speed against 43 Nm continuous high load for at least 1s, which is expected to provide sufficient power output to assist level walking for a 70 kg amputee.

Chapter 5

Amputee Trial with Passive Ankle

An amputee trial with the ankle functioning passively has been undertaken in order to gather ankle sensor signals for the controller design. The ankle prosthesis prototype was worn by a 70 kg transtibial amputee. The servomotor was controlled to zero velocity in this trial. The test setup is described at the beginning. Several stance conditions have been tested by the amputee and the ankle sensor signals have been recorded and analysed for the comparison with the treadmill walking results. The ankle prosthesis prototype was then tested at 14 different speeds from 2.8 km/h to 5.4 km/h. The sensor signal characteristics of a typical gait are presented and discussed. The relationship between the different walking speeds and ankle sensor signal features is summarized at the end of this chapter.

5.1. Test Introduction and Setup

Referring to the previous patient trial on the MK3 prototype [80], the window for the powered walking assistance in the terminal stance phase is limited and the start time point is very important to make the most use of the power from the EHA. To improve the controller design and study the passive prosthetic ankle performance, it is important to find the relationship between the characteristics of the sensor signals and the ankle motion. The characteristics of the ankle sensor signals should be collected in different conditions according to the daily activities of the amputee, e.g. stand-still, standing at different stance conditions and walking at different speeds. In order to obtain a control signal for the powered ankle with active PF assist, which should have clear features in level walking especially in the heel strike phase, the characteristics and range of ankle sensor signals should be analysed by comparing between different activities. The comparison and analysis of the ankle sensor signals at different walking speeds are intended to study the ankle performance in passive mode, direct the future controller design and gather information for the amputee trial with powered ankle.

The MK4 prototype has been tested by a 70 kg transtibial amputee in the indoor test site in Chas A Blatchford & Sons Ltd. The ankle prosthesis prototype was connected to the below-knee socket of the transtibial amputee by an adapter and a tube. The mounting angle of the ankle could be adjusted using the adapter within the adjustment range. When the amputee first put on the ankle prosthesis prototype, the mounting angle was tuned to give a comfortable inversion/eversion angle and the maximum available dorsiflexion/plantarflexion rotation range. The DF and PF restrictor valves have been adjusted to meet the damping requirement of the amputee when the ankle is in the passive mode.

5.2. Stance Test

The amputee with the ankle prosthesis prototype has been asked to do several movements in both double stance and single stance conditions including: standing still, dorsiflexing the ankle prosthesis to the maximum angle, plantarflexing the ankle prosthesis to the maximum angle, standing on the healthy leg only and standing on the prosthetic leg only. The recorded ankle rotation angle and the strain gauge signals for stand-still are shown in Figure 5-1.

The ankle rotation angle in Figure 5-1 is recorded by the displacement sensor (Figure 4-29). The output voltage of the displacement sensor has been converted into rotation angle as shown in Figure 4-30. In this passive ankle amputee trial, the ankle angle when the amputee was standing uprightly has been set to be the reference, i.e. 0°, and PF has been set to be the positive rotation direction. As shown in Figure 5-1, the ankle rotation angle drifts away 0° within a small range. The heel strain gauge signal and the average toe strain gauge signals are measured by the strain gauges shown in Figure 4-31 and recorded by the NI 9235 quarter bridge completion module on the CRIO shown in Figure 4-33 [87]. Since the left toe and the right toe strain gauge signals were observed to be approximately the same through the tests, the average strain gauge signal of the left toe and the right toe is shown in Figure 5-1 instead of the separate toe strain gauge signals. Because of the lack of information of the foot spring stiffness, the recorded voltage signal from the quarter bridge completion module has been plotted, which means the strain gauge signals are indicating the force change on the foot springs but not showing the actual force value. When the amputee is standing still and upright, both the feet (healthy and prosthetic) share the body weight (double-stance condition).

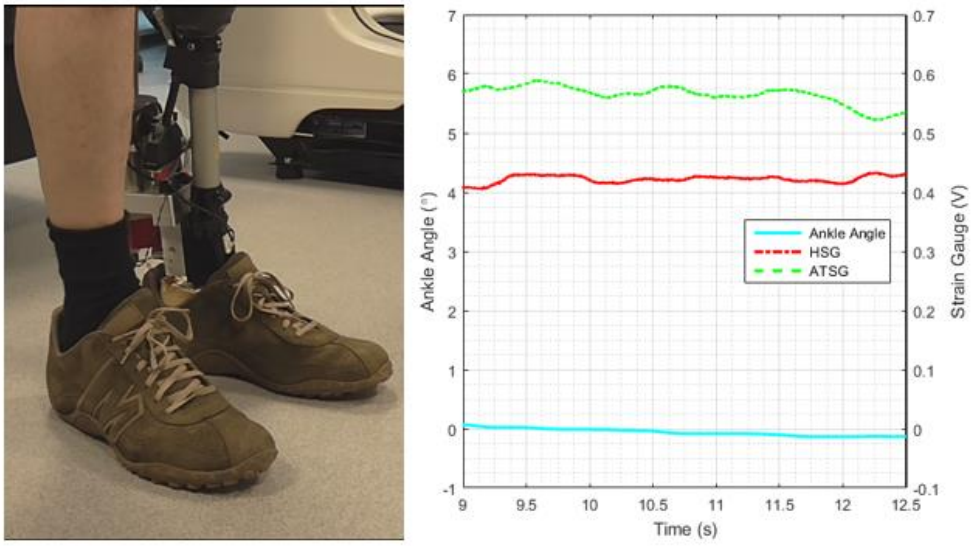

(a) **(b)**

Figure 5-1: Ankle rotation angle and the strain gauge signals at stand-still. (a) Stand-still posture. (b) Ankle angle and foot strain gauge signals.

For the prosthetic foot, both the toe springs and the heel spring are bearing the body weight. The strain gauge signals are approximately constant since the amputee's body is stable in this short period shown in Figure 5-1. For a long standing time, the strain gauge signals were observed to vary within +/- 0.1 V in the tests.

Figure 5-2 shows the ankle sensor signals when the amputee rotated the ankle prosthesis from the maximum DF position to the maximum PF position. The maximum DF angle is -10.0° and the maximum PF angle is 14.4°. In the maximum DF period, the majority of the body weight is acting on the toe springs and the average toe strain gauge signal is about 1.25 V. When the amputee dorsiflexes the ankle (18.5~19.5s), the body weight moves from the toe springs to the heel spring and the healthy leg, which results in the decline of the average toe strain gauge signal and the slight increase of the heel strain gauge signal. When the ankle has been plantarflexed to the maximum, the majority of the body weight is supported by the healthy leg and both the strain gauge signals are less than 0.6 V.

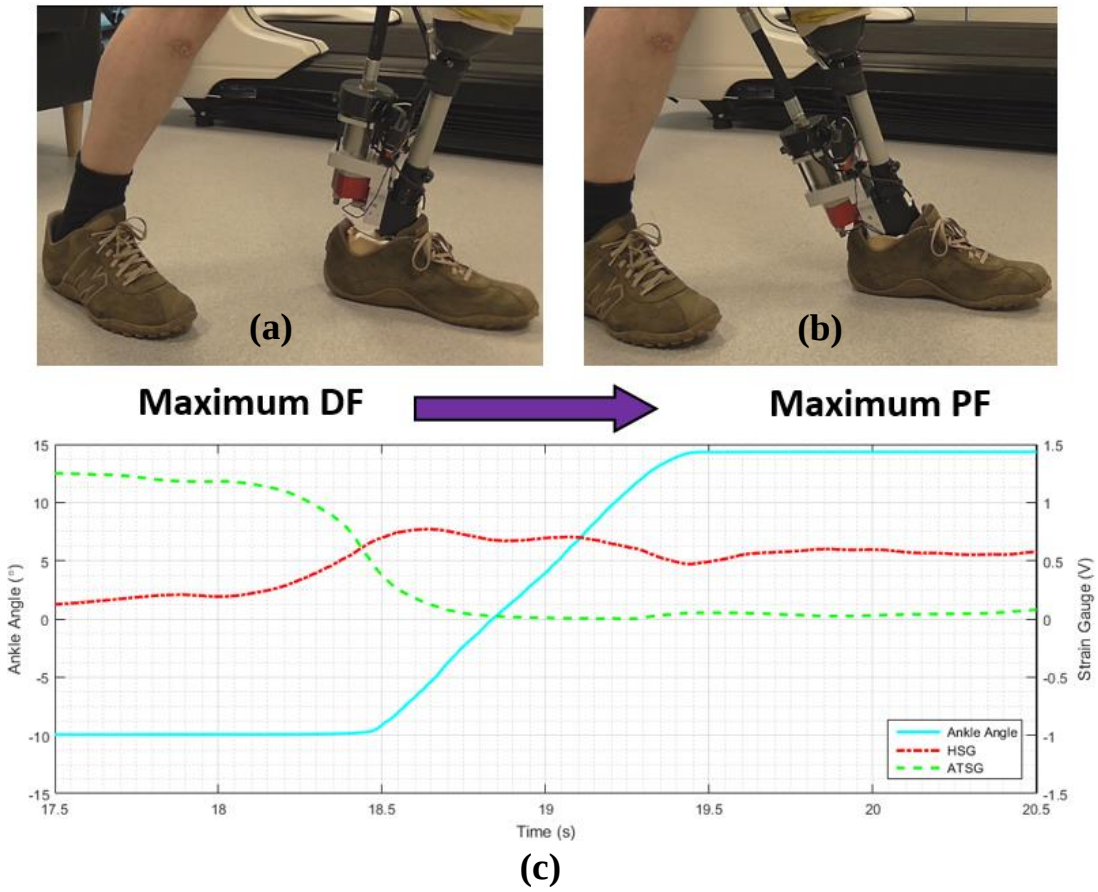

Figure 5-2: Ankle rotation angle and the strain gauge signals of the maximum DF and the maximum PF situation. (a) Maximum DF posture. (b) Maximum PF posture. (c) Ankle angle and foot strain gauge signals.

Figure 5-3 shows the ankle rotation angle and the strain gauge signals of the single leg stance. When the prosthetic foot is lifted up, the strain gauge signals are zero and the ankle angle is constant. Both the average toe strain gauge and the heel strain gauge signals increase when the stance leg is switched to the prosthetic leg. The strain gauge signals vary since it is difficult for the amputee to balance on the prosthetic leg.

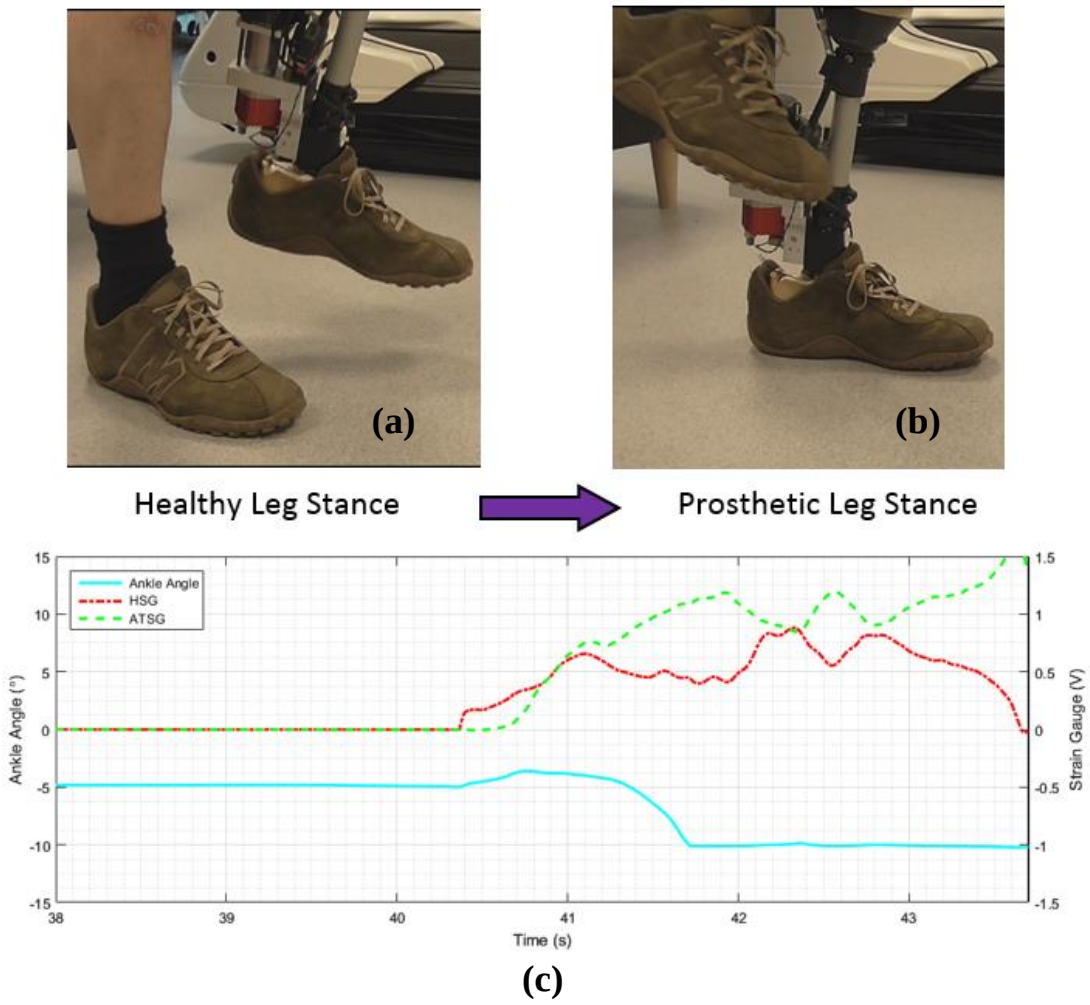

Figure 5-3: Ankle rotation angle and the strain gauge signals of single stance situations. (a) Single stance on healthy leg posture. (b) Single stance on prosthetic leg posture. (c) Ankle angle and foot strain gauge signals.

5.3. Treadmill Walking with the Passive Ankle

According to the amputee who took part in this test, his daily walking speed range is from 2.8 km/h to 4.8 km/h and a walking speed of 3.8 km/h is considered to be a nominal and comfortable speed for him. In the treadmill walking test with the passive

ankle, the treadmill speed increments by 0.2 km/h from 2.8 km/h to 5.4 km/h and the amputee walks for about 100 seconds at each speed.

A typical gait cycle at 3.8 km/h treadmill speed is shown in Figure 5-4. The ankle starts to passively plantarflex once the heel contacts the ground at the beginning of the heel strike phase (phase <1>). The PF of the ankle joint piston pushes the hydraulic fluid through the passive-PF bypass restriction valve (valve ② in Figure 4-11). The damping generated by the restriction valve prevents the ankle from plantarflexing too quickly. In the heel strike phase (phase <1>), a peak pressure difference across the ankle joint cylinder of 22 bar occurs, which corresponds to the HSG signal peak (1.45 V) in the bottom graph. The grey bar between phase <1> and phase <2> indicates the finish of the heel strike when the ankle plantarflexes to the maximum in this gait. Compared to the stance test results shown in Figure 5-2, only half the ankle rotation range is used. At the beginning of phase <2>, the HSG signal and the ATSG cross each other, which indicates the bodyweight is moving forward. Within phase <2>, the damping is controlled by the passive-DF bypass restriction valve (valve ① in Figure 4-11). Phase <2> and phase <3> are divided by the grey bar, which indicates the time point when the ankle dorsiflexes to the maximum. Due to the lack of the powered PF movement in the terminal stance phase, the ankle joint keeps the maximum DF position until the start of the next gait. The ATSG signal keeps increasing in phase <2> and peaks at 2.65 V in phase <3> after the ankle piston reaches the end stroke. Phase <4> is the swing phase and the dark grey bar between phase <3> and phase <4> indicates the toe-off.

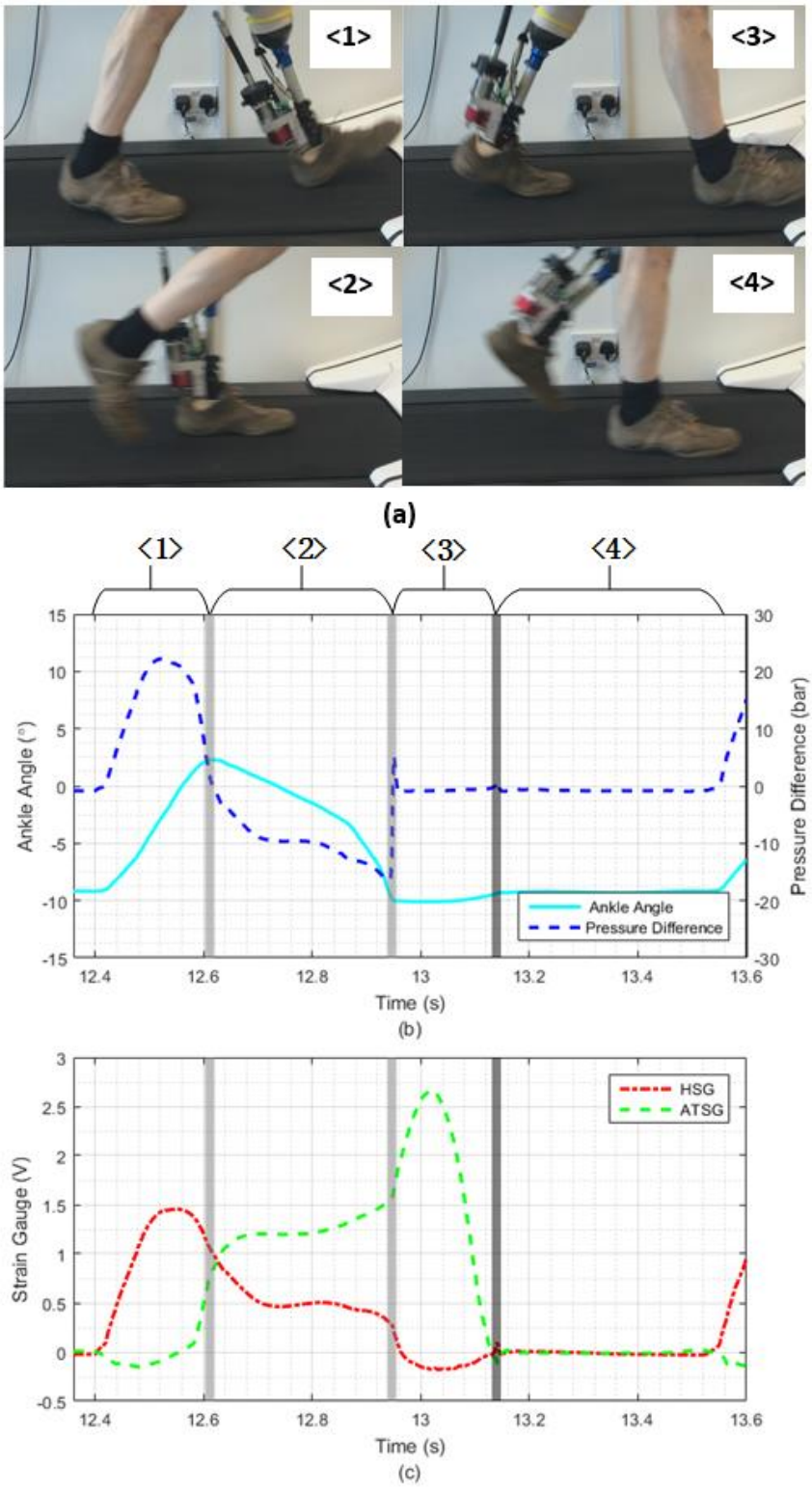

Figure 5-4: A typical gait with passive ankle at 3.8km/h walking speed. (a) Different phases in a gait cycle. (b) Ankle angle and pressure difference across pump. (c) Foot strain gauge signals.

The gait length, heel strike length, peak value of HSG signal and the maximum PF angle of the tests at different walking speeds are summarized in Figure 5-5. On each box in Figure 5-5, the red line at the centre indicates the median, and the bottom and top edges of the box indicate the 25th and 75th percentiles respectively. The bottom and top whiskers extend to the most extreme data points which are not considered outliers. The '+' symbol indicates the outliers. Figure 5-5 (a) shows the gait duration of the amputee at different walking speeds. The start of a gait is found by the heel strain gauge signal increasing above a certain value (0.29 V). The gait duration is the time length between the start of two adjacent gaits. As can be seen from Figure 5-5 (a), the gait duration reduces along with the increasing walking speed when the walking speed is higher than 3.2 km/h. According to [18], the gait cycle duration of a healthy subject when level walking is 1.11+/-0.05 s, which is similar to the gait duration for 3.4~4 km/h walking speed with the passive ankle. When the amputee is walking faster than 3.6 km/h, he is matching the treadmill speed by increasing step frequency, which may be linked to the lack of the powered PF phase before toe-off and the weight increment from ankle prosthesis prototype. The gait is more ‘relaxed’ when walking at low speed (2.8~3.2 km/h), which results in less correlation between walking speed and gait duration, indicating that the amputee is sometimes adjusting step length to achieve the walking speed change.

Figure 5-5(b) compares the percentage of the heel strike phase duration in a gait cycle at different walking speeds. The heel strike duration is defined as the time length between the start of the gait (the heel strain gauge signal increasing above 0.29V) and the time point when the heel strain gauge signal and average toe strain gauge signal cross each other (grey bar between phase <1> and phase <2> in Figure 5-4). As shown in the figure, the heel strike duration is significantly reduced when high speed walking.

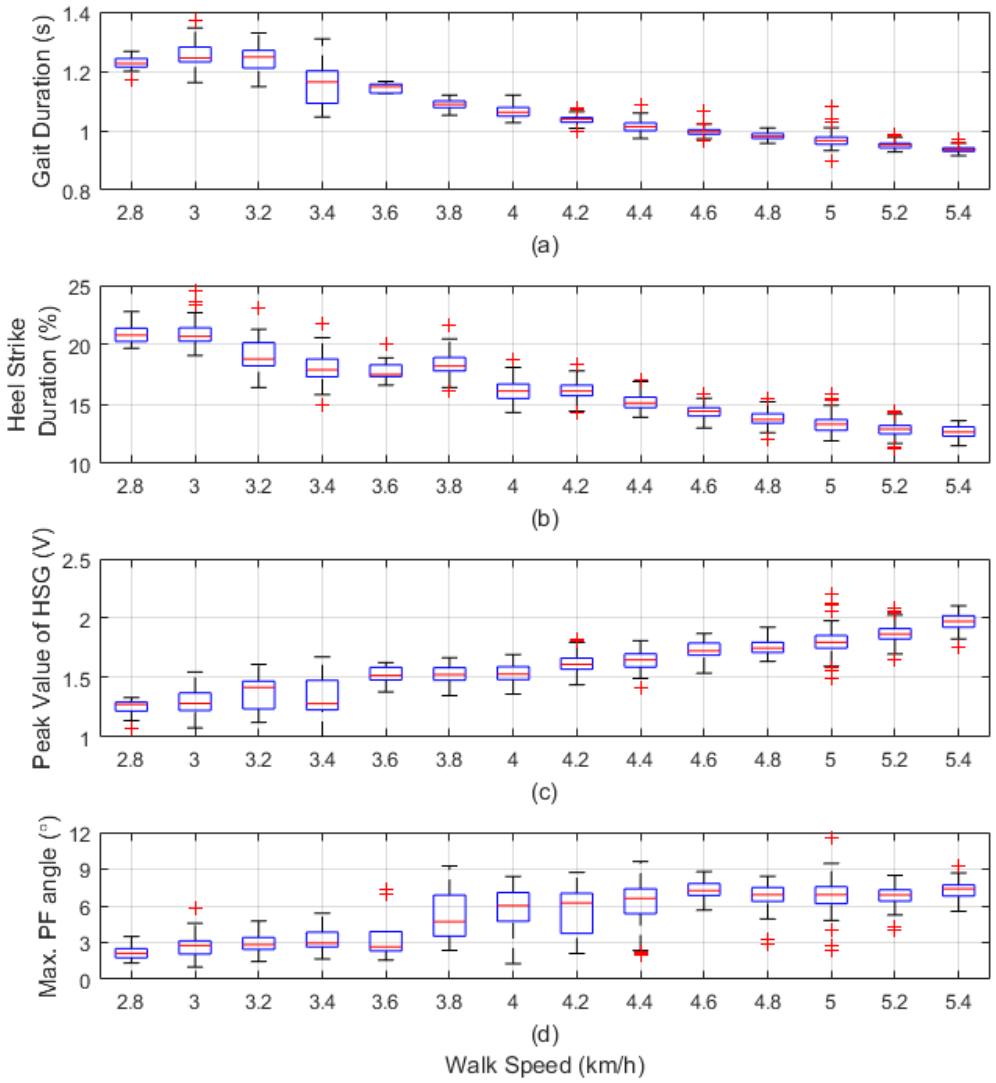

Figure 5-5: Summary of the passive ankle treadmill walking test results. (a) Gait duration. (b) Heel strike duration. (c) Peak value of HSG in heel. (d) Maximum ankle PF angle.

The maximum heel strain gauge signal always occurs in the heel strike phase as shown in Figure 5-4 and the peak values at different walking speeds are shown in Figure 5-5(c). A high peak heel strain gauge signal indicates a heavy heel strike impact. Compared to the heel strain gauge signal in double-stance (Figure 5-1), the peak value of the heel strain gauge signal is about three times as high even for the slowest walking speed.

The bypass restriction valves were pre-set before the amputee trial and kept the same through the tests. But the damping provided by the bypass restriction valve is found to be insufficient when walking at high speed according to the feedback of the amputee. As shown in Figure 5-5(d), the maximum PF angle when walking at high speed (4.6~5.4 km/h) is about 4 times that of low speed walking.

5.4. Conclusions

Walking characteristics with a passive ankle were measured using foot spring strain gauges, a displacement sensor and pressure transducers in different stance conditions and different speed treadmill walking tests. The passively operated ankle prosthesis prototype can provide damping in the stance phase. Without the powered assist from the ankle prosthesis, the amputee reported that it was difficult to maintain a high walking speed. By comparing the measurements in the stance situation and the walking situation, some critical thresholds required by the controller can be derived, which will be further discussed in chapter 6. The inter-subject deviations have not be studied, due to the availability of the test amputee, which will limit the applicability of the controller for powered ankle prosthesis.

Chapter 6

Timing Control

The start time point of the powered PF assist is critical for the powered ankle prosthesis performance. The timing control method for the MK4 prototype is presented in this chapter, which is based on heel strike recognition and a middle stance time delay. The heel strike can be recognised using the strain gauge signal features obtained in the patient trial with the passive ankle. To avoid false triggering of the powered PF assist by other movements, a heel strike recognition method is proposed which is based on the difference between the heel strain gauge and the average toe strain gauge signals. The time delay in the middle stance phase can be adjusted to fit different walking speeds. A reference middle stance time delay is found according to the patient trial results. The servo motor is controlled by a closed loop speed controller and is demanded to run at the maximum speed in the powered PF and DF phases. The control program algorithm and the selected thresholds are summarized in a flow chart. A pressure difference signal based timing control method is also proposed and discussed at the end of the Chapter.

6.1. Timing Control Introduction

In order to assist the PF in the terminal stance phase efficiently and safely, the start time of the powered PF phase is critical and a timing control program to trigger the powered PF is necessary. Powering the PF too early will result in the power being wasted to lift the body upwards instead of push the body forwards. Powering the PF too late will result in a lack of support of the body weight, which means the amputee is in danger of stumbling.

According to the ankle sensor signals obtained in chapter 5, the heel strike has unique features which could be used to recognise the walking intention of the amputee and to demarcate the start of a gait. The peak of the heel strain gauge (HSG) signal in particular clearly shows the impact on the heel (Figure 5-4). The powered PF assist should be started when most of the body weight is moved to the toe spring at the end of the middle stance phase (phase <2> in Figure 3-1), which could be triggered by a time delay after the HSG signal crosses the average toe strain gauge (ATSG) signal. According to the patient trial results using the MK3 prototype [80], the powered PF assist requires the full power output from the EHA.

The control program is compiled using Labview [93] and is running on the CRIO shown in chapter 4 [74]. The control program scans the sensor readings from the FPGA (field-programmable gate arrays) in the CRIO at 1000 Hz, which will give about 250 readings in the heel strike and mid stance phase respectively. The high scan rate is important since the amputee is sensitive about the start time point of the powered PF. According to the feedback of the amputees who took part in the patient trial described in [80], 5 ms variation can be clearly perceived by the amputee.

6.2. Heel Strike Recognition

As shown in Figure 5-4, the HSG shows a clear peak in the heel strike. This signal peak could be recognised by setting two detection point, as shown in Figure 6-1.

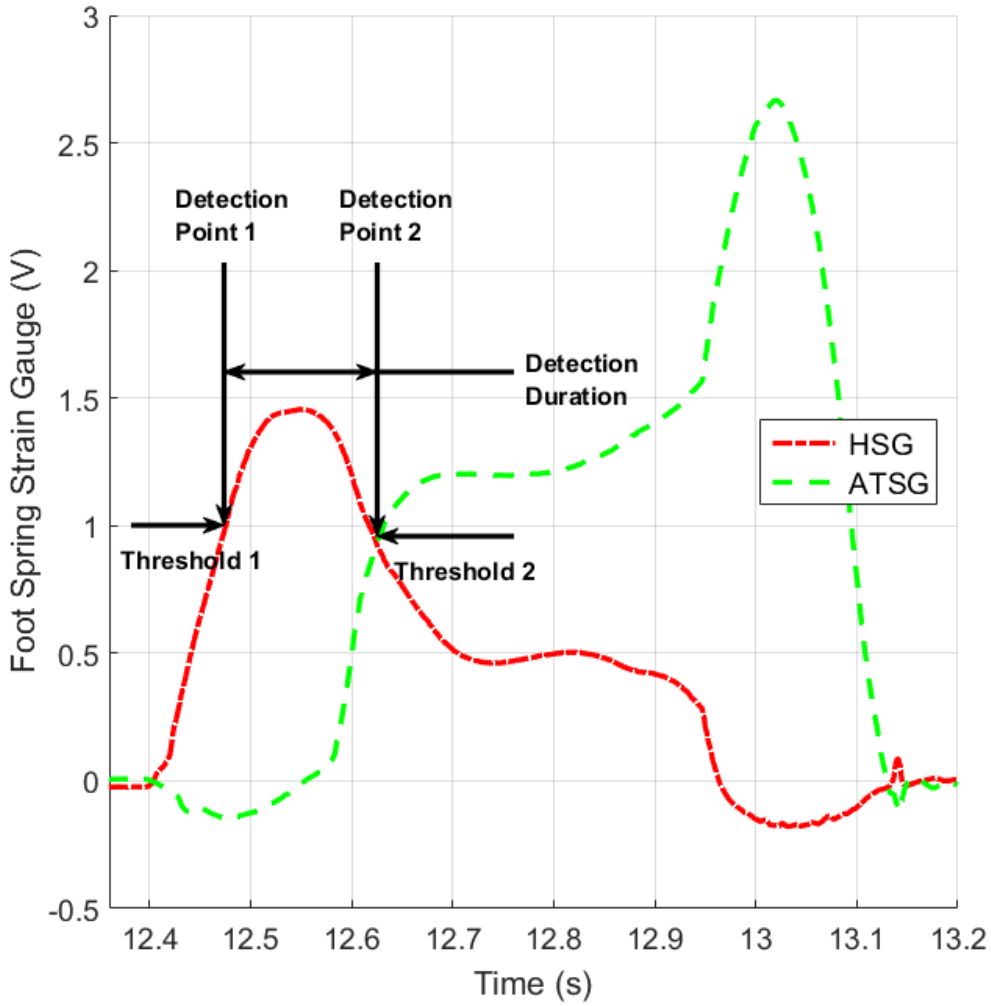

Figure 6-1: Detection points of heel strike recognition.

Table 6-1: The strain gauge signals comparison between different movements

		HSG Peak (0.1V)	HSG Minimum (0.1V)	HSG-ATSG Peak (0.1V)	HSG-ATSG Minimum (0.1V)	Duration (ms)
Heel Strike	Low speed walk	10~15	5 (after peak)	10~15	-7 (after peak)	<250
	High speed walk	15~20		15~20		<150
Double Stance	Balanced body weight	3~5		-2		-
	Unbalanced body weight	15	0	-2		uncertain
Single Stance	Full body weight	15	10	15	0	
	No body weight	0	0	0	0	-
Stamp	Stamping on the heel	20	0 (after peak)	20	0 (after peak)	<100

The first detection point is when the HSG signal crosses a pre-set threshold 1 upwards and the second detection point is when the HSG signal crosses a pre-set threshold 2 downwards. But this simple method may cause false recognition since the HSG signal peak also exists in other movement, e.g. single stance on the prosthetic foot or stamping on the prosthetic heel. The strain gauge signal comparison between several different movements is summarized in Table 6-1.

The peak and minimum HSG values of the heel strike in low speed and high speed walking in Table 6-1 are obtained from the amputee trial with passive ankle (Figure 5-5). To recognise the heel strike, threshold 1 at the first detection point should be lower than the peak HSG value and threshold 2 at the second detection point should be higher than the minimum HSG value after peak within the detection duration.

The strain gauge values of the balanced body weight in double stance situation is when the amputee is standing still as shown in Figure 5-1. The unbalanced body weight in

double stance situation is when the amputee is swaying the body between the prosthetic foot and the healthy foot. The HSG values in this situation are considered to change between the two extreme single stance situations (full body weight and nobody weight on the prosthetic foot as shown in Figure 5-3). When the amputee is releasing the body weight from the prosthetic foot, it is possible to falsely trigger the powered PF assist since both the thresholds will be crossed, which will cause the amputee to fall over. This possibility can be reduced by using the difference value between the HSG and the ATSG (HSG-ATSG in Table 6-1) instead of the HSG signal alone.

The HSG-ATSG signal in a typical gait in shown in Figure 6-2. In the beginning of the heel strike during level walking, HSG-ATSG signal is approximately the same as the HSG signal since the toe spring is not contacting the ground. After the peak value, the HSG-ATSG signal drops below zero rapidly since the heel spring is released and the body weight is switched to the toe springs. In the unbalanced body weight double stance situation described above, the HSG-ATSG is estimated to change around zero based on the observation in the patient trial. In other words, HSG-ATSG in the stance phase when level walking directly indicates the body is moving forwards, which means that the heel strike can be distinguished from standing.

According to the patient trial results shown in Figure 5-3, the HSG and the HSG-ATSG vary significantly in the extreme single stance situation which could also falsely trigger the powered PF. But this situation is not expected to happen in daily activities of the amputee.

Another movement may cause the false trigger of the powered PF assist is when the amputee is stamping on the heel spring of the prosthetic foot. The sizes of the HSG and HSG-ATSG signals are estimated based on the observations in the patient trial. During stamping, the HSG-ATSG signal can also peak to a high value and return to zero due to the quick release of the heel spring compression. One of the methods to distinguish this stamp movement from the heel strike is by setting threshold 2 of the HSG-ATSG signal at detection point 2 to be negative. But this methods resulted in several missed triggers of the powered PF in the patient trial. Another method which

is applied in the controller is adding another judgement condition at detection point 2. When the HSG-ATSG crosses the second threshold, the HSG signal is also required to be higher than a certain value to make sure the heel is on the ground.

The duration between the two detection points are also important to avoid false triggering of the powered PF assist. The second threshold should be crossed within a certain time after the first threshold is passed to avoid false triggers which result from the body weight not being evenly supported by the heel spring and the toe springs

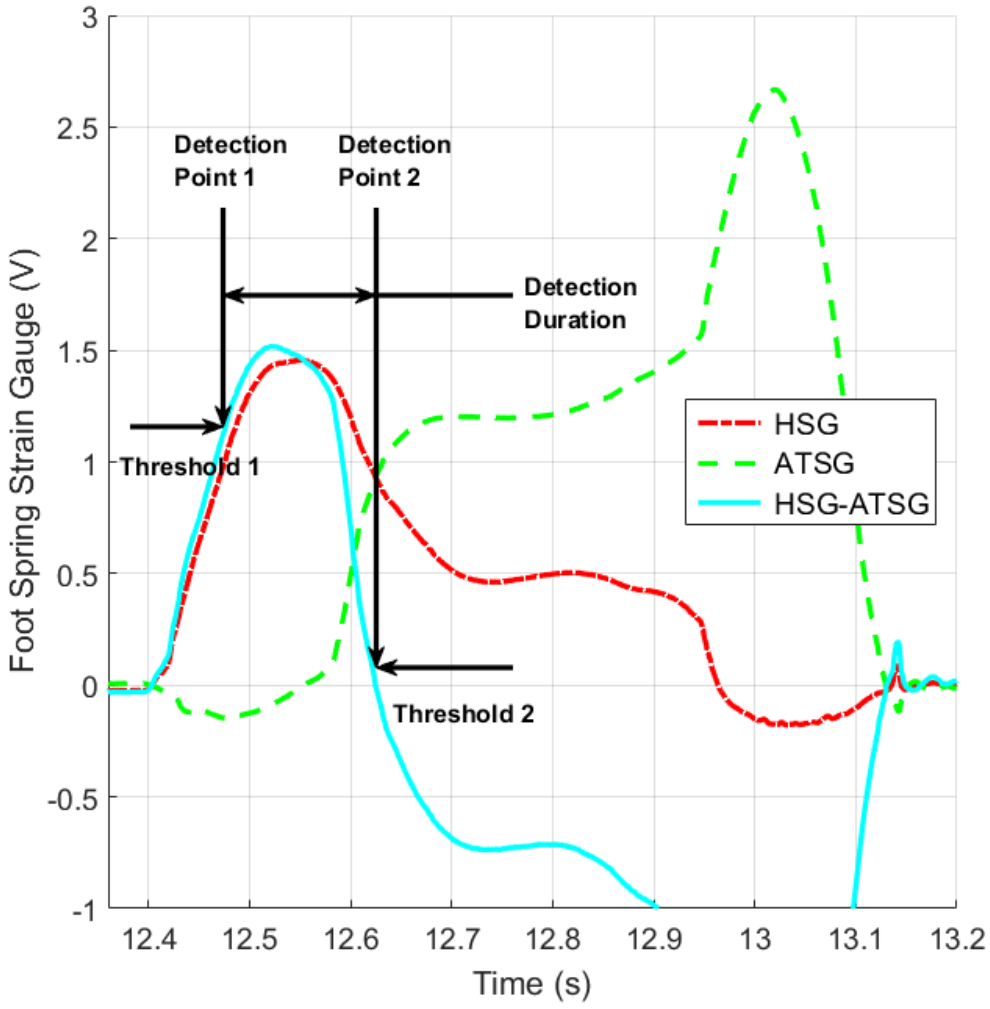

Figure 6-2: Comparison between HSG and HSG-ATSG signals.

6.3. Time Delay in Middle Stance

When the heel strike is recognised by the control program, the powered PF assist can be triggered after a certain time delay. This delay time length can be adjusted to fit different walking speeds.

According to Table 3-1 [18] and Figure 5-4, the stance phase duration for either a healthy subject or a lower limb amputee is about 60% of a gait cycle and the terminal stance phase (powered PF phase) is about 20% of a gait cycle, which means the heel strike and the middle stance phase (phase <1> and phase <2> in Figure 5-4) make up the other 40% of a gait cycle. The middle stance duration can be calculated from the gait duration and the heel strike duration (Figure 5-5) and is shown in Figure 6-3. During low speed walking (2.8 ~ 3.6 km/h) the middle stance duration is 270~300 ms. When the walking speed is higher than 3.6 km/h, the middle stance duration is approximately constant at 250 ms. If the second threshold in the control program is set as HSG-ATSG=0, which is equivalent to the end of heel strike defined in Figure 5-5, this 250 ms middle stance duration can be used as a reference delay time length in the control program.

6.4. Motor Control in Powered Phases

Within the powered PF phase, the servo motor is demanded to run at the highest speed (6000 rpm) to maximize the output power of the EHA. The servo motor is controlled by the ESCON controller [90] described in chapter 4. Using the ESCON studio software [91], the servo motor controller operation mode and parameters can be adjusted, which are summarized in Table 6-2.

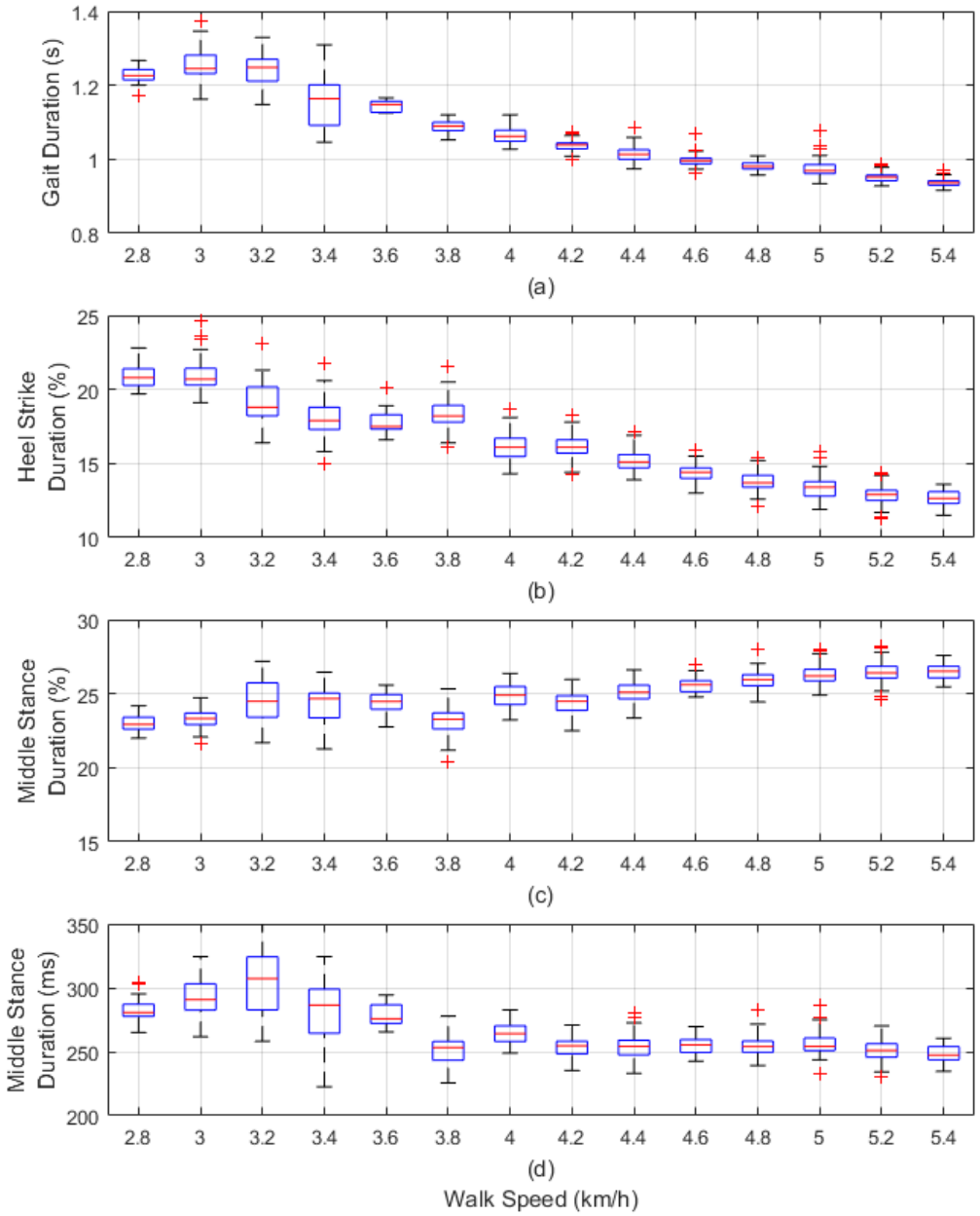

Figure 6-3: Middle stance duration at different walking speeds. (a) Gait duration. (b) Heel strike duration percentage. (c) Middle stance duration. (d) Middle stance duration percentage.

Table 6-2: Settings of the servo motor controller [91].

Main Features	Setting
Operation Mode	Closed loop speed control
Thermal Time Constant	200 seconds
Maximum Output Current Limit	15 A
Proportional Gain	515
IxR Factor	500

The thermal time constant is an important setting to protect the motor from overheating. This 200 s thermal time constant is a compromise setting allowing the motor to run long enough against a high load torque in the powered PF phase while maintaining a safe operation temperature. The IxR factor is a forward gain in the IxR compensation in the ESCON controller [90, 91]. This IxR factor and the proportional gain are found using the tuning program in the ESCON controller [91].

The motor is stopped by the control program when the ATSG drops below a small value, which allows the EHA to power the PF until the toe spring leaves the ground. The motor will also be shut down if the duration of the powered PF phase exceeds a certain time length to protect the motor and the amputee. After a short delay, the motor is demanded to reverse the direction and dorsiflexes the ankle to the maximum DF position.

6.5. System Response Analysis

At the transaction from the passive mode to active mode, the response time of the EHA system is important to avoid missing the correct power injection time point.

In the MK4 prototype described in chapter 4, the motor drive (Eason controller) receive the step speed demand from the cRIO and start to accelerate the motor-pump. The mechanical time constant of the motor used in MK4 prototype is 0.483ms [84] and is considered to be much higher than the electrical time constant. In this EHA system, the effective inertia of the motor-pump is affected by the inertia of the pump

and the pressured hydraulic oil in the motor case which will extend the acceleration time length. The acceleration time length of the motor-pump is also expected to be extended since there is certain amount of load pressure applied on the pump as shown in Figure 5-4(b) when the motor-pump start running in the level walking situation.

As the same time when the motor is demanded to accelerate, the on/off valve (valve ③ in Figure 4-11) is demanded to close the bypass flow rate. This on/off valve is driven by NI9505 motor drive module and its pull-in response time (at 200 bar working pressure) is 40 ms maximum. Even this pull-in response time is expected to be smaller in lower working pressure conditions, it is still considered to limit the power input to the ankle cylinder.

The compressibility of the fluid in the manifold is considered to have limited effect on the system response, since the fluid volume in the manifold is relatively small.

At the start time point of the powered PF phase in level walking condition, the response of the whole system highly depends on the acceleration time length of the motor-pump and the pull-in response time of the on-off valve. The system response time is difficult to be estimated since the load situation when level walking is hard to be simulated. In the control method proposed in this chapter, the middle stance time delay can be adjusted according to the amputee. In this way, the system response time is included in the middle stance time delay and will not affect the performance of the powered PF assist.

6.6. Control Algorithm and Threshold Selection

The control program algorithm is summarised in Figure 6-4. The decision {1} and {2} are equivalent to the detection point 1 and 2 in Figure 6-2. The threshold 1 (1V) is the lowest peak HSG-ATSG value as shown in Table 6-1. The middle stance time

delay in decision {3} can be manually adjusted in the patient trial. The time delay between the powered PF phase and the powered DF phase (decision {4}) is a period for the motor to brake, which will avoid energy loss when reversing the motor rotation direction. The displacement sensor threshold (8.7 V) in decision {5} is slightly smaller than the displacement sensor value when the ankle is at the maximum DF position (9 V). This will stop the motor before the actuator reaches the end stroke, preventing energy from being wasted, as described in [80].

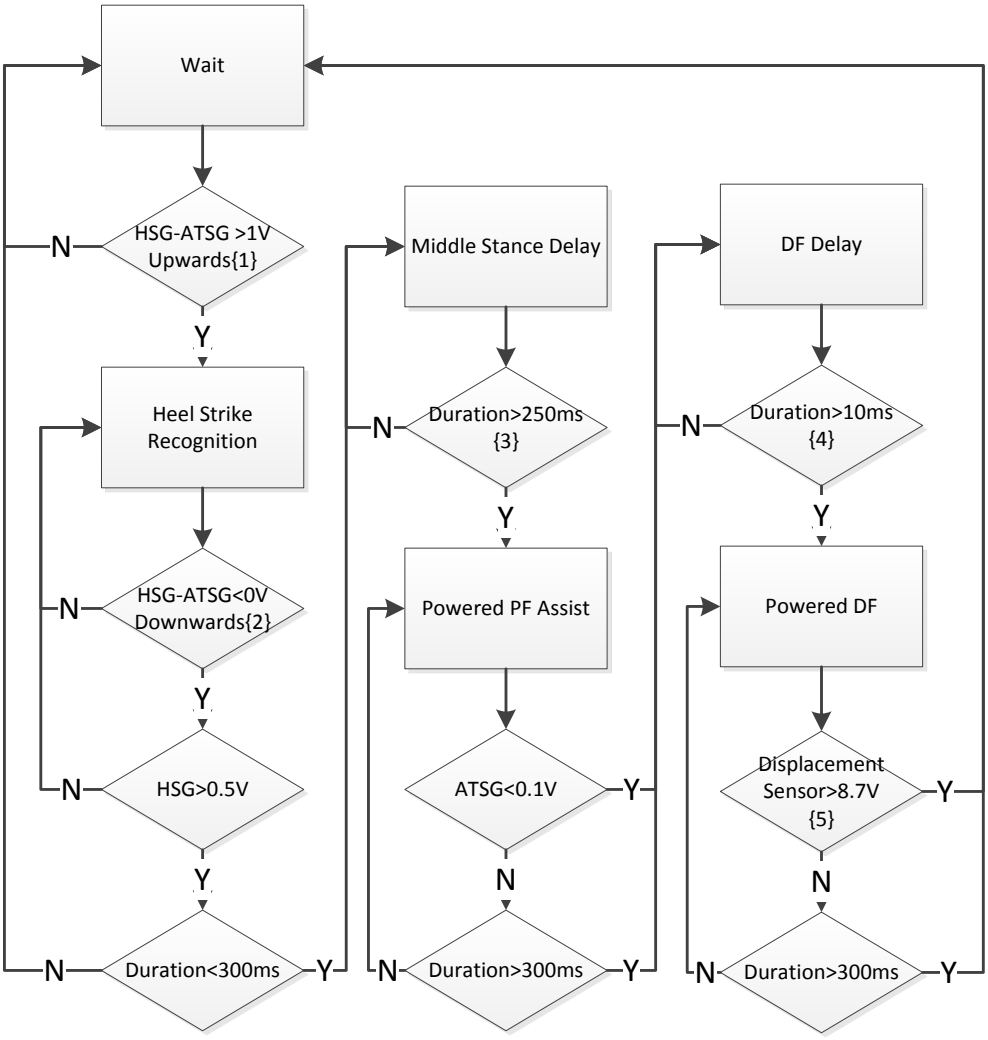

Figure 6-4: Control program flow chart.

6.7. Pressure Based Timing Control

The strain gauges and their wires are fragile and a quarter bridge completion module is required to provide a usable signal. Furthermore, easy interchange of foot springs is prevented if they need to be instrumented with strain gauges. Using the pressure difference signal to recognise the heel strike might be an alternative, avoiding the need for the strain gauges on the foot spring. As shown in Figure 5-4 and Figure 6-5, the pressure signal also shows a clear peak at the heel strike. At detection point 2, the pressure difference signal crosses zero, which indicates the ankle moment direction is reversed. The disadvantage of using the pressure difference signal is that the opportunities to avoid false triggering are reduced. The powered PF phase could not be stopped by detecting when the toe leaves the ground either since the ATSG signal is not available.

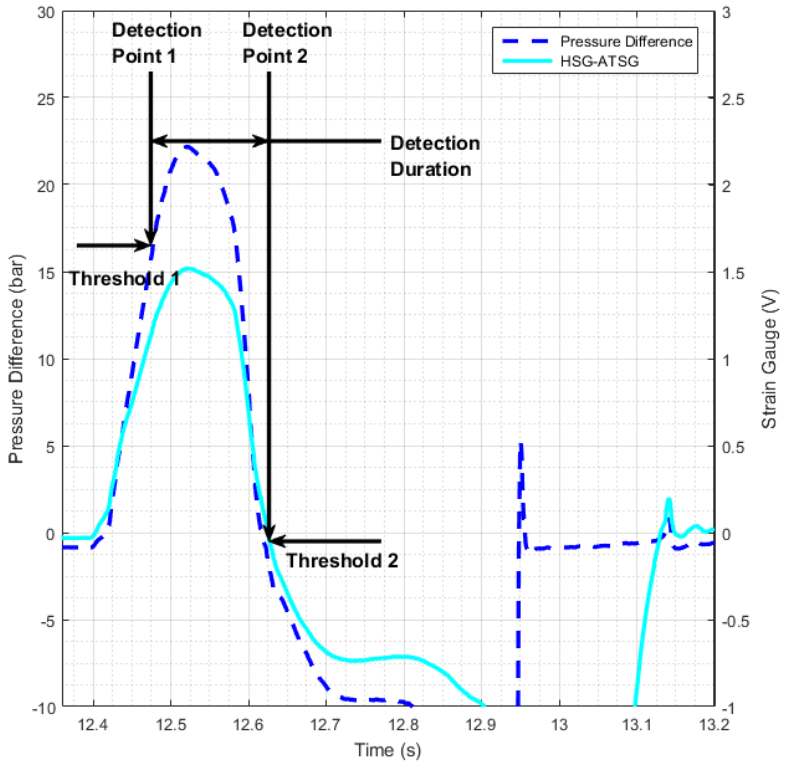

Figure 6-5: Pressure difference peak in the heel strike.

6.8. Conclusions

The HSG-ATSG signal can be used to recognise the heel strike by setting two detection points. The two thresholds are selected to be 1 V and 0 V. The combination of the HSG and the ATSG signals can be used to reduce the false triggering of the powered PF assist by other movements. The time delay in the middle stance is found to be 250 ms when the walking speed is higher than 3.6 km/h, which can be used as a reference middle stance time delay in the control program. The closed loop servo motor controller is tuned to maximize the EHA output power. The pressure difference signal can also be used in this timing control program, which could avoid the need for strain gauges on the foot spring.

Chapter 7

Amputee Trial with Powered Ankle

This chapter presents and discusses the results of the amputee trial with the powered ankle prosthesis. A transtibial amputee was monitored while walking on the treadmill at three different walking speeds with the powered assist from the MK4 prototype. The EHA performance and its timing control method is validated in the amputee trial. The characteristics of the powered ankle prosthesis are analysed by comparing with the healthy ankle and by testing at different walking speeds. The shank rotation angle obtained by the IMU is also presented in this chapter. The feedback from the amputee, the timing control method, the optimization of the powered PF and DF phases and the battery capacity are discussed at the end.

7.1. Amputee Trial Introduction and Set Up

In order to validate the EHA performance and its timing control method and investigate the ankle motions with powered ankle prosthesis at different walking speeds, an amputee trial with powered ankle prosthesis prototype has been taken place. In this amputee trial, the powered PF assist is triggered using the strain gauge based timing control method described in chapter 6. The validation of the performance of the EHA powered ankle prosthesis and its controller is based on the ankle sensor signals recorded in the amputee trial and the feedback of the amputee. The ankle motions and EHA performance are investigated by analysing the EHA performance and ankle motion in a gait cycle, comparing with ankle motion data of healthy subject and comparing between different walking speeds. The analysis on the EHA power and efficiency, alternative control method and working life is intended to be used for controller improvement and actuation system optimization.

The MK4 prototype of the powered ankle prosthesis has been tested by a transtibial amputee in the indoor and outdoor test site in Chas A Blatchford & Sons Ltd. The amputee has been asked to walk on a treadmill at three different speeds: slow speed at 2.8 km/h; medium speed at 3.8 km/h; high speed at 4.8 km/h, which are selected according to the daily walking speed range of the amputee. The amputee has also walked outside on a slightly upslope with the powered ankle prosthesis at a self-selected speed. The same transtibial amputee as has taken part in the trial with the passive ankle is used. His body weight is 70 kg. The pre-test mounting and tuning progress is the same as described in section 5.1.

According to the amputee trial results with passive ankle, the servo motor will be back driven by the load pressure difference across pump if the motor is disabled in the heel strike and the middle stance phase, which results in a lack of damping in the heel strike and uncertain ankle motion in the middle stance phase. Thus the servo motor was demanded to be 0 rpm in the heel strike and the middle stance phase.

7.2. EHA Performance and Ankle Motion

7.2.1. EHA Performance and Timing Control

The EHA performance and the ankle sensor signals in a typical gait cycle in the amputee trial is shown in Figure 7-1. The chosen gait is when the amputee is walking on the treadmill at 3.8 km/h. The gait cycle starts from the heel strike and the gait duration is 1.155 s. The first grey bar at 17% of the gait cycle indicates the transaction time point between heel trike phase and middle stance phase. The second grey bar at 40% of the gait cycle indicates the start time point of the powered PF phase. The third grey bar at 60% of the gait cycle indicates the end of the powered PF phase when the toe leaves the ground.

The recorded motor speed, motor current and pressure difference across the pump are shown in Figure 7-1(b) & (c). The direction of the positive pressure difference in Figure 7-1(c) is opposite to that in Figure 6-5. Resulting from the impact on the heel spring in the heel strike, a 20 bar pressure difference across the pump is seen at 10% gait cycle time. Since the motor is demanded to keep 0 rpm in the heel strike phase and the middle stance phase, about -3 A motor current is generated to hold the motor against the load pressure difference in the heel strike and about 1.5 A at the beginning of the middle stance phase.

The motor current peaks at the beginning of the powered PF phase to accelerate the motor. Within the powered PF phase, the mean velocity of the motor is about 3100 rpm against the peak pressure difference at 60 bar and the peak motor current is 6 A. The powered PF assist duration is about 250 ms. After the toe spring leaves the ground (ATSG signal is lower than 0.1 V) at 60% of the gait, the motor reverses rotation direction to dorsiflex the ankle. In the powered DF phase, the motor is running at approximately 4000 rpm for about 200 ms and the load pressure across pump is 7 bar.

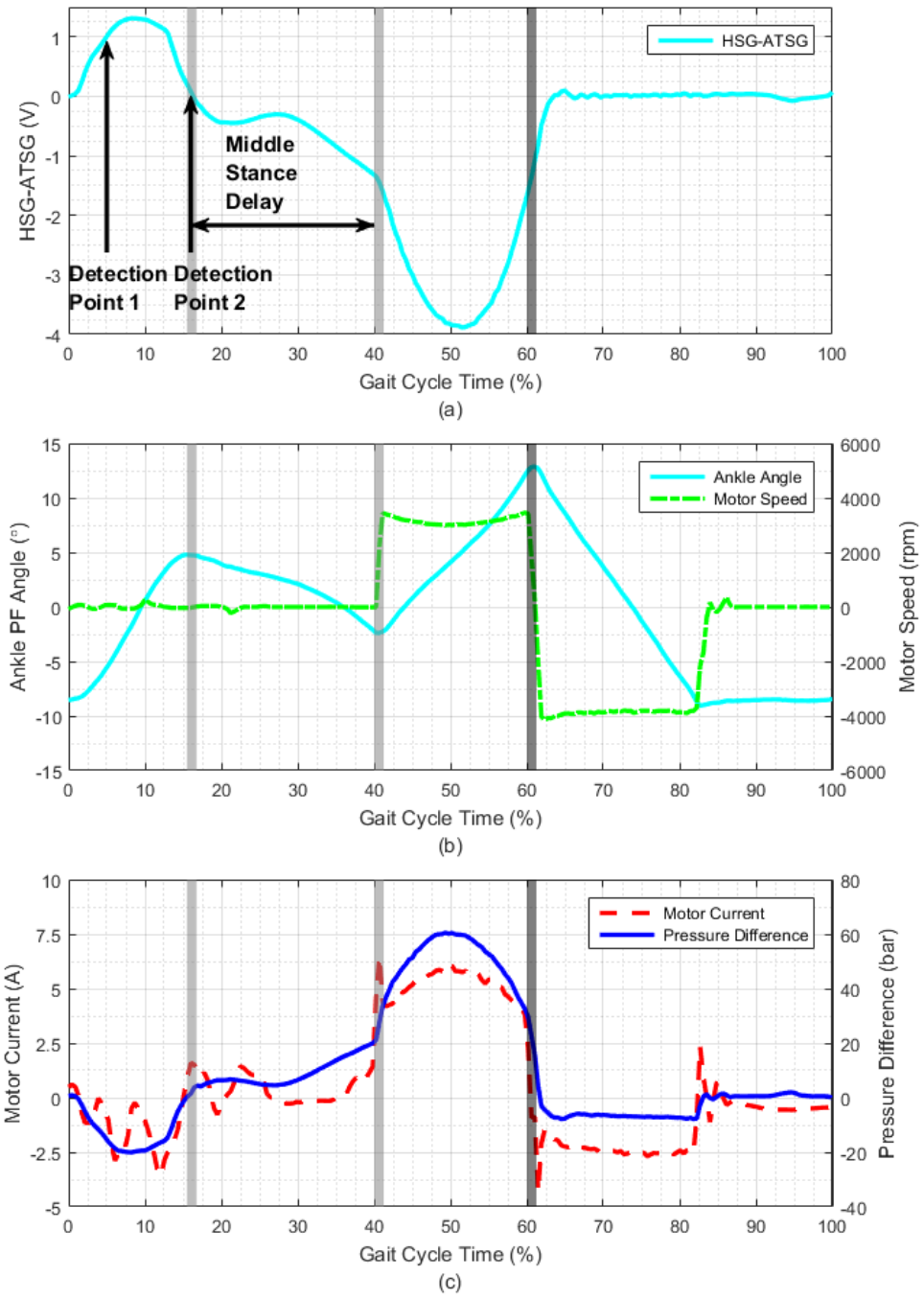

Figure 7-1: EHA performance and ankle motion in 3.8km/h treadmill walking. (a) Foot strain gauge signal. (b) Ankle PF angle and motor speed. (c) Motor current and pressure difference across pump.

7.2.2. Ankle Motion Comparison with Healthy Subject

The comparison of the ankle motion between the transtibial amputee and a healthy subject is shown in Figure 7-2. The healthy subject level ground walking data is from the data bank of the Centro di Bioingegneria gait laboratory which presented in [18]. There are 6 gaits overlapping in the figure. The gait cycle starts from the heel strike and the gait duration is 1.140+/-0.015 s. As shown in Figure 7-2(a), the ankle plantarflexes from -8.5° to 5° in the heel strike. Because the ankle prosthesis has been dorsiflexed to the maximum DF angle in the previous gait and the lack of the cushion effect of the heel, the ankle PF angle in the heel strike of the amputee is much bigger than a healthy subject. The DF range of the ankle in the middle stance phase is about 7° for the transtibial amputee, which is about half of a healthy subject. In the powered PF phase (22% of the gait cycle between the two grey bars), the ankle has been actively plantarflexed to the maximum 13° in about 250 ms. It takes another 200 ms for the ankle prosthesis EHA to dorsiflex the ankle to the maximum DF position. Comparing to the healthy subject, the available ankle rotation range of the transtibial amputee with prosthetic ankle is slightly smaller. But the rotation range is not fully used in the middle stance phase. In the swing phase, the ankle prosthesis over-dorsiflexes the ankle to the maximum DF position which causes a small amount of energy to be wasted.

The ankle torque T_{an} in Figure 7-2(b) is calculated from:

$$T_{an} = \Delta P A_a L_a \qquad (7-1)$$

where ΔP is the pressure difference across pump; A_a is the annulus area of a double acting cylinder; L_a is the arm length between the cylinder rod and the ankle joint axis.

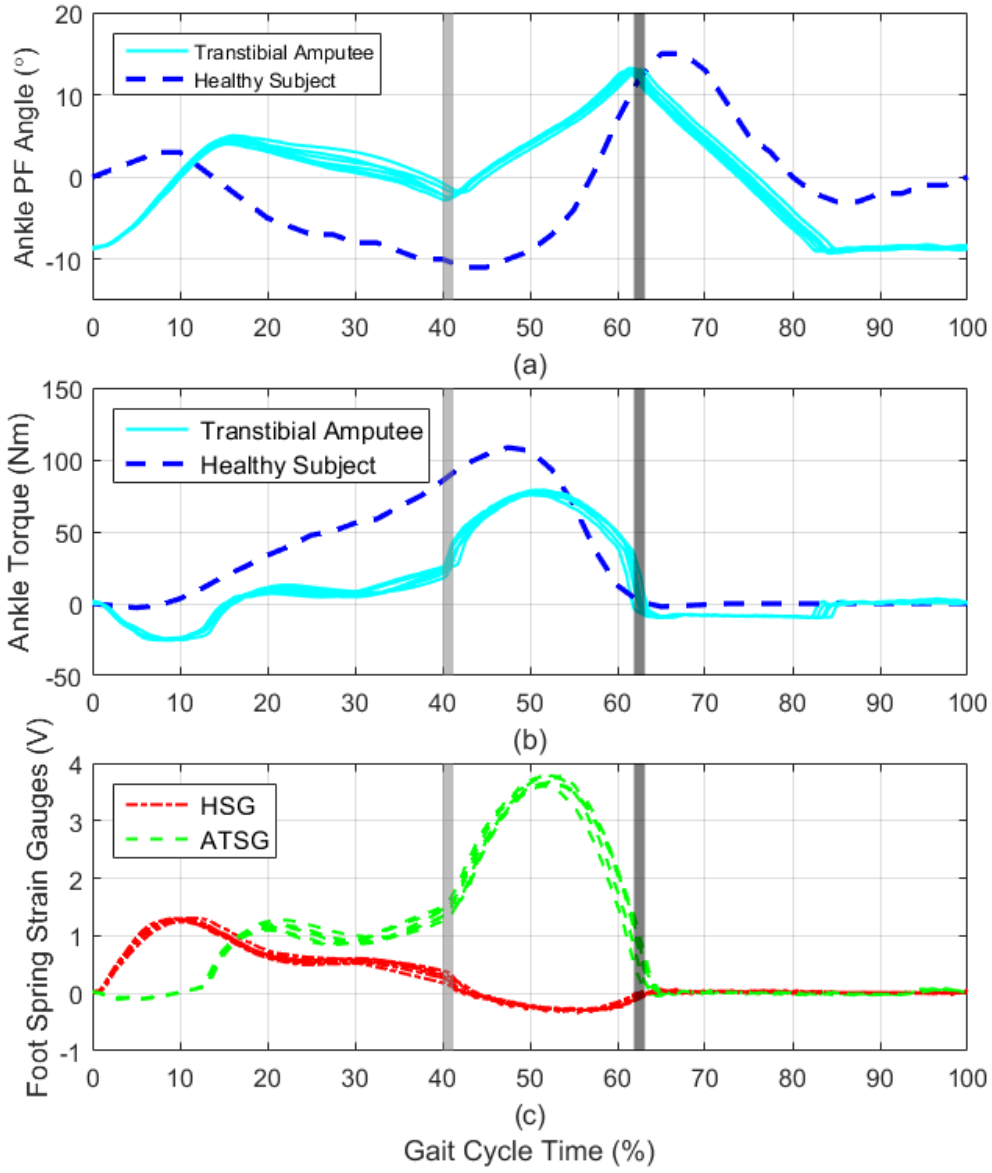

Figure 7-2: Ankle motion compared with healthy subject in a gait cycle of 3.8km/h [18]. (a) Comparison of ankle rotation angle. (b) Comparison of ankle torque. (c) Foot strain gauge signals.

Since the pressure loss in the hydraulic manifold and the friction in the actuator cylinder are not included in the calculation, the actual ankle output torque is approximate. In the heel strike phase, the prosthetic ankle provides 20 Nm resistance torque instead of zero of a healthy subject. The ankle torque keeps on increasing in the

middle stance phase until the start of the powered PF assist, but is only 1/4 of the ankle torque of a 70 kg healthy subject. The peak torque provided by the EHA (80 Nm at 50% of the gait cycle) during the powered PF is smaller and later than the peak torque of a healthy ankle (110 Nm at 47% of the gait cycle). For a healthy subject, the ankle torque is quickly released in the second half of the terminal stance phase, which results in the high speed ankle rotation at the end of the stance phase. However for the transtibial amputee with the prosthetic ankle, the ankle torque kept over 40 Nm in the majority of the powered PF phase. A probable reason is that the function of the upper joint (knee or hip) is restricted by the weight of the ankle prosthesis.

The HSG and ATSG signals shown in Figure 7-2(c) clearly show the switch of the body weight from the heel to the toe. The HSG signal peaks at 1.2 V in the heel strike and drops crossing the ATSG signal at about 18% of the gait. After the powered PF assist started, the ATSG signal increases and peaks at 3.8 V. The HSG is negative in the powered PF phase since the toe springs are supporting all the body weight and results from the stretch of the shoe.

7.2.3. Ankle Power Analysis

The power consumption of the EHA in a gait cycle is shown in Figure 7-3. The motor input power P_m is calculated from:

$$P_m = (K_b \omega_m + IR)I \qquad (7-2)$$

where ω_m is the recorded motor velocity; K_b is the back-EMF (back electromotive force) coefficient of the brushless DC motor; I is the recorded motor current and R is the resistance in the motor.

The pump output power P_p is calculated from:

$$P_p = \omega_m D \Delta P \qquad (7-3)$$

where D is the pump displacement. The ankle output power P_a is calculated from:

$$P_a = \omega_{an} T_{an} \qquad (7-4)$$

where ω_{an} is the ankle rotation speed, which is obtained by differentiating from the ankle angular position. T_{an} is an estimate as given by equation (7-1).

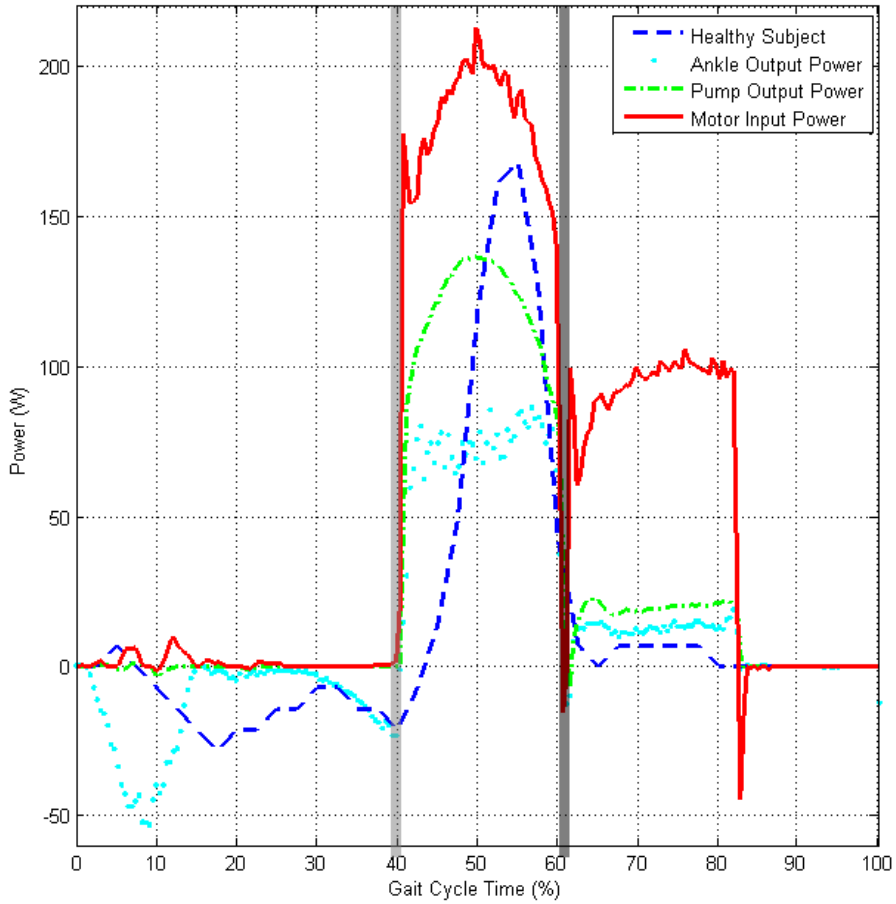

Figure 7-3: Ankle power in a gait cycle at 3.8km/h walking speed.

In the heel strike, the impact on the heel causes the hydraulic fluid in the cylinder chamber to be pressurised and bypassed through the restriction valve (valve ② in Figure 4-11). The negative ankle output power in the heel strike in Figure 7-3, which peaks at -50 W, shows that power is dissipated in this procedure. For the healthy ankle, the heel strike is mainly absorbed by the cushion effect of the heel. The human body is pushed forwards, by the other leg in the middle stance phase, prosthetic ankle is passively dorsiflexed, which results in the negative ankle output power being

dissipated by restriction valve ① (Figure 4-11). But comparing to the healthy ankle, the ankle output power of the prosthetic ankle in this period is relatively low except at the end of the middle stance phase. Because the motor is kept immobile ($\omega_m = 0$) during the heel strike and the middle stance phase, the calculated ankle pump output power is zero and the motor input power is the power consumed by the motor resistance.

Since the ankle PF velocity is obtained by differentiating the ankle angular position, the estimated ankle output power is noisy in the powered PF phase. Unlike the ankle power of a 70 kg healthy subject which peaks at 168 W at the end of the terminal stance phase, the prosthetic ankle output power oscillates within 60~85 W. Although the peak ankle power is not achieved, the mean power in the terminal stance phase is approximately the same as the healthy ankle. When the powered PF assist starts, a peak motor input power of 177 W is used to accelerate the motor. The peak motor input power (210 W) and pump output power (135 W) occur at about 50% of the gait when the load torque is at the highest (Figure 7-2). The efficiency between the motor input power and the pump output power is about 64%. The majority power loss in the motor-pump is due to the friction and the pump internal leakage. The efficiency between the ankle output power and the pump output power is estimated to be 70% and the overall efficiency is about 45%.

The negative power between the powered PF and DF phases is because the motor is actively braking, which indicates the delay time (10 ms) should be longer to avoid battery energy being wasted to brake the motor. In the powered DF phase, the ankle output power is a little higher than the healthy subject and is about 70% of the pump output power. The efficiency between the motor input power and the pump output power is only 18%. This is because the pressure difference across pump is very small due to the low load on the ankle in this period. Relatively high amount of power from the motor input is wasted on the friction in the pump and motor. There is also some energy being wasted when braking the motor after the powered DF, which could be avoided by optimizing the control programme.

7.2.4. Ankle Motion Comparison between Different walking speeds

A typical gait of high speed walking (4.8 km/h) and low speed walking (2.8km/h) is shown in Figure 7-4 and Figure 7-5 respectively. The characteristics of powered ankle prosthesis performance in daily walking speed range can be analysed by comparing between different walking speeds, which will direct the future controller design and actuation system optimization.

In the heel strike phase shown in Figure 7-4(a), the HSG-ATSG signal barely crosses the threshold (1V) at detection point 1, which indicates the possibility of the missed detection of the heel strike in low speed walking. The servo motor speed was demanded to be 0 rpm in the heel strike and the middle stance phase, the current used to drive the motor against load in this period shows no relationship to the walking speed or load pressure. This may result from the poor control of the motor speed around 0 rpm since the motor speed is obtained by the hall effect sensors. The comparison between the heel strike features at different walking speeds is summarized in Figure 7-6. There are 30 gait samples included in each speed group. When the amputee is walking at high speed (4.8 km/h), the peak HSG and peak pressure difference in the heel strike is much higher and the heel strike duration is smaller compared to low speed walking (2.8 km/h), which indicates the impact of the heel strike is more acute when the walking speed is higher. These heel strike features at different walking speeds could be used for real-time walking speed detection.

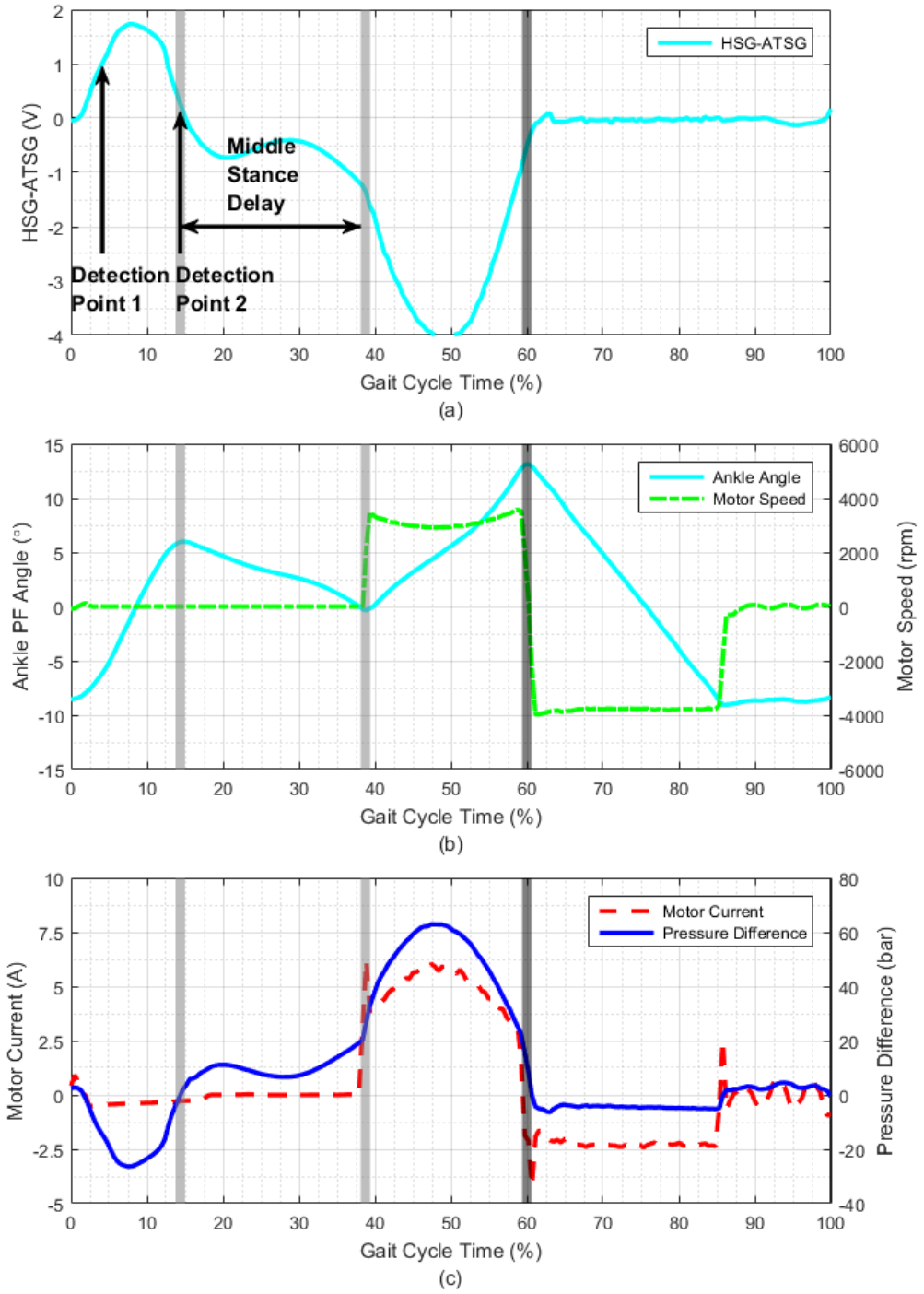

Figure 7-4: EHA performance and ankle motion in 4.8km/h treadmill walking. (a) Foot strain gauge signal. (b) Ankle PF angle and motor speed. (c) Motor current and pressure difference across pump.

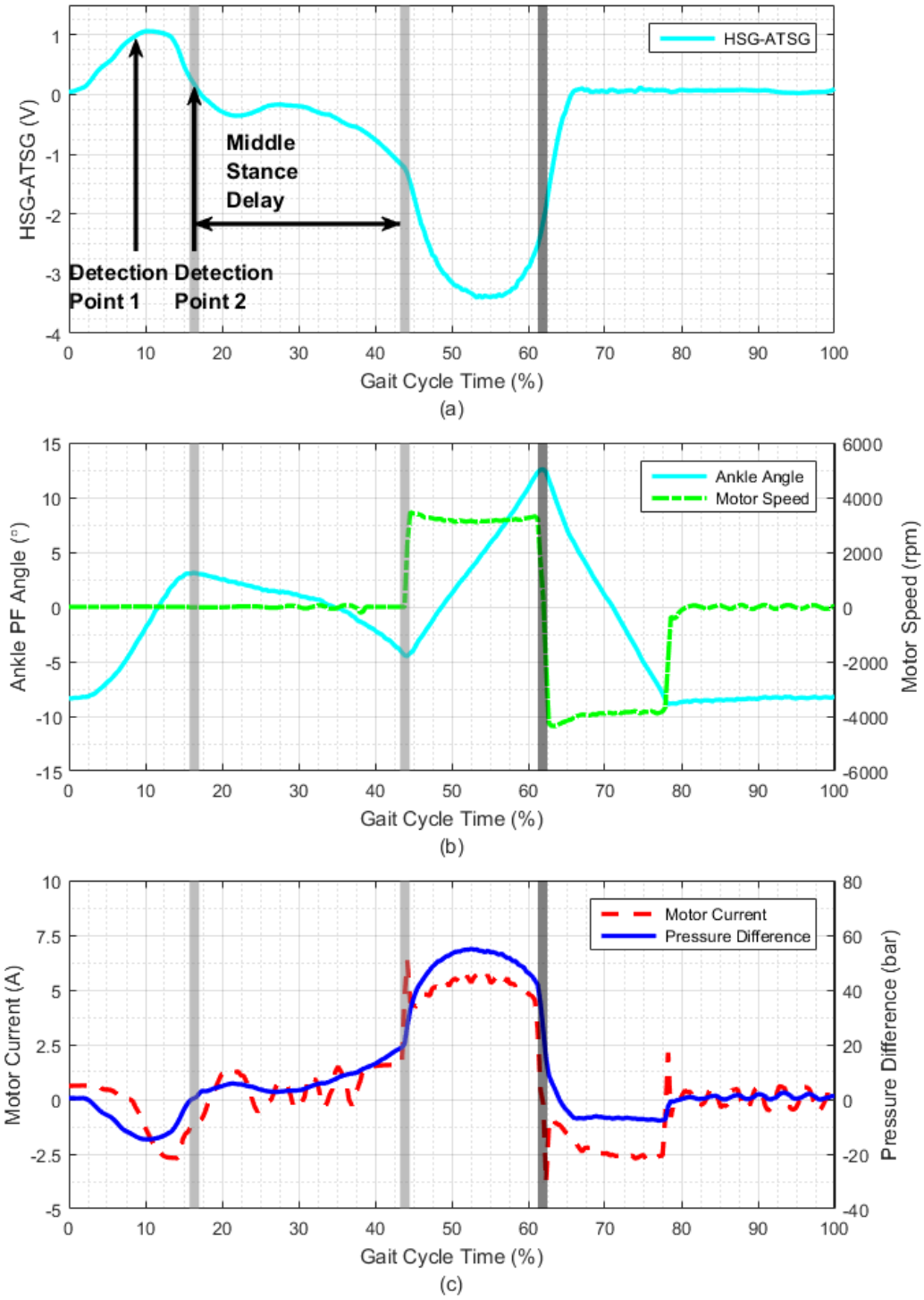

Figure 7-5: EHA performance and ankle motion in 2.8km/h treadmill walking. (a) Foot strain gauge signal. (b) Ankle PF angle and motor speed. (c) Motor current and pressure difference across pump.

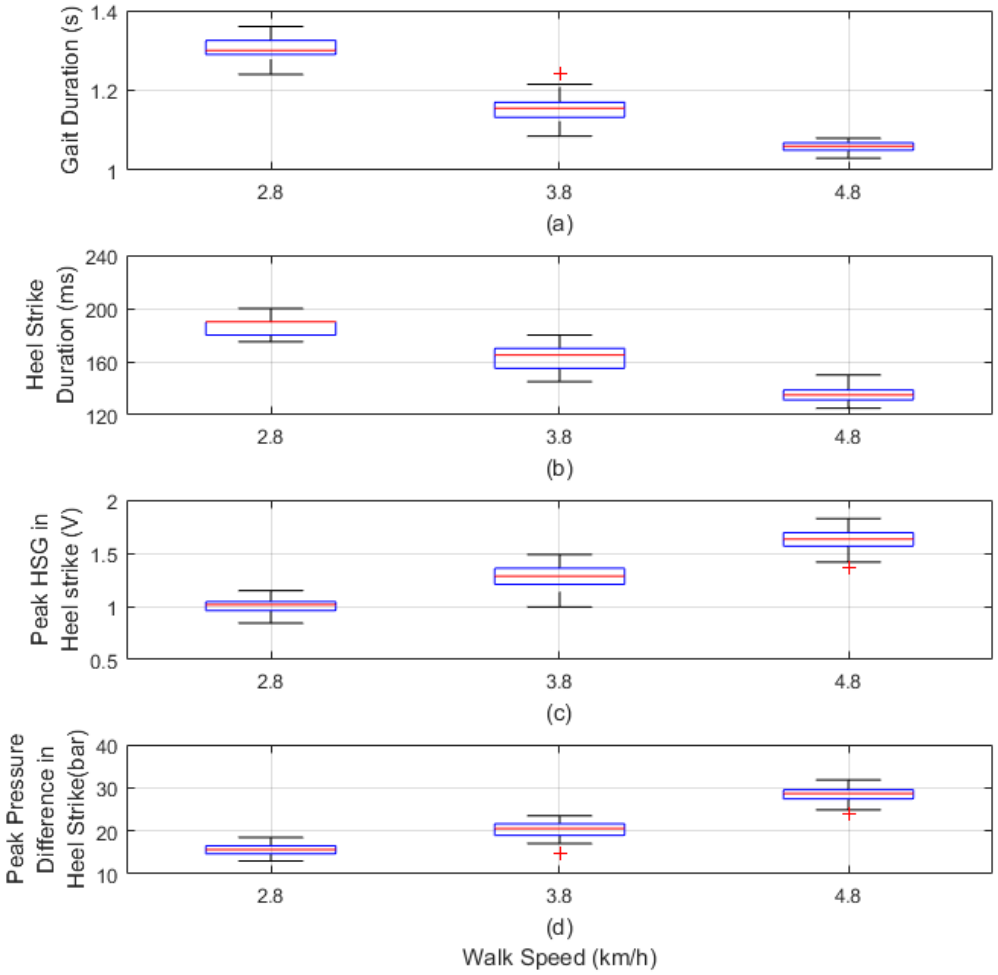

Figure 7-6: Comparison of ankle characteristics in the heel strike between different walking speeds. (a) Gait duration. (b) Heel strike duration. (c) Peak HSG in heel strike. (d) Peak pressure difference in heel strike.

The comparison between the powered PF features at different walking speeds is summarized in Figure 7-7. The gaits included in Figure 7-7 are the same as in Figure 7-6. The powered PF duration is approximately the same between different walking speeds. The peak ATSG and the peak pressure difference in the powered PF phase shown in Figure 7-5(b)&(c) indicates the ankle torque requirements increase along with the increment of the walking speed. The average motor velocity is limited by the high load pressure difference in high speed walking as shown in Figure 7-7(d).

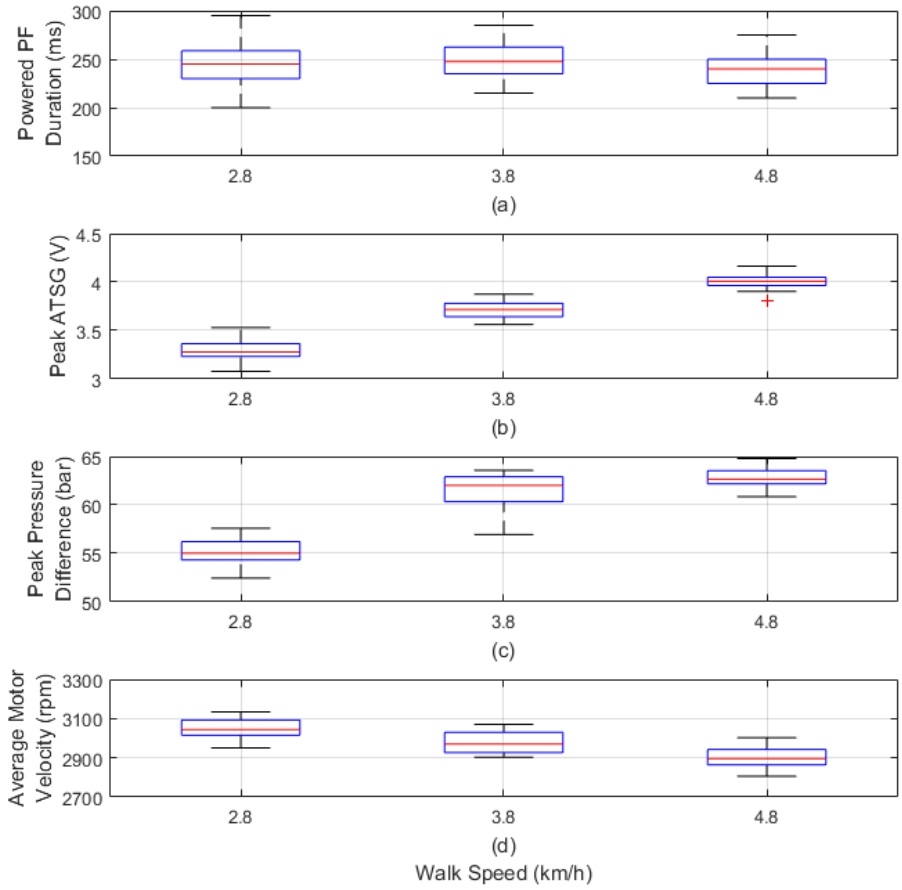

Figure 7-7: Comparison of ankle characteristics in the powered PF phase between different walking speeds. (a) Powered PF duration. (b) Peak ATSG. (c) Peak pressure difference. (d) Average motor speed.

7.3. Shank Rotation Angle

The rotation of the shank (ankle cylinder block) is recorded by the IMU and presented by the rotation displacement between the coordinate frame of the IMU and a reference frame. The three axis coordinate frame of the IMU is defined as shown in Figure 7-8, where the axis x′ is parallel to the shank tube and pointing upwards; the axis y′ is perpendicular to the surface of the ankle cylinder block and pointing into the paper and the axis z′ follows the right hand rule.

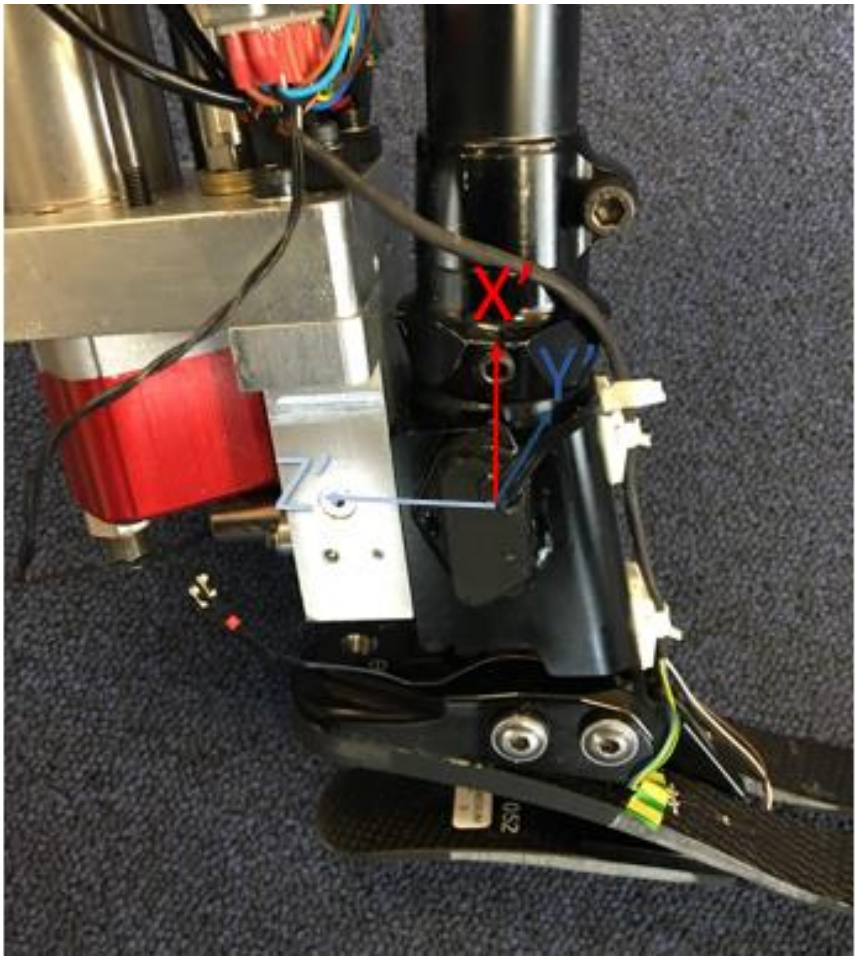

Figure 7-8: Shank IMU and its coordinate frame.

The reference three axes coordinate frame is defined as shown in Figure 7-9 (a), where the axis x is perpendicular to the ground and its positive direction is upwards; the axis y is parallel to the initial ankle joint axis y_0; the yz plane is parallel to the ground. When the amputee is standing still as shown in Figure 7-9 (a), the IMU coordinate frame x′, y′, z′ is approximately aligned with the reference frame x, y, z. When the amputee is walking, the shank is mainly rotating around the axis y and the rotations around the axes x and z are neglectable. The ankle rotation angle is shown as angle α and the shank rotation angle is shown as angle β in Figure 7-9.

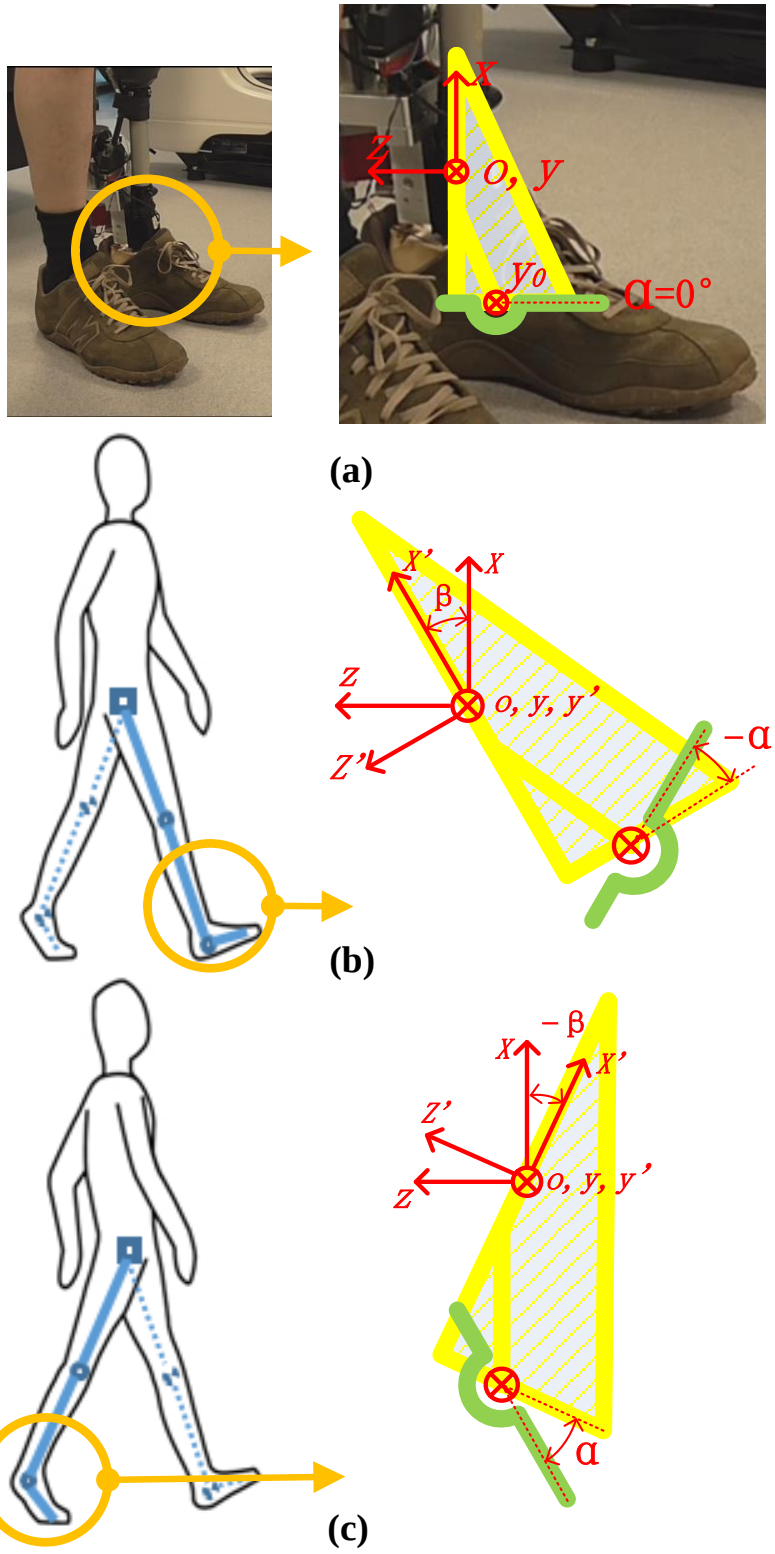

Figure 7-9: The rotation of the shank when standing and walking. (a) Coordinate frame at stand-still. (b) Ankle and shank angle when the shank-ankle is in front of the torso. (c) Ankle and shank angle when the shank-ankle is behind the torso.

Figure 7-9(b) shows the status at the beginning of the stance phase of a gait cycle, when the shank-ankle is in front of the torso. In this position, the shank rotation angle β is at the maximum value and the ankle rotation angle α is at the maximum DF angle. Figure 7-9(c) shows the status at the end of the stance phase, when the shank-ankle is behind the torso. In this position, the shank rotation angle β is negative and the ankle rotation angle α is at the maximum PF angle.

The comparison of shank angle and ankle angle in a typical gait cycle is shown in Figure 7-10. The chosen gait is the same as in Figure 7-1. The shank angle is at the maximum at the start of the heel strike. The shank is rotating in a single direction in the stance phase which is from the beginning of the gait cycle to the toe-off (grey bar in the figure). After the toe left the ground at 60% of the gait cycle, the shank is still rotating in the same direction until 72% of the gait cycle. The shank and ankle is lifted by the upper joint (knee and hip). When the shank angle crossing zero at about 87% of the gait cycle, the shank tube is approximately perpendicular to the ground, the ankle-foot prosthesis is at the nearest position to the ground. The toe spring should be lifted (DF) before this time point to clear the ground.

The comparison of the shank rotation angle between different walking speeds is summarized in Table 7-1. The maximum, minimum and rang of the shank rotation angles shown in Table 7-1 are given as: mean (standard deviation). There are 30 gait samples included in each speed group. The maximum shank rotation angle, which occurs at the beginning of the heel strike, is bigger at higher walking speed. This could be used for real-time walking speed detection. The minimum shank rotation angle did not show clear variation with the walking speed. The rotation range of the shank increases along with the walking speed increment.

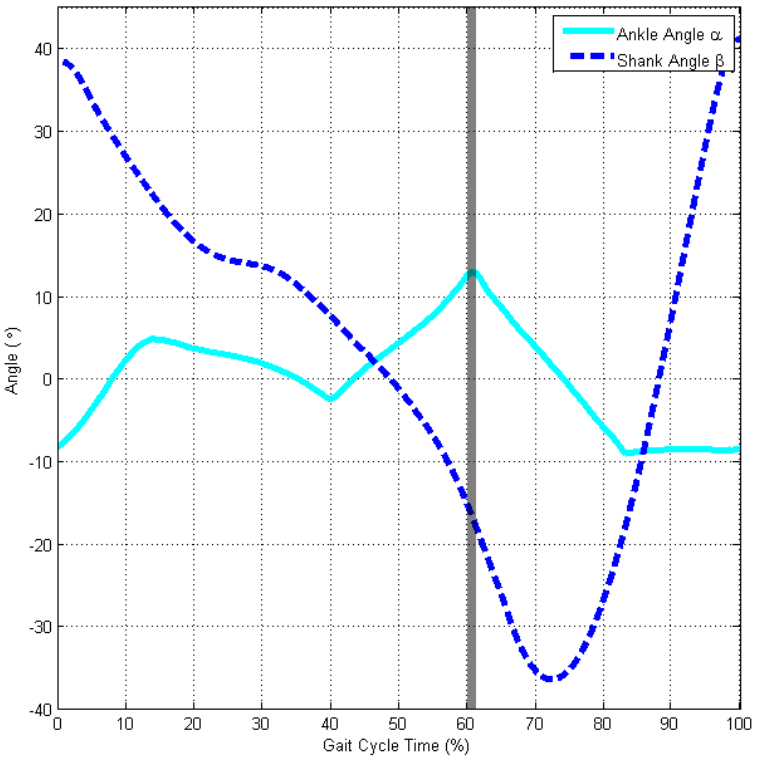

Figure 7-10: Shank rotation angle in a gait cycle.

Table 7-1: Comparison of the shank rotation angle between different walking speeds.

Walking Speed	Shank Rotation Angle, β (°)		
	Maximum	Minimum	Range
2.8 km/h	34.7 (1.48)	-36.2 (1.29)	70.9 (2.05)
3.8 km/h	38.3 (2.33)	-37.5 (1.65)	75.9 (2.74)
4.8 km/h	47.5 (1.29)	-35.2 (1.26)	82.7 (1.07)

7.4. Amputee Test Discussions

7.4.1. Feedbacks from the Amputee

Both the controller settings and the amputee test set-up are highly reliant on the feedbacks from the transtibial amputee who took part in the tests, including middle stance delay time length in different walking speeds, trigger thresholds, restriction valve settings, treadmill walking test speed range and ankle-shank adapter mounting angle. The feedback from the amputee also helped to evaluate the performance of the powered ankle prosthesis. Some of the feedback from the amputee is summarized below.

As shown in Figure 7-3, the characteristic of the ankle output power in the powered PF phase is different from the ankle power of a healthy subject. But according to the amputee, he received sufficient assistance from the powered ankle prosthesis. Without the powered ankle prosthesis, it is difficult for him to attain a high walking speed (4.8 km/h) [94]. In the low speed walking test (2.8 km/h), the amputee suggested the injected power could be reduced for a more comfortable walking experience.

The amputee claimed that the powered ankle prosthesis kept pushing him forward instead of lifting him up, especially the injected power at the end of the stance phase, which is very useful to help him walking [95]. This also indicates that beside the start time point of the powered PF assist, the end of the powered PF phase is also important. The amputee also claimed that the gait with the powered ankle prosthesis is very natural and the prosthesis ankle feels like the healthy ankle [96].

The dependence on one amputee limited the general conclusions which can be made about the powered ankle prosthesis controller. The performance of this prototype also needs to be verified by other amputees.

7.4.2. Timing Control Method Discussion

In the amputee trial presented in this chapter, the timing control method is based on the detection of the heel strike and the middle stance time delay. The heel strike detection is achieved by using the foot spring strain gauge signals. The middle stance delay time length is tuned according to the amputee.

The pressure based timing control method described in section 6.6 has also been verified by a series of treadmill walking tests. The gait cycle shown in Figure 7-11 is from the amputee trial with pressure based timing control, in which the same transtibial amputee (as described in section 7.1) is walking on the treadmill at 3.8 km/h walking speed. As shown in Figure 7-11(a), the heel strike is recognised by: pressure difference signal crossing the first threshold (-10 bar) at detection point 1 and crossing the second threshold (0 bar) at detection point 2. The powered PF phase is started at 40% of the gait cycle (the first grey bar in Figure 7-11), which is the same as the results shown in Figure 7-1.

To achieve automatic adjustment on the middle stance time delay to fit different walking speeds, instead of the pre-tuned delay length according to the expected walking speed, real-time walking speed detection is required. By analysing the amputee trial results presented in this chapter, several sensor signals have the potential, including peak HSG signal in heel strike, peak pressure difference in heel strike, heel strike duration and maximum shank rotation angle.

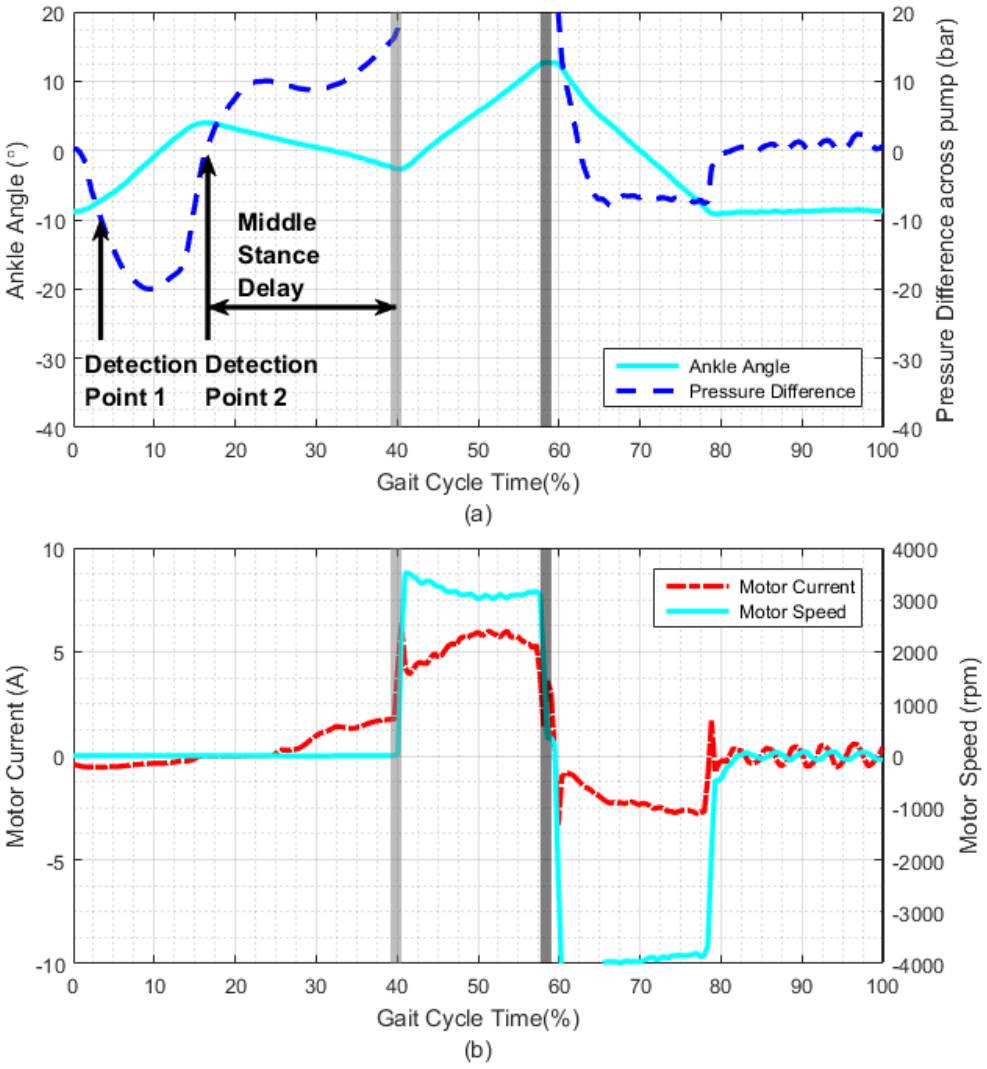

Figure 7-11: Pressure signal based timing control method. (a) Ankle angle and pressure difference across pump. (b) Motor current and speed.

7.4.3. Powered PF Control Optimization

A comparison between two gaits at the same walking speed (3.8 km/h) but with different characteristics is shown in Figure 7-12. The start and end time point of the powered PF phase is approximately the same. In gait 1, the motor is accelerated to a high velocity before the load pressure difference builds up at the beginning of the powered PF phase. However in gait 2, the motor fails to accelerate at the beginning of

the powered PF phase. Instead, the peak motor velocity occurs at the end of the stance phase, after the peak load pressure difference. Since the ankle rotation speed is approximately proportional to the motor-pump velocity, the ankle is re-accelerated before the toe-off, which is similar to the ankle characteristics of a healthy subject shown in Figure 7-2. In another words, the active power should be injected into the ankle joint at the end of the powered PF phase to push the amputee forwards, and should not be wasted at the beginning of the powered PF phase to lift the amputee upwards. This optimization could be achieved by postponing the start time point of the powered PF assist or limiting the input power level in the first half of the powered PF phase.

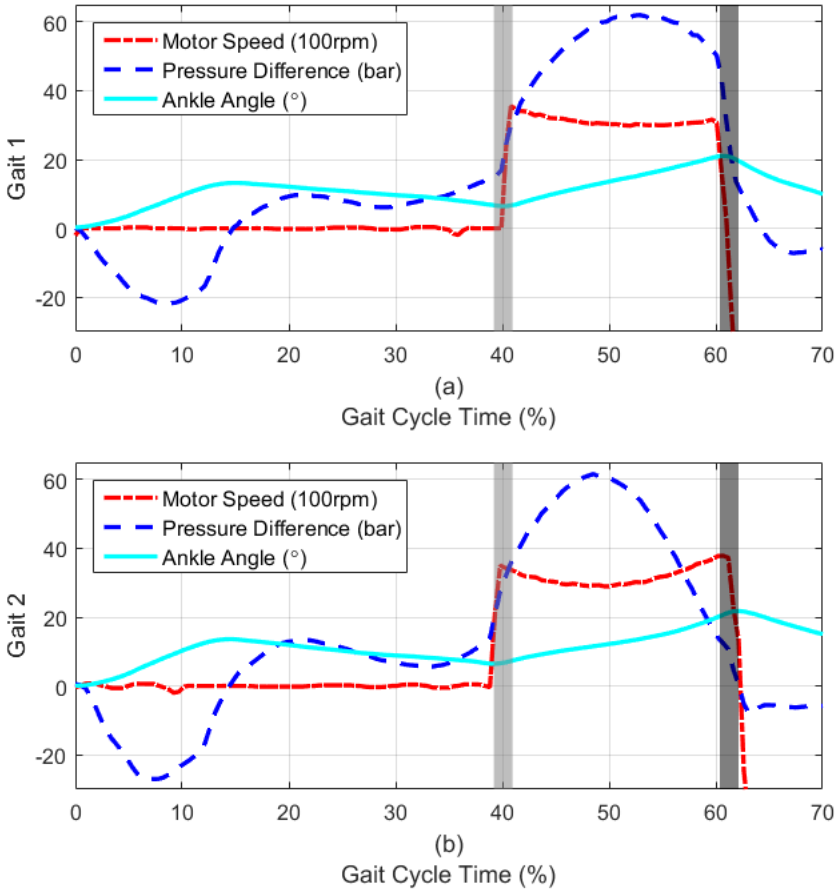

Figure 7-12: Comparison of the different powered PF characteristics. (a) EHA performance and ankle motion of gait 1. (b) EHA performance and ankle motion of gait 2.

7.4.4. Powered DF Optimization

As shown in Figure 7-3, a large amount of energy is wasted by the bypass fluid via the restriction valve ② since the manually controlled restriction valve cannot be closed in the middle of a gait. A micro-motor controlled restriction valve used in MK2 (Figure 4-7) or another on/off valve could be applied to close the active DF bypass line in the swing phase. Another advantage of reducing the bypass flow rate in the powered DF phase is to lift the toe spring quicker to clear the ground.

7.4.5. Battery Capacity Discussion

Several assumptions can be made to estimate the battery working time length:

- The amputee is walking on level ground at a middle speed around 3.8 km/h.
- The majority power is consumed in the powered PF phase. The power consumption in the other phases in a gait cycle is neglectable.
- The output voltage drop of the battery is limited and would not affect the performance of the ankle prosthesis.
- The system would not shut down by over-heating.

According to the amputee trial results shown in Figure 7-1, the average motor current is about 5.2 A during the 250 ms powered PF phase. The charge consumption of one step is 1.3 As. The 48 V, 2 Ah Lithium-Ion Battery [92] used in MK4 prototype (Figure 4-35) is able to power over 5500 steps. Note that at 48 V the 1.3 As per step charge is equal to an energy of 63 J.

7.5. Conclusions

The performance of the EHA powered ankle prosthesis prototype and its controller are validated in the treadmill walking test with a transtibial amputee. According to the amputee trial results shown in this chapter, the EHA is operated passively with approximately zero energy consumption and the damping of the ankle is controlled by the bypass restriction valves in the heel strike and middle stance phase. In the terminal stance phase, the EHA provided 80 Nm peak torque in the terminal stance phase when the amputee walking on a treadmill at 3.8 km/h walking speed. The 2 Ah, 1.1 kg Lithium-Ion battery used in the amputee trial is able to power over 5500 steps. The amputee trial results also show the proposed timing control method (chapter 6) can:

- correctly recognise the heel strike using the strain gauge signals or pressure signals;
- trigger the powered PF walking assistance in the terminal stance phase after a pre-set middle stance time delay;
- dorsiflex the ankle in the early swing phase to clear the ground.

The characteristics of the powered prosthetic ankle at three different walking speeds (2.8, 3.8 and 4.8 km/h) are obtained in the amputee trial. The gait duration and heel strike duration are found to be reduced with the increment of the walking speed, but the powered PF duration is similar. The comparisons of the heel strike features between the different walking speeds indicate the peak HSG signal and the peak pressure difference in the heel strike are higher when the walking speed is higher, i.e. the impact of the heel strike is more acute at higher walking speed. The ankle torque requirements in the terminal stance phase also increase at higher walking speed. The shank rotation angle features at different walking speeds have also been analysed in this chapter. The amputee walking experience and the timing control method are discussed. Based on the amputee trial results, several changes have been proposed to improve the power efficiency and the amputee's walking experience.

Chapter 8

EHA Simulation

A simulation model has been developed to help analyse the performance of the EHA. The EHA simulation model includes two parts: the brushless DC motor model and the hydraulic actuation model. The simulation model of the brushless DC motor and its controller is established and validated by no-load and high-load bench tests results respectively. The model only represents the characteristics of the motor controller used in the prototype approximately because of the lack of the access to its control program parameters. The hydraulic actuation model is a simplified symmetric model, which has been presented in [28]. The whole EHA simulation model results are discussed at the end by comparing with the treadmill walking test results.

8.1. EHA Simulation Overview

The EHA simulation model is established in Matlab Simulink to help analyse the performance of the EHA powered ankle prosthesis. As presented in chapter 7, a series of amputee tests has been done when the amputee is walking on level ground with the assistance from the active ankle prosthesis and many test results have been obtained. The EHA model is used to simulate the ankle prosthesis in the level walking situation, including the switch between the passive and the active mode.

The EHA simulation model structure is shown in Figure 8-1 which can be separated into two main parts: the brushless DC motor model and the hydraulic actuation model. The demand motor velocity is used as the demand signal to the model and the recorded pressure difference across pump is used as the main load on the motor-pump. The simulated motor velocity from the brushless DC motor model is used as the input signal of the hydraulic actuation model. For the hydraulic actuation model, the real load on the prosthetic foot when the amputee is walking is not easy to simulate, thus the recorded pressure difference across the pump is used again as an input signal to complete the model. As described in section 4.3.4, there is an on/off valve (valve ③ in Figure 4-11) to fully close the bypass line in the powered PF assist phase. To avoid the detailed model on the on/off valve, the recorded on/off valve drive current is used as another input signal to simulate the bypass flow rate. The output signal of the EHA simulation model is the ankle angular position which could be compared with the recorded ankle angular position for model validation.

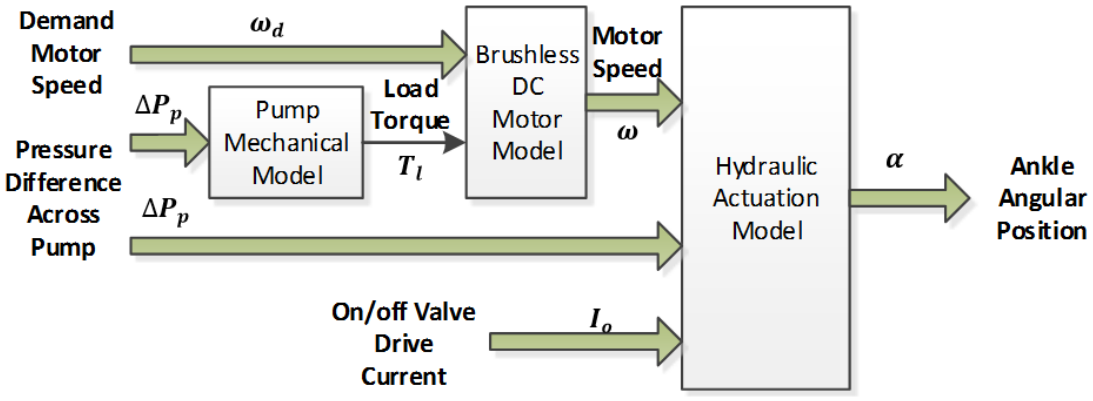

Figure 8-1: EHA simulation model structure.

8.2. Motor model

8.2.1. Motor Model Overview

The brushless DC motor simulation model structure is summarized in Figure 8-2.

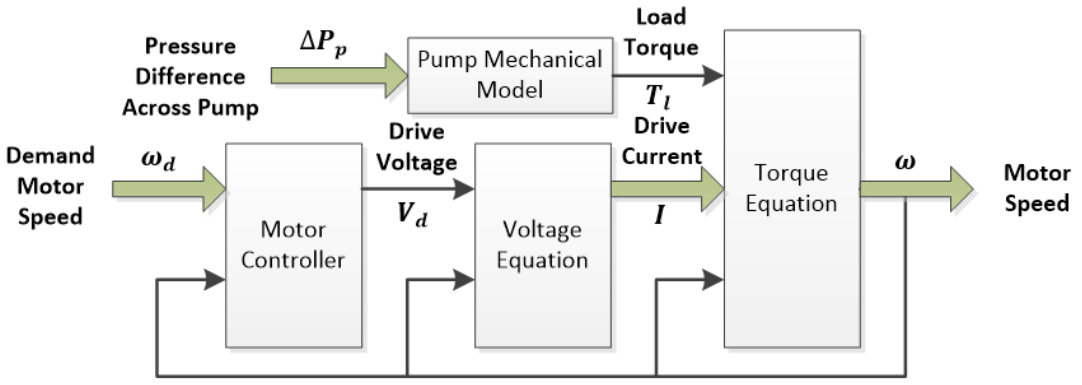

Figure 8-2: Brushless DC motor simulation model structure.

8.2.2. Closed-loop motor control

The brushless DC motor is controlled by the ESCON controller [90] as shown in Figure 4-34. A closed-loop controller, including a PI (Proportional-integral) controller and IxR compensator, was used to control the motor and was set up in the ESCON studio software [91]. The drive voltage V_d is given by:

$$V_d = (K + K_i/s)(\omega_d - \omega_m) + K_r IR \qquad (8-1)$$

where K is the proportional gain; K_i is the integral gain; s is the differential operator; ω_d is the demand motor speed; ω_m is the motor-pump speed; K_r is the IxR compensation coefficient; I is the motor drive current and R is the motor resistance.

In the amputee trial and most of the bench tests, the motor is demanded to run at the maximum speed to maximize the output power. But the maximum motor power is limited by the maximum battery voltage, the controller saturation voltage and the controller current limitation. As observed in the experiments, the controller current limitation (15A) is seldom reached, but the saturation voltage always affects the motor performance. Thus the motor model is given as:

$$\begin{cases} V_d = (K + K_i/s)(\omega_d - \omega_m) + K_r IR & for \quad |V_d| \le V_b \\ V_d = V_b & for \quad V_d > V_b \\ V_d = -V_b & for \quad V_d < -V_b \end{cases} \qquad (8-2)$$

where V_b is the saturation voltage.

8.2.3. Motor Voltage Equation and Torque Equation

The motor voltage equation is given by:

$$V_d = K_b\omega_m + (R + Ls)I \qquad (8-3)$$

where K_b is the back-EMF coefficient; L is the motor inductance. The pump mechanical model is given by:

$$T_l = \Delta P_p(D + K_{pf}) \qquad (8-4)$$

where T_l is the load torque; ΔP_p is the pressure difference across pump; D is the pump displacement; K_{pf} is the pressure-based friction coefficient. The motor torque balance is given by:

$$K_t I = T_l + T_{cf} + K_{vf}\omega_m + (J_m + J_p)s\omega_m \qquad (8-5)$$

where K_t is the torque constant of the motor; T_{cf} is the coulomb friction; K_{vf} is the viscous friction coefficient; J_m is the motor inertia and J_p is the pump inertia.

8.2.4. Low Pass Filter in Motor Model

In the no-load motor tests, the motor current and velocity are initially recorded by the ESCON controller [90]. The CRIO [74] acquires the motor current and velocity from the output channels on the ESCON controller [90] at a high scan rate of 2.5 kHz. By analysing the experiment results, the motor current and motor velocity signals are found to be recorded via a low pass filter, which might be embedded in the ESCON controller [90]. Thus, two second order Butterworth low pass filters with 200 Hz cut-off frequency have been inserted into the motor simulation model.

8.2.5. Motor Model Validation

The motor model is tuned and validated by comparing the simulated motor current and motor velocity with the experiment results in the no-load and the high-load conditions. The no-load motor test condition is when there is no pump attached and the motor is running without external load torque. The comparison between the simulation result and experiment result when the motor respond to a step demand velocity (1000 rpm) is shown in Figure 8-3. The simulation model parameters are summarized in Table 8-1.

Table 8-1: Motor model parameters in no load motor test.

Symbol	Specification	Value
K	Proportional Gain	0.515 V/rad/s
K_i	Integral Gain	95.5 V/rad
K_r	IxR compensation coefficient	0
K_b	Back-EMF Coefficient	0.091 V/rad/s
R	Motor Resistance	3.535 Ω
L	Motor Inductance	0.995 mH
V_b	Saturation Voltage	42 V
K_t	Torque Constant	0.091 Nm/A
T_{cf}	Coulomb Friction	0 Nm
K_{vf}	Viscous Friction Coefficient	17.5×10^{-5} Nm/rad/s
J_m	Motor Inertia	44 gcm^2

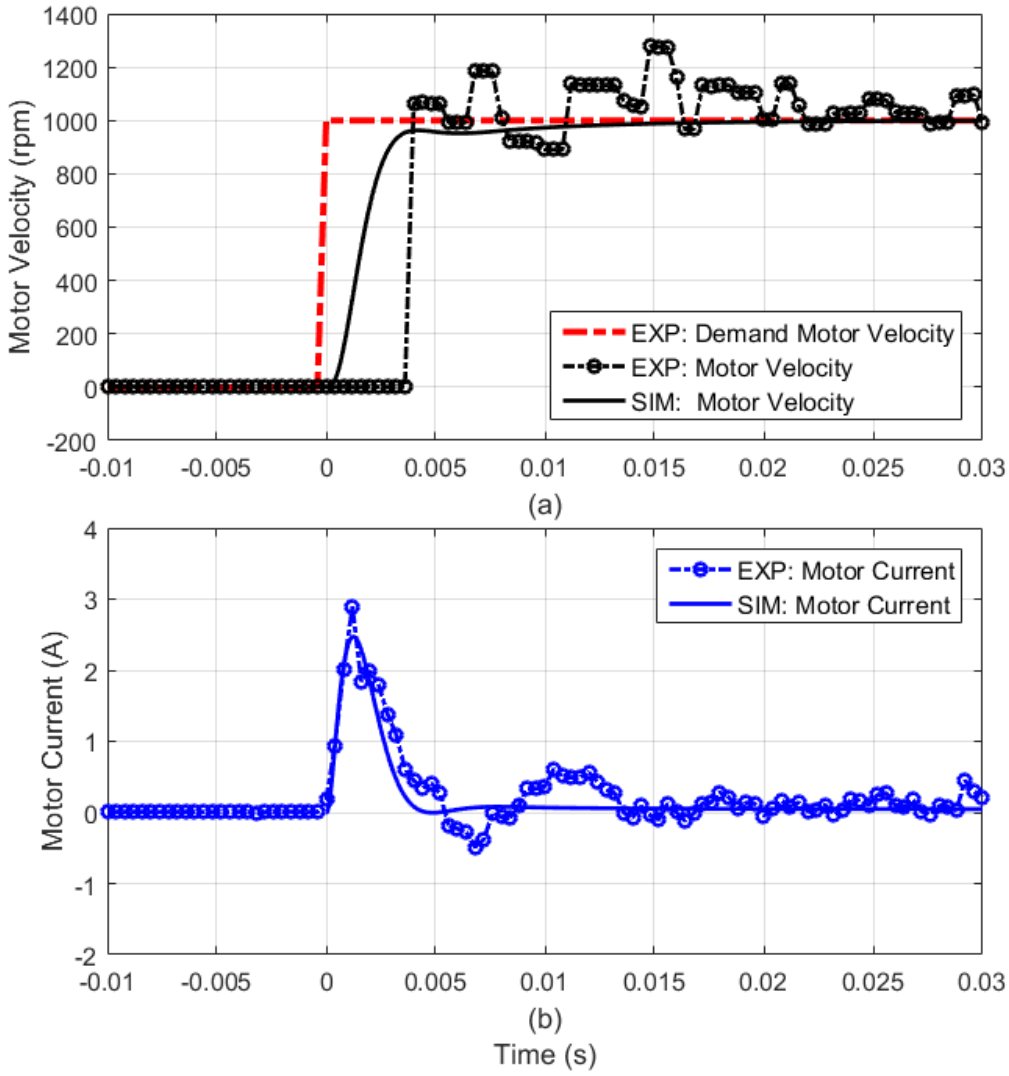

Figure 8-3: Comparison between the no-load motor test result and the simulation result (1000 rpm demand velocity). (a) Comparison of motor velocity. (b) Comparison of motor current.

Since there is not a pump coupled on the motor, the T_l and $J_p s\omega$ terms in equation 8-5 are zero. The saturation voltage V_b of the motor is decided by the battery maximum output voltage. Since the battery was not fully charged in this experiment, the maximum output voltage was 42V, which is smaller than the output voltage when the battery is fully charged (48V) [92]. The torque constant K_t and the motor inertia J_m

are found from the motor catalogue [84]. The other coefficients in Table 8-1 were estimated by matching the simulated motor speed and the no load motor test results.

The PI controller and the IxR compensator is tuned and set using the tuning program in ESCON studio software [91]. But the parameters are not clearly shown in the software. And the actual control program in the ESCON controller is more complicated including several protection functions, which are not in public domain. Thus the proportional gain K, the integral gain K_i and the IxR compensation coefficient K_r are estimated as shown in Table 8-1.

In the development of the simulation model, the motor resistance are found to be much bigger than the claimed values in the motor catalogue, which are 3.5 times of the original value.

The coulomb friction is found to be negligible in this load situation. The viscous friction coefficient is calculated by using the recorded motor current and motor speed when the motor is running at a constant velocity:

$$K_{vf} = (K_t I - T_{cf})/\omega_m \qquad (8-6)$$

The motor velocity is recorded by three hall effect sensors in this brushless DC motor, which results in the lag between the start of the motor acceleration and the first recorded motor velocity value. As shown in Figure 8-3 (a), the acceleration progress of the motor was not recorded in the no-load motor test with 1000 rpm demand velocity.

In the steady state, both the simulated current and the recorded motor current are approximately zero. The simulated motor velocity steady state error is very small, but the irregularly oscillation of the recorded motor velocity (between 900 and 1300 rpm) need further study.

The brushless DC motor has been further validated by another no-load step response (6000 rpm) test as shown in Figure 8-4. As shown in Figure 8-4, the peak simulated motor current to accelerate the motor is higher than the recorded motor current. The acceleration current might be limited to a certain value by the ESCON controller in this no-load motor test, which cannot be accurately simulated in the motor model. As

shown in Figure 8-4(a), the acceleration progress of the motor is well represented by the motor model.

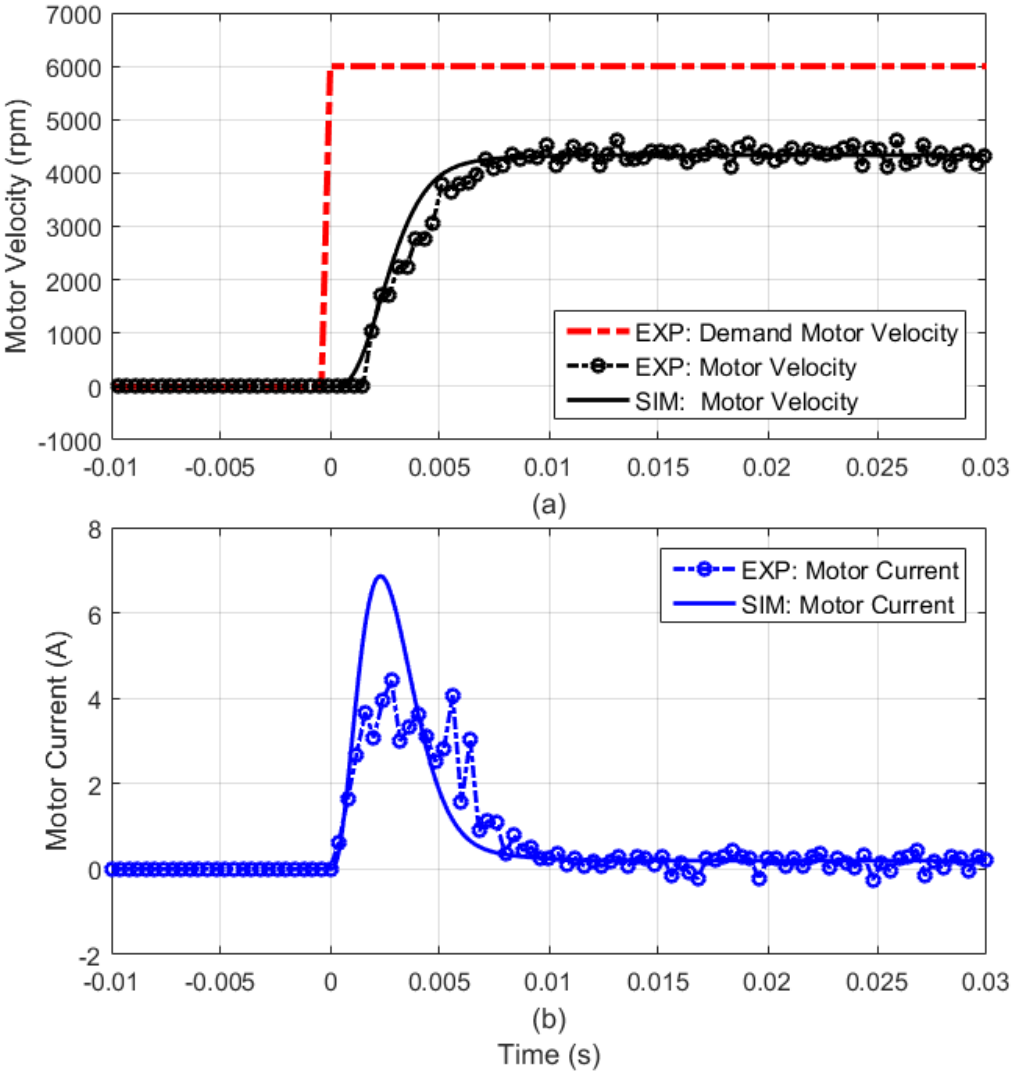

Figure 8-4: Comparison between the no-load motor test result and the simulation result (6000 rpm demand velocity). (a) Comparison of motor velocity. (b) Comparison of motor current.

In the steady state, the simulation result shows about 0.2A motor current is required against friction, which is same as in the experimented result. The motor velocity error between the simulation and the experiment in the steady state is small. Considering the lack of the access to the motor control programme, the brushless DC motor

simulation model can present the performance of the motor in the no-load situation to some extent.

Another test condition is the high-load motor test as described in section 4.5, in which the EHA is used to lift a weight via a lever. The comparison between the simulation result and the experiment result is shown in Figure 8-5. Since a pump is attached on the motor, the friction characteristics are considered to be changed as shown in Table 8-2. The maximum drive voltage is 48V in this high-load motor test since the battery was fully charged, i.e. saturation voltage $V_b = 48V$. The other motor parameters are kept the same.

The motor is demanded to run at 6000 rpm to maximize the EHA output power, which is higher than the nominal speed of the motor (4390 rpm). As shown in the simulation results, the drive current is kept over 6A in this high load situation, which result in the voltage across motor resistant shares approximately 1/3 of the drive voltage. The motor velocity is limited to 3000 rpm in this high load situation as shown in Figure 8-5(a).

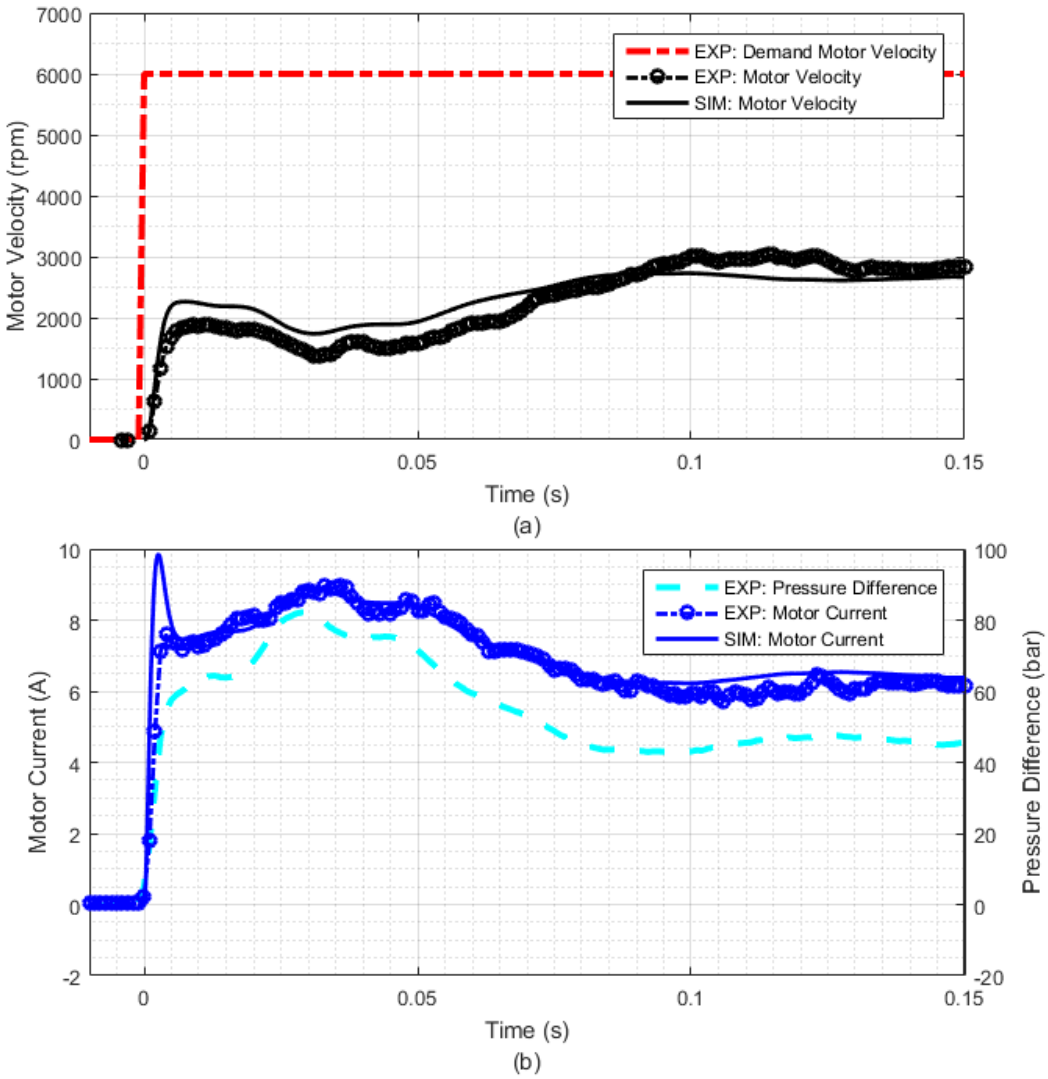

Figure 8-5: Comparison between high load motor test results and the simulation result. (a) Comparison of motor velocity. (b) Pressure difference and comparison of motor current.

Table 8-2: New model parameters for the high-load motor test.

Symbol	Specification	Value
V_b	Saturation Voltage	48 V
T_{cf}	Coulomb Friction	0.013 Nm
K_{vf}	Viscous Friction Coefficient	7 x10^{-4} Nm/rad/s
K_{pf}	Pressure-based Friction Coefficient	1.07 x10^{-3} Nm/bar
J_p	Pump Inertia	22 gcm^2
D	Pump Displacement	0.45 cc/rev

In the high-load motor test, the coulomb friction and the viscous friction of the pump are added. For an external gear pump, the friction is also increasing when the load pressure is higher [97], which results in the insertion of the pressure-based friction term in the model (included in the pump mechanical model as shown in equation 8-4). These friction coefficients are obtained by matching the simulated motor current and the recorded motor current under high load. As shown in Figure 8-5(b), the simulated motor current is very close to the recorded motor current in the experiment. The recorded motor velocity is more sensitive to the high load, when the load pressure difference peaks at 80 bar at 0.15s, which may result from a non-linear relationship between friction change and load pressure change.

8.3. Hydraulic Actuation Model

A detailed simulation motor of the hydraulic actuation in the ankle prosthesis has been presented in [5]. The hydraulic actuation model for MK4 prototype is simplified as a symmetric model and its structure is shown in Figure 8-7. The simulation hydraulic circuit is shown in Figure 8-8.

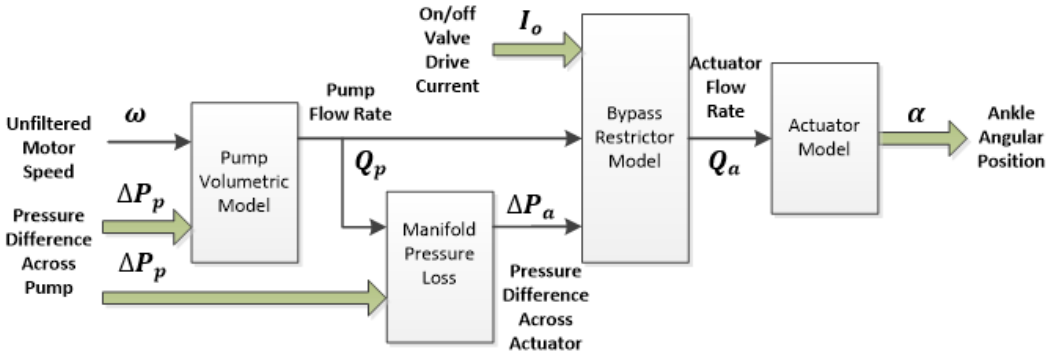

Figure 8-6: Hydraulic actuation simulation model structure.

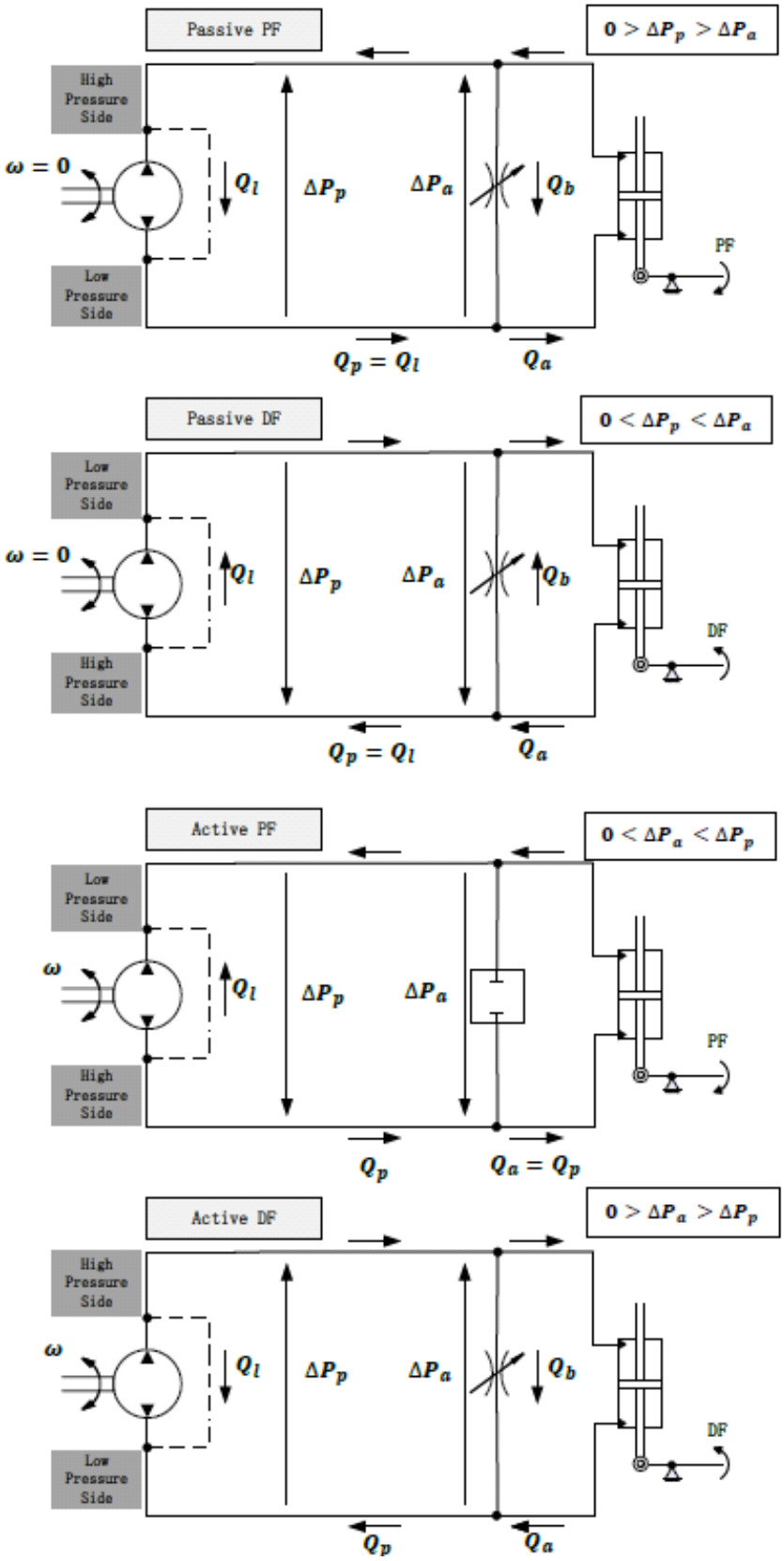

Figure 8-7: Simulation hydraulic circuit.

The compressibility flow loss was found to have limited effect on the simulated result, and is not included in the model. The external leakage of the pump is collected in the accumulator hose and re-fed into the closed circuit. To keep the model simple, this leakage flow is not included in the model. The pump flow model is given by:

$$Q_p = D\omega_m - K_{in}\Delta P_p \qquad (8-7)$$

where Q_p is the pump flow rate; ΔP_p is the pressure difference across the pump; K_{in} is the internal leakage coefficient.

The pressure loss in the manifold was found to be significant. Especially between passive and active modes, the flow rate in the manifold is totally causing a reduced pressure difference across the bypass restriction valves, hence reducing the bypass flow rate. According to the experiment results, the linear pressure loss model matches the manifold pressure loss of this EHA prototype well. The pressure loss in the manifold is modelled as:

$$\Delta P_a = \Delta P_p - K_l Q_p \qquad (8-8)$$

where ΔP_a is the pressure difference across the actuator, which is also the pressure difference across the bypass restriction valve (valve ① and valve ② in Figure 4-11); K_l is the manifold pressure loss coefficient. The bypass valve is modelled as:

$$\begin{cases} Q_a = Q_p - K_B\left(K_{bp1}\sqrt{\Delta P_a} + K_{bp2}\Delta P_a\right) & for\ \Delta P_a \geq 0 \\ Q_a = Q_p - \left(-K_{bd1}\sqrt{|\Delta P_a|} + K_{bd2}\Delta P_a\right) & for\ \Delta P_a < 0 \end{cases} \qquad (8-9)$$

where Q_a is the flow rate in/out of the actuator; K_B is the coefficient for on/off valve ($K_B = 1$ if the on/off valve is open and $K_B = 0$ if the on/off valve is closed); K_{bp1} and K_{bp2} are the bypass pressure difference to flow rate coefficients for the active PF phase and the passive DF phase (valve ① in Figure 4-11 activated), which combines both the square-root and the proportional relationship in the bypass line. K_{bd1} and K_{bd1} are the bypass pressure difference to flow rate coefficients for the active DF phase and the passive PF phase (valve ② in Figure 4-11 activated). The actuator was simplified as a proportional relationship between the actuator flow rate and ankle rotation speed:

$$s\alpha = K_a Q_a / A_a \qquad (8-10)$$

where α is the ankle angular position; A_a is the annular area of the double-ended cylinder; K_a is a lever ratio between the piston rod extension speed and the ankle angular speed.

8.4. Simulation Results and Discussions

The treadmill walking test results presented in chapter 7 are used to validate the simulation model. The comparison of the amputee test result and the simulation result is shown in Figure 8-8. The walking speed of the gait in the figure is 3.8 km/h.

The recorded pressure difference across the pump, demand motor velocity and on/off valve current signals shown in the upper graph of Figure 8-8 were used as the input signals of the simulation model. By matching the simulated ankle angular position with the treadmill walk test result, the parameters of the hydraulic actuation simulation model were estimated and summarized in Table 8-3.

Table 8-3: EHA simulation model parameters (hydraulic actuation part).

Symbol	Specification	Value
K_{in}	Pump Internal Leakage Coefficient	1.46×10^{-12} $m^3/s/Pa$
K_l	Manifold Pressure Loss Coefficient	9×10^9 $Pa/m^3/s$
K_{bp1}	Active PF Bypass Coefficient 1 (square-root)	4.275×10^{-9} $m^3/s/Pa$
K_{bp2}	Active PF Bypass Coefficient 2 (linear)	1.575×10^{-12} $m^3/s/Pa$
K_{bd1}	Active DF Bypass Coefficient 1 (square-root)	6.75×10^{-8} $m^3/s/Pa$
K_{bd2}	Active DF Bypass Coefficient 2 (linear)	1.1×10^{-11} $m^3/s/Pa$
A	Actuator Annular Area	6.28 cm^2
K_a	Ankle Joint Lever Coefficient	2.64 °/mm

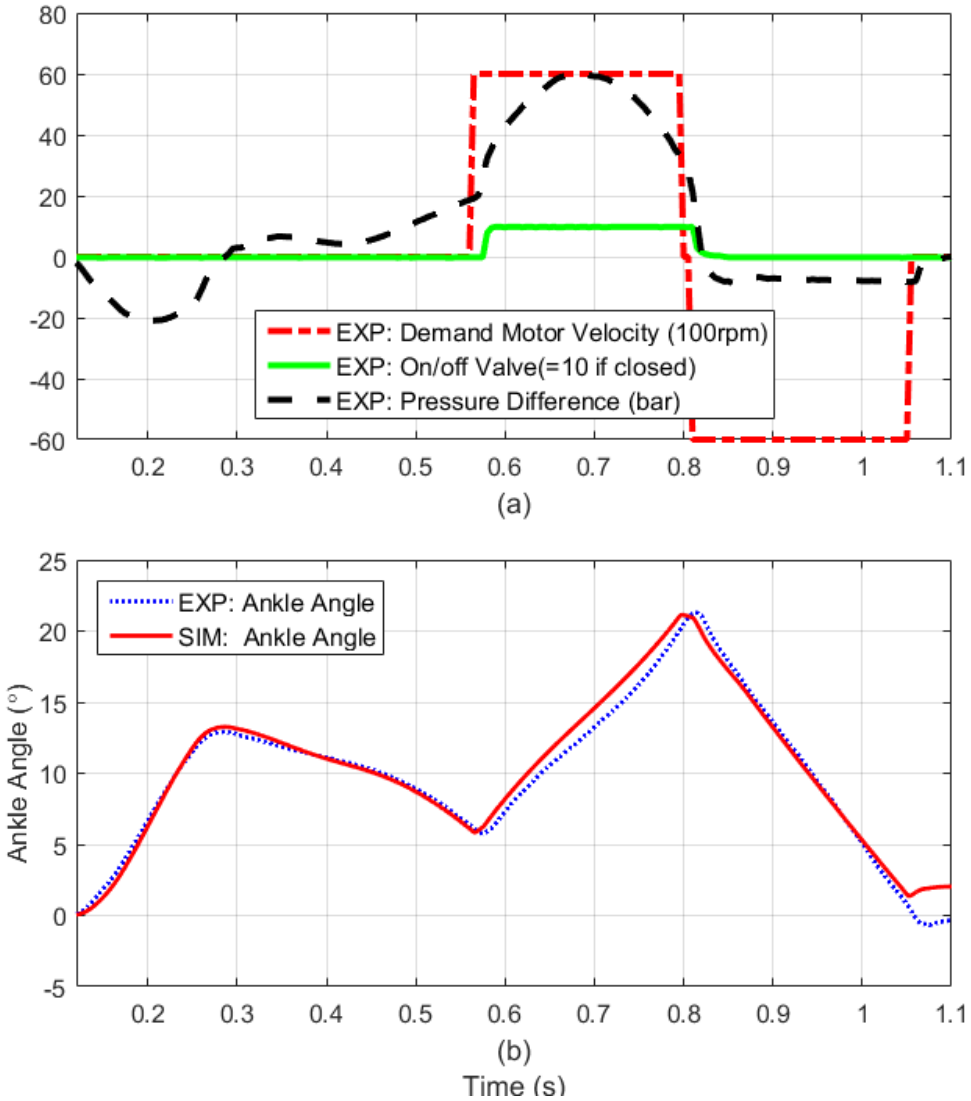

Figure 8-8: Comparison between 3.8 km/h treadmill walking test result and the simulation result. (a) Input signals of the simulation model. (b) Comparison of the ankle angle.

The comparison between the ankle angular positions from simulation and experiment are shown in the bottom graph of Figure 8-9. The gait shown in the figure starts from the heel strike, where a pulse of high pressure causes the passive PF movement of the ankle. The ankle then passively DF under a small damping along with the body weight moving forwards until the powered PF phase is started at about 0.57s. Within the powered PF phase, the motor is demanded to run at the highest speed against the high load and the on/off valve is closed to ensure the full power from the motor is delivered

to the ankle actuator. The motor is demanded to reverse the direction to rotate the ankle to the maximum DF position once the powered PF phase has ended. As shown in Figure 8-9, the EHA simulation model, using the recorded pressure difference as the load signal, successfully simulates the ankle angular position in both the passive and the active phases.

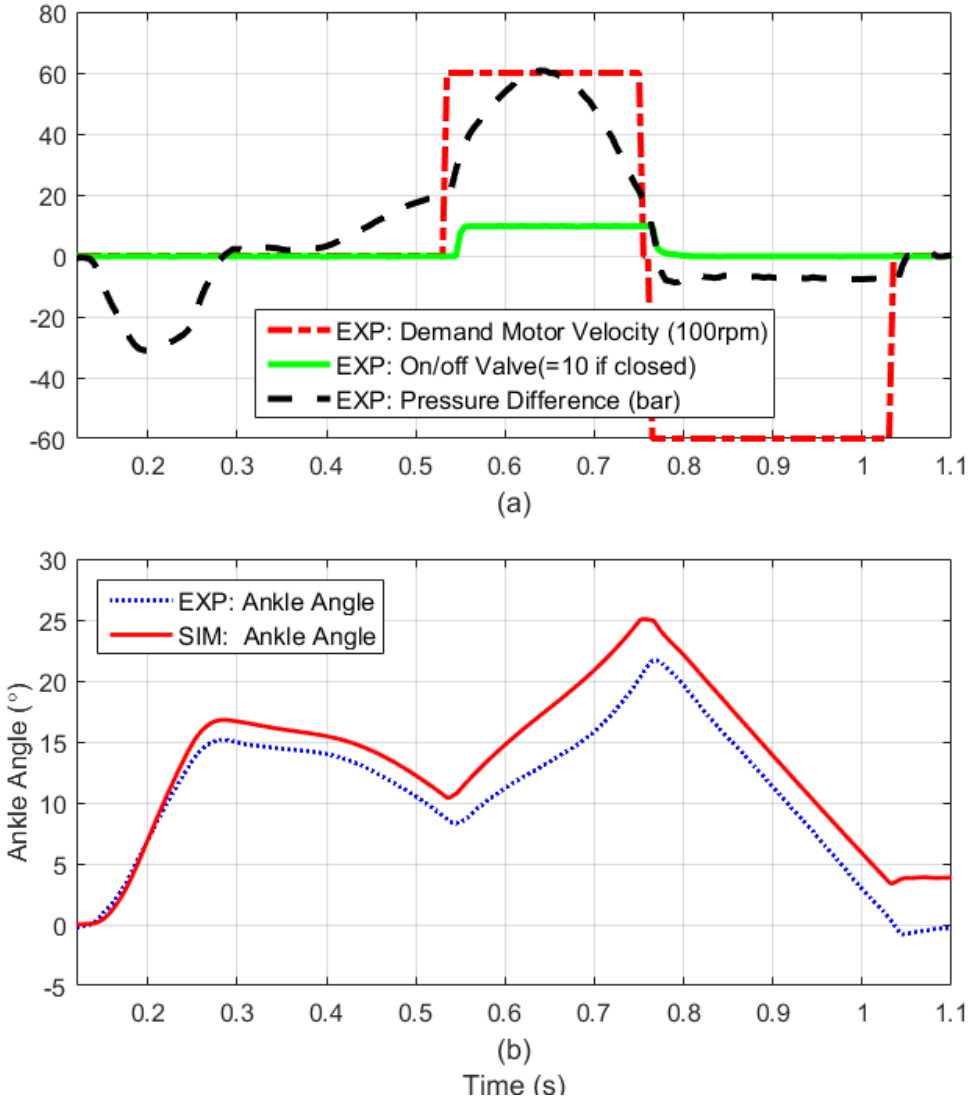

Figure 8-9: Comparison between 4.8 km/h treadmill walking test result and the simulation result. (a) Input signals of the simulation model. (b) Comparison of the ankle angle.

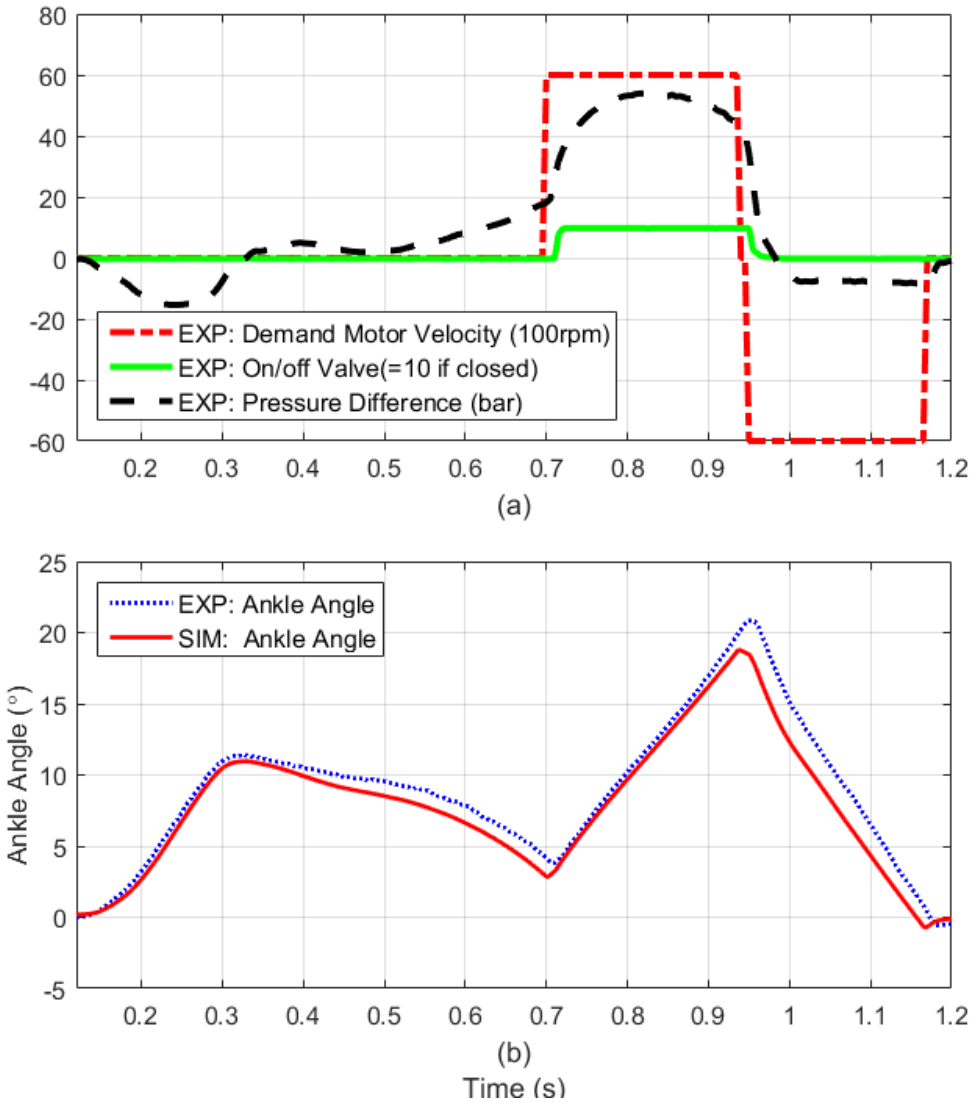

Figure 8-10: Comparison between 2.8 km/h treadmill walking test result and the simulation result. (a) Input signals of the simulation model. (b) Comparison of the ankle angle.

Figure 8-9 shows the comparison of the amputee test result and the simulation result when the walking speed of the amputee is 4.8 km/h. Figure 8-10 shows the comparison of the amputee test result and the simulation result when the walking speed of the amputee is 2.8 km/h. In the heel strike phase, the high pressure difference at 4.8 walking speed cause the ankle to PF to 15° in the amputee trial. But according to the

simulation result, the ankle rotation angle in the same load situation can be up to 17°. In the heel strike phase of the other two walking speed conditions, the simulation results (using the same parameters in Table 8-3) match the amputee test results well. This shows the ankle motion in passive phases is less sensitive to the walking speeds in the amputee tests. The simulation results in Figure 8-9(b) also indicate the RoM of the ankle is required to be larger than the current prototype (21°) if the amputee walking speed is increased. According to the simulation results, which is not showing in this section, the high bypass flow rate in the active DF phase lead to the slow DF speed and high energy waste, which indicate the bypass line should be closed in active DF phase to quickly lift-up the toe for ground clearance.

8.5. Conclusions

The uncertain parameters in the motor controller result in the imperfect simulation result but the brushless DC motor model can represent the motor performance in different load conditions reasonably well. The hydraulic actuation model using the measured pressure difference signal and the on/off valve drive current can successfully simulate the flow rate in the hydraulic circuit. The EHA simulation model described in this chapter can accurately predict the ankle motion under the real load situation in both passive and active phases.

Chapter 9

Conclusions and Future Work

The development of the EHA powered ankle prosthesis prototype and its controller are summarized. Main findings in the amputee trial results and the simulation model are briefly discussed. Recommendations for the future works at different aspects are given at the end.

9.1. Conclusions

This research focuses on the development and study of an EHA powered ankle prosthesis. The EHA described in this thesis can quickly and smoothly switch between active and passive modes, which gives the ability of the ankle prosthesis to operate passively with controllable damping and to assist walking by powering PF in the terminal-stance phase and toe-lifting in the early swing phase. According to the amputee trial results and the feedback from the amputee, the EHA powered ankle prosthesis prototype can successfully assist level walking.

The powered ankle prosthesis prototype has the EHA integrated at the ankle joint which weights 2.2 kg. The main components include a 100 W brushless DC motor, a 0.45 cc/rev bi-directional gear pump, bypass restriction valves, ankle cylinder, and foot springs. The RoM of this ankle prosthesis prototype is 21°. A timing control method based on the heel strike detection and the middle stance time delay is proposed. The HSG and the ATSG strain gauge signals are used to recognize the heel strike and trigger the powered PF phase. The signal thresholds and middle stance time delay used in the controller are derived from the walking characteristics obtained in an amputee trial with a passive ankle.

The powered ankle prosthesis prototype and its controller has been tested by a 70 kg transtibial amputee. According to the amputee trial results, the EHA is operated passively with approximately zero energy consumption and the damping of the ankle is controlled by the bypass restriction valves in the heel strike and middle stance phase. In the terminal stance phase, the EHA provided 80 Nm peak torque when the amputee was walking on a treadmill at 3.8 km/h, and is able to provide more than 100 Nm according to the bench test results. A 2 Ah, 1.1 kg Lithium-Ion battery was used as an on-board power source in the amputee trial with powered ankle, which is able to power over 5500 steps. This ankle prosthesis can still operate passively after the battery is drained, which cannot be achieved by most of the other actuation solutions. In the amputee trial with the powered ankle prosthesis, the heel strike is correctly recognised

by the controller and the middle time delay is adjusted according to different walking speeds to trigger the powered PF assist. According to the feedback of the amputee, he received sufficient assistance from the powered ankle prosthesis and the gait with the powered ankle prosthesis was very natural.

The characteristics of the powered prosthetic ankle at three different walking speeds (2.8, 3.8 and 4.8 km/h) are obtained in the amputee trial. The gait duration and heel strike duration are found to be reduced with the increment of the walking speed, but the powered PF duration is similar. The comparisons of the heel strike features between the different walking speeds indicate the impact of the heel strike is more acute when the walking speed is higher. The ankle torque requirements also increase at higher walking speed. Other amputee trial results are also analysed and discussed in the thesis, including shank rotation angle features, amputee walking experience, controller optimization, etc.

A simulation model has been developed to help analyse the performance of the EHA. The simulation model of the brushless DC motor and its controller is established and validated by no-load and high-load bench tests results respectively. The uncertain parameters in the motor controller result in the imperfect simulation result but the brushless DC motor model can represent the motor performance in different load conditions reasonably well. The hydraulic actuation model is a simplified symmetric model, which can use the measured pressure difference signal and the on/off valve drive current to successfully simulate the flow rate in the hydraulic circuit. The EHA simulation model described in this thesis can accurately predict the ankle motion under the real load situation in both passive and active phases.

9.2. Recommendations for future work

Although there are still several aspects which need be further studied or improved, the proof of principle prototype of the EHA powered ankle prosthesis has been successfully developed in this research and the amputee trial results show a promising future.

Hardware improvements:

- The size and weight of the EHA can be significantly reduced if additive manufacture is used to optimise material placement and avoid the use of plugs and seals. This would also allow integration of the pump within the ankle/cylinder structure.
- The leakage at the end cap of the motor can be significantly reduced if a commercially available high pressure feedthrough is applied. Another approach is to redesign the shaft seal of the pump to hold higher pressure, but will increase the friction and result in the relocation of the accumulator.
- The accumulator hose used in the prototype has the potential to be minimized by resizing the length or replaced by a bespoke integrated accumulator.
- The current structure of the EHA limits the access to the shank adapter (Figure 4-12), which reduces the available mounting angle range. A new type of shank adapter or the redesign of the EHA structure may worth investigating.
- The size and weight of the controller can be minimized if the NI CRIO used in the prototype is replaced by an embedded microcontroller.

Control improvements:

- There are several refinements of the actuator control (low level control) which can be realized as described in the previous chapter.

- Based on the current timing control method, the middle stance time delay should be automatically adjusted according to different walking speeds. This requires the real-time walking speed detection and a correct relationship between the middle stance time delay and the walking pace. The walking speed detection can be achieved by monitoring the sensor signal features in the heel strike, which has been presented in this research.
- The foot spring strain gauge signals, used for gait phase recognizing and user intent detection, may be replaced by other sensor signals to improve the robustness and applicability of the ankle prosthesis controller, for example the pressure transducer and the shank IMU signals discussed in this thesis. A single signal may be enough to recognise the gait phase.
- For user intent detection, multi-activity assist, environment awareness and safety, the combination of different sensor signals are necessary. This 'middle' and 'high' level control requirement has not been the subject of this research, but will be critical for the future development.

Towards a commercially available powered ankle prosthesis:

- The height of the ankle joint EHA should be reduced to fit more users. Robustness, waterproof quality and appearance of the ankle prosthesis will lead to the redesign of the EHA structure.
- The costs of the main components in the prototype, e.g. motor and its controller, pump, bypass restriction valves, ankle cylinder and foot springs are within an acceptable range, but the total cost still need to be limited. This requires an alternative solution to replace the micro on/off valve and to avoid purchasing high pressure feedthroughs.
- The noise might be a critical problem for a commercially available powered ankle prosthesis. For some customers, a quiet device may be even more important than the fully powered walking assist.

- The EHA described in this thesis can also be applied to the development of a powered knee prosthesis or a powered bi-articular transfemoral prosthesis with both knee and ankle actuations. This will further expand the daily activities for the amputee, especially the powered knee prosthesis plays an important role to assist stair ascent. Shared controller, sensor signals, shank space and energy source will allow more flexibility of the actuation design and the possibility for cooperative motion control of both the actuations.

- The energy density of the battery is a key technology to boost the future development of a lower limb prosthesis. To fulfil one day of level walking assist, a battery of 2 Ah capacity is recommended. The weight of the battery is limited to approximately 0.3 kg if the battery is placed at the ankle joint. Other choices for the location of battery may increase the weight limitation margin, e.g. a battery belt, but the existence of long power wires are not acceptable for a product.

Other aspects:

- Amputee trials should involve multi subjects, including amputees of different weights, heights, levels of amputation (transfemoral or transtibial) and walking habits to further test the performance of EHA powered ankle prosthesis and its controller. The inter-subject variations should be studied for the controller design.

- A more detailed simulation model should be established to further research the performance of the EHA under different load conditions and can be used for controller design studies.

- Considering the active power can be delivered to the ankle more gently in a bigger time window in the middle stance phase, the EHA described in the thesis also has the potential to assist walking by additionally powering the DF movement in the middle stance phase. The amputee trial mentioned in [5] indicates the above-knee amputee with a knee prosthesis considered that it was very helpful to assist walking.

References

[1] National Health Service. (2014, July 21). *Amputation Introduction* [Online]. Available: http://www.nhs.uk/Conditions/Amputation/Pages/Introduction.aspx

[2] K. Ziegler-Graham et al., "Estimating the Prevalence of Limb Loss in the United States: 2005 to 2050," *Archives of physical medicine and rehabilitation*, vol. 89, no. 3, pp. 422-429, 2008.

[3] K. J. Griffin et al., "Toe Amputation: A predictor of future limb loss?," *Journal of Diabetes and its Complications*, vol. 26, no.3, pp. 251-254, Apr. 2012.

[4] M. I. Awad et al., "Estimation of Actuation System Parameters for Lower Limb Prostheses," in *MECATRONICS - REM 2016*, Compiègne, France, 2016.

[5] T. Yu et al., "THE DESIGN OF A POWERED ANKLE PROSTHESIS WITH ELECTROHYDROSTATIC ACTUATION," in *Proc. Of the ASME/BATH 2015 Symposium on Fluid Power*, Chicago, Illinois, USA, 2015.

[6] C. Marchall and G. Stansby, "Amputation and rehabilitation," *Surgery (Oxford)*, vol. 28, no.6, pp. 284-287, 2012.

[7] Chas A Blatchford and Sons Ltd. (2017). *Our Heritage* [Online]. Available: http://www.blatchford.co.uk/about-blatchford/our-heritage/

[8] Chas A Blatchford and Sons Ltd. (2017). *Elan* [Online]. Available: http://www.blatchford.co.uk/endolite/elan/

[9] Chas A Blatchford and Sons Ltd. (2017). *Echelon* [Online]. Available: http://www.blatchford.co.uk/endolite/echelon/

[10] YOGA DIVINITY (2017). *Stress Management through Yoga* [Online]. http://www.yogadivinity.com/stress-management-through-yoga

[11] M. R. Tucker et al., "Control strategies for active lower extremity prosthetics and orthotics: a review," *Journal of Neuro Engineering and Rehabilitation*, vol. 12, pp. 1, 2015.

[12] O. Fliegel and S. G. Feuer, "Historical Development of Lower-Extremity Prostheses," *Orthopedic & Prosthetic Appliance Journal*, vol. 47, no. 5, pp. 275-85, Dec. 1966.

[13] D. P. Ferris and B. R. Schlink, "Robotic Devices to Enhance Human Movement Performance," *Kinesiology Review*, vol. 6, no.1, pp. 70-77, 2017.

[14] R. Versluys et al., "From Conventional Prosthetic Feet to Bionic Feet: A Review Study," in *Proc. Of the 2nd Biennial IEEE/RAS-EMBS Int. Conf. on Biomedical Robotics and Biomechatronics*, Scottsdale, AZ, USA, 2008.

[15] Chas A Blatchford and Sons Ltd. (2017). *Esprit* [Online]. Available: http://www.blatchford.co.uk/endolite/esprit/

[16] Chas A Blatchford and Sons Ltd. (2017). *BladeXT* [Online]. Available: http://www.endolite.com/products/bladext

[17] Chas A Blatchford and Sons Ltd. (2017). *EliteVT* [Online]. Available: http://www.blatchford.co.uk/endolite/elitevt/

[18] R. Riener et al., "Stair ascent and descent at different inclinations," *Gait & posture*, vol. 15, No.1, pp. 32-44, 2002.

[19] D. A. Winter. “Energy generation and absorption at the ankle and knee during fast, natural, and slow cadences,” *Clinical orthopaedics and related research,* vol. 175, pp. 147-154, May. 1983.
[20] J. Breakey, “Gait of unilateral below-knee amputees,” *Orthotics and Prosthetics*, vol. 30, No. 3, pp. 17-24, Sep. 1976.
[21] D. A. Winter and S. E. Sienko, “BIOMECHANICS OF BELOW-KNEE AMPUTEE GAIT,” *Journal of Biomechanics,* vol. 2, no. 5, pp. 361-367, 1988.
[22] S. K. Au and H. M. Herr, “Powered Ankle-Foot Prosthesis: The Importance of Series and Parallel Motor Elasticity,” *IEEE Robotics & Automation Magazine,* pp. 52-59, 2008.
[23] Ottobock. (2017). *BiOM* [Online]. Available: http://www.ottobock.co.uk/prosthetics/lower_limb_prosthetics/prosthetic-product-systems/biom_ankle-contentupdate/
[24] J. M et al., “Modelling and Simulating the Pump of an Aerospace Electro-Hydrostatic Module for Fault Detection and Identification Purpose,” in *Proc. Of the ASME/BATH 2014 Symposium on Fluid Power*, Bath, UK, 2014.
[25] H. Yang and M. Pan, “Engineering research in fluid power: a review,” *Journal of Zhejiang University-SCIENCE A (Applied Physics & Engineering),* vol. 15, no. 6, pp. 427-442, 2015.
[26] Parker Hannifin Corporation, *Innovations in Flight Control Systems and Subsystems* [Online]. Parker Hannifin Corporation, 2011. Available: https://www.parker.com/literature/Control%20Systems%20Division/CSD%20literature/CSDBrochure.pdf
[27] M. A. EI Sayed and S. Habibi, ‘‘INNER-LOOP CONTROL FOR ELECTRO-HYDRAULIC (EHA) ACTUATION SYSTEMS,’’ in *Proc. Of the ASME 2009 Dynamic Systems and Control Conference*, Hollywood, California, USA, 2009.
[28] T. Yu et al., “THE DESIGN, ANALYSIS AND TESTING OF A COMPACT ELECTROHYDROSTATIC POWERED ANKLE PROSTHESIS,” in *Proc. Of the ASME/BATH 2016 Symposium on Fluid Power*, Bath, UK, 2016.
[29] M. V. Pillai, “Design of a Semi-Active Knee-Ankle Prosthesis,” in *2011 IEEE Int. Conf. on Robotics and Automation*, Shanghai, China, 2011.
[30] D. A. Winter. “KINEMATIC AND KINETIC PATTERNS IN HUMAN GAIT: VARIABILITY AND COMPENSATING EFFECTS,” *Human Movement Science,* vol. 3, pp. 51-76, 1984.
[31] D. A. Winter, *The biomechanics and motor control of human gait: normal, elderly and pathological,* 2nd ed. Waterloo, Ont.: Waterloo Biomechanics, 1991.
[32] G. Bovi et al., “A multiple-task gait analysis approach: Kinematic, kinetic and EMG reference data for healthy young and adult subjects,” *Gait & Posture,* vol. 33, pp. 6-13, 2011.
[33] J. Gardiner et al., “Transtibial amputee gait efficiency: Energy storage and return versus solid ankle cushioned heel prosthetic feet,” *Journal of Rehabilitation Research & Development*, vol. 53, no. 6, pp. 1133-39, 2016.
[34] Chas A Blatchford and Sons Ltd., *élan*: *Experience smoother, safer and more natural walking* [Online]. Available: http://www.blatchford.co.uk/catalogue/feet/new-elan/flyer/936562%20Elan%20Flyer%20iss5_Web.pdf

[35] Ottobock. (2017). *Triton smart ankle* [Online]. Available: http://www.ottobockus.com/prosthetics/lower-limb-prosthetics/solution-overview/triton-smart-ankle/
[36] Össur. (2017). *PROPRIO FOOT* [Online]. Available: https://www.ossur.com/prosthetic-solutions/products/dynamic-solutions/proprio-foot
[37] Ottobock. (2017). t*riton-smart-ankle-brochure* [Online]. Available: http://www.ottobockus.com/media/local-media/prosthetics/lower-limb/triton-smart-ankle/triton-smart-ankle-brochure.pdf
[38] Össur. (2017). *PROPRIO FOOT Technical Manual* [Online]. Available: https://assets.ossur.com/library/26721/PROPRIO%20FOOT%20Technical%20manual%20-%20PROPRIO%20FOOT%20Technical%20Manual.pdf
[39] H. M. Herr and A. M. Grabowski, "Bionic ankle–foot prosthesis normalizes walking gait for persons with leg amputation," *Proceedings of The Royal Society B*, vol. 279, pp. 457-464, 2012.
[40] S. K. Au et al., "Powered Ankle–Foot Prosthesis Improves Walking Metabolic Economy," *IEEE TRANSACTIONS ON ROBOTICS*, vol. 25, no. 1, pp. 51-66, 2009.
[41] A. E. Ferris et al., "Evaluation of a Powered Ankle-Foot Prosthetic System During Walking," *Arch Phys Med Rehabil*, vol. 93, no. 1, pp. 1911-8, 2012.
[42] E. J. Rouse et al., "Design and Testing of a Bionic Dancing Prosthesis," *PLoS ONER*, 10(8): e0135148. 2015.
[43] Össur. (2017). *Elation* [Online]. Available: https://www.ossur.com/prosthetic-solutions/products/all-products/feet/elation
[44] F. Sup et al., "Preliminary Evaluations of a Self-Contained Anthropomorphic Transfemoral Prosthesis," *IEEE/ASME TRANSACTIONS ON MECHATRONICS*, vol. 14, no. 6, pp. 667-676, 2009.
[45] F. Sup et al., "Upslope Walking With a Powered Knee and Ankle Prosthesis: Initial Results With an Amputee Subject," *IEEE TRANSACTIONS ON NEURAL SYSTEMS AND REHABILITATION ENGINEERING*, vol. 19, no. 1, pp. 71-78, 2011.
[46] J. K. Hitt et al., "An Active Foot-Ankle Prosthesis With Biomechanical Energy Regeneration," *Journal of Medical Devices*, vol. 4, pp. 0110031-8, 2010.
[47] J. K. Hitt et al., "DYNAMICALLY CONTROLLED ANKLE-FOOT ORTHOSIS (DCO) WITH REGENERATIVE KINETICS: INCREMENTALLY ATTAINING USER PORTABILITY," in *2007 IEEE Int. Conf. on Robotics and Automation*, Roma, Italy, 2007.
[48] R. D. Bellman et al., "SPARKy 3: Design of an Active Robotic Ankle Prosthesis with Two Actuated Degrees of Freedom Using Regenerative Kinetics.," in *Proc. Of the 2nd Biennial IEEE/RAS-EMBS Int. Conf. on Biomedical Robotics and Biomechatronics*, Scottsdale, AZ, USA, 2008.
[49] B. Lambrecht and H. Kazerooni, "Design of a Semi-Active Knee Prosthesis," in *2009 IEEE Int. Conf. on Robotics and Automation*, Kobe, Japan, 2009.
[50] G. K. Klute et al., "Development of powered prosthetic lower limb," in *the 1st Natl Meeting, Veterans Affairs Rehabil. R&D Service*, Washington DC, USA, 1998.

[51] F. Sup et al., “Design and Control of a Powered Knee and Ankle Prosthesis,” in *2007 IEEE Int. Conf. on Robotics and Automation*, Roma, Italy, 2007.
[52] F. Sup and M. Goldfard, “Design of a pneumatically actuated transfemoral prosthesis,” in *Proc. Of the ASME Int. Mech. Eng. Congress and Exposition*, Chicago, Illinois, USA, 2006.
[53] R. Versluys et al., “A Pneumatically Powered Below-Knee Prosthesis: Design Specifications and First Experiments with an Amputee,” in *Proc. Of the 2nd Biennial IEEE/RAS-EMBS Int. Conf. on Biomedical Robotics and Biomechatronics*, Scottsdale, AZ, USA, 2008.
[54] H. Zheng and X. Shen, “Design and Control of a Pneumatically Actuated Transtibial Prosthesis,” *Journal of Bionic Engineering*, vol. 12, no. 2, pp. 217-226, 2015.
[55] R. Jiménez-Fabián and O. Verlinden, “Review of control algorithms for robotic ankle systems in lower-limb orthoses, prostheses, and exoskeletons,” *Medical Engineering & Physics*, vol. 34, no. 4, pp. 397-408, 2012.
[56] H. A. Varol and M. Goldfarb, “Decomposition-Based Control for a Powered Knee and Ankle Transfemoral Prosthesis,” in *Proc. Of 2007 IEEE Int. Conf. on Rehabilitation Robotics*, Noordwijk, The Netherlands, 2007.
[57] H. A. Varol et al., “Real-time gait mode intent recognition of a powered knee and ankle prosthesis for standing and walking,” in *Proc. Of the 2nd Biennial IEEE/RAS-EMBS Int. Conf. on Biomedical Robotics and Biomechatronics*, Scottsdale, AZ, USA, 2008.
[58] H. A. Varol et al., “Powered sit-to-stand and assistive stand-to-sit framework for a powered transfemoral prosthesis,” in *Proc. Of the 2009 IEEE Int. Conf. on Rehabilitation Robotics*, Kyoto, Japan, 2009.
[59] S. Au et al., “Powered ankle–foot prosthesis to assist level-ground and stair descent gaits,” *Neural Networks*, vol. 21, no. 4, pp. 654-66, 2008.
[60] S. Au et al., “An EMG-position controlled system for an active ankle–foot prosthesis: an initial experimental study,” in *Proc. Of the 2005 IEEE Int. Conf. on Rehabilitation Robotics*, Chicago, Illinois, USA, 2005.
[61] F. Sup et al., “Design and Control of a Powered Transfemoral Prosthesis,” *The International Journal of Robotics Research*, vol. 27, no. 2, pp. 263-273, 2008.
[62] K. A. Shorter et al., “Technologies for powered ankle-foot orthotic systems: Possibilities and challenges.,” *IEEE/ASME Transactions on Mechatonics*, vol. 18, no. 1, pp. 337-347, 2013.
[63] H. M. Herr and A. Wilkenfeld, “User-adaptive control of a magnetorheological prosthetic knee,” *Industrial Robot: An International Journal*, vol. 30, no. 1, pp. 42-55, 2003.
[64] R. Kobetic et al., “Development of hybrid orthosis for standing, walking, and stair climbing after spinal cord injury,” *Journal of Rehabilitation Research & Development*, vol. 46, no. 3, pp. 447-462, 2009.
[65] Y. D. Li and E. T. Hsiao-Wecksler, “Gait Mode Recognition and Control for a Portable-Powered Ankle-Foot Orthosis,” in *2013 IEEE Int. Conf. on Rehabilitation Robotics*, Seattle, Washington, USA, 2013.
[66] F. Zhang et al., “Effects of Locomotion Mode Recognition Errors on Volitional Control of Powered Above-Knee Prostheses,” *IEEE TRANSACTIONS ON*

NEURAL SYSTEMS AND REHABILITATION ENGINEERING, vol. 23, no. 1, pp. 64-72, 2015.

[67] F. Sup et al., "Design and Control of an Active Electrical Knee and Ankle Prosthesis," in *Proc. Of the 2nd Biennial IEEE/RAS-EMBS Int. Conf. on Biomedical Robotics and Biomechatronics*, Scottsdale, AZ, USA, 2008.

[68] T. Kikuchi et al., "Development of Third-Generation Intelligently Controllable Ankle-Foot Orthosis with Compact MR Fluid Brake," in *2010 IEEE Int. Conf. on Robotics and Automation*, Anchorage, Alaska, USA, 2010.

[69] J. C. Moreno et al., "Design and implementation of an inertial measurement unit for control of artificial limbs: Application on leg orthoses," *Sensors and Actuators B: Chemical*, vol. 118, no. 1-2, pp. 333-337, 2006.

[70] H.F. Maqbool et al., "Real-time gait event detection for lower limb amputees using a single wearable sensor," in 38th *IEEE Annual Int. Conf. Of the Engineering in Medicine and Biology Society*, Orlando, Fla., USA, 2016.

[71] Y. D. Li et al., "Estimating system state during human walking with a powered ankle-foot orthosis," *IEEE/ASME Transactions on Mechatronics*, vol. 16, no. 5, pp. 835-844, 2011.

[72] The Lee Company. (2017). *Axial Flow Screened 187 Lee Chek* [Online]. Available: http://www.ottobock.com/cps/rde/xchg/ob_com_en/hs.xsl/38138.html

[73] Maxon Motor. (2017). *ESCON 50/5 Servo Controller Hardware Reference* [Online]. Available: http://www.maxonmotorusa.com/medias/sys_master/8810873815070/409510-ESCON-50-5-Hardware-Reference-En.pdf

[74] National Instruments. (2017). *CRIO 9076* [Online]. Available: http://www.ni.com/en-gb/support/model.crio-9076.html

[75] Maxon Motor. (2017). *EC 60 flat* [Online]. Available: http://www.maxonmotor.com/medias/sys_master/root/8825435324446/17-EN-270.pdf

[76] Hydraproducts. (2017). *KV0R04RBZZE Reversible Gear Pump* [Online]. Available: http://www.hydraproducts.co.uk/portals/0/PDFimages/micro/TI11003ACDCHPR.pdf

[77] Hydrotechnik UK Ltd. (2017). *Dn4 Microbore Hose* [Online]. Available: http://www.hydrotechnik.co.uk/catalog/minimess-test-points-hoses-kits/microbore-hoses/dn2-dn4-microbore-hose

[78] Variohm. (2017). *EPT1200 Pressure Transducer* [Online]. Available: https://www.variohm.com/images/datasheets/EPT1200%20_%201500.pdf

[79] The Lee Company. (2017). *250 Series Solenoid Valve* [Online]. Available: http://leecat.theleeco.com/ecatalog/piloting-solenoid-valves/en/SDBA2531013B

[80] T. Yu et al., "Testing an Electrohydrostatic Powered Ankle Prosthesis with Transtibial and Transfemoral Amputees," in *Proc. Of the 7th IFAC Symposium on Mechatronic Systems*, Loughborough, UK, 2016.

[81] Parker Hannifin. (2017). *Oildyne Miniature Piston Pumps and Cartridge Piston Pumps* [Online]. Available: https://www.parker.com/literature/Hydraulic%20Pump%20Division/Oildyne%20Compact%20Piston%20Pumps/Miniature%20and%20Cartridge%20Pumps%20Instruction%20Manual%20Nov%202011.pdf

[82] Takako Industries. (2017). *Small Axial Piston Pump* [Online]. Available: http://www.takako-inc.com/english/products/pdf/pump.pdf
[83] JUNG-FLUIDTECHNIK. (2017). *Jung IPZ 1-HRL-7 Reversible Internal Gear Pump* [Online]. Available: http://www.jung-fluid.de/standard-right-handed-ipz-1-hr.html
[84] Maxon Motor. (2017). *EC-I 40 High Torque* [Online]. Available: http://www.ensatek.com.tr/image/urun/eci/5EC-I40_100.pdf
[85] MICRO-EPSILON. (2017). *Magneto-inductive sensors MDS-45-K-SA* [Online]. http://www.micro-epsilon.co.uk/download/products/cat--mainSENSOR--en.pdf
[86] National Instruments. (2017). *NI 9505 DC Brushed Servo Drive* [Online]. Available: http://www.ni.com/pdf/manuals/374211h.pdf
[87] National Instruments. (2017). *NI 9235 120Ω Quarter Bridge Completion* [Online]. http://www.ni.com/pdf/manuals/374645a_02.pdf
[88] National Instruments. (2017). *NI 9205 Analog Input Module* [Online]. Available: http://www.ni.com/pdf/manuals/374188a_02.pdf
[89] National Instruments. (2017). *NI 9264 Analog Voltage Output Module* [Online]. Available: http://www.ni.com/pdf/manuals/378025a_02.pdf
[90] Maxon Motor. (2017). *ESCON Module 50/5 Servo Controller Hardware Reference* [Online]. Available: http://www.maxonmotor.com/medias/sys_master/root/8818448859166/438725-ESCON-Module-50-5-Hardware-Reference-En.pdf
[91] Maxon Motor. (2017). *ESCON Studio 2.2* [Online]. Available: http://www.maxonmotor.com/maxon/view/content/ESCON-Detailsite
[92] Mountfield. (2017). *MBT4820Li 2.0Ah Lithium-Ion Battery* [Online]. Available: https://www.mountfieldlawnmowers.co.uk/products/freedom48-cordless/mbt4820li-2ah-lithium-ion-battery
[93] National Instruments. (2017). *Labview* [Online]. Available: http://www.ni.com/en-gb/shop/labview.html
[94] Amputee Trial with Powered Ankle Prosthesis Video 1. (2017). [CD] Basingstoke, UK: Tian Yu.
[95] Amputee Trial with Powered Ankle Prosthesis Video 2. (2017). [CD] Basingstoke, UK: Tian Yu.
[96] Amputee Trial with Powered Ankle Prosthesis Video 3. (2017). [CD] Basingstoke, UK: Tian Yu.
[97] Centre for PTMC, *ME40058 Fluid Power Lecture Notes*, Bath Univ. Bath, UK, Aug. 2015

Appendixes

Appendix 1: Publication 1

This appendix includes the conference paper titled '**The design of a powered ankle prosthesis with electrohydrostatic actuation**', which is published in Proceedings of the ASME/BATH 2015 Symposium on Fluid Power and Motion Control, Oct 12-14, 2015, Chicago, Illinois, United States. Authors including:

Tian Yu, Andrew Plummer, Pejman Iravani

Department of Mechanical Engineering, Centre for Power Transmission and Motion Control, University of Bath, Bath, United Kingdom

Jawaad Bhatti

Chas A Blatchford & Sons Ltd., Kingsland Business Park, Basingstoke, United Kingdom

Abstract

This paper presents the design and modelling of a new powered ankle prosthesis which combines electrohydrostatic actuation with a controllable passive damper. The new powered ankle prosthesis can switch quickly between passive mode and powered assistance mode, and is intended to just give assistance at certain points within the gait cycles, such as during toe push-off. The design concept and a prototype built to demonstrate the concept are presented. A simulation model was developed to help analyse the performance characteristics. The structure and parameterisation of the simulation model are described. A comparison between simulation results and experiment results is undertaken in order to validate the model and assist in the optimisation of the design. Some results from an initial trial with amputees are included in the paper. According to

subjective feedback from the amputees, the new powered ankle prosthesis provides sufficient force at push-off to assist with walking. Future investigations will be focusing on the compactness, weight reduction and control of the powered ankle prosthesis.

INTRODUCTION

It was estimated that there were 623 000 major lower limb amputees in the United States in 2005 [1]. In England, there are approximately 5-6000 major limb amputations carried out every year, and the most common type are lower limb amputations [2]. Among all the physiological and psychological approaches to help amputees rehabilitate, well-functioning lower limb prostheses are essential to enable the amputees' daily activities. Efforts have been devoted to the investigations of both knee joint and ankle joint prostheses. This paper will focus on a new type of ankle joint prosthesis.

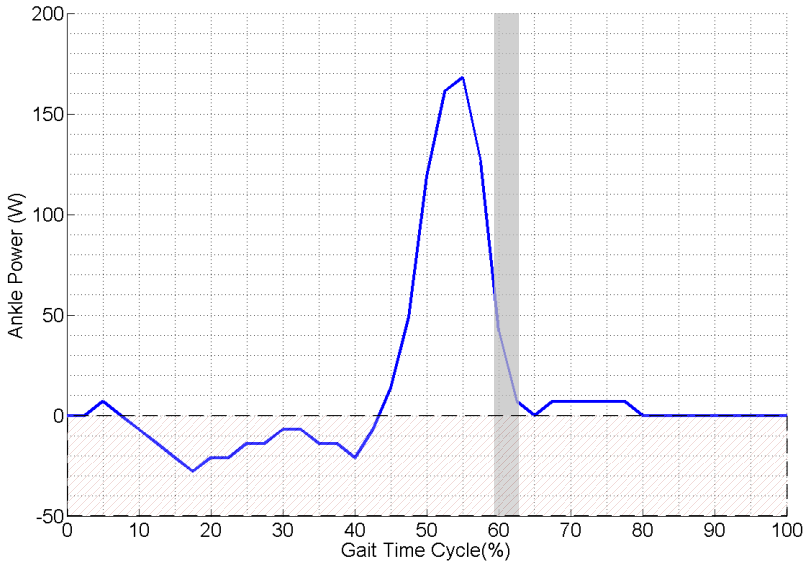

Fig.1: Ankle power of a typical healthy subject (70 kg) during level walking. The grey bar indicates the toe off [3].

The development of ankle prostheses mirrors the increasing level of human ankle function realization. The solid ankle-cushion heel (SACH) foot prostheses were designed to realize the fundamental function of supporting the body weight in the stance phase and absorb

the shock during heel strike [4]. As shown in figure 1, the ankle of a nonpathologic subject has a negative work phase in the mid stance and a burst of positive work before toe off during level walking [3, 5]. Some energy-storing below knee prostheses using an elastic structure to absorb the energy in the early stance phase and return the energy during push off to assist walking. The energy storage structure can be carbon composite leaf springs in the artificial feet [6-10], a shank-ankle-foot structure made of a specially developed carbon composite [11, 12], an elastic bumper spring [13] or other types [14]. To extend the practicability of the ankle prosthesis to stair ascent and descent, up slope and down slope walking, microprocessors-based control has been used to adjust the damping [8]. The PROPRIO FOOT® integrates an electric motor to adjust the ankle angular position, which improved the ground clearance in different walking and sitting conditions [15].

Subjects with a nonpathologic gait require high net power in the stance phase at the ankle during level walking and stair ascent, which the conventional passive ankle prosthesis cannot achieve [3]. A study in [16] showed that the lack of the push-off function at the ankle resulted in an early toe-off. Several active ankle prostheses using different kind of actuation have been developed by researchers, including off-board electric motor with flexible tether [17], pneumatic actuation [18], pneumatic artificial muscles [19], a DC motor with a ball screw [6, 20] and a DC motor with a lead screw [21]. The first commercially available ankle prosthesis providing active power in the stance phase was the BiOM [22].

The main challenge of the development of an active ankle prosthesis is to reach the kinematic and kinetic characteristics of a human's ankle-foot within the weight and volume limitation. This requires the prosthesis actuation to be high power to weight/volume ratio, high torque to weight/volume ratio and to have a strike absorption ability. To extend the ambulation range to stair ascent and descent, and slope climbing and descending, the peak power and peak torque of the actuation does not necessarily have to be increased comparing to level walking [3]. But the ankle dorsiflexion/plantarflexion range needs to be wider and the damping ratio should be adjustable. Besides these factors, the weight and size of the on-board energy source, noise and biomimetic shape are also essential for ankle prosthesis design.

We describe a powered ankle prosthesis which combines the advantages of an energy-storing damping-controllable ankle-foot prosthesis and an electrohydrostatic actuator. A prototype was built and the performance of which has been verified in bench tests and lower limb amputee trials.

DESIGN CONCEPT

The new powered ankle prosthesis was designed to achieve a quick switch between the passive and active mode. The major power was intended to be input into the ankle joint actuator to assist push-off at the end of stance phase and lift up the toes in the swing phase.

The ankle actuator was modified from a commercial available ankle prosthesis which is shown in figure 2 [8]. This élan foot has separated elastic carbon forefoot and heel, which could absorb the energy in early-middle stance and feedback the energy before toe-off. The ankle joint itself is a damper (hydraulic cylinder) with two bypass restriction valves. As shown in figure 2, the damping in either direction can be controlled by adjusting the orifices area of the restriction valves respectively. The restriction valves are controlled by two micro motors and a microprocessor.

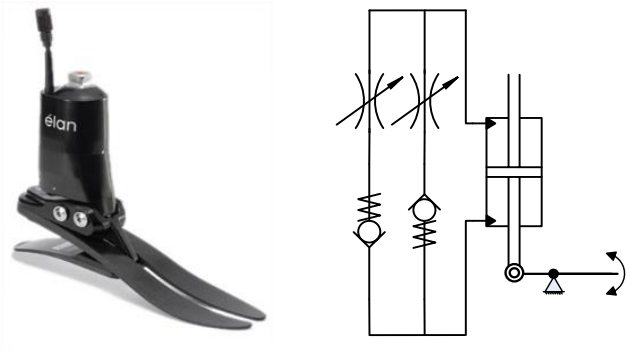

Fig.2: The élan foot and its hydraulic circuit [8].

A brushless DC motor and a bi-directional gear pump were used to deliver hydraulic oil to either side of the ankle cylinder via two flexible hoses. The hydraulic circuit is shown in figure 3. An accumulator is connected to the case drain of the pump, and the pump leakage is collected and re-fed into the closed-circuit via a pair of check valves. This

accumulator was pre-charged and maintained the low pressure in the circuit at about 5 bar.

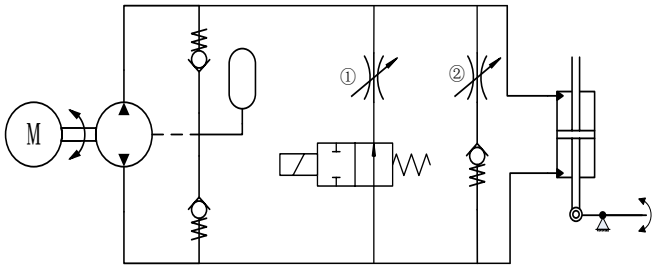

Fig.3: The hydraulic circuit of the new powered ankle prosthesis concept.

A hall effect sensor was attached between the ankle cylinder block and the foot carriage to measure the ankle angular position in a certain range, as shown in figure 4. When the ankle joint rotates across a threshold position in the dorsiflexion direction in the middle stance phase, after a certain length of delay, the electrohydrostatic actuation will be triggered to power a plantarflexion movement. The threshold position and the delay length before push-off could be manually adjusted to fit different walking speeds and different walking habit. The motor-pump will then reverse the rotation direction to lift the toe. The prosthesis will operate passively until the next trigger condition is matched. This simple control method has been used in initial tests of the prosthesis, and more sophisticated control approaches will be investigated in the future.

During powered push-off period, when the pressure in the bottom side of ankle cylinder is high, the bypass line ① (figure 3) would be fully closed by an on/off valve to ensure there is no leakage through that line

The Ankle dorsiflexion angle of a healthy subject is shown in figure 5 [3]. The timing control of a complete gait cycle is indicated in table 1.

DESIGN SPECIFICATIONS

Derived from the level walking kinematic and kinetic data of a typical person (70 kg), in the stance phase, the peak angular speed of ankle joint is about 73 °/s, the total movement range of ankle joint is about 27°, the peak moment is about 112 Nm and the mean power during push-off is about 133 Watts [3]. The angular movement range of the new ankle prosthesis was enlarged to 25° from the standard élan foot. The brushless DC motor from Maxon motor (EC 60 flat motor) was selected, which was rated to 100 Watts. The pump was a bi-directional gear pump with a displacement as 0.45 cc/rev, which was one of the smallest commercial bidirectional gear pumps. A piece of PVC hose was acted as the accumulator. The check valves used in the fluid feedback paths were from Lee Products Ltd [23].

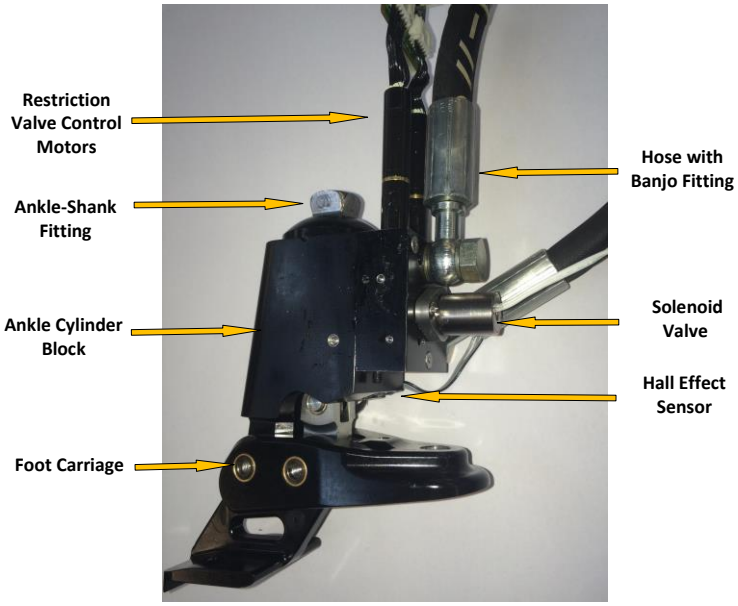

Fig.4: The ankle side assembly of the new powered ankle prosthesis

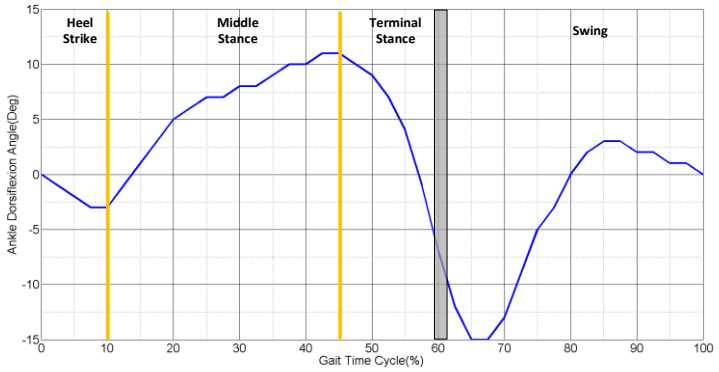

Fig.5: The ankle dorsiflexion angle of a healthy subject during level walking. The thick grey bar indicates toe off [3].

Table.1: The timing control of the prototype in a gait cycle.

Gait Phase	Heel strike	Middle stance	Terminal stance	Swing	
Ankle Spin Direction	PF	DF	PF	DF	-
Active/Passive Mode	Passive	Passive	Active	Active	Passive
Motor-pump Direction	0	0	Positive	Negative	0
Cylinder High Pressure Side	Top	Bottom	Bottom	Top	-
Activated Restriction Valve	②	①	-	②	-
On/off Valve	Open	Open	Close	Open	Open

The motor-pump unit was kept in a backpack, and connected with the ankle block by a pair of 1 meter hydraulic hoses. The diameter of these hoses are ¼ inch. The hydraulic oil would flow into the ankle cylinder via a pair of banjo fittings as shown in figure 4.

The manifold holes were machined to about 3 mm diameter to minimise the pressure loss within the space constraints of the ankle block. The on/off valve is a 3 way/2 position normally closed solenoid valve from Lee Products Ltd [24]. When the valve is opened, the fluid could only flow though the valve in one direction, which also included the function of the check valve in the line.

The control program was run on a National Instruments Compact RIO. Via a wireless router, the real-time data could be monitored on a laptop and the control parameters could be adjusted. A DC brushed servo drive module (NI 9505) was added to the Compact RIO to drive the solenoid valve. The motor was powered by a 48V battery, via an amplifier. The amplifier used in the prototype was the Escon controller from Maxon, which could record the motor speed and drive current. The weight of the batteries for the motor, controller and sensors were summed up to about 3 kg, which could be gathered into one single battery in the future. The capacity of the batteries will be discussed along with the patient trial results. All the battery and controllers were also held in the backpack. The total weight of the prototype was about 11 kg.

SIMULATION MODEL

A simulation model was built in Matlab/Simulink to help analyse the performance of the actuation in the new powered ankle prosthesis. As the focus here is to understand the hydraulic performance, the DC motor model is not presented. The actual experimental motor (pump) speed was used as the input signal to the simulation. The hydraulic circuit simulated is shown in figure 6. The arrows in figure 6 indicate the positive flow rate direction in the simulation model.

The accumulator hose in the prototype is simplified as a fluid source at a constant pressure in the simulation model. When the pressure in either side of the pump is lower than the pre-set pressure, a restricted flow will be added into that side. Because relatively significant volume of fluid is in the hose between the pump and the actuator, the compliance of the hoses is included in the model. The pressure losses due to the fittings and narrow holes are also important in the simulation model and can be used to assess hydraulic manifold design.

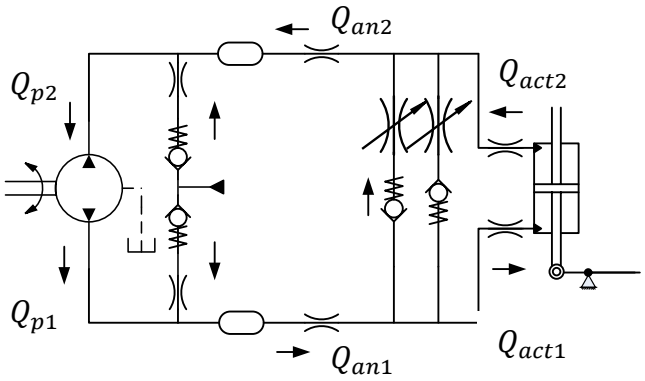

Fig.6: Simulated hydraulic circuit.

The flow equations for the fluid in either side of the hydraulic pump are given by:

$$Q_{p1} = D\omega - K_{in}\left(P_{p1} - P_{p2}\right) - K_{ex}P_{p1} \tag{1}$$

$$Q_{p2} = D\omega - K_{in}\left(P_{p1} - P_{p2}\right) + K_{ex}P_{p2} \tag{2}$$

where, Q_{p1} and Q_{p2} are the pump flows; D is the displacement of pump, ω is the motor-pump rotation speed; K_{in} is the internal leakage coefficient; K_{ex} is the external leakage coefficient; P_{p1} and P_{p2} are the pressures at either side of the pump. The simplified fluid compensation path and the compressible fluid in the hoses are given by:

$$\begin{cases} P_{p1} = \frac{1}{s}\left[\frac{B_{eh}\left(Q_{p1} - Q_{an1} + K_{acc}\sqrt{P_{acc} - P_{p1}}\right)}{V_{hose}}\right] \cdots (P_{p1} \le P_{acc}) \\ P_{p1} = \frac{1}{s}\left[\frac{B_{eh}\left(Q_{p1} - Q_{an1}\right)}{V_{hose}}\right] \cdots (P_{p1} > P_{acc}\ ) \end{cases} \tag{3}$$

$$\begin{cases} P_{p2} = \frac{1}{s}\left[\frac{B_{eh}\left(Q_{an2} - Q_{p2} + K_{acc}\sqrt{P_{acc} - P_{p2}}\right)}{V_{hose}}\right] \cdots (P_{p2} \le P_{acc}) \\ P_{p2} = \frac{1}{s}\left[\frac{B_{eh}\left(Q_{an2} - Q_{p2}\right)}{V_{hose}}\right] \cdots (P_{p2} > P_{acc}) \end{cases} \tag{4}$$

where, s is the differential operator; B_{eh} is the effective bulk modulus for rubber hoses; V_{hose} is the oil volume in the one hose; Q_{an1} and Q_{an2} are the flow rates at the inlet and outlet ports of ankle block; P_{acc} is the pre-set pressure in the constant pressure fluid source (simplified accumulator hose); K_{acc} is the orifice coefficient of the compensation flow. Linear pressure loss of the hoses and fittings is given by:

$$P_{an1} = P_{p1} - K_{hose}Q_{an1} \tag{5}$$

$$P_{an2} = P_{p2} + K_{hose} Q_{an2} \tag{6}$$

where, P_{an1} and P_{an2} are the pressures at the ankle inlet and outlet ports; K_{hose} is the pressure loss coefficient of the hoses and fittings. The bypass restriction orifice model is given by:

$$\begin{cases} \begin{cases} Q_{act1} = Q_{an1} - K_{PF}\sqrt{|P_{an1} - P_{an2}|} \\ Q_{act2} = Q_{an2} - K_{PF}\sqrt{|P_{an1} - P_{an2}|} \end{cases} \cdots (P_{an1} \geq P_{an2}) \\ \begin{cases} Q_{act1} = Q_{an1} + K_{DF}\sqrt{|P_{an1} - P_{an2}|} \\ Q_{act2} = Q_{an2} + K_{DF}\sqrt{|P_{an1} - P_{an2}|} \end{cases} \cdots (P_{an1} < P_{an2}) \end{cases} \tag{7}$$

where, Q_{act1} and Q_{act2} are the flow rates into/out of the actuator cylinder; K_{PF} is the orifice coefficient of the operation valve when active plantarflexion; K_{DF} is the orifice coefficient of the operation valve when active dorsiflexion. The pressure loss of the manifold in the ankle block is given by:

$$P_{act1} = P_{an1} - K_{an} Q_{act1} \tag{8}$$

$$P_{act2} = P_{an2} + K_{an} Q_{act2} \tag{9}$$

where, P_{act1} and P_{act2} are the pressures at the different side of the actuator cylinder; K_{an} is the pressure loss coefficient of the manifold in the ankle. The actuator and load model is:

$$P_{act1} = \frac{1}{s}\left[\frac{B_{eh}(Q_{act1} - A\dot{x})}{V_1 + Ax}\right] \tag{10}$$

$$P_{act2} = \frac{1}{s}\left[\frac{B_{eh}(A\dot{x} - Q_{act2})}{V_2 - Ax}\right] \tag{11}$$

$$AP_{act1} - AP_{act2} - F_{cushion} - F_c = F_{out} \tag{12}$$

$$\frac{F_{out}}{K_l} - Mg = K_l \ddot{x} M \tag{13}$$

where, A is the annual area of the cylinder; x is the displacement of cylinder rod, the zero position of which is at the middle position in the cylinder; V_1 and V_2 are the initial oil volume in the actuator; $F_{cushion}$ is the cushion force to stop the rod when it get to the end of the cylinder; F_c is the coulomb friction between the rod and the cylinder; F_{out} is the

output force from ankle actuator; K_l is the lever ratio of the weight lifting lever in the experiment; M is the load weight mass and g is the acceleration of gravity.

A series of tests was undertaken to help parametrize the model. The internal and external leakage coefficients were obtained by comparing both the mean outlet flow rate and the mean case drain flow rate in different load conditions with the theoretical flow rate which was calculated from the recorded motor-pump speed. The pump test results indicated that the volumetric efficiency was over 90% at the constant load condition but dropped significantly when the load was a pressure rapid pulse, which was more similar to the practical condition. The external leakage was much smaller than internal leakage. The obtained leakage coefficient was then adjusted by comparing the experiment result and the simulation result, giving were $K_{in} = 1 \times 10^{-12}\ \frac{m^3}{s}/Pa$ and $K_{ex} = 7.2 \times 10^{-15}\ \frac{m^3}{s}/Pa$.

An approximate linear relationship between pressure loss and flow rate was found in a series of loaded motion tests. In the test, the ankle actuation was powered against a series of constant loads at different motor speeds. The pressure was measured near the pump inlet and outlet ports. As shown in figure 7, the pressure loss characteristic of the actuation could be fitted by a linear equation:

$$P_d = kQ + P_c + P_l \tag{14}$$

where, P_d is the pressure difference between the inlet and outlet ports of the pump; k is the pressure loss coefficient; P_c is a constant pressure loss due to the friction in the actuator; P_l is the load pressure. By fitting the test results of 0, 5 and 10 kg loaded motion tests, an averaged pressure loss coefficient could be obtained as $k = 1.1 \times 10^{11}\ \text{Pa}/\frac{m^3}{s}$ and a flow rate independent pressure loss as $P_c = 2.4\ bar$. Resulting from the flow rate difference before or after the bypass line, the pressure loss has been divided into two parts in the simulation model, which are $K_{hose} = 7.4 \times 10^{10}\ \text{Pa}/\frac{m^3}{s}$ and $K_{an} = 2.6 \times 10^{10}\ \text{Pa}/\frac{m^3}{s}$.

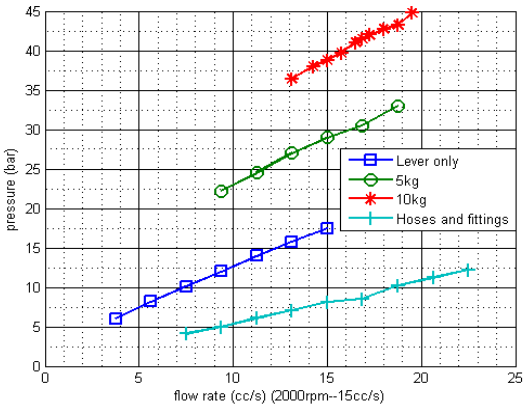

Fig.7: Pressure loss test with different load (hoses& fittings, 0kg, 5kg and 10kg).

Fig.8: Powered ankle prosthesis bench test rig.

The bench test rig is shown in figure 8. The ankle prosthesis was mounted upside down to lift a lever. Weights could be hung at the end of the lever to provide certain load. In figure 9, the comparison between the simulation result and experiment result indicates that the simulated actuation characteristics (pressures and ankle angular position) match the experiment result well. In this particular test, a 16 kg weight was hanging at the end of a lever, and the motor demand movement was 3500 rpm for 1 second. The pressure increased to 100 bar when the actuator rod reached the end of the cylinder. Some shortcomings of the simulation model can also be seen from figure 9. For example, the low pressure in the experiment dropped to about 1 bar, instead of maintaining over the pre-set 5 bar accumulator pressure in the simulation result. The ankle acceleration characteristic was also different between experiment and simulation which should be further investigated.

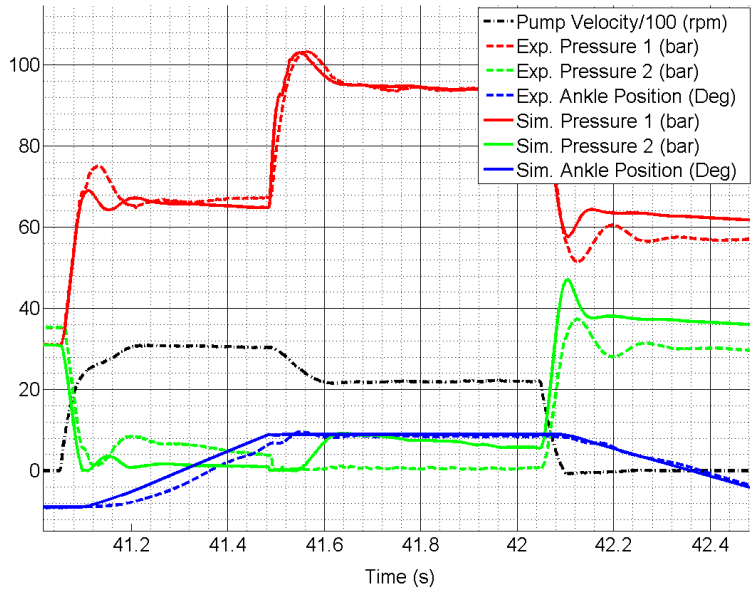

Fig.9: Comparison between simulation and experiment result.

With the assistance of the simulation model, it was proven that the on/off valve was essential to fully close the bypass line rather than relying on the adjustable orifice. The model was also applied to predict the pressure loss when designing the manifold in the ankle block.

Initial Trial with amputees

The new powered ankle prosthesis prototype has been tested in Chas A Blatchford & Sons Ltd with a transfemoral amputee and a transtibial amputee respectively. Considering the safety issue, a push button was attached onto the controller and could be held by the amputee. The active mode of the ankle prosthesis actuation could only be enabled when the button has been pressed down. To obtain the performance data of the prototype in the amputee's natural ambulation, the power source backpack was carried by an assistant instead of being worn by the amputee.

Both the amputees confirmed that the new powered ankle prosthesis could provide sufficient assistance at push-off. Some other preliminary results were:

The powered ankle prosthesis consumed about 112 J energy in each gait. The batteries currently used in the prototype could support over 3000 steps. This working range could be increased if the motor-pump could decelerate before the cylinder rod reach the end stroke.

The right timing to inject power into the ankle actuator is critical to effectively assist amputee walking forward.

Noise of the powered actuation was obvious, which should be abated in the future.

An additional trial has taken place which was to assist the dorsiflexion movement in the stance phase instead, considering the active power could be delivered to the ankle more gently in a bigger time window. A contrary feedback from the transfemoral amputee and transtibial amputee was received. Only the above-knee amputee with a knee prosthesis considered that it was very helpful to assist walking.

Conclusion

As a result of the high power density of electrohydrostatic actuation, it is suitable for the new powered ankle prosthesis. With the advantages of the passive prosthesis being retained, this new powered ankle prosthesis could sufficiently assist lower limb amputees' walking by providing active power at push-off.

The simulation model of the actuation system could represent the performance of the prototype and helped to design the new powered ankle prosthesis.

The future work will be focusing on the compact prototype of the powered ankle prosthesis, in which the whole actuation will be mounted nearby the ankle joint. The weight could be significantly reduced by optimising the batteries. The control of the powered ankle prosthesis could be further investigated to optimize the timing of power injection, and it should be self-adjusting according to different walking speed and ambulation condition.

Acknowledgments

We thank Chas A Blatchford & Sons Ltd., the University of Bath, and the UK Higher Education Innovation Fund for supporting this research.

References

[1] K. Ziegler-Graham et al., "Estimating the Prevalence of Limb Loss in the United States: 2005 to 2050," *Archives of physical medicine and rehabilitation*, vol. 89, no. 3, pp. 422-429, 2008.
[2] National Health Service. (2014, July 21). *Amputation Introduction* [Online]. Available: http://www.nhs.uk/Conditions/Amputation/Pages/Introduction.aspx
[3] R. Riener et al., "Stair ascent and descent at different inclinations," *Gait & posture*, vol. 15, No.1, pp. 32-44, 2002.
[4] A. L. Muilenburg and A. B. Wilson, jr. (1996) *A Manual for Below-Knee Amputees Ankle-Foot Systems.* [Online]. Available:http://www.oandp.com/resources/patientinfo/manuals/9.htm
[5] D.A. Winter, "Energy generation and absorption at the ankle and knee during fast, natural, and slow cadences," *Clin Orthop Relat Res*, vol.175, pp. 147-54, May. 1983.
[6] S. Au et al., ''Powered ankle-foot prosthesis for the improvement of amputee ambulation,'' in *Proc. 29th Annu. Int. Conf. IEEE Engineering in Medicine and Biology Society*, Lyon, France, 2007, pp. 3020–3026.
[7] Chas A Blatchford and Sons Ltd. (2015). *Esprit* [Online]. Available: http://www.endolite.co.uk/products/esprit
[8] Chas A Blatchford and Sons Ltd. (2015). *élan* [Online]. Available: http://www.endolite.co.uk/products/elan
[9] Ottobock. (2015). *1C60 Triton* [Online]. Available: http://www.ottobock.com/cps/rde/xchg/ob_com_en/hs.xsl/38138.html
[10] Össur. (2015). *Flex-Foot® Junior* [Online]. Available: http://www.ossur.co.uk/prosthetic-solutions/products/feet/feet/flex-foot-junior
[11] Chas A Blatchford and Sons Ltd. (2015). *bladeXT* [Online]. Available: http://www.endolite.co.uk/products/bladext
[12] Össur. (2015). *Flex-Foot Cheetah* [Online]. Available: http://www.ossur.co.uk/prosthetic-solutions/products/feet/feet/cheetah
[13] Chas A Blatchford and Sons Ltd. (2015). *eliteVT* [Online]. Available: http://www.endolite.co.uk/products/elitevt
[14] MJ. Hsu et al., "The Effects of Prosthetic Foot Design on Physiologic Measurements, Self-Selected Walking Velocity, and Physical Activity in People With Transtibial Amputation," *Arch Phys Med Rehabil*, vol.87, pp. 123-9, 2006.
[15] Össur. (2015). *PROPRIO FOOT®* [Online]. Available: http://www.ossur.co.uk/prosthetic-solutions/products/feet/bionic-feet/proprio-foot
[16] J. Breakey, "Gait of unilateral below-knee amputees," *Orthotics and Prosthetics*, vol. 30, No. 3, pp. 17-24, September 1976

[17] M. Joshua et al., "An Experimental Robotic Testbed for Accelerated Development of Ankle Prostheses," in *IEEE Int. Conf. on Robotics and Automation*, Karlsruhe, Germay, 2013

[18] F. Sup et al., "Design and Control of a Powered Transfemoral Prosthesis," *The International Journal of Robotics Research*, vol. 27, No. 2, pp. 263–273, February 2008.

[19] R. Versluys et al., "A Pneumatically Powered Below-Knee Prosthesis: Design Specifications and First Experiments with an Amputee," in *Proc. Of the 2nd Biennial IEEE/RAS-EMBS Int. Conf. on Biomedical Robotics and Biomechatronics*, Scottsdale, AZ, USA, 2008.

[20] F. Sup et al., "Design and Control of an Active Electrical Knee and Ankle Prosthesis," in *Proc. Of the 2nd Biennial IEEE/RAS-EMBS Int. Conf. on Biomedical Robotics and Biomechatronics*, Scottsdale, AZ, USA, 2008.

[21] J.K. Hitt et al., "An Active Foot-Ankle Prosthesis With Biomechanical Energy Regeneration," Journal of Medical Devices, vol. 4, pp. 011003-1-9, Mar. 2010.

[22] BiOM. (2015). *BiOM® T2 System* [Online]. Available: http://www.biom.com/prosthetists/personal-bionics/

[23] The Lee Company. (2015). *Axial Flow Screened 187 Lee Chek* [Online]. Available: http://www.ottobock.com/cps/rde/xchg/ob_com_en/hs.xsl/38138.html

[24] The Lee Company. (2015). *250 Series Solenoid Valve* [Online]. Available: http://leecat.theleeco.com/ecatalog/piloting-solenoid-valves/en/SDBA2531013B

Appendix 2: Publication 2

This appendix includes the conference paper titled '**Testing an Electrohydrostatic Powered Ankle Prosthesis with Transtibial and Transfemoral Amputees**', which is published in Proceedings of the 7th IFAC Symposium on Mechatronic Systems, Sep 5-8, 2016, Loughborough University, UK, Authors including:

Tian Yu, Andrew Plummer, Pejman Iravani

Department of Mechanical Engineering, Centre for Power Transmission and Motion Control, University of Bath, Bath, United Kingdom

Jawaad Bhatti, Saeed Zahedi OBE, David Moser

Chas A Blatchford & Sons Ltd., Kingsland Business Park, Basingstoke, United Kingdom

Abstract

Powered lower-limb prostheses have the potential to assist amputees in the push-off phase during level walking, as well as stair and slope ascent. Compared to electromechanical actuation, the advantages of using eletrohydrostatic actuation (EHA) including high power density, low noise and good controllability. Especially for the application in lower limb prosthetic joints, an EHA provides a quick and smooth switch between passive and active operation modes. This paper presents the testing results using a new eletrohydrostatic powered ankle prosthesis which combines an EHA with a controllable passive damper. The new powered ankle prosthesis has been tested by both a transtibial and a transfemoral amputee. The test results show that the ankle prosthesis can provide sufficient power to assist toe push-off and subsequent foot lift (dorsiflexion) and operating passively in the rest of a gait cycle. The test results are compared with the ankle dorsiflexion angle and torque for healthy subjects. The timing control method and the performance of the EHA are discussed.

INTRODUCTION

A well-functioning lower limb prosthesis is essential to enable an amputee's daily activities. The development of ankle prostheses mirrors the increasing level of human ankle function realization. The solid ankle-cushion heel (SACH) foot prostheses were designed to realize the fundamental function of supporting the body weight in the stance phase and absorb the shock during heel strike (Muilenburg and Bennett Wilson, 1996). As shown in figure 1, the ankle of a nonpathologic subject has a negative work phase in the mid stance and a burst of positive work before toe off during level walking (Winter, 1988; Riener, et al. 2002). Some energy-storing below knee prostheses using an elastic structure to absorb the energy in the early stance phase and return the energy during push off to assist walking. The energy storage structure can be carbon composite leaf springs in the artificial feet (Au et al., 2007; Blatchford, 2016a; Blatchford, 2016b; Ottobock, 2016; Össur, 2016a), a shank-ankle-foot structure made of a specially developed carbon composite (Blatchford, 2016c; Össur, 2016b), an elastic bumper spring (Blatchford, 2016d) or other types (Hsu, et al., 2006). To extend the practicability of the ankle prosthesis to stair ascent and descent, up slope and down slope walking, microprocessors-based control has been used to adjust the damping (Blatchford, 2016b).The PROPRIO FOOT® integrates an electric motor to adjust the ankle angular position, which improved the ground clearance in different walking and sitting conditions (Össur, 2016c).

Subjects with a nonpathologic gait require high net power in the stance phase at the ankle during level walking and stair ascent, which the conventional passive ankle prosthesis cannot achieve (Riener, et al., 2002). The study by Breakey (1976) showed that the lack of the push-off function at the ankle resulted in an early toe-off. Several active ankle prostheses using different kind of actuation have been developed by researchers, including off-board electric motor with flexible tether (Caputo and Collins, 2013), pneumatic actuation (Sup, Bohara and Goldfarb, 2008), pneumatic artificial muscles (Versluys, et al., 2008), a DC motor with a ball screw (Au, et al., 2007; Sup, et al., 2008) and a DC

motor with a lead screw (Hitt, et al., 2010). The first commercially available ankle prosthesis providing active power in the stance phase was the BiOM (BiOM, 2016).

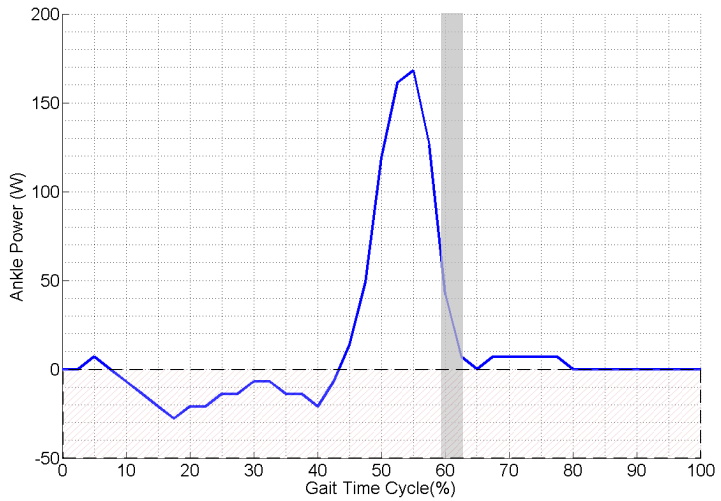

Fig. 1. Ankle power of a typical healthy subject (70 kg) during level walking. The grey bar indicates the toe off (Riener, et al., 2002).

The main challenge of the development of an active ankle prosthesis is to reach the kinematic and kinetic characteristics of a human's ankle-foot within the weight and volume limitation. This requires the prosthesis actuation to be high power to weight/volume ratio, high torque to weight/volume ratio and to have a strike absorption ability. To extend the ambulation range to stair ascent and descent, and slope climbing and descending, the peak power and peak torque of the actuation does not necessarily have to be increased comparing to level walking (Riener, et al., 2002). But the ankle dorsiflexion/plantarflexion range needs to be wider and the damping ratio should be adjustable. Besides these factors, the weight and size of the on-board energy source, noise and biomimetic shape are also essential for ankle prosthesis design.

We describe a powered ankle prosthesis which combines the advantages of an energy-storing damping-controllable ankle-foot prosthesis and an electrohydrostatic actuator. A prototype was built and the performance of which has been verified in bench tests and lower limb amputee trials.

DESIGN and CONTROL

The new powered ankle prosthesis was designed to achieve a quick switch between the passive and active modes. Power was intended to be input into the ankle joint actuator to assist push-off at the end of the stance phase and lift up the toes in the swing phase. A prototype has been built and tested in a lab environment and with transtibial and transfemoral amputees.

The prototype was developed from a commercially available passive ankle prosthesis which is shown in figure 2 (Blatchford, 2016b). This élan foot has separated elastic carbon forefoot and heel, which can absorb energy in early-middle stance and return energy before toe-off. The ankle joint itself has a damper (hydraulic cylinder) with two bypass restrictor valves. As shown in figure 2, the damping in either direction can be controlled by adjusting the orifice areas of the restrictor valves respectively. The restrictor valves are controlled by two micro motors and a microprocessor.

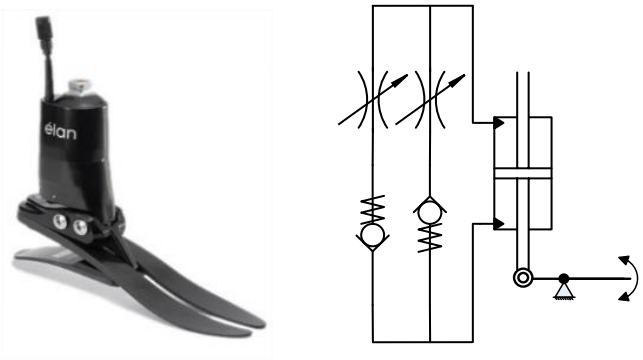

Fig. 2. The élan foot and its hydraulic circuit (Blatchford, 2016b).

A brushless DC motor (Maxon EC 60 flat motor) and a bi-directional gear pump (displacement: 0.45 cc/rev) were used to deliver hydraulic oil to either side of the ankle cylinder via two flexible hoses. The hydraulic circuit is shown in figure 3. A piece of low pressure hose acts as the accumulator, which is connected to the case drain of the pump, and the pump leakage is collected and re-fed into the closed-circuit via a pair of check valves (The Lee Company, 2016a). This accumulator was pre-charged and maintained the low pressure level in the circuit at about 5 bar.

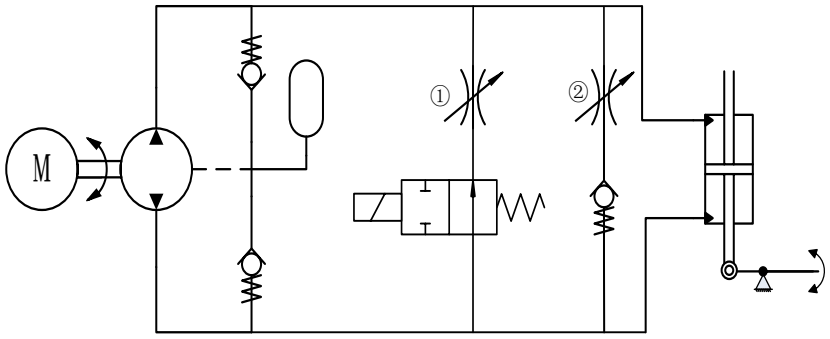

Fig. 3. The hydraulic circuit of the new powered ankle prosthesis concept.

A Hall effect sensor was attached between the ankle cylinder block and the foot carriage to measure the ankle angular position in a certain range, as shown in figure 4. During the powered push-off period, when the pressure in the bottom side of ankle cylinder is high, the bypass line ① (figure 3) would be fully closed by an on/off valve to ensure there is no leakage through that line. The on/off valve is a 3 way/2 position normally closed solenoid valve from Lee Products Ltd as shown in figure 4 (The Lee Company, 2016b). When the valve is opened, the fluid could only flow through the valve in one direction, as it also functions as a check valve in the line.

The control program was run on a National Instruments Compact RIO. The motor was powered by a 48 V battery via an amplifier. The amplifier used in the prototype was the Escon controller from Maxon. The total weight of the batteries, controller and sensors was about 3 kg. The battery, controllers and motor-pump were held in a backpack. The total weight of the prototype was about 11 kg. Additional detail of the design specification is presented in Yu, et al. (2015).

The timing control of a complete gait cycle is indicated in figure 5 and table 1. By monitoring the ankle flexion angle using the Hall effect sensor, a threshold angle could be set. The active mode would only be triggered when the ankle flex passed the threshold angle in the dorsiflexion (DF) direction. A time delay was added between the active mode trigger and the start of the powered plantarflexion (PF) phase. The threshold and the time delay could be manually adjusted recording to different walking speeds and different patients. This simple control method has been used in initial tests of the prosthesis, and more sophisticated control approaches will be investigated in the future. The powered PF and powered DF time length was pre-set at a certain value.

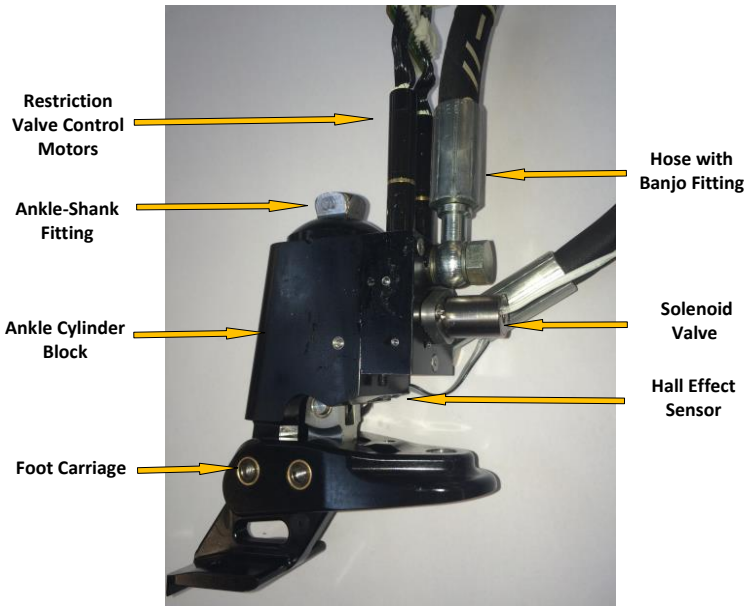

Fig. 4. The ankle side assembly of the new powered ankle prosthesis.

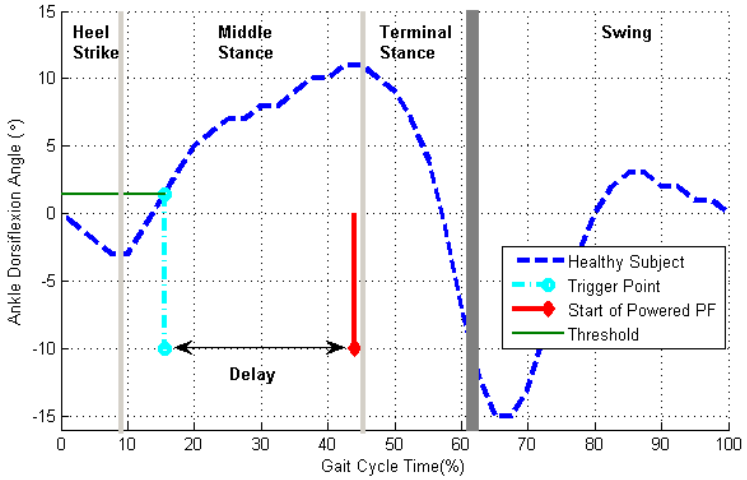

Fig. 5. The ankle dorsiflexion angle of a healthy subject during level walking. The thick grey bar indicates toe off (Riener, et al., 2002).

Table 1. The timing control of the prototype in a gait cycle.

Gait Phase	Stance					Swing		
	Heel strike	Middle stance	Trigger	Delay	Powered PF	Delay	Powered DF	Swing
Ankle Rotation Direction	PF	DF	Ankle dorsiflex pass a threshold angle	DF	PF	-	DF	-
Active/Passive Mode	Passive	Passive		Passive	Active	Passive	Active	Passive
Motor-pump Direction	0	0		0	Positive	0	Negative	0
Cylinder High Pressure Side	Top	Bottom		Bottom	Bottom	Bottom	Top	-
Activated Restriction Valve	②	①		①	-	–	②	-
On/off Valve	Open	Open		Open	Close	lose	Open	Open

AMPUTEE TEST RESULTS

3.1 Test Introduction and Setup

The new powered ankle prosthesis prototype has been tested by two amputees (a transtibial amputee and a transfemoral amputee) in the indoor test site in Chas A Blatchford & Sons Ltd. The transtibial amputee is 70 kg and the transfemoral amputee is 80 kg. The new powered ankle prosthesis was connected to the amputee's socket (below-knee socket of the transtibial amputee and prosthetic knee of the transfemoral) by an adapter and a tube. The mounting angle of the ankle could be adjusted using the adapter within the adjustment range. When the amputees first put on the new powered ankle prosthesis, the mounting angle was tuned to fit a comfortable inversion/eversion angle and the maximum available dorsiflexion/plantarflexion rotation range. The settings of the DF and PF restrictor valves have been tuned to meet the damping requirement of the amputees when the ankle is in the passive mode. An assistant held the backpack and followed the amputee to avoid increasing the body weight of the amputee in the test. A push button was connected to the controller and held by the amputees. The active mode of the powered ankle prosthesis could only be enabled when the push button was pressed

down, which gives the ability to disable the motor when the amputee intends to stop walking.

Each amputee walked around the indoor test site. The amputees turned around after each 4-5 steps because of the limitation of the test area. The threshold angle to trigger the active mode was set according to the amputee's preference. Since the threshold and time delay could not be adjusted automatically according to different walking speeds, the patient walked at a constant speed so that the power from the EHA was applied in the correct time window. When the delay time length matched the walking speed, the amputees reported that they could get useful degree of assistance from the powered ankle prosthesis.

3.2 Test Results for the Transtibial Amputee

The comparison of the ankle dorsiflexion angle between the transtibial amputee with powered ankle prosthesis and a healthy subject is shown in figure 6. The dashed line in the figure indicates the ankle dorsiflexion angle of the healthy subject (Riener, et al., 2002). There are 5 steps overlaid in the upper graph. The gait cycles start from heel strike and the gait durations are 1.293-1.437 s, which are slower than a normal walking speed of healthy people (1.11±0.05 s) (Riener, et al., 2002). The total ankle rotation range is about 22°.

Since the ankle was driven to the maximum dorsiflexion angle in each powered DF phase, the heel strike was always starting at maximum dorsiflexion. It can be seen in figure 6 that the PF angle for the transtibial amputee with the prosthesis (about 5-9°) is much bigger than for healthy people (3°) (Riener, et al., 2002). The time length of the PF in heel strike is also longer than in the healthy subject, which indicates that the passive PF damping could be higher at this walking speed. The grey bar in figures 6 and 7 indicate when the cylinder rod reaches the end of its stroke in the mid stance before the start of the powered PF phase, which results from the total available dorsiflexion range of this

prosthesis being smaller than health people. Recording to the amputee's feedback, the lack of dorsiflexion angle did not affect the walk experience.

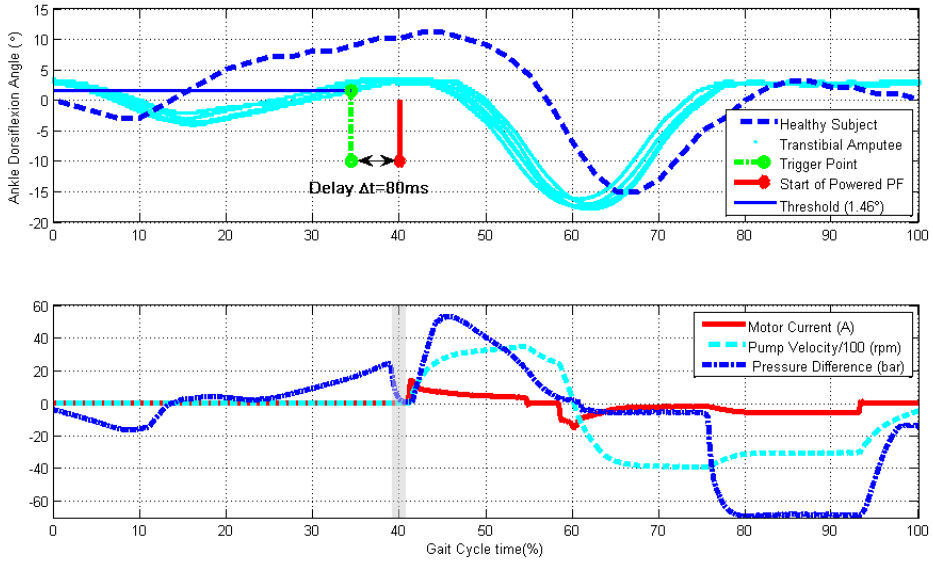

Fig. 6. The comparison of the ankle dorsiflexion angle between the transtibial amputee with powered ankle prosthesis and a healthy subject (Riener, et al., 2002).

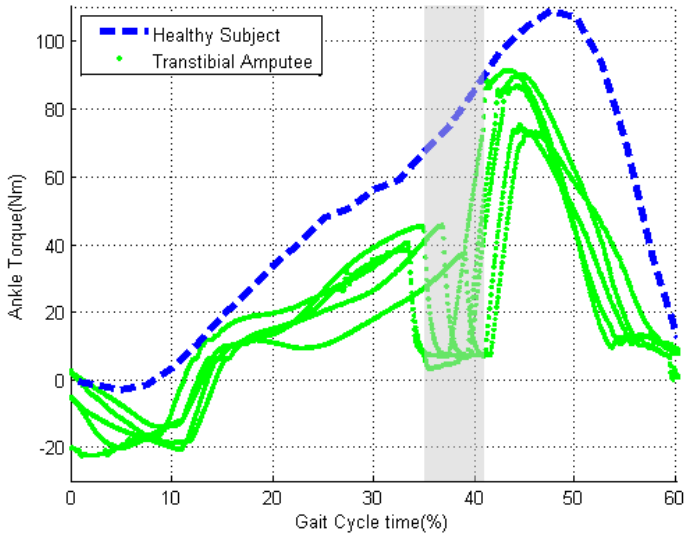

Fig. 7. The comparison of the ankle torque between the transtibial amputee with powered ankle prosthesis and a 70kg healthy subject (Riener, et al., 2002).

The threshold angle was 1.46° and the time delay before the start of the powered PF was 80 ms as shown in figure 6. In these series of steps, the start of the powered PF was at about 35-40% of the gait cycle. The EHA performance for a typical step is shown in the bottom graph in figure 6. In this step, the motor started running at about 40% of the gait cycle and was demanded to run at the highest speed for 200 ms. At the same time, the on/off valve was closed. The load pressure increased to 58bar in the middle of the powered PF phase and then reduced during the toe-off. The motor velocity was about 3000 rpm in the powered PF period. The current consumption was about 5 A. The ankle plantar flexed to the maximum 22° within 200 ms, which is approximately the same PF speed of health people (26° in 250 ms). After another period of delay, the motor was demanded to run in the reverse direction for 500ms to lift the toe. The current consumption was very small in this powered DF phase, but a lot of energy was wasted after the maximum DF angle is reached at about 80% of the gait cycle. This results from the simple control strategy which does not detect this condition to turn off the motor.

The ankle torque during the stance phase of the transtibial amputee is shown in figure 7. The ankle torque was calculated from the pressure difference in the hydraulic circuit. The dashed line in the figure indicates the ankle torque of a healthy subject (Riener, et al., 2002). As shown in figure 7, during the heel strike, the prosthetic ankle provides more resistance torque (20 Nm) compared to the healthy ankle (about zero), i.e. cushioning heel strike is not as good. In the middle stance, the ankle torque calculated from the pressure difference disappears for about 5% of the gait cycle which is because the rod of the actuator reach the end of its stroke. This does not translate to a drop in total torque at the ankle (i.e. additional torque is provided by the cylinder end-stop).The peak torque (90 Nm) during the powered PF phase is smaller than the peak torque of the normal ankle (110 Nm).

3.3 Test Results for the Transfemoral Amputee

The comparison of the ankle dorsiflexion angle between the transfemoral amputee with powered ankle prosthesis and the healthy subject is shown in figure 8. The dashed line in the figure indicates the ankle dorsiflexion angle of a healthy subject (Riener, et al., 2002). There are 7 steps overlaid in the upper graph. The gait sizes are 1.439-1.505 s, which are longer than the transtibial amputee. Comparing with the transtibial amputee, the ankle PF angle in heel strike of transfemoral amputee is much bigger, approximately 15-18°, but the length of the heel strike is about the same (16-17%). As can been seen in figure 8, the full rotary range of the prosthetic ankle joint has been used in the stance phase, which avoids the lack of the dorsiflexion angle occurred in the test with the transtibial amputee.

The threshold angle was -3.53° and the time delay before the start of the powered PF was 60 ms as shown in figure 8. In these series of steps, the start of the powered PF was at about 37-43% of the gait cycle. The EHA performance of a typical step is shown in the bottom graph in figure 8. In this step, the motor started running at about 42% of the gait cycle and was demanded to run at the highest speed for 300 ms. The first peak pressure difference reached during the powered PF phase is 82 bar, which is the load pressure in the terminal stance. The second peak at the end of this powered PF period is because the ankle has been plantar flexed to the maximum and the actuator rod reached the end of the stroke, which is indicated by the grey bar in figures 8 and 9. The motor velocity was about 2500 rpm and the current consumption was about 5 A. The ankle plantar flexed to the maximum 22° within about 300 ms, which is slower than the transtibial amputee because the body weight of the transfemoral amputee in the test is heavier than the transtibial amputee.

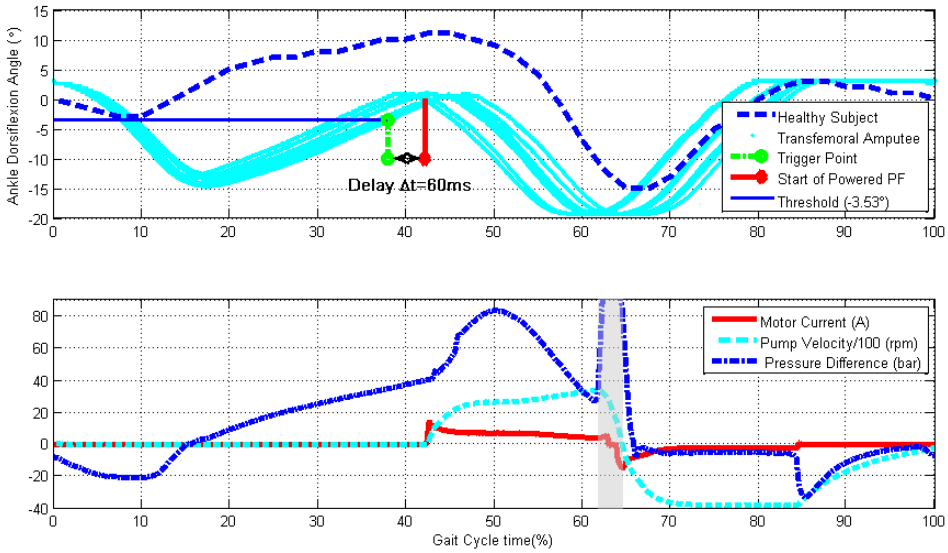

Fig. 8. The comparison of the ankle dorsiflexion angle between the transfemoral amputee with powered ankle prosthesis and the healthy subject (Riener, et al., 2002).

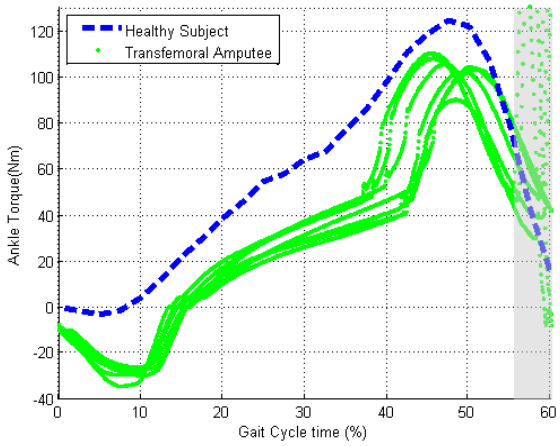

Fig. 9. The comparison of the ankle torque between the transfemoral amputee with powered ankle prosthesis and an 80kg healthy subject (Riener, et al., 2002).

The ankle torque during the stance phase of the transfemoral amputee is shown in figure 9. The dashed line in the figure indicates the ankle torque of a health subject (Riener, et al., 2002). As shown in figure 9, during the heel strike, the prosthetic ankle provides more torque (30 Nm) compare to the transtibial amputee. The peak torque (110 Nm) during the powered PF phase, which is higher than the transtibial amputee but still smaller than for a healthy person of the same weight (120 Nm).

3.4 Testing Conclusions

As seen in the test results, the ankle prosthesis was operating in passive mode in the majority of the gait cycle without using any net power. The passive damping in the hydraulic circuit played an important role in heel strike, helping to absorb the heel strike impact. The heel strike PF angle of both the transtibial amputee (5-9°) and the transfemoral amputee (15-18°) are bigger than healthy people (3°, Riener, et al., 2002), which indicates the passive PF damping could be set higher.

In the amputee tests, the prosthesis only needs to be powered in the push-off PF phase to assist walking, which is about 15-20% of the gait cycle. Within this powered PF period in the terminal stance phase, the peak ankle torque of the transtibial amputee is 90 Nm (110 Nm for 70 kg healthy subject, Riener, et al., 2002), which is equivalent to 58 bar pressure difference in the EHA. Under this load pressure difference, the motor-pump is running at a speed of about 3000 rpm and the ankle rotation speed is about 110 °/s, which is approximately the same speed as for a healthy subject (104 °/s, Riener, et al., 2002). The peak ankle torque of the transfemoral amputee is 110 Nm (120 Nm for 80kg healthy subject, Riener, et al., 2002), which is equivalent to 82 bar pressure difference in the EHA. Due to the high load, the motor-pump is running at a speed of about 2500rpm and the ankle speed is about 73 °/s. In both tests, the EHA provides high ankle torque and high ankle rotation speed in the powered PF period to assist walking. Even though the output power is less than that measured for healthy people, especially for the heavier amputee,

both the transtibial amputee and the transfemoral amputee reported that they received significant assistance from the powered ankle prosthesis.

It is essential that the torque is applied to the ankle joint at the correct timing point. Premature triggering would result in the power being wasted by lifting the body instead of pushing forward. Late triggering would reduce the assistance before toe off. The tests indicate an appropriate timing point is about 40% of the gait cycle at a gait duration of around 1.293-1.505 s. In the amputee tests, the transtibial amputee consumed approximately 44 J per step in the powered PF phase and the value for the transfemoral amputee is about 63 J per step, which mostly results from the body weight difference and the timing of the powered PF. The power used to dorsiflex the ankle in the swing phase is about 2.4 J per step. A 48 V battery with 2AH capacity can thus sustain more than 5000 steps of level walking.

The walking speed of both the amputees is slower than healthy subjects. The ankle joint rotation range is smaller than for the non-amputee, but if the mounting angle was adjusted to fit the amputee's walking gait, the rotation range of the prosthesis ankle could satisfy the full rotation requirement. Also, the noise from the actuation was noticeable in the powered PF phase.

CONCLUSIONS and FUTURE WORK

The design presented in this paper using an EHA allows quick switch between powered and passive modes. Recording to the test results and the feedback of both the amputees who involved in the testing, the new powered ankle prosthesis can provide damping to absorb impact and support body weight in the passive phase avoid the consumption of net power, and provide high ankle torque and high ankle rotation speed in the active phase to effectively assist them walking.

The future work will be focusing on two aspects: the development of compact actuation integrated in the ankle joint and study of the intelligent control of the ankle prosthesis.

According to feedback from both amputees, the hydraulic hoses which link the motor-pump in the backpack and the actuator at the ankle end not only limited the motion of the amputee. These also reduce the stiffness and efficiency of the hydraulic transmission. The motor-pump will be mounted at the ankle end to overcome this. Beside the reduction in weight by removing the hydraulic hoses, the weight of the whole prototype will be significantly reduced by better integration.

Additional sensors will be used to investigate the relationship between the different features at different walking speeds and the timing point of the powered PF. For example strain gauges at the heel and the toe can detect the centre of the body weight moving forward along with walking, which could be used to compute the walking speed and also help to detect the movement intention of the amputee. An inertial measurement unit will also be useful in this regard.

ACKNOWLEDGMENTS

We thank Chas A Blatchford & Sons Ltd., the University of Bath, and the UK Higher Education Innovation Fund for supporting this research.

REFERENCES

Au, S., Herr, H., Weber, J. and Martinez-Villalpando, E. (2007). Powered Ankle-Foot Prosthesis for the Improvement of Amputee Ambulation. *Proceedings of the 29th Annual International Conference of the IEEE EMBS*, pp.3020-6.

BiOM. (2016). *Flex-Foot Cheetah*. [online] Available at:< http://www.bionxmed.com/patients/the-biom-advantage/> [Accessed 12 February 2016].

Blatchford. (2016a). *Esprit*. [online] Available at:<http://www.endolite.co.uk/products/esprit> [Accessed 12 February 2016].

Blatchford. (2016b). *élan*. [online] Available at:<http://www.endolite.co.uk/products/elan> [Accessed 12 February 2016].

Blatchford. (2016c). *bladeXT*. [online] Available at:<http://www.endolite.co.uk/products/bladext> [Accessed 12 February 2016].

Blatchford. (2016d). *eliteVT*. [online] Available at:<http://www.endolite.co.uk/products/elitevt> [Accessed 12 February 2016].

Breakey, J. (1976). Gait of unilateral below-knee amputees. *Orthotics and Prosthetics*, 30(3), p.17-24.

Caputo, J. and Collins, S. (2013). An Experimental Robotic Testbed for Accelerated Development of Ankle Prostheses. *2013 IEEE International Conference on Robotics and Automation (ICRA)*, pp.2645-2650.

Hitt, J., Sugar, T., Holgate, M. and Bellman, R. (2010). An Active Foot-Ankle Prosthesis With Biomechanical Energy Regeneration. *Journal of Medical Devices*, 4, pp.011003-1-9.

Hsu, M., Nielsen, D., Lin-Chan, S. and Shurr, D. (2006). The Effects of Prosthetic Foot Design on Physiologic Measurements, Self-Selected Walking Velocity, and Physical Activity in People With Transtibial Amputation. *Arch Phys Med Rehabil*, 87, pp.123-9.

Muilenburg, A.L. and Bennett Wilson, A. (1996). *A Manual for Below-Knee Amputees Ankle-Foot Systems*. [online] Available at:<http://www.oandp.com/resources/patientinfo/manuals/9.htm> [Accessed 12 February 2016].

Ottobock. (2016). *Triton*. [online] Available at:<http://corporate.ottobock.co.uk/cps/rde/xchg/ob_uk_en/hs.xsl/38130.html> [Accessed 12 February 2016].

Össur. (2016a). *Flex-Foot® Junior*. [online] Available at:<http://www.ossur.co.uk/prosthetic-solutions/products/feet/feet/flex-foot-junior> [Accessed 12 February 2016].

Össur. (2016b). *Flex-Foot Cheetah*. [online] Available at:<http://www.ossur.co.uk/prosthetic-solutions/products/feet/feet/cheetah > [Accessed 12 February 2016].

Össur. (2016c). *PROPRIO FOOT®*. [online] Available at:<http://www.ossur.co.uk/prosthetic-solutions/products/feet/bionic-feet/proprio-foot> [Accessed 12 February 2016].

Riener, R., Rabuffetti, M. and Frigo, C. (2002). Stair ascent and descent at different inclinations. *Gait and Posture*, 15(1), pp.32-44.

Sup, F., Bohara, A. and Goldfarb, M. (2008). Design and Control of a Powered Transfemoral Prosthesis. The *International Journal of Robotics Research*, 27(2), pp.263-73.

Sup, F., Varol, H., Mitchell, J. Withrow, T. and Goldfarb, M. (2008). Design and Control of an Active Electrical Knee and Ankle Prosthesis. *Proceedings of the 2nd Biennial IEEE/RAS-EMBS International Conference on Biomedical Robotics and Biomechatronics*, pp.523-8.

The Lee Company. (2016a). *Axial Flow Screened 187 Lee Chek.* [online] Available at:< http://leecat.theleeco.com/ecatalog/chek-valves/en/CKFA1875001A > [Accessed 12 February 2016].

The Lee Company. (2016b). *250 Series Solenoid Valve*. [online] Available at:< http://leecat.theleeco.com/ecatalog/piloting-solenoid-valves/en/SDBA2531013B > [Accessed 12 February 2016].

Versluys, R., Desomer, A., Lenaerts, G., Damme, M., Perre, P., Peeraer, L. and Lefeber, D. (2008). A Pneumatically Powered Below-Knee Prosthesis: Design Specifications and First Experiments with an Amputee. *Proceedings of the 2nd Biennial IEEE/RAS-EMBS International Conference on Biomedical Robotics and Biomechatronics*, pp.372-7.

Winter, D. A. and Sienko, S. E. (1988). Biomechanics of below-knee amputee gait. *Journal of Biomechanics*, 21(5), pp.361–67.

Yu, T., Plummer, A., Iravani, P. and Bhatti, J. (2015). THE DESIGN OF A POWERED ANKLE PROSTHESIS WITH ELECTROHYDROSTATIC ACTUATION. *Proceedings of the ASME/BATH 2015 Symposium on Fluid Power and Motion Control*, pp.1-6.

Appendix 3: Publication 3

This appendix includes the conference paper titled '**The design of a powered ankle prosthesis with electrohydrostatic actuation**', which is published in Proceedings of the ASME/BATH 2016 Symposium on Fluid Power and Motion Control, Sep 7-9, 2016, Bath, UK. Authors including:

Tian Yu, Andrew Plummer, Pejman Iravani

Department of Mechanical Engineering, Centre for Power Transmission and Motion Control, University of Bath, Bath, United Kingdom

Jawaad Bhatti, Saeed Zahedi OBE, David Moser

Chas A Blatchford & Sons Ltd., Kingsland Business Park, Basingstoke, United Kingdom

Abstract

This paper presents a prototype powered ankle prosthesis which can operate passively in most of the gait cycle and provide assistance for toe push-off and subsequent foot dorsiflexion. The use of electrohydrostatic actuation (EHA) gives the ability to switch quickly and smoothly between passive and active modes. In this new powered ankle prosthesis, the motor-pump unit is integrated with the ankle joint and the battery and controller are held in a backpack. A 100W brushless DC motor is used driving a 0.45cc/rev gear pump. The motor runs in hydraulic fluid, pressurised to 60bar, avoiding the need for a pump shaft seal and a refeeding circuit for external leakage. A simulation model was developed to help analyse the performance characteristics of the EHA. The simulation results are compared with laboratory-based experiment results to validate the model. The compact prototype is suitable for prolonged testing with amputees, and an example set of results from amputee testing is presented.

INTRODUCTION

Passive spring-based ankle-foot prostheses are now common. They use an elastic structure to absorb the energy in the early-stance phase (heel strike) and mid-stance phase (dorsiflexion). The stored energy can be returned to assist walking in the terminal-stance phase (toe-off) [1-3]. This kind of passive spring-based ankle-foot prosthesis can achieve a nature gait to some extent (especially in low speed walking), and has several advantages including low weight, quietness, un-limited range, robustness and relatively low cost. Some more intelligent ankle prostheses are also commercially available. As an example, the Elan Foot uses controllable hydraulic damping to offer smooth ankle joint motion, which significantly improves the walking experience of amputees [4]. The PROPRIO Foot has electrical actuation at the ankle joint to adjust the ankle angle, so it can lift the toe in the swing phase to improve ground clearance and assist stand-up [5].

To further extend the daily activities of the lower limb amputees, researchers are investigating powered ankle prostheses in which active power will be used to assist walking particularly at higher speed and up slopes, and for stair climbing. Several kinds of actuation have been investigated, including off-board electric motor with flexible tether [6], pneumatic actuation [7], pneumatic artificial muscles [8], a DC motor with a ball screw [9,10], a DC motor with a lead screw [11] and electrohydrostatic actuation [12]. The main challenge is to reach the high torque and power requirement (figure 1) within the weight and volume limitation. How this actuation can be controlled to achieve a natural gait for users is also important. Different control strategies for active lower limb prostheses have been reviewed in [13]. BioM [14] is the first commercially available powered ankle prosthesis, but its power requirement significantly limits walking range.

Electrohydrostatic actuation (EHA) is widely used in aerospace, and increasingly used in industrial hydraulics. Its high power to weight/volume ratio, high torque to weight/volume ratio, good controllability and robustness give its great potential to be used in lower limb

prosthesis applications. The authors described a powered ankle prosthesis using EHA which could quickly and smoothly switch between passive and active mode in [12]. The EHA in this powered ankle prosthesis could be activated to assist walking within certain time windows, the plantarflexion (PF) before toe-off, and dorsiflexion (DF) in the early swing phase for toe-lifting. In the rest of the gait, the ankle prosthesis actuation system could operate passively with controllable damping, which could increase the working time range and ensure safe passive prosthetic function after the battery discharged.

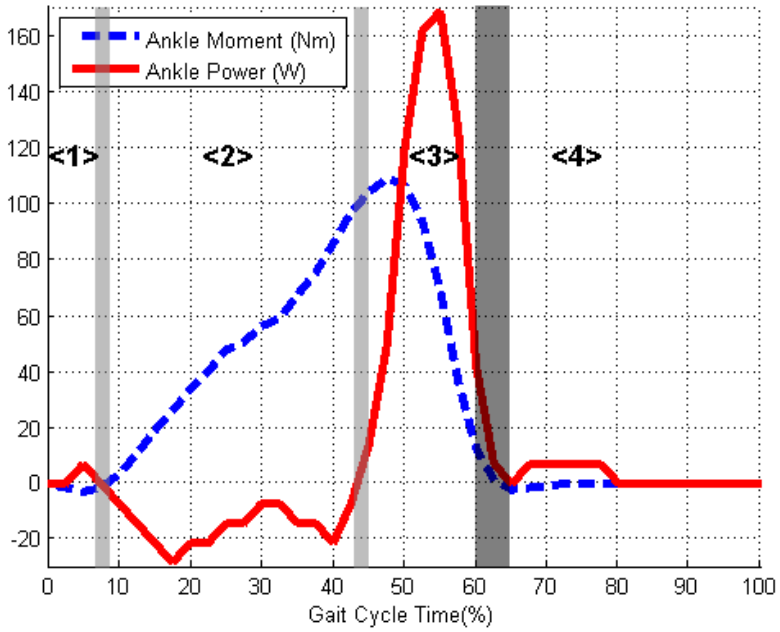

Fig.1: Ankle moment and power of healthy subjects (70kg) [15]. <1>Early-stance phase (heel strike); <2>Mid-stance phase; <3>Terminal-stance phase (active PF); <4> Swing phase. The thick dark bar in the figure indicates the toe-off.

The prototype in [12,16] has already been shown to give assistance with sufficient power. But this prototype was heavy and had a pair of hydraulic hoses to connect the motor-pump unit in the backpack to the actuator at the ankle joint. The new prototype describe in this paper is a compact powered ankle prosthesis which integrates the EHA at the ankle joint.

This new prototype can deliver the same level of assistance power with a 2.2kg integrated actuation system and a 1kg battery in the backpack. A new foot strain gauge signal based trigger method was also applied on the new prototype instead of the previous ankle angle based trigger method.

PROTOTYPE DESIGN

The hydraulic circuit is shown in figure 2. The main components are summarized in table 1. The compact powered ankle prosthesis prototype and its weight contribution are shown in figure 3.

1. Motor-pump Unit Integration

In this compact motor-pump unit, the motor runs in hydraulic fluid of about 60 bar mean pressure. With the pump shaft seal removed, the pressurised fluid in the motor cavity is refed into the closed circuit via the leakage path of the pump to compensate for oil volume variation in the closed circuit.

Apart from the electrical connections, the motor is designed to withstand an internal pressure (it has a welded steel motor casing). An end cap with o-ring has been made to seal at the end of the motor. Instead of an accumulator, a piece of compliant power steering hose is attached on the top of the end cap to supplement the volume in the motor cavity, which is shown as an accumulator symbol in figure 2. Since commercially available electrical multi-wire high pressure feedthroughs are too large for this application, a special feedthrough structure has been assembled with the endcap, which is using a ring piece of PVC material as isolator and 8 metal screws (3 for motor power wires and 5 for motor hall effect sensors) as conductors.

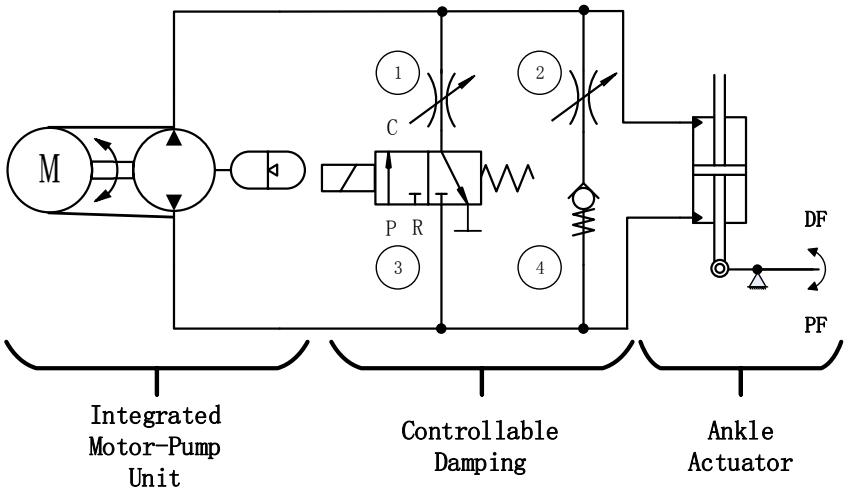

Fig.2: The hydraulic circuit of the new compact powered ankle prosthesis.

Table.1: Main components in the compact powered ankle prosthesis prototype.

Component	**Main Feature**	
Maxon EC-i 40 High Torque Brushless DC Motor	Nominal Voltage	48 V
	Rated Power	100 W
	Nominal Speed	4460 rpm
	Stall Torque	5.02 Nm
Escon Module 50/5 Servo Controller	Nominal Voltage	10-50 V
	Maximum Output Current	15 A
Hydraproducts KV0R04RBZZE Reversible Gear Pump	Displacement	0.45 cc/rev
Lee SDBA2531012B 3-way Normally Open Solenoid Valve	Pull-in Voltage	12 V
	Current Drain	0.4 A
Mountfield MBT4820Li Lithium-Ion Battery	Output Voltage	48 V
	Capacity	2 Ah

	Weight	1 kg
Blatchford Elan Ankle Joint Cylinder	Actuator Working Area	6.28 cm^2
	Movement Range	21°

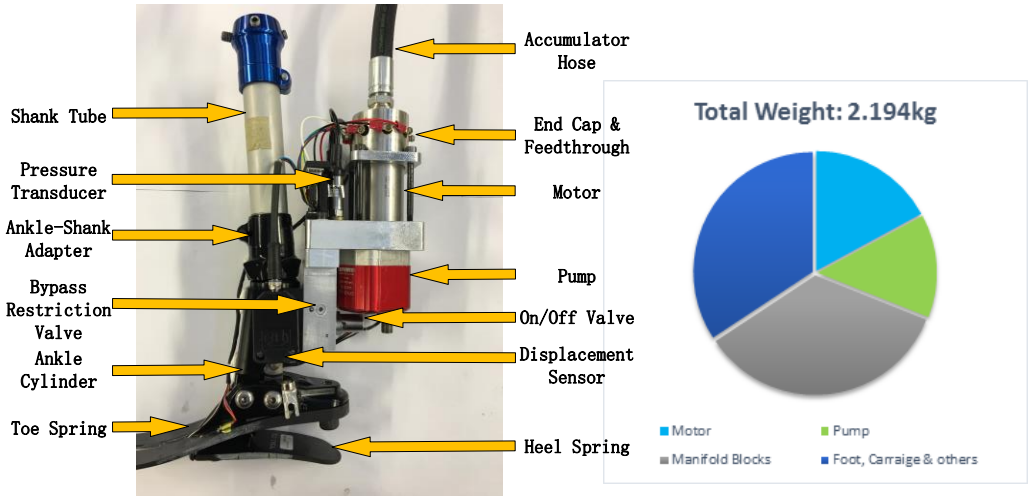

Fig.3: The compact powered ankle prosthesis prototype and its weight contribution.

Table.2: The controllable damping of the prototype in a gait cycle.

Gait Phase	Heel strike	Middle stance	Terminal stance	Swing	
Ankle Rotation Direction	PF	DF	PF	DF	-
Active/Passive Mode	Passive	Passive	Active	Active	Passive
Cylinder High Pressure Side	Top	Bottom	Bottom	Top	-
Activated Restriction Valve	②	①	-	②	-
On/off Valve	Open	Open	Close	Open	Open

2. Controllable Damping

The bypass restriction valves (valve 1&2 in figure 2) are from the Echelon foot manufactured by Blatchford [17], which can be manually adjusted to set the damping ratio in either the direction. A 3-way solenoid valve (valve 3 in figure 2) is in series with the passive DF restriction valve (valve 1). This 3-way valve works as an on/off valve, which is normally open (from port P to port C) in the passive phase and lets the fluid go through valve 1 in the passive DF phase (mid-stance). In the active PF phase, this on/off valve will be closed (P, R port blocked) to avoid flow loss through valve 1. The other bypass restriction valve (valve 2) will be activated in passive PF phase (heel

strike) and active DF phase (toe lifting in the swing phase), which is decided by the check valve 4. This controllable damping operation is summarized in table 2.

3. Ankle Joint Actuator

The actuator is the ankle joint cylinder from the élan foot of Blatchford (enlarged stroke version) [4]. An adapter is used to connect the dome of the actuator and the shank tube, as shown in figure 3. The mounting angle can be tuned by adjusting the screws on the adapter to fit a comfortable inversion/eversion angle and the maximum available dorsiflexion/plantarflexion rotation range.

4. Sensors and Electronics

Two pressure transducers are connected at the output ports of the pump to monitor the pressure in the circuit. A magnetic inductive displacement sensor is attached on the ankle cylinder and its target magnet is glued on the foot carriage. The angular position of the ankle joint can be recorded by measuring the distance between the displacement sensor and its magnet target. Three strain gauges have been attached on the foot spring as shown in figure 4.

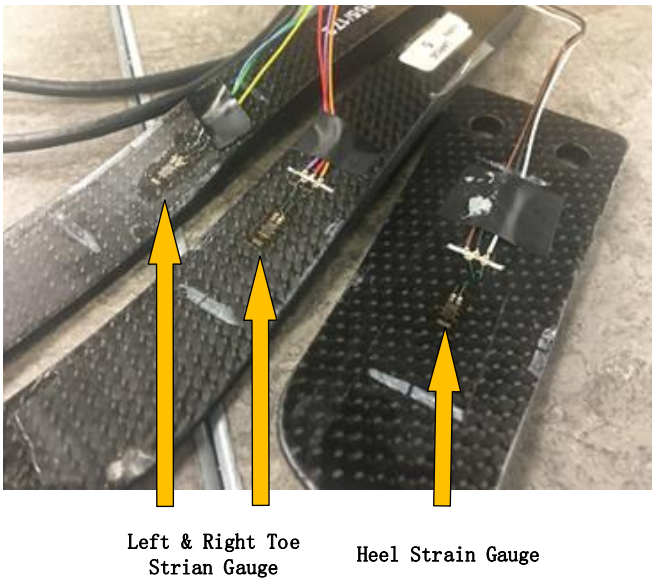

Fig.4: The strain gauges on the toe and heel spring.

A single 48V battery is carried in the backpack. A National Instruments Compact RIO is used to run the control program and record data. Via a wireless router, the real-time

data can be monitored and stored on a laptop and the control parameters can be adjusted, which means the prototype is suitable for tests with amputees. The solenoid on/off valve is driven by a servo drive module (NI 9505) on the Compact RIO. The motor was powered by the 48V battery via an amplifier (Escon 50/5 Servo Controller), which weighs only 12g. This amplifier/servo controller can also monitor and record the motor speed and current.

5. Bench Test

The new prototype has been tested in the laboratory to verify the EHA performance. In the laboratory test, the compact powered ankle prosthesis prototype was powered against a constant load. The test rig has been described in [12]. The result of an example test, in which the EHA was running against a high load (43Nm), is shown in figure 5 and summarized in table 3. Based on amputee test results using the previous prototype [16], the new prototype can provide sufficient power to assist amputee walking. Efficiency however is only about 36% in this high-load condition.

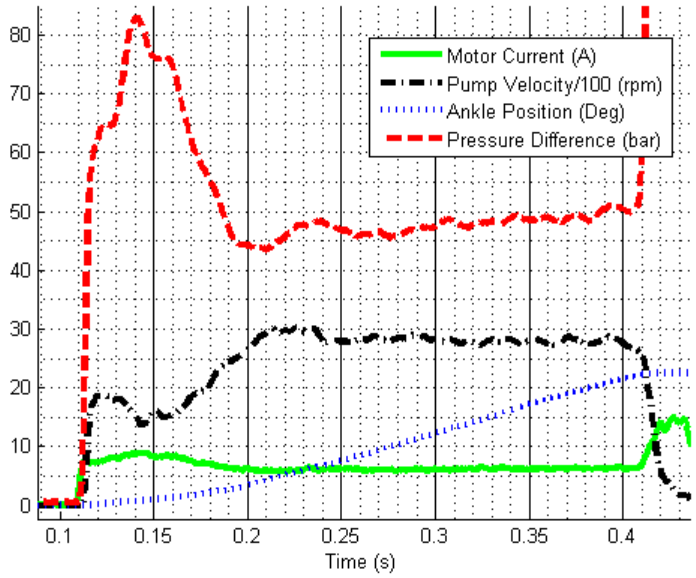

Fig.5: Bench test result of 43Nm constant load.

Mechanical output	Pump output	Motor output	Motor input
43 Nm	46 bar	0.558 Nm	6 A
1.344 rad/s	1.01 L/min	272 rad/s	27.13 V

Table 3. Summary of the EHA performance from laboratory based test.

57.8 W	77.7 W	151.8 W	162.8 W

Control method

Referring to the previous patient trials [16], the window for the powered walking assistance in the terminal stance phase is limited and the start time point is very important to make the most use of the power from the EHA. Compared to the ankle angle based trigger timing control method described in [16], the strain gauges on the foot spring directly indicate body weight transfer from the heel to the toe.

As shown in figure 4, two of the strain gauges are on each toe spring and the third one is on the heel spring. The strain gauge signal characteristics in a gait cycle have been obtained via a patient trial, in which the amputee was walking on a treadmill at a constant speed wearing the compact ankle prosthesis and the foot with strain gauges in figure 4. The EHA was operating passively in this trial. The result is shown in figure 6. The heel foot spring was compressed in the heel strike at the beginning of the gait cycle. As the body weight was transferred forward, the heel spring was released and the toe spring was compressed until toe-off. These foot spring strain gauge signals were also found to be very repeatable in this constant speed passive treadmill walking test.

Based on this result, two detection points have been set to decide the start time point of the powered PF (toe-off) assistance as shown in figure 6. The first detection point is when the heel strain gauge signal crosses a pre-set threshold, which is used to recognize the heel strike. The second trigger point is when the heel strain gauge signal and toe strain gauge signal cross each other, which indicates when the body weight is transferred from the heel to the toe. A time delay is added between the second trigger

point and the start of the powered PF phase. This delay time length can be adjusted to fit different walking speeds.

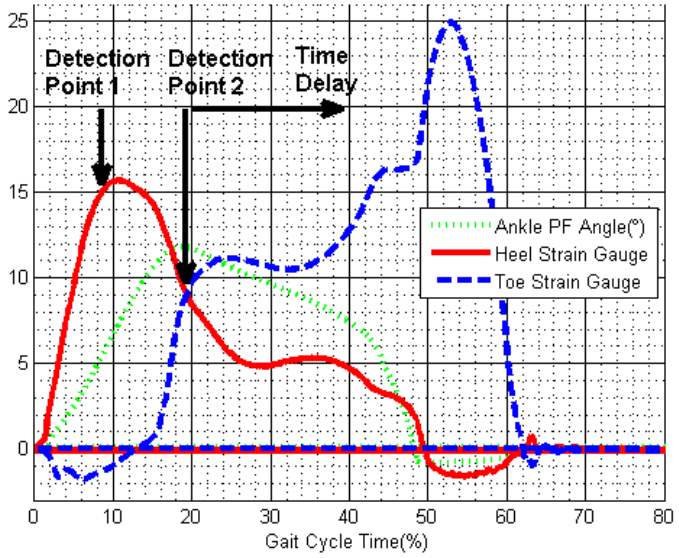

Fig.6: Strain gauge signal characters in a passive gait cycle. The toe strain gauge signal is shown as the average value of the left and right toe strain gauge.

Simulation model

A simulation model has been established to help analyse the performance of the EHA and will be used for further development of the controller. The characteristics of the hydraulic actuation system in both the passive and active phases is modelled.

The hydraulic actuation model is simplified as a symmetric model. The compressibility flow loss was found to have limited effect on the simulated result, and is not included in the model. The external leakage of the pump will be collected in the accumulator hose and be refed into the closed circuit. To keep the model simple, the leakage flow into the accumulator hose and the refed flow from the accumulator hose are also not included in the model. The pump model is given by:

$$Q_p = D\omega - K_{in}\Delta P_p \quad (1)$$

Where D is the pump displacement; ω is the motor-pump velocity; Q_p is the pump flow rate; ΔP_p is the pressure difference across the pump; K_{in} in is the internal leakage coefficient.

The pressure loss in the manifold was found to be significant. Especially between passive and active mode, the flow rate in the manifold is totally different and will be revealed as the reduced pressure difference beside the bypass restriction valves, hence affects the bypass flow rate. According to the experiment results, the linear pressure loss model matches the manifold pressure loss of this EHA prototype well. The pressure loss in the manifold is modelled as:

$$\Delta P_a = \Delta P_p - K_l Q_p \tag{2}$$

Where ΔP_a is the pressure difference across the actuator, which is also the pressure difference across the bypass restriction valve (valve 1&2 in figure 2); K_l is the manifold pressure loss coefficient. The bypass valve is modelled as:

$$\begin{cases} Q_a = Q_p - K_B\left(K_{bp1}\sqrt{\Delta P_a} + K_{bp2}\Delta P_a\right) & for\ \Delta P_a \geq 0 \\ Q_a = Q_p - \left(-K_{bd1}\sqrt{|\Delta P_a|} + K_{bd2}\Delta P_a\right) & for\ \Delta P_a < 0 \end{cases} \tag{3}$$

Where Q_a is the flow rate in/out of the actuator; K_B is the coefficient for on/off valve ($K_B = 1$ if the on/off valve is open and $K_B = 0$ if the on/off valve is closed); K_{bp1} and K_{bp2} are the bypass pressure difference to flow rate coefficients for the active PF phase and the passive DF phase (valve 1 in figure 2 activated), which combines both the square-root and the proportional relationship in the bypass line. K_{bd1} and K_{bd1} are the bypass pressure difference to flow rate coefficients for the active DF phase and the passive PF phase (valve 2 in figure 2 activated). The actuator was simplified as a proportional relationship between the actuator flow rate and ankle rotation speed:

$$\dot{\theta} = K_a Q_a A^{-1} \tag{4}$$

Where $\dot{\theta}$ is the ankle rotation speed; A is the annular area of the double-ended cylinder; K_a is a lever ratio between the piston rod extension speed and the ankle angular speed.

The results from a treadmill walk experiment have been used to validate the simulation model. In this treadmill walking experiment, a transtibial amputee was walking on a treadmill at a constant speed of 3.8km/h wearing the compact powered ankle prosthesis. The pressure difference across the pump, motor speed and on/off valve current signals shown in the upper graph of figure 7 were recorded and were used as the input signals of the simulation model. By matching the simulated ankle angular

position with the treadmill walk experiment results, the coefficients in the simulation model were estimated. The comparison between the ankle angular positions of simulation and experiment results are shown in the bottom graph of figure 7. The gait shown in the figure 7 starts from the heel strike, where a burst high pressure causes the passively PF movement of the ankle. The ankle then passively DF under a small damping along with the body weight moving forwards until the powered PF phase is started at about 0.57s of the gait. Within the powered PF phase, the motor is demand to run at the highest speed against the high load and the on/off valve is closed to ensure the full power from the motor to be delivered to the ankle actuator. The motor is demanded to reverse the direction to rotate the ankle to the maximum DF position once the powered PF phase is ended. The parameters in the model are summarized in table 4.

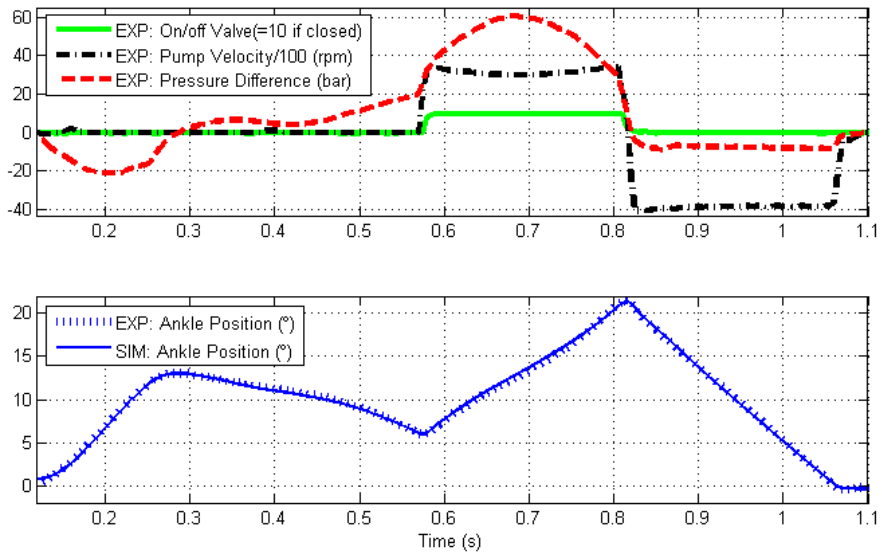

Fig.7: Comparison between treadmill walk experiment results and the simulation result.

As shown in figure 7, the simulation model can accurately predict the ankle motion under the real load situation in both passive and active phases. More detailed model including the accumulator hose and the brushless DC motor will be developed in the future to study the limits of performance in different loading scenarios.

Table.4: The summary of the simulation model parameters

Symbol	Specification	Value
D	Pump Displacement	0.45 cc/rev
K_{in}	Pump Internal Leakage Coefficient	1.46×10^{-12} $m^3/s/Pa$
K_l	Manifold Pressure Loss Coefficient	9×10^9 $Pa/m^3/s$
K_{bp1}	Active PF Bypass Coefficient 1 (square-root)	4.275×10^{-9} $m^3/s/Pa$
K_{bp2}	Active PF Bypass Coefficient 2 (linear)	1.575×10^{-12} $m^3/s/Pa$
K_{bd1}	Active DF Bypass Coefficient 1 (square-root)	6.75×10^{-8} $m^3/s/Pa$
K_{bd2}	Active DF Bypass Coefficient 2 (linear)	1.1×10^{-11} $m^3/s/Pa$
A	Actuator Annular Area	6.28 cm^2
K_a	Ankle Joint Lever Coefficient	2.64 °/mm

CONCLUSION AND FUTURE DEVELOPMENT

The EHA described in this paper can quickly switch between active and passive mode, which gives the ability of the ankle prosthesis to operate passively with controllable damping and to assist walking by powering PF in the terminal-stance phase (toe-off) and toe-lifting in the early swing phase. The new compact powered ankle prosthesis prototype has the EHA integrated at the ankle joint. The EHA can provide sufficient power to assist walking with the reduced size and weight (under 2.2kg).

The size and weight of the EHA could be further reduced if additive manufacture were used to optimise material placement and avoid the use of plugs and seals. This would also allow integration of the pump within the ankle/cylinder structure. A more detailed simulation model will be established to further research the performance of the EHA under different load conditions and will be used for controller design studies. Future investigation will also include intelligent control of the ankle prosthesis, to vary the input power level for different walking speeds, powered PF assist trigger timing

control based on other sensor signals and intelligent detection of different movement intent.

ACKNOWLEDGMENTS

We thank Chas A Blatchford & Sons Ltd., the University of Bath, and the UK Higher Education Innovation Fund for supporting this research.

References

[1] Chas A Blatchford and Sons Ltd. (2016). *Prosthetic Feet* [Online]. Available: http://www.blatchford.co.uk/endolite/category/feet/

[2] Ottobock. (2016). *1C60 Triton* [Online]. Available: http://www.ottobock.com/cps/rde/xchg/ob_com_en/hs.xsl/38138.html

[3] Össur. (2016). *Prosthetic-Solutions/ Feet* [Online]. Available: http://www.ossur.com/prosthetic-solutions/products/all-products/feet

[4] Chas A Blatchford and Sons Ltd. (2016). *élan* [Online]. Available: http://www.endolite.co.uk/products/elan

[5] Össur. (2016). *PROPRIO FOOT®* [Online]. Available: http://www.ossur.co.uk/prosthetic-solutions/products/feet/bionic-feet/proprio-foot

[6] M. Joshua et al., "An Experimental Robotic Testbed for Accelerated Development of Ankle Prostheses," in *IEEE Int. Conf. on Robotics and Automation*, Karlsruhe, Germay, 2013

[7] F. Sup et al., "Design and Control of a Powered Transfemoral Prosthesis," *The International Journal of Robotics Research*, vol. 27, No. 2, pp. 263–273, February 2008.

[8] R. Versluys et al., "A Pneumatically Powered Below-Knee Prosthesis: Design Specifications and First Experiments with an Amputee," in *Proc. Of the 2nd Biennial IEEE/RAS-EMBS Int. Conf. on Biomedical Robotics and Biomechatronics*, Scottsdale, AZ, USA, 2008.

[9] S. Au et al., ''Powered ankle-foot prosthesis for the improvement of amputee ambulation,'' in *Proc. 29th Annu. Int. Conf. IEEE Engineering in Medicine and Biology Society*, Lyon, France, 2007, pp. 3020–3026.

[10] F. Sup et al., "Design and Control of an Active Electrical Knee and Ankle Prosthesis," in *Proc. Of the 2nd Biennial IEEE/RAS-EMBS Int. Conf. on Biomedical Robotics and Biomechatronics*, Scottsdale, AZ, USA, 2008.

[11] J.K. Hitt et al., "An Active Foot-Ankle Prosthesis With Biomechanical Energy Regeneration," Journal of Medical Devices, vol. 4, pp. 011003-1-9, Mar. 2010.

[12] T. Yu et al., "THE DESIGN OF A POWERED ANKLE PROSTHESIS WITH ELECTROHYDROSTATIC ACTUATION," in *Proc. Of the ASME/BATH 2015 Symposium on Fluid Power*, Chicago, Illinois, USA, 2015.

[13] M. Tucker et al., "Control Strategies for Active Lower Extremity Prosthetics and Orthotics: A Review," *Journal of NeuroEngineering and Rehabilitation,* vol. 12, No.1, 2015.
[14] BiOM. (2016). *BiOM® T2 System* [Online]. Available: http://www.biom.com/prosthetists/personal-bionics/
[15] R. Riener et al., "Stair ascent and descent at different inclinations," *Gait & posture,* vol. 15, No.1, pp. 32-44, 2002.
[16] T. Yu et al., "Testing an Electrohydrostatic Powered Ankle Prosthesis with Transtibial and Transfemoral Amputees," in *Proc. Of the 7th IFAC Symposium on Mechatronic Systems,* Loughborough, UK, 2016.
[17] Chas A Blatchford and Sons Ltd. (2016). *Echelon* [Online]. Available: http://www.blatchford.co.uk/endolite/echelon/